

Identification of BK Polyomavirus Agnoprotein as a Novel Viroporin

Gemma Ede Swinscoe

Submitted in accordance with the requirements for the
degree of

Doctor of Philosophy

The Astbury Centre for Structural Molecular Biology

School of Molecular and Cellular Biology

The University of Leeds

November, 2019

The candidate confirms that the work submitted is her own. The contribution of the candidate and the other authors to this work has been explicitly indicated below. The candidate confirms that appropriate credit has been given within the thesis where reference has been made to the work of others.

Chapter 3: All experiments were performed, and figures generated by Gemma Ede Swinscoe (myself).

Chapter 4: All experiments were performed by myself, except figure 4.1A, which was performed by Katharine Ramshorn under my supervision, and initial modelling of BK agnoprotein was created by Dr. Richard Foster. All figures were generated by myself.

Chapter 5: All experiments were performed, and figures generated by myself.

This copy has been supplied on the understanding that it is copyright material and that no quotation from the thesis may be published without proper acknowledgement.

The right of Gemma Ede Swinscoe to be identified as Author of this work has been asserted by her in accordance with the Copyright, Designs and Patents Act 1988.

© 2019 The University of Leeds and Gemma Ede Swinscoe.

Acknowledgments

I would like to thank my supervisors: Dr Andrew Macdonald for the opportunity to undertake such a challenging and rewarding PhD project, and for his invaluable guidance throughout; and Dr Thomas Edwards for often playing devil's advocate and for his expertise in all things protein related.

I would like to thank all the past and present members of the Macdonald group for providing a thoroughly entertaining environment in lab that I will forever miss. I wish them all the best of luck in the future, wherever that might take them. Dr Emma Prescott for the time she spent training me, and the invaluable initial work she carried out before I adopted the project. Dr Margarita Panou, Dr Ethan Morgan, Dr David Kealey, and Michelle Antoni for all their advice and perspectives as we all descended into insanity. Molly Patterson for being the little pessimistic ray of sunshine that never failed to brighten the day. Dr Eleni Loundras for all Post-It notes, and always being there whenever I needed her help or advice. I would like to thank Dr Ian Manfield and Dr Sally Boxall for their training and help with troubleshooting.

I would like to thank Jack Kirk for everything. I would not have gotten through this PhD without him. Thank you for always believing in me and being there when everything got too much. Thank you to my family for their unwavering support and care throughout the entirety of my academic life.

Abstract

BK polyomavirus (BKPyV) is a small dsDNA virus and a common opportunistic infection in kidney transplant patients where it causes polyomavirus associated nephropathy (PVAN). In addition to the standard complement of structural and non- structural proteins, BKPyV also encodes a small auxiliary protein termed the agnoprotein. This is a small, highly basic protein that is expressed late during the viral life cycle. Previous studies have shown that agnoprotein is a novel viral egress factor. Polyomaviruses lacking agnoprotein show a profound defect in virus release into cell culture media. Despite these observations the mechanism by which the agnoprotein regulates such a critical stage in the viral lifecycle is poorly understood.

In 2010, the agnoprotein encoded for by JC polyomavirus (JCPyV) was shown to have a viroporin function. Viroporins are a family of virally encoded channel forming proteins, which are well characterised to have essential functions during virus egress. Viroporins have become ubiquitous across many viral families and popular drug targets in many cases. We have developed a detergent-free purification system for the production of recombinant BKPyV agnoprotein. Using this system, we have been able to show that this viroporin function is conserved in BKPyV and that the channel formed is sensitive to classical viroporin inhibitors.

Contents

Acknowledgements	II
Abstract	III
Contents of Figures	IX
Contents of Tables	XI
Abbreviations	XII
Chapter 1 : Introduction	1
1.1 Polyomaviruses	1
1.1.1 Discovery of Polyomaviruses	1
1.1.2 Classification of Polyomaviruses.....	1
1.2 Human Polyomaviruses.....	2
1.2.1 Discovery of Human Polyomaviruses	2
1.2.1 Epidemiology of Human Polyomaviruses.....	5
1.2.2 Transmission of Human Polyomaviruses	7
1.3 BK polyomavirus (BKPyV).....	8
1.3.1 Pathology of BK polyomavirus	8
1.3.2 BK polyomavirus and Cancer.....	9
1.3.3 Treatment.....	9
1.4 JC Polyomavirus (JCPyV)	10
1.4.1 Pathology of JC polyomavirus.....	10
1.4.2 JC Polyomavirus and Cancer.....	11
1.4.3 Treatment.....	11
1.5 Molecular Virology of Human Polyomaviruses	12
1.5.1 Genome Organisation	12
1.6 Non-coding Control Region (NCCR)	14
1.7 Early Non-Structural Proteins	16
1.7.1 Large Tumour Antigen (LT).....	16
1.7.2 Small Tumour Antigen (sT)	16
1.7.3 Alternative-Spliced LT	17
1.8 Late Structural Proteins	17
1.8.1 VP1 and VP2/3.....	17
1.8.2 VP4, VP5, VP6	20
1.9 Late Non-Structural Protein	21

1.9.1	Agnoprotein	21
1.10	Human Polyomavirus Lifecycle	24
1.10.1	Virus Entry and Uncoating	26
1.10.2	Persistence	31
1.10.3	Viral Replication and Transcription	32
1.10.4	Viral Assembly	33
1.10.5	Viral Egress and Release.....	34
1.11	Viroporins	35
1.11.1	Influenza M2.....	37
1.11.2	Hepatitis C virus (HCV) p7	41
1.11.3	Human Immunodeficiency Virus (HIV) Vpu.....	42
1.11.4	Enterovirus 2B.....	43
1.11.5	Human Papillomavirus (HPV) E5	44
1.12	Aims and Objectives.....	46
Chapter 2	: Materials and Methods.....	47
2.1	Materials	47
2.1.1	Mammalian Cell Lines and Primary Cells	47
2.1.2	Bacterial Strains	47
2.1.3	Plasmids.....	47
2.1.4	Antibodies	48
2.1.5	Lipids.....	48
2.1.6	Inhibitors and Control Compounds.....	48
2.2	Manipulation of Recombinant DNA	50
2.2.1	Oligonucleotides.....	50
2.2.2	Polymerase Chain Reaction (PCR).....	50
2.2.3	Restriction Endonuclease Digestion	51
2.2.4	DNA Clean Up.....	52
2.2.5	Agarose Gel Electrophoresis	52
2.2.6	DNA ligation	52
2.2.7	Colony PCR Screening	53
2.3	Preparation of Plasmid DNA.....	54
2.3.1	Transformation and Plating of Chemically Competent Bacterial Cells	54
2.3.2	Preparation of Small-Scale Bacterial Cultures, Extraction and Purification of Plasmid DNA (Miniprep).....	54

2.3.3	Preparation of Large-Scale Bacterial Cultures, Extraction and Purification of Plasmid DNA (Maxiprep).....	54
2.3.4	Storage of Plasmid DNA as a Glycerol Stock	55
2.3.5	Quantification of Plasmid DNA.....	55
2.4	Expression and Purification of His-BK agnoprotein.....	55
2.4.1	IPTG Induced Protein Expression.....	55
2.4.2	Bacterial Cell Lysis.....	56
2.4.3	Nickel Affinity Purification of His-BK agnoprotein.....	56
2.4.4	Ion Exchange Chromatography of His-BK agnoprotein	56
2.4.5	Reverse Phase High Pressure Liquid Chromatography (rpHPLC) of 10x His BK agnoprotein	57
2.4.6	Concentration of Recombinant 10x His BKPyV agnoprotein	57
2.4.7	Quantification of Recombinant 10x His BKPyV agnoprotein.	58
2.5	<i>In Vitro</i> Liposome Assays	58
2.5.1	Preparation of Unilamellar Liposomes	58
2.5.2	Real Time <i>In Vitro</i> Liposome Assay	59
2.5.3	Inhibitor Assays.....	59
2.5.4	Floatation Assays.....	59
2.6	Mammalian Cell Culture	60
2.6.1	Maintenance and Passage of Cells.....	60
2.6.2	Seeding of Cells	60
2.6.3	Storage and recovery of frozen cell stocks	61
2.7	Preparation of BK Polyomavirus Stocks.....	61
2.7.1	Transfection of RPTE cells with BKPyV genome.....	61
2.7.2	Infection of RPTE cells with BKPyV	62
2.7.3	Quantification of BKPyV – Fluorescence Focus Assay.....	62
2.8	Protein Biochemistry.....	64
2.8.1	Preparation of Cell Lysates for SDS Polyacrylamide Gel Electrophoresis (PAGE)	64
2.8.2	Preparation of Immunoprecipitations/GST Pull Down for SDS PAGE	64
2.8.3	Preparing and Running SDS PAGE Gels	65
2.8.4	Semi-Dry Transfer of Proteins to Nitrocellulose	65
2.8.5	Western Blotting.....	65
2.8.6	Coomassie-based Staining of Polyacrylamide Gels	66
2.8.7	GST Pull Down.....	66

2.9	Cell-based Assays	67
2.9.1	Transfection	67
2.9.2	Preparation of Cells for Immunofluorescence	68
2.9.3	Lysis of Mammalian Cells	68
2.9.4	Merocyanine 540 Assay	68
2.9.5	Hygromycin Assay	69
2.9.6	Subcellular Fractionations	69
2.9.7	Cytotoxicity Assay	70
2.9.8	Treatment of BK polyomavirus Infection	70
2.10	Statistical Analysis	70
Chapter 3 : Expression and Purification of Recombinant BKPyV Agnoprotein		
	71	71
3.1	Introduction	71
3.2	Cloning of 10x His BKPyV agnoprotein	75
3.3	Expression of Recombinant 10x His BKPyV agnoprotein	77
3.4	Isolation of 10x His BKPyV agnoprotein	81
3.5	Purification of isolated 10x His BKPyV agnoprotein	83
3.6	Concentration of purified 10x His BKPyV agnoprotein	87
3.7	Discussion	91
Chapter 4 : BKPyV agnoprotein Oligomerises and Displays Channel-Forming Ability		
	98	98
4.1	Introduction	98
4.2	BKPyV agnoprotein Forms Oligomers	100
4.3	BKPyV agnoprotein associates with membranes in mammalian cells. 102	
4.4	BKPyV agnoprotein has a varying orientation in membranes	102
4.5	10x His BKPyV agnoprotein Displays Channel-forming Activity...	106
4.5.1	BKPyV agnoprotein disrupts cellular membranes	106
4.5.2	BKPyV agnoprotein does not permeabilise the plasma membrane	113
4.5.3	10x His BKPyV agnoprotein associated with and integrates into Liposomal membranes	115
4.5.4	10x His BKPyV agnoprotein facilitates dose-dependent release of carboxyfluorescein from Liposomes	120
4.6	Discussion	124
4.6.1	<i>in silico</i> Modelling of BKPyV agnoprotein	129

Chapter 5 : Inhibition of BKPyV agnoprotein Channel Activity	135
5.1 Introduction	135
5.2 Channel formed by BKPyV agnoprotein is sensitive to classical viroporin inhibitors	137
5.2.1 Adamantanes	138
5.2.2 MNDNJ	138
5.3 Channel formed by BKPyV agnoprotein is sensitive to the anion channel inhibitor DIDs	138
5.3.1 Rimantadine, MNDNJ, and DIDs inhibit BKPyV viral release from RPTE cells.	142
5.4 Discussion	145
5.4.1 Could Resistant Strains of BKPyV form?	146
Chapter 6 : Conclusions	150
Chapter 7 : Reference	153
Appendix	180

Contents of Figures

<i>Figure 1.1: Polyomaviridae phylogenetic family, based on identity similarity of large tumour antigen</i>	3
<i>Figure 1.2: Polyomavirus Virion Architecture</i>	4
<i>Figure 1.3: Generalised schematic of polyomavirus genome.</i>	13
<i>Figure 1.4: Polyomavirus VP1 Arrangement</i>	19
<i>Figure 1.5: Schematic of polyomavirus life cycle</i>	25
<i>Figure 1.6: Schematic of Sialic Acid Receptors</i>	27
<i>Figure 1.7: EM structure of BKPyV in complex with GT1b</i>	28
<i>Figure 1.8: Schematic diagram of the classification of viroporin.</i>	38
<i>Figure 2.1: Schematic of BKPyV production</i>	63
<i>Figure 3.1: Amino acid conservation and hydrophobicity of polyomavirus agnoproteins</i>	72
<i>Figure 3.2: Computational Characterisation of agnoproteins from BKPyV, JCPyV and SV40</i>	73
<i>Figure 3.3: Cloning of pET19b BKPyV agnoprotein</i>	76
<i>Figure 3.4: Test Expression of pET17b BKPyV agnoprotein</i>	78
<i>Figure 3.5: Effect of His BK agnoprotein on E coli proliferation</i>	80
<i>Figure 3.6: Nickle affinity chromatography purification of 10x His BKPyV agnoprotein</i>	82
<i>Figure 3.7: rpHPLC of 10x His BKPyV agnoprotein</i>	85
<i>Figure 3.8: cIEX purification of recombinant 10x His BKPyV agnoprotein</i> ...	88
<i>Figure 3.9: Aggrescan prediction of aggregation-prone “hot spots” in 10x His BKPyV agnoprotein</i>	90
<i>Figure 3.10: Schematic of purification method for recombinant 10x His BKPyV agnoprotein</i>	96
<i>Figure 4.1: Oligomerisation of BKPyV agnoprotein</i>	101
<i>Figure 4.2: Subcellular fractionation of BKPyV agnoprotein</i>	103
<i>Figure 4.3: Topology of BKPyV agnoprotein</i>	104
<i>Figure 4.4: Merocyanine 540 (MC540) Assay</i>	107
<i>Figure 4.5: Flow cytometry gates applied during merocyanine analysis</i>	108
<i>Figure 4.6: Merocyanine 540 Assay with BKPyV and JCPyV agnoprotein</i>	110
<i>Figure 4.7: A schematic of BKPyV agnoprotein mutants cloned into peGFP-C1</i>	111

<i>Figure 4.8: Merocyanine 540 Assay with BKPyV agnoprotein truncations</i>	112
<i>Figure 4.9: Merocyanine 540 Assay with BKPyV agnoprotein point mutants</i>	114
<i>Figure 4.10: Hygromycin Assay</i>	116
<i>Figure 4.11: Hygromycin Assay with BKPyV and JCPyV agnoprotein</i>	117
<i>Figure 4.12: Flootation Assay with recombinant BKPyV agnoprotein</i>	119
<i>Figure 4.13: Dye Release Assay with recombinant BKPyV agnoprotein</i> ...	121
<i>Figure 4.14: Dye Release Assay with Agnoprotein 20-42 aa. Peptide</i>	123
<i>Figure 4.15: in silico Model of BKPyV agnoprotein</i>	130
<i>Figure 4.16: Iterative Oligomeric Modelling of BKPyV agnoprotein using CCbuilder</i>	133
<i>Figure 4.17: CCbuilder 2.0 Model of BKPyV agnoprotein</i>	134
<i>Figure 5.1: Inhibition of Dye Release with Adamantanes</i>	139
<i>Figure 5.2: Inhibition of Dye Release with NNDNJ</i>	140
<i>Figure 5.3: Inhibition of Dye Release with DIDs</i>	141
<i>Figure 5.4: MTT Assays in RPTE cells</i>	143
<i>Figure 5.5: Treatment of BKPyV Infections in RPTE cells</i>	144
<i>Figure A.1: Dye Release Controls</i>	182
<i>Figure A.2: Alignment of BKPyV agnoproteins from multiple stains</i>	183

Content of Tables

<i>Table 1.1: A summary of human polyomaviruses (HPyV) – in order of discovery– with their associated seroprevalence, diseases, and site(s) of infection.....</i>	<i>6</i>
<i>Table 1.2: A summary of identified interaction partners for the agnoproteins of JCPyV and BKPyV.....</i>	<i>23</i>
<i>Table 1.3: Table of viroporins and their functions</i>	<i>36</i>
<i>Table 2.1: Table of Inhibitors and Compounds, with their structures and source</i>	<i>50</i>
<i>Table 2.2: Composition of PCR mix used for amplification of agnogene</i>	<i>51</i>
<i>Table 2.3: Step-by-step PCR protocol used for amplification of agnogene .</i>	<i>51</i>
<i>Table 2.4: Composition of PCR mix used for amplification of agnogene</i>	<i>53</i>
<i>Table 2.5: Step-by-step PCR protocol used for colony PCR</i>	<i>53</i>
<i>Table 2.6: Recipe for revolving and stacking acrylamide gels</i>	<i>65</i>
<i>Table 5.1: List of characterised viroporin inhibitors, their structures, target and system in which they were characterised</i>	<i>137</i>
<i>Table 5.2: Mutations found in the helical domain of agnoprotein from clinically isolated BKPyV stains.....</i>	<i>147</i>
<i>Table A.1: List of Oligonucleotides.....</i>	<i>180</i>

Abbreviations

-HF	- high fidelity
(-)	Negative sense
(+)	Positive sense
5HT2A	Serotonin 2A receptor
aa	Amino acid
ADP	Adenosine diphosphate
AF	Alexa fluor
AIDS	Acquired immunodeficiency syndrome
Ala or A	Alanine
AM2	Influenza A virus matrix protein 2
AP-3	Adaptor protein complex 3
APS	Ammonium persulfate
APyV	Avian polyomavirus
Arg or R	Arginine
ARV	Avian reovirus
Asn or N	Asparagine
ATCC	American Type Culture Collection
ATP	Adenosine triphosphate
B	Buffer
BCA	Bicinchoninic acid
BIT225	N-[5-(1-methyl-1H-pyrazol-4-yl)-naphthalene-2-carbonyl]-guanidine
BKPyV	BK polyomavirus
BM2	Influenza B virus matrix protein 2
BPyV	Bovine polyomavirus
BSA	Bovine serum albumin

BUDE	Bristol University Docking Engine
bv	Bed volume
BVDV	Bovine viral diarrhoea virus
Ca ²⁺	Calcium
Cdc42	Cell division control protein 42 homolog
CF	Carboxyfluorescein
cIEX	Cation exchange chromatography
CM2	Influenza C virus matrix protein 2
CNS	Central nervous system
Conc.	Concentration
CoxV B	Coxsackie 3B virus
CPyV	Crow polyomavirus
CSFV	Classical swine fever virus
DIDs	4,4'-Diisothiocyano-2,2'-stilbenedisulfonic acid
DM2	Influenza D virus matrix protein 2
DMEM	Dulbecco's Modified Eagle Media
DMSO	Dimethyl sulfoxide
DNA	Deoxyribose nucleic acid
dNTP	Deoxyribonucleotide triphosphate
ds-	Double stranded
E5	HPV early protein 5
EBV	Epstein Barr Virus
ECL	Electrochemiluminescence
EDTA	Ethylenediaminetetraacetic acid
EGF	Epidermal growth factor
eGFP	Enhance green fluorescence protein
EGFR	Epidermal growth factor receptor
EM	Electron microscopy

ER	Endoplasmic reticulum
ERAD	Endoplasmic-reticulum-associated protein degradation
ERK	Extracellular Receptor Kinase
ERp29	Endoplasmic Reticulum Protein 29
EV71	Enterovirus 71
FBS	Foetal bovine serum
FDA	Food and Drug Administration
FEZ1	Fasciculation and elongation protein zeta-1
FL	Full length
FLAG	DYKDDDK tag
FMDV	Foot-and-mouth disease virus
FPyV	Finch polyomavirus
GAPDH	Glyceraldehyde 3-phosphate dehydrogenase
GHPyV	Goose haemorrhagic polyomavirus
Gln or Q	Glutamine
Glu or E	Glutamic acid
Gly or G	Glycine
GST	Glutathione S-transferases
GTP	Guanosine triphosphate
H1	Histone 1
HA	Hemagglutinin
HAART	Highly active antiretroviral therapy
HaPyV	Hamster polyomavirus
HCV	Hepatitis C virus
HEK	Human embryonic kidney
HEK293T	Human embryonic kidney cells transformed with heat sensitive SV40 LT
His or H	Histidine

HIV	Human immunodeficiency virus
HMA	5-(N,N-Hexamethylene) amiloride
HP1 α	Heterochromatin protein 1
HPV	Human papillomavirus
HPyV	Human polyomavirus
HPyV12	Human polyomavirus 12
HPyV6	Human polyomavirus 6
HPyV7	Human polyomavirus 7
HPyV9	Human polyomavirus 9
hr	Hour
hRSV	Human respiratory syncytial virus
Hsp70	Heat shock protein 70
HSV	Herpes simplex virus
HTERT	Human telomerase reverse transcriptase
HTLV	Human immunodeficiency virus type-1
IAV	Influenza A virus
IBV	Influenza B virus
ICV	Influenza C virus
IF	Immunofluorescence
Ile or I	Isoleucine
IPTG	Isopropyl β - d-1-thiogalactopyranoside
IU	Infectious units
IV	Influenza virus
JCPyV	JC polyomavirus
kDa	Kilo dalton
KIPyV	Karolinska Institute polyomavirus
L1	HPV late protein 1
LB	Luria-Bertani

Leu or L	Leucine
LIPyV	Leon IARC polyomavirus
LPyV	African green monkey B-lymphotropic polyomavirus
LSTc	lactoseries tetrasaccharide c
LT	Large tumor antigen
Lys or K	Lysine
M	Melittin
m-	milli-
M2	Matrix protein 2
MaPyV	Mastomys polyomavirus
MBP	Maltose-binding protein
MC540	Merocyanine 540
MCPyV	Merkle cell polyomavirus
MD	Molecular dynamics
MEK	Mitogen-activated protein kinase kinase
MHV	Murine hepatitis virus
mins	Minutes
miRNA	Micro ribose nucleic acid
MNK1	MAP kinase-interacting serine/threonine-protein kinase 1
MOI	Multiplicity of infection
MPtV	Murine pneumotropic polyomavirus
mPyV	Murine polyomavirus
mT	Middle tumor antigen
MTT	4,5-dimethylthiazol-2-yl)-2,5-diphenyltetrazolium bromide
MWPyV	Malawi polyomavirus
MXPyV	Mexico polyomavirus

MyPyV	Myotis polyomavirus
n-	nano-
NaCl	Sodium Chloride
NCCR	Non-coding Control Region
NF- κ B	Nuclear factor kappa-light-chain-enhancer of activated B cells
NHS	National health service
Ni	Nickle
NJPyV	New Jersey polyomavirus
NK cell	Natural killer cell
NMR	Nuclear magnetic resonance
NNDNJ	N-(n-Nonyl)-1-deoxynojirimycin
OD	Optical density
OPP	O-propargyl-puromycin
OraPyV 1/2	Bornean orangutan polyomavirus 1/2
ORF	Open reading frame
PA	L- α -Phosphatidic acid
PAGE	Polyacrylamide gel electrophoresis
PBS	Phosphate buffered saline
PC	L- α -Phosphatidylcholine
PCNA	Proliferating cell nuclear antigen
PCR	Polymerase chain reaction
PDI	Protein disulphide isomerase
PE	L- α -Phosphatidylethanolamine with lissamine rhodamine B labelled head groups
PEI	Polyethylenimine
Phe or F	Phenylalanine
PI	Protease inhibitors
PML	Progressive Multifocal leukoencephalopathy

PML-NBs	Promyelocytic leukaemia nuclear bodies
PP2A	Protein phosphatase 2
pRb	Retinoblastoma protein
PV	Poliovirus
PVAN	Polyomavirus associated nephropathy
rpHPLC	Reverse phase high performance liquid chromatography
rpm	Rotation per minutes
RPTE	Renal proximal tubule epithelial
RV	Rotavirus
SARS-CoV	Severe acute respiratory distress syndrome-associated coronavirus
SDS	Sodium dodecyl sulphate
sec	Seconds
Ser or S	Serine
SH	Small hydrophobic protein
SLPyV	California sea lion polyomavirus
SqPyV	Squirrel monkey polyomavirus
ss-	Single stranded
sT	Small tumor antigen
STLPyV	St Louis polyomavirus
SV40	Simian vacuolating virus 40
SVG-A	Human foetal astrocyte cell line
TAE	Tris base, acetic acid and EDTA
Tat	Trans-Activator of Transcription
TBST	Tris buffered saline with tween
TEMED	Tetramethylethylenediamine
TEV	Tobacco etch virus protease

TFA	Trifluoroacetic acid
TGN	Trans-Golgi Network
TM	Transmembrane
Trp or W	Tryptophan
TSPyV	Trichodysplasia spinulosa-associated polyomavirus
tT	Truncated tumor antigen
TX	Triton X100
Tyr or T	Tyrosine
U	Units
ULBP3	UL16 Binding Protein 3
UV	Ultraviolet
V	Volts
Val or V	Valine
Vero	African green monkey kidney cells
VLP	Viral-like particles
Vol.	Volume
VP	Viral protein
Vpu	Viral protein U
WB	Western blot
wt.	Wild type
WUPuV	Washington university polyomavirus
YB-1	Y box binding protein 1
α -SNAP	N-ethylmaleimide-sensitive factor Attachment Protein Alpha
Δ agno	Agnoprotein-deficient
μ -	Micro-

Chapter 1 : Introduction

1.1 Polyomaviruses

1.1.1 Discovery of Polyomaviruses

The first polyomavirus was isolated from AKR mice by Eddy and Stewart in 1959. This virus, initially dubbed SE polyomavirus, is now referred to as murine polyomavirus [1]. The term polyoma originates from the Greek roots poly- meaning "many" and -oma meaning "tumor", which is indicative of the multiple tumors observed in the pathogenesis of many animal polyomaviruses [2]. Since 1959, polyomaviruses have been found in a wide range of vertebrates, including birds, fish, humans, monkeys, and bats.

1.1.2 Classification of Polyomaviruses

Polyomaviruses were originally classed, alongside papillomaviruses, under the *Papovaviridae*. In 2000, The International Committee on Taxonomy of Viruses concluded that polyoma- and papillomaviruses are fundamentally different, and therefore *Papovaviridae* was divided into *Polyomaviridae* and *Papillomaviridae* [3].

Inclusion of new family members in *Polyomaviridae* is now determined using the following species criteria [4]:

1. The complete genome is published and available on a public database.
2. The genome displays the characteristic polyomavirus arrangement.
3. The natural host is well characterised.
4. The genetic difference between it and the closest species is >15% based on the large t antigen.

5. If two members exhibit <15% genetic difference based on their large t antigen, then profound differences in biological tropism, pathogenesis, or host can be used as justification of inclusion.

Polyomaviridae are further divided into four genera; Alphapolyomavirus, Betapolyomavirus, Deltapolyomavirus, and Gammapolyomavirus (figure 1.1), based on the identity similarity of the large tumor antigens. Alpha-, Beta-, and Deltapolyomaviruses are known only to infect mammals, whilst Gammapolyomaviruses infect avian species [5]. These genera classifications will undoubtedly need expanding upon in the future to accommodate the clear phylogenetic differences exhibited by emerging fish polyomaviruses [6].

1.2 Human Polyomaviruses

1.2.1 Discovery of Human Polyomaviruses

The first evidence of a human polyomavirus was found in 1965 from electron microscopy of virus particles isolated from a progressive multifocal leukoencephalopathy patient, which resembled polyoma-like architecture [7] (figure 1.2). These virus particles were later identified as JC polyomavirus (JCPyV) by Padgett et al. in 1971 [8]. 1971 also saw the discovery of the second human polyomavirus, described by Gardner et al. and coined BK polyomavirus [9] (BKPyV). There have since been 12 more polyomaviruses discovered; KI polyomavirus (KIPyV) [10], WU polyomavirus (WUPyV) [11], Merkel cell polyomavirus (MCPyV) [12], trichodysplasia spinulosa-associated polyomavirus (TSPyV) [13], MW polyomavirus (MWPyV) [14], STL polyomavirus (STLPyV) [15], New Jersey polyomavirus (NJPyV) [16], Lyon IARC polyomavirus (LIPyV) [18], human polyomavirus-6 (HPyV6) [19], -7 (HPyV7) [19], -9 (HPyV9) [20], and -12 (HPyV12) [21].

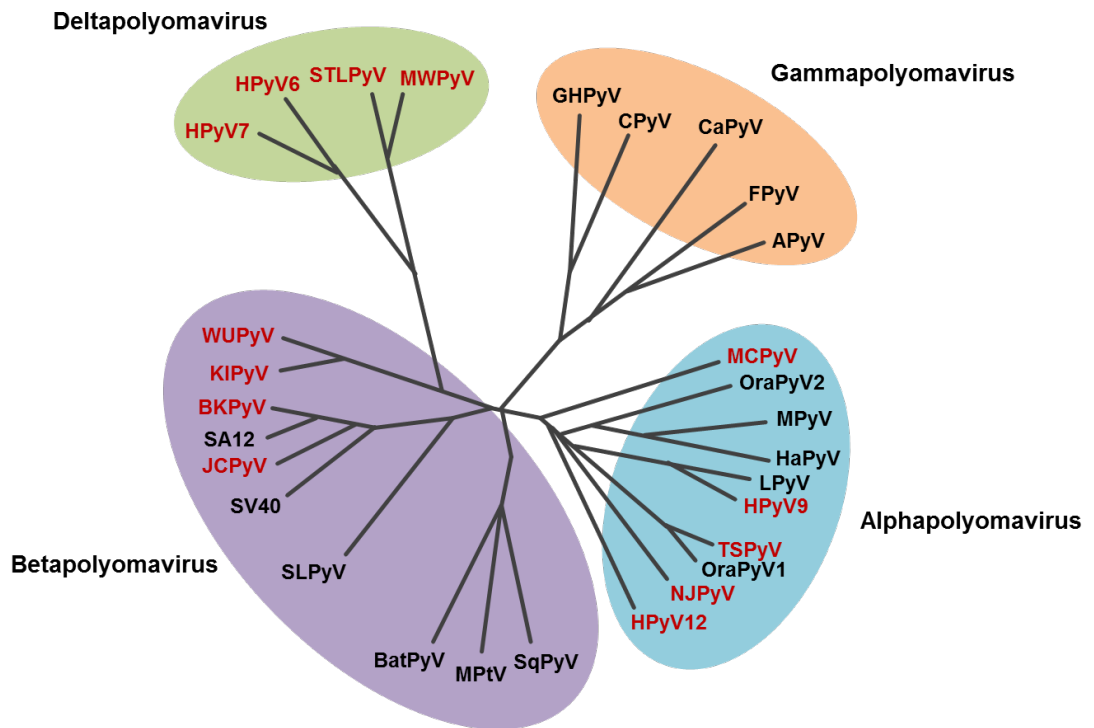
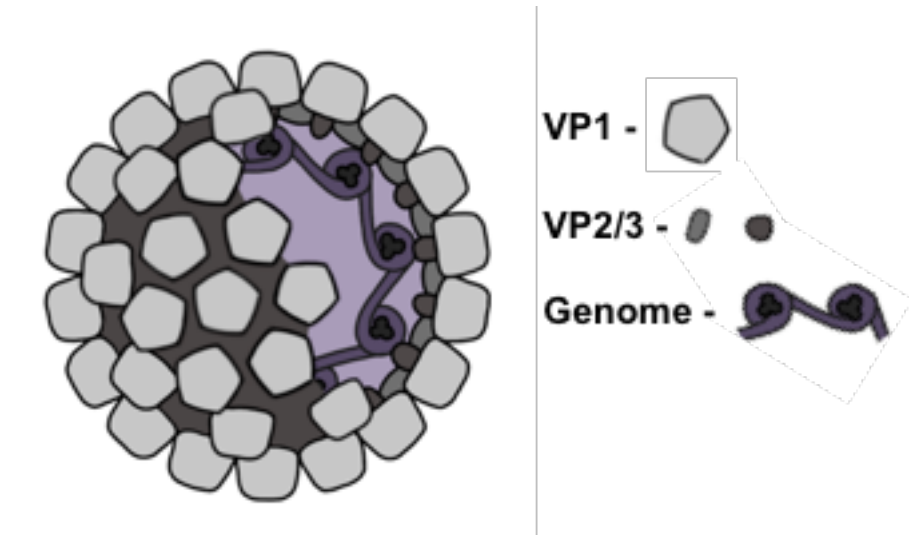


Figure 1.1: Polyomaviridae phylogenetic family, based on identity similarity of large tumour antigen

Human polyomaviruses (HPyVs) are highlighted in red. Goose haemorrhagic polyomavirus (GHPyV); crow polyomavirus (CPyV); finch polyomavirus (FPyV); avian polyomavirus (APyV); bornean orangutan polyomavirus 1/2 (OraPyV 1/2); murine polyomavirus (mPyV); hamster polyomavirus (HaPyV); African green monkey B-lymphotropic polyomavirus (LPyV); murine pneumotropic polyomavirus (MPtV); California sea lion polyomavirus (SLPyV); squirrel monkey polyomavirus (SqPyV).

A



B

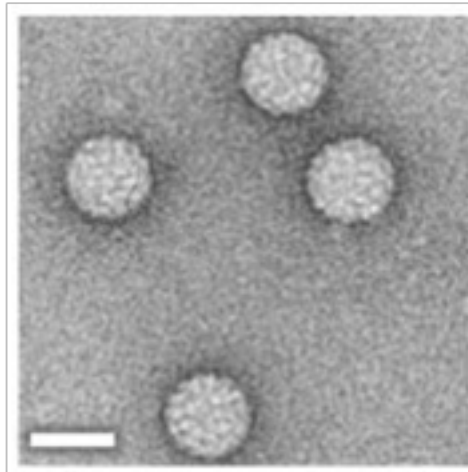


Figure 1.2: Polyomavirus Virion Architecture

(A) Generalised schematic of polyomavirus architecture. (B) Morphology of a polyomavirus. BK polyomavirus visualised via negative stain electron microscopy. Scale bar 50 nm [22].

1.2.1 Epidemiology of Human Polyomaviruses

All human polyomaviruses are associated with childhood/young-adult asymptomatic infections that establish lifelong episomal persistence [23], with periodic shedding from viral reactivation. The seroprevalence of human polyomaviruses, in the general population, ranges from 20% to >90% (table 1.1). LIPyV and NJPyV are reported to have the lowest seroprevalence of ~5% [24], whilst BKPyV is reported to have a >90% seroprevalence [23].

Virus Name	Year of Isolation	Seroprevalence	Associated Disease	Site of Isolation
JCPyV	1971	50-80% [23, 25]	Progressive Multifocal Leukoencephalopathy (PML) [8]	Urine [26], Brain [8]
BKPyV	1971	>90% [23, 25]	BK-associated nephropathy [26], ureteral stenosis [27], haemorrhagic cystitis [28]	Urine [9]
KIPyV	2007	>55% [25]	None known	Respiratory tract [10]
WUPyV	2007	>69% [25]	None known	Respiratory tract [11]
MCPyV	2008	60-80% [25]	Merkel Cell Carcinoma	Skin [19]
HPyV 6	2010	>83% [25]	Pruritic and dyskeratotic dermatitis [29]	Skin [29]
HPyV 7	2010	>64% [25]	Pruritic and dyskeratotic dermatoses [29]	Skin [29]
TSPyV	2010	70-80% [23, 25]	Trichodysplasia spinulosa [30]	Skin [30]
HPyV 9	2011	19-70% [24, 25]	None known	Plasma, Serum, Urine, Blood [20]
MWPyV	2012	~40-70% [31]	None known	Digestive tract [17]

STLPyV	2013	70%[33]	None known	Intestinal tract [15]
HPyV 12	2013	~15-30% [21]	None known	Digestive tract, Liver [21]
NJPyV	2014	~5% [24]	None known	Skin [16]
LIPyV	2017	~5% [24]	None known	Skin [18], Blood [24]

Table 1.1: A summary of human polyomaviruses (HPyV) – in order of discovery– with their associated seroprevalence, diseases, and site(s) of infection.

The clinical relevance of the human polyomaviruses is strongly associated with immunocompromised patients, who have either received solid organ transplants [29, 34, 35] or have acquired/congenital immunodeficiencies [36-38]. Multiple etiological studies have investigated pathological complications where HPyVs were isolated from unhealthy/anomalous tissues [24]. However, to date only BKPyV, JCPyV, MCPyV, TSPyV, HPyV6, and HPyV7 have been determined as causal factors of disease.

1.2.1.1 Human Polyomaviruses and Cancer

Consequently, etiological studies have also contributed to an increasing amount of evidence for the involvement of HPyVs in cancers. Excluding MCPyV -which has been identified as the causative agent in ~80% of Merkel cell carcinomas [39]- there are multiple examples in the literature where HPyV DNA or proteins have been isolated from cancerous tissues [40].

The current school of thought about these etiological observations suggest that polyomavirus tumour antigens are responsible for the oncogenic transformation of cells. In the case of MCPyV, oncogenic transformation is thought to be triggered via a UV-dependent integration of the viral genome [41]. This integration

leads to the eradication of viral replication, constitutive expression of sT gene, and truncation of the LT gene. The sT antigen and truncated LT antigen are then able to initiate oncogenesis and transformation. Integration events for other polyomaviruses have also been observed, for example BKPyV CH-1 (KP984526.1). BKPyV CH-1 was found integrated in a high-grade urothelial tumour that developed in a renal allograft. It was unable to complete a production virus lifecycle due to a disruption in the VP1 gene at the site of integration, but importantly maintained LT expression [42, 43].

So far, no clear mechanistic details of oncogenesis have been described for other polyomaviruses, and the idea of HPyV-driven oncogenesis is challenged by [44]:

1. The “hit-and-run” mechanism, where HPyVs play critical roles in early oncogenic mutation, through inducing chromosomal instability, but are subsequently lost from malignant cells.
2. The “passenger” mechanism, by which HPyVs favour the conditions within a transformed cell, but contribute nothing towards oncogenesis.
3. The “by-stander” mechanism, where HPyVs infect surrounding non-malignant cells and contribute nothing towards neighbouring abnormal cells.

1.2.2 Transmission of Human Polyomaviruses

Several modes of transmission have been suggested for HPyVs. Oral transmission has strong support from multiple studies which report the presences of HPyVs in sewage [45] and drinking water sources [46]. This is perhaps not surprising, seeing as latently infected individuals periodically shed viruses in both their urine and/or faeces [47]. Respiratory transmission, through aerosols or fomites, is also a likely mechanism of spread, due to primary infections often presenting themselves with mild cold-like symptoms in children and active infections being detected in the respiratory tract [10, 11, 48]. This could explain the rapid infection of young children, especially if they are exposed to other infected children within the confines of a school or nursery environment.

Other mechanisms of transmission that potentially play minor roles in the transmission of HPyVs include; sexual transmission, as BKPyV has been detected in sperm and the male reproductive system [49, 50]; transmission through contaminated blood from individuals experiencing spikes in viraemia [24]; and placental transmission from mother to child [51], due to virus reactivation being more prominent during the immunoprivileged environment that is created during pregnancy.

1.3 BK polyomavirus (BKPyV)

Gardner et al. [9] isolated BKPyV from biopsies and urine of a Sudanese patient who developed ureteric obstruction after a renal transplantation in 1971. Electron microscopy, cytological investigation, and viral propagation at the time revealed viral particles whose morphology resembled that of the polyoma subgroup of the *Papovaviridae*.

1.3.1 Pathology of BK polyomavirus

BKPyV has now emerged as the causative agent of late-onset haemorrhagic cystitis in hematopoietic stem cell transplantations [52], and nephropathies and urethral stenosis in renal transplant patients receiving immunosuppression therapy [25, 27, 53]. It is associated with BKPyV-associated nephropathy (PVAN) in up to 10% of renal transplantations, and 90% of cases lead to the development of acute renal rejection [54]. PVAN is characterised as an inflammatory interstitial nephropathy which usually manifests within the first year after transplantation [26, 55]. Less commonly, PVAN has been reported in native kidney of patients with AIDs [36], malignancies [56], and non-renal solid organ transplants [35, 57, 58]. All reported cases of PVAN, whether transplanted or native kidneys are involved, occur in immunocompromised patients with kidney traumas.

Several other clinical manifestations have also been reported in relation to BKPyV infection, these include; meningoencephalitis [59], bilateral atypical retinitis [60], and progressive multifocal leukoencephalopathy (PML) [61]. These unusual

pathologies were associated with long-term immunodeficiencies through either immunosuppression or HIV.

1.3.2 BK polyomavirus and Cancer

BKPyV has been observed to be oncogenic when intracerebrally or intravenously injected into newly born rodents, and has been reported to form ependymoma, neuroblastoma, pancreatic tumours, fibrosarcoma and osteosarcoma. Similar transformative properties have also been observed in cultured embryonic cells from rodents, however BKPyV is unable to effectively transform human embryonic kidney (HEK) cells in culture [62].

The involvement of BKPyV in human cancers has been studied over the last few decades, across a variety of cancer types. BKPyV DNA and LT antigen have been detected in brain [63, 64], bladder [65, 66], kidney, prostate [67], and cervical [68] tumours [44, 69]. Although the occurrence is considered rare, BKPyV genome has also been found integrated in cases of urothelial carcinoma [42, 43]. The integration of BKPyV always resulted in loss of active viral replication, and it has been suggested that the expression of LT and other viral proteins may contribute to the progression of tumorigenesis.

1.3.3 Treatment

Treatment options for PVAN are limited, with current guidelines recommending careful modulation of a patient's immunosuppressive therapies [70]. This allows a patient's own immune system to combat the infection, however, also runs the risk of causing acute rejection. Over the years, several broad-acting antimicrobial agents have been shown to target BKPyV in cell culture, but many of these antimicrobials fail to perform in the clinical setting.

Cidofovir; a nucleotide analogue used against cytomegalovirus and human simplex virus (HSV) infection, was shown to have a potent effect on BKPyV in cell culture. However, limited success has been observed in clinical cases, and

high nephrotoxicity has been reported [71]. Ciprofloxacin; a DNA gyrase and topoisomerase IV inhibitor [72, 73], and Leflunomide; a pyrimidine synthesis inhibitor [74], have also been shown to reduce virus load in renal transplant patients, though exact mechanism of how these inhibit polyomavirus replication is poorly understood and they have mixed results in the clinic.

Recently, a virus-like particle vaccine against BKPyV has entered commercial development, with the potential use in transplant patients for the purpose of preventing PVAN [75]. Though, it is strongly contested whether or not these vaccines will be sufficient enough to reduce the seroprevalence of persistent BKPyV. This is mainly due to the difficulties associated with administering a vaccine for an infectious agent which is observed to asymptotically infect a large proportion of the population from a very young age. Any vaccine developed would have to be given very early to children to be effective at reducing seroprevalence. Alternatively, if the vaccine was used as a therapeutic there is the problem with the large majority of patients being immunosuppressed, which would likely interfere with the effectiveness of the vaccine.

1.4 JC Polyomavirus (JCPyV)

Padgett et al. first isolated and cultivated JCPyV in 1971 from PML lesions. Electron microscopy of both brain sections and infected primary human foetal glial revealed virions with the characteristic polyoma-like structure [8].

1.4.1 Pathology of JC polyomavirus

PML was first coined in 1958 as a neuropathological complication in chronic lymphatic leukaemia and Hodgkin's lymphoma patients [76]. PML is characterised as progressive demyelination and inflammation at multiple sites within the white matter of the brain, resulting in deterioration of neurological function. In 1965, this neuropathology was linked to a viral infection [77], but it was not until 1971 that JCPyV was propagated from a PML lesion [8].

PML is now associated with solid organ transplants [78, 79], AIDS [80, 81], multiple sclerosis [37], and Hodgkin's lymphoma [76]. Epidemiology studies have shown that PML is most commonly associated with HIV with an incidence of 3-5% in HIV positive individuals [25]. PML is less common in solid organ transplants, multiple sclerosis, and Hodgkin's lymphoma; although, incidence in multiple sclerosis patients is dramatically increased with natalizumab therapy [37].

Recently, several cases of JCPyV reactivation have also been reported in renal transplant patients, resulting in PVAN [82-84]. Although, cases of JC-related PVAN are less frequent than BK-related PVAN, these studies have shown that JCPyV is also capable of initiating nephropathologies similar to BKPyV.

1.4.2 JC Polyomavirus and Cancer

The occurrence of brain tumours and PML have been reported in multiple cases, before even the connection was made between JCPyV and PML. The first case indicating JCPyV involvement in the formation of human brain tumours was reported in 1990s [85], in an immunodeficient individual. Since then, the presences of JCPyV has also been reported in a variety of human brain tumours [62]. JCPyV genome and viral proteins have also been detected in colon cancers, with the suggestion that JCPyV LT antigen leads to enhanced transcription at the c-myc promoter [86]. However, limited evidence exists to support the oncogenic nature of JCPyV LT antigen in humans, and integration of JCPyV into a human genome is yet to be reported.

1.4.3 Treatment

Treatment options for PML are very limited and results are inconsistent. Current guidelines recommend attempting to restore a patient's immune system. This may involve removal of any immunosuppressants or starting HIV positive individuals on HAART in attempt to slow disease progression. AIDs patients have been reported to have an improved prognosis if HAART is administered [87].

Other therapeutic approaches have been used, such as: cidofovir [88, 89], cytarabine [90]; a chemotherapy drug, mefloquine [91]; an anti-malarial drug, interleukin-2 [92], and mirtazapine [93]; an antidepressant. These drugs have been shown as successful therapies against PML, however, there is limited clinical data and many of them have to be considered on a case-by-case basis. Similarly to BKPyV, a virus-like particle vaccine against JCPyV has entered commercial development [94].

1.5 Molecular Virology of Human Polyomaviruses

1.5.1 Genome Organisation

Polyomaviruses have circular dsDNA genomes (figure 1.3) of approximately 5000 base pairs, which are packaged around ~25 host-derived histones. The nucleosomal structures in the virions do not include linker histone (H1), though this is acquired from host cells during infection [95, 96]. Polyomavirus genomes are functionally divided into three regions: a non-coding-control region (NCCR), early region, and late region.

The NCCR contains many elements that are important for replication and viral protein expression; these elements include the viral origin of replication and multiple binding sites for host transcription factors. This region contains the highest variability between viral strains, and recombination within the NCCR is thought to play a role in the reactivation of latent virus [25].

The early region encodes the regulatory proteins; large tumour antigen (LT), alternatively-spliced LT, and small tumour antigen (sT), which are named as such because of the oncogenic roles they have in animal polyomaviruses [97, 98] and multiple miRNAs which regulate early gene expression and play roles in immune evasion [99, 100].

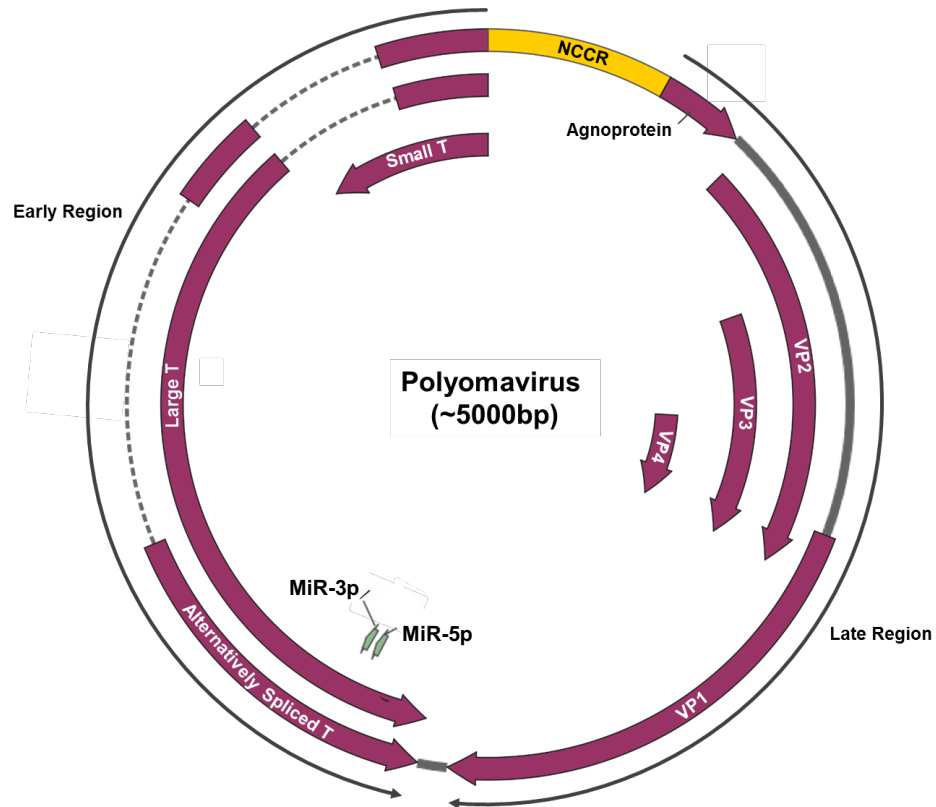


Figure 1.3: Generalised schematic of polyomavirus genome.

The Polyomavirus genome is divided into three regions; non-coding control region (NCCR), early region, and late region. The NCCR encodes a bi-directional promoter which drives expression of the OFR in a temporal manner, dependant on the concentration of large tumour antigen. The early region encodes for the small, large and alternative spliced tumour antigen. The late region encodes for agnoprotein, VP1, VP2, VP3, VP4, and contains ORF for VP5 and 6 (truncations of VP4; not shown above) though expression products of these have yet to be identified. Furthermore, the late region transcription extends into the early region to express MiR-3p and MiR-5p which act as negative feedback regulation of LT.

The late region encodes for the three structural proteins: VP1, VP2, and VP3; the non-structural protein VP4; open reading frames (ORF) for putative VP5 and VP6 proteins [101]; and a small accessory protein, coined the agnoprotein [102, 103].

1.5.1.1 Reverse Genetics of the Polyomavirus Genome

Reverse genetics of polyomavirus genomes has been somewhat unsuccessful in the past, with the integration of any proteins tags within the genome resulting in the loss of genome packaging and mature capsid assembly. This is most likely because polyomaviruses are highly evolved to utilise such a small compact genome for their replication. Loss of function studies have been performing by incorporation of stop codons in place of ORF start codons. These studies have enabled the determination of VP2/3 and agnoprotein function. It may be possible in the future to perform further reverse genetics, but a greater understanding of polyomavirus genomes is required.

1.6 Non-coding Control Region (NCCR)

NCCRs are highly variable segment of the polyomavirus genome, that functionally act as a bi-directional promoter and origin of replication during the viral lifecycle [104]. The bi-directional promoter function of the NCCR drives and regulates expression for the early and later regions of the genome. Upon infection expression of the early open reading frames (OFR) is initiated until levels of large tumour antigen (LT) reach a negative feedback threshold. LT is then recruited to the NCCR to initiate switching to the expression of late OFR and replication.

Significant recombination of this region has been observed between archetypal and disease-associated stains of human polyomaviruses. Archetypal virus strains contain a NCCR specifically arranged to dampen down viral gene expression through reduced promoter activity and increase miRNA expression [105, 106]. Recombination events, in disease-associated stains [107-109], are thought to reactivate the viral genome and lead to uncontrolled replication in the immunosuppressed. It is unclear exactly when, where, and how these

recombination events occur as disease-associated recombination are also found in healthy individuals [110]. Archetypal strains are typically thought to be the transmissible form of the virus, though they replicate very poorly in cell culture compared to rearranged stains. It is thought that low level of LT expression is the limiting factor in these cases [51, 52]. Recombination seems to be required for reactivation of viral replication and disease progression.

Multiple recombination models have been proposed for the conversion between archetypal and disease-associated NCCRs. The first of these suggests the involvement of V(D)J recombination machinery, as it has been noted that JCPyV can infect B cells. However, this model seems unlikely as no V(D)J-like recombination signal sequences have been reported within the NCCR sequences of polyomaviruses [25]. Other studies have suggested that recombination could take place between JCPyV and Epstein Barr Virus (EBV) in B cells, as there are regions of homology between the JCPyV NCCR and the EBV genome [111]. Though whether this is relevant in terms of a PML pathogenesis it remains unclear but could highlight a mechanism for recombination of persistent DNA viruses within humans.

A different model that has been suggested from work on SV40's and JCPyV's NCCR identifies palindromic sequences within the NCCR which are capable of forming hairpin structures during replication. The formation of these hairpin structures in SV40's replication was thought to lead to the stalling replication and could possibly lead to the collapse of the active replication fork. This event leads to increase risk of double strand breaks, which could initiate a recombination event [112]. This model remains unvalidated though, as the existence of palindromic sequences do not directly correlate with replication stall sites. Further investigation is required to fully understand the mechanism by which polyomavirus NCCR recombine, but it is evident that NCCR recombination is essential for reactivation of transcription and replication. Establishment of a cell culture model which allows persistent infection of archetypal stains is required to

perform investigations into what factors lead to the NCCR recombination and whether this recombination leads to reactivation of viral replication.

1.7 Early Non-Structural Proteins

1.7.1 Large Tumour Antigen (LT)

LT is expressed early in the polyomavirus life cycle and contributes many functions that are essential for infection. LT drives changes to the host cell through interactions with multiple host factors. During early infection, LT is required to drive the cell cycle into S phase and initiate a DNA damage response. These changes in cell metabolism are essential for an environment that provides all the host machinery and substrates; such as nucleotides, required for viral replication [98]. Similarly, LT is also responsible for preventing cell cycle arrest and apoptosis through binding p53 and inhibition of the expression of p53-dependant genes. This function is the proposed oncogenic function [113, 114], although in human cells LT antigens have never been shown to have transformative properties. The exception to this is a truncated variant which occurs during integration of MCPyV genome. This truncated LT antigen has been shown to play an active role in MCPyV oncogenesis [114].

Additionally, LT functions later in the polyomavirus lifecycle as a replicative DNA helicase and recruiter of host replication machinery to the viral origin of replication (ori) [98]. It is also responsible in the later lifecycle events for the LT-mediated transactivation of the late promoter, which controls the expression of the late viral proteins [115]. Without this transactivation viral replication is severely affected, and it is the levels of LT antigen that determine how efficiently a polyomavirus will replicate in cell culture [116, 117].

1.7.2 Small Tumour Antigen (sT)

sT is involved in promoting an accelerated G1 and S phase through inhibition of protein phosphatases, which leads to a transactivation of promoters that drive the

expression of cyclin A and cyclin D1 [118, 119]. Interactions between MCPyV sT and host phosphatases has been shown to also lead to modulation of the NF- κ B pathway and subversion of the host innate immunity response, allowing a persistent infection to be established [120]. Additionally, sT also upregulates early transcript levels and facilitates LT-mediate activation of the late viral promoter [97].

1.7.3 Alternative-Spliced LT

The polyomavirus genome also encodes alternatively spliced forms of LT. All of these proteins contribute to the modulation of the cellular environment and have been linked to transformation. Murine polyomavirus encodes a middle T antigen (mT) and a tiny T antigen (tT). mT is a membrane-associated protein which promotes proliferation through interactions with PP2A and dysregulation of signalling cascades such as MEK/ERK/MNK1 [30, 113], whilst tT increases the ATPase activity of heat shock protein 70 [121]. Simian vacuolating virus-40 (SV40), JCPyV and BKPyV also encode spliced variations of the LT and these proteins have all been linked to transformation in cell culture [122-124].

1.8 Late Structural Proteins

1.8.1 VP1 and VP2/3

VP1 is the major capsid protein in polyomavirus particles. Polyomavirus capsids are made from 72 VP1 pentamers arranged in a T=7d icosahedral lattice. Published EM structures of BKPyV's capsid [125] (figure 1.4C) showed that within the capsid there are 6 distinct conformations of VP1, which each share a common β -sandwich, "jelly roll" fold. The VP1 pentamers are held together through interactions between a C-terminal arm and neighbouring pentamer (figure 1.4A). Minor rearrangements were noted in 3 of the C-terminal arms in the BKPyV EM structures compared to the SV40 crystal structure (figure 1.4B). These rearrangements allow for potentially 10 additional hydrogen bonding events. Differences in arrangement of BKPyV and SV40 were also seen on the

icosahedral 2-fold axes, where conformational difference may allow for interactions between Arg²¹⁴ and Asn³¹⁰ in BKPyV's capsid. Although these rearrangements may be an artefact of experimental procedure, the BKPyV EM structure gives the most physiologically relevant insight and is potentially shedding light on regions in the polyomavirus capsid that supply stability to the virion.

Other than these minor rearrangements, the gross-fold of VP1 pentamers in SV40 and BKPyV are very similar. Crystallographic studies have produced multiple structures of isolated VP1 pentamers from many different polyomaviruses in complex with their receptor (JCPyV, SV40, mPyV). Each VP1 pentamer contains 5 receptor binding sites, which are created by the surface exposed loops and bind cellular oligosaccharides.

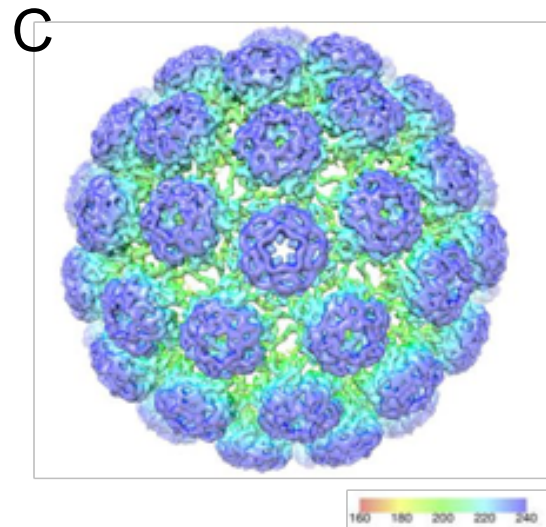
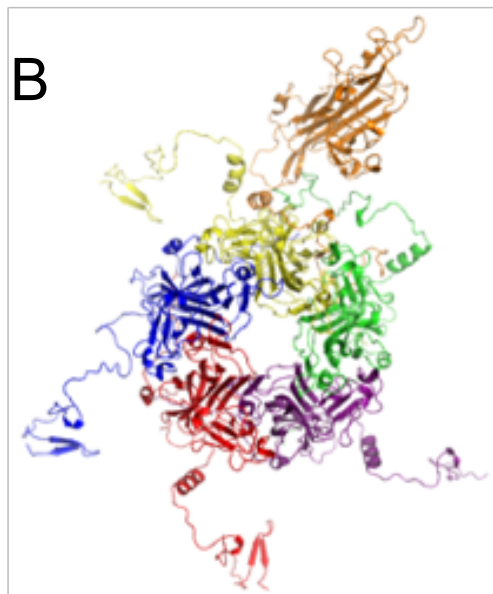
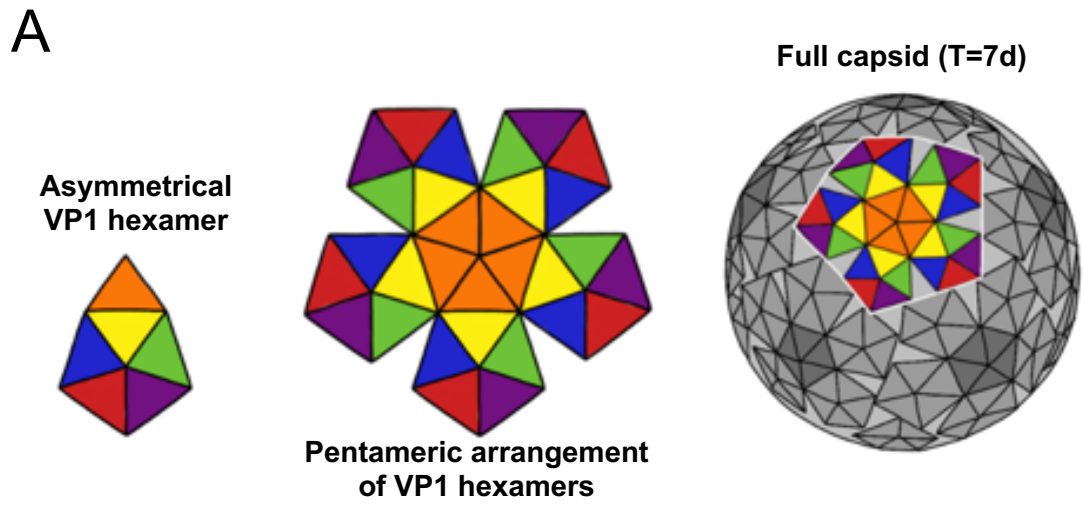


Figure 1.4: Polyomavirus VP1 Arrangement

(A) Schematic of T=7d virus capsid assembly. (B) 3.1 Å crystallographic model of SV40 VP1 pentamer [127]. (C) 7.6 Å electron microscopy structure of BK polyomavirus capsid [125].

Most recently the full BKPyV capsid has been resolved by cryo-EM in complex with GT1b ganglioside [126], giving the first visualisation of the multivalent nature of receptor binding by polyomaviruses. This recent 3.4Å EM structure of BKPyV also gave us the first evidence of the location of VP2/3 within the BKPyV capsid. The capsid structure was resolved enough to identify residues 288–301 of VP2 and showed density for a small hydrophobic helix at the base of the VP1 pentamers. Unfortunately, due to symmetrical averaging in the BKPyV EM structure, no data concerning the stoichiometry of the minor capsid proteins within the capsid could be obtained. To date it is thought that VP2/3 are distributed in a 1:1 ratio with each VP1 pentamers, but the ratio between the two minor proteins is unknown.

VP2/3 have been suggested to play important roles associated with entry and capsid disassembly. Studies have suggested that VP2/3 are involved with virions exiting the ER [128, 129], and are thought to contain nuclear localisation signals responsible for delivering the viral genome to the nucleus [130, 131]. Although these mechanisms are unclear, it has been observed in SV40 that the absence of the minor capsid proteins prevents successful viral entry [128]. VP2/3 also appear to have a function during the later stages of the viral life cycle. Loss of VP2/3 from JCPyV has been shown to result in a packaging defect [132], and VP2/3 of mPyV has been shown to cause apoptosis of the host cell [133].

1.8.2 VP4, VP5, VP6

The structural protein; VP4, was first discovered to be expressed in SV40 [134], where a downstream methionine in VP2/3 transcripts was found to be a translational initiation site. Initially, SV40 VP4 was suggested to have viroporin function and have essential roles in viral release, although, later studies have shown that VP4 is not required for SV40 release [101]. VP4 has now also been reported to be expressed by BKPyV and JCPyV, though VP4 is not incorporated into these viral capsids. Furthermore, ORFs have been reported for putative VP5 and VP6 proteins in the BKPyV genome.

1.9 Late Non-Structural Protein

1.9.1 Agnoprotein

Agnoproteins are not expressed by all members of the *Polyomaviridae*, although, the sequences of agnoproteins are highly conserved. This conservation brings into question the function of the agnoprotein and why only some members of the family require it [135, 136].

The gene sequence, which encodes agnoprotein, was first discovered in SV40 [102], located in the late region of the genome. It was predicted that this sequence contained an open reading frame, which encoded a 62 amino acid protein, however evidence showing the expression of this gene, dubbed the agnogene, was not detected until the 1980s by Jay et al. Similar open reading frames for the agnogene were also found in the genome sequences of JCPyV [137] and BKPyV [103] polyomaviruses, and shown to express the agnoprotein in both cases.

Agnoprotein is small highly basic protein that is abundantly expressed during the late stages of polyomavirus infection [138]. It is thought to play multiple roles during infection and interact with a growing number of host proteins, though so far very little detail is known about its exact function.

1.9.1.1 Function of Agnoprotein

The function of the agnoprotein within the polyomavirus life cycle is not at all clear, but many studies suggest that it corresponds to release and egress of the virus. Knockout viruses have shown that the absence of the agnoprotein results in phenotypes with: impaired viral release and reduced viral titres in BKPyV [22] and JCPyV [139]; and additional packaging defects in SV40 [140]. This suggests that agnoprotein by an unknown mechanism catalyses the trafficking of progeny virus out of infected cells, and for SV40 plays roles in viral assembly. Studies investigating the role of agnoprotein in the lifecycle of BKPyV, showed that infectious progeny of an agnoprotein-deficient virus (Δ agno) become trapped in the nucleus of infected cells [22]. This suggested that the role of agnoproteins is

essential for viral egress and is involved in active release from the nucleus/retrograde trafficking through the cytoplasm to the plasma membrane.

A small number of host binding partners of the BKPyV agnoprotein have been reported, however, there is little information as to their contribution to agnoprotein function. In contrast, more is known of the function of agnoprotein encoded for by JCPyV. A greater range of host binding partners have been suggested for JCPyV agnoprotein (table 1.2), and a putative viroporin activity is strongly supported by evidence in the literature [141, 142]. The agnoprotein of JCPyV is reported to increase permeability of the plasma membrane to hygromycin in an agnoprotein-inducible SVG-A cell line, and it is suggested that this viroporin activity, at least in JCPyV, is regulated by interactions with the adaptor protein complex 3 [141, 142].

PyV	Interaction partner	Functional implication	Interacting domain partner	Interacting domain agnoprotein	Ref.
BKPyV	α -SNAP	Interference secretion	Not determined	N-terminus	[22, 143]
	PCNA	Inhibition DNA synthesis			[144]
	p50	Unknown	Unknown	Unknown	[103]
	p75	Unknown	Unknown	Unknown	[49]
	p100	Unknown	Unknown	Unknown	[49]
JCPyV	FEZ1	Facilitates viral release	Coiled-coil domain	Not determined	[145]
	HP1 α	Nuclear egress virions	Not determined	N-terminus	[146]
	Ku70	Aberrant DNA repair	Not determined	N-terminus	[147]
	p53	Dysregulation cell cycle	Not determined	N-terminus (aa 1-36)	[148]
	p52	Unknown	Unknown	Unknown	[149]
	p103	Unknown	Unknown	Unknown	[149]
	p112	Unknown	Unknown	Unknown	[149]

p158	Unknown	Unknown	Unknown	[149]
HIV-1 Tat	Inhibition HIV-1 gene expression	Residues 1-50	Residues 18-54	[150]
Tubulin	Unknown	Unknown	Unknown	[149]
YB-1	Altered gene expression	C-terminal half	Residues 18-36	[151]
LT-ag	Repression viral transcription and DNA replication	Central domain	N-terminus	[152]
st-ag	Disrupt PP2A:st-ag interaction?	C-terminus	N-terminus	[153]
PP2A	Dephosphorylation of agnoprotein	Not determined	Residues 18-36	[153]

Table 1.2: A summary of identified interaction partners for the agnoproteins of JCPyV and BKPyV

1.9.1.2 Subcellular Localisation of Agnoprotein

The agnoprotein has been observed in the ER, cytoplasm and nucleus of infected cells [103, 135, 142, 154]. The distribution between these two compartments varies slightly from virus to virus, with JCPyV having a greater accumulation of agnoprotein in the nucleus [154]. Nuclear localisation of the agnoprotein is consistent with the existence of a weak bipartite nuclear localisation signal, which is predicted to be located within the N-terminal region [135]. It is also evident that localisation varies from virus to virus in studies which suggest that JCPyV agnoprotein localises to the plasma membrane, and it is here that JCPyV agnoprotein functions as a viroporin [141, 142]: and there is evidence that BKPyV agnoprotein has a propensity for co-localising with lipid droplets in infected cells [155, 156]. The variation in localisation sites may highlight the multifunctional nature of the agnoprotein or be a consequence of its role in polyomavirus lifecycle.

1.9.1.3 Structure of Agnoprotein

Solving the structure of any agnoprotein has proven difficult due to their ability to transiently oligomerise, which is inhibiting the obtainment of ordered crystals for x-ray crystallography studies. The agnoprotein has been observed to exist in transient dimeric and oligomeric forms during infection, and although transient it has been shown that these oligomeric forms are SDS resistant [157, 158]. Electron microscopy approaches are also unsuitable due to the small size of agnoproteins. Recently, an NMR approach has been successful in solving the monomeric structure of JCPyV agnoprotein [157, 159]. The structure has confirmed the existence of an amphipathic helix encompassing residues R24 to F39. Mutagenesis studies have shown there is a Leu/Ile/Phe-rich domain within this helix which is critical for oligomerisation [157, 158], and hydrophobicity plots show a region of high hydrophobicity correlating to this helix which suggests that it is a putative transmembrane domain. The published NMR structure does not, however, give any information about the oligomeric or membrane associated forms of the agnoprotein; and because of the difficulties associated with maintaining the protein as a monomer the conditions of the NMR experiment are far from physiological.

1.10 Human Polyomavirus Lifecycle

The life cycle of polyomaviruses lacks many details, concerning mechanisms and pathways that are utilised to facilitate polyomavirus replication. The current dogma of polyomavirus infection (figure 1.5) states that;

- Polyomaviruses can enter cells through a variety of pathways, seemingly dependent on cell type [160, 161].
- Virions are trafficked through endosomes to unidentified acidic compartments, and on to pH neutral caveosomes [162].
- Virions then pass through the ER where disassembly is initiated, are released into the cytoplasm, and enter the nucleus [163-165].

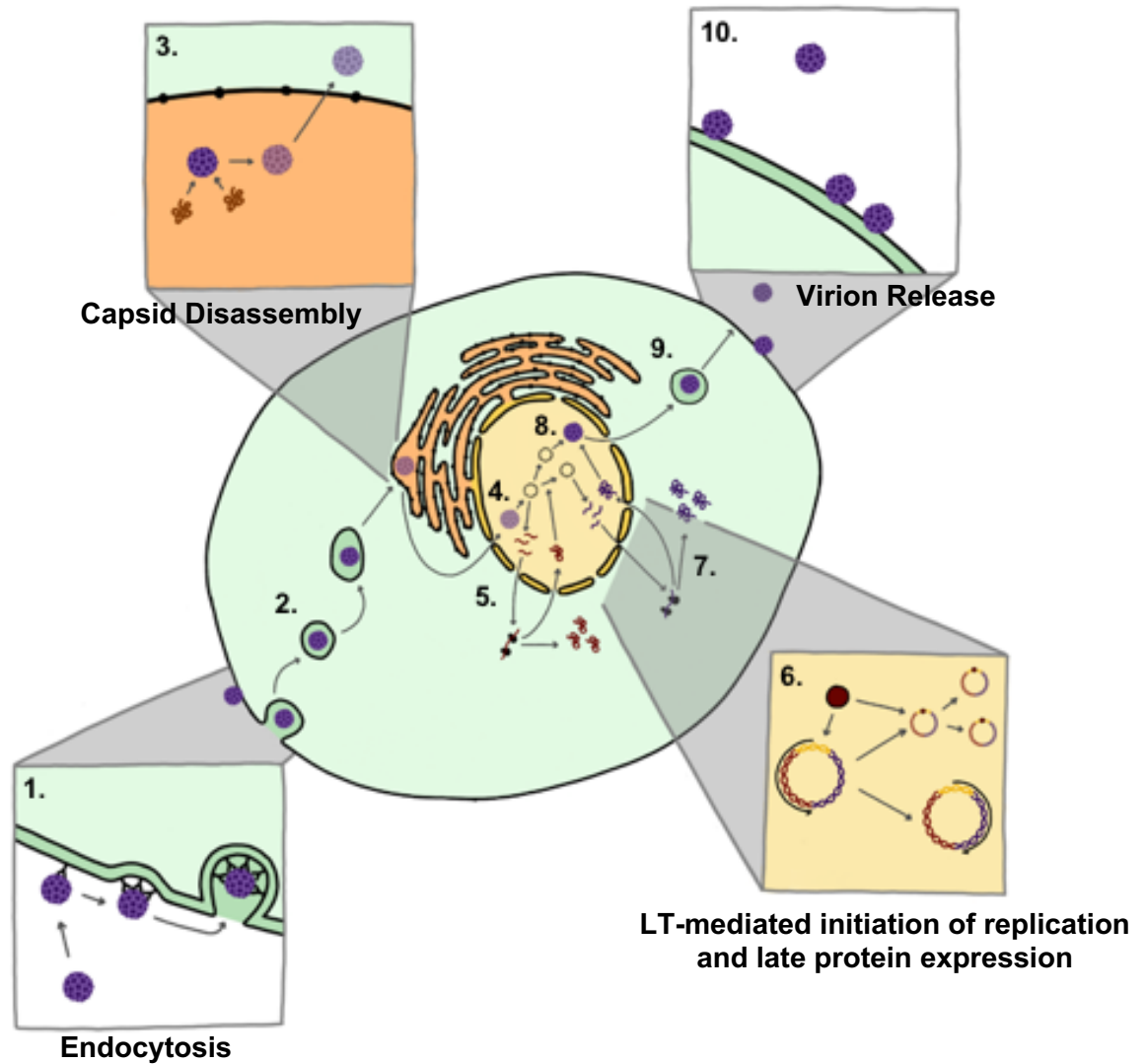


Figure 1.5: Schematic of polyomavirus life cycle

(1) Receptor mediated endocytosis via ganglioside receptors. (2) Endocytic trafficking through acidified compartment. (3) Initiation of capsid disassembly in endoplasmic reticulum via host protein folding machinery and protein disulphide isomerase. (4) Release of viral genome into nucleus. (5) Early gene expression. (6) Large tumour antigen (LT)-mediated initiation of replication and switch to late promoter. (7) Late gene expression. (8) Viral replication and virion assembly. (9) Viral egress. (10) Virion release.

- Translation of early viral proteins occurs to manipulate the cellular environment for viral replication and production. The accumulation of LT results in a LT-mediated initiation of replication and switch to late promoter [115].
- Replication of late genes and replication of the genome leads to assembly of viral particles and viral egress [166].
- Progeny virions release from the plasma membrane, with a large proportion remaining membrane associated [167].

1.10.1 Virus Entry and Uncoating

1.10.1.1 Receptor and Cellular Tropisms

All viruses have natural tropisms for specific host cells, often defined by the receptors displayed on the surface of plasma membrane. Viruses, in general, rely on a vast range of receptors and co-receptors to enable their attachment and subsequent entry into host cells. Most viral receptors are proteinaceous in nature but binding to viral capsids is often through interactions with oligosaccharide post-modification displayed on these proteins.

Most polyomavirus capsids have an affinity for gangliosides, through interactions with sialic acid motifs (figure 1.6) and the binding-pocket formed by VP1 [126, 168]. Gangliosides contribute considerably towards the complex profile of glycans within cells and are ubiquitously found across many cell/tissue types. Notably for polyomavirus infections, gangliosides are found in neuronal, bone marrow derived, intestinal, and renal tissues [169, 170]. In general, VP1 has a mM binding affinity for gangliosides, which in itself seems unsuitable to facilitate binding of virions to a plasma membrane. In context of a polyomavirus capsid, however, there are 360 VP1 monomers providing an equal number of binding sites (figure 1.7). This reduces the binding affinity from mM to nM for the binding of an intact capsid.

Research in the past has determined that there is a difference, between polyomaviruses, in specificity for particular gangliosides (figure 1.6) and co-receptors. BKPyV utilises GD1b and GT1b to infect renal proximal tubular

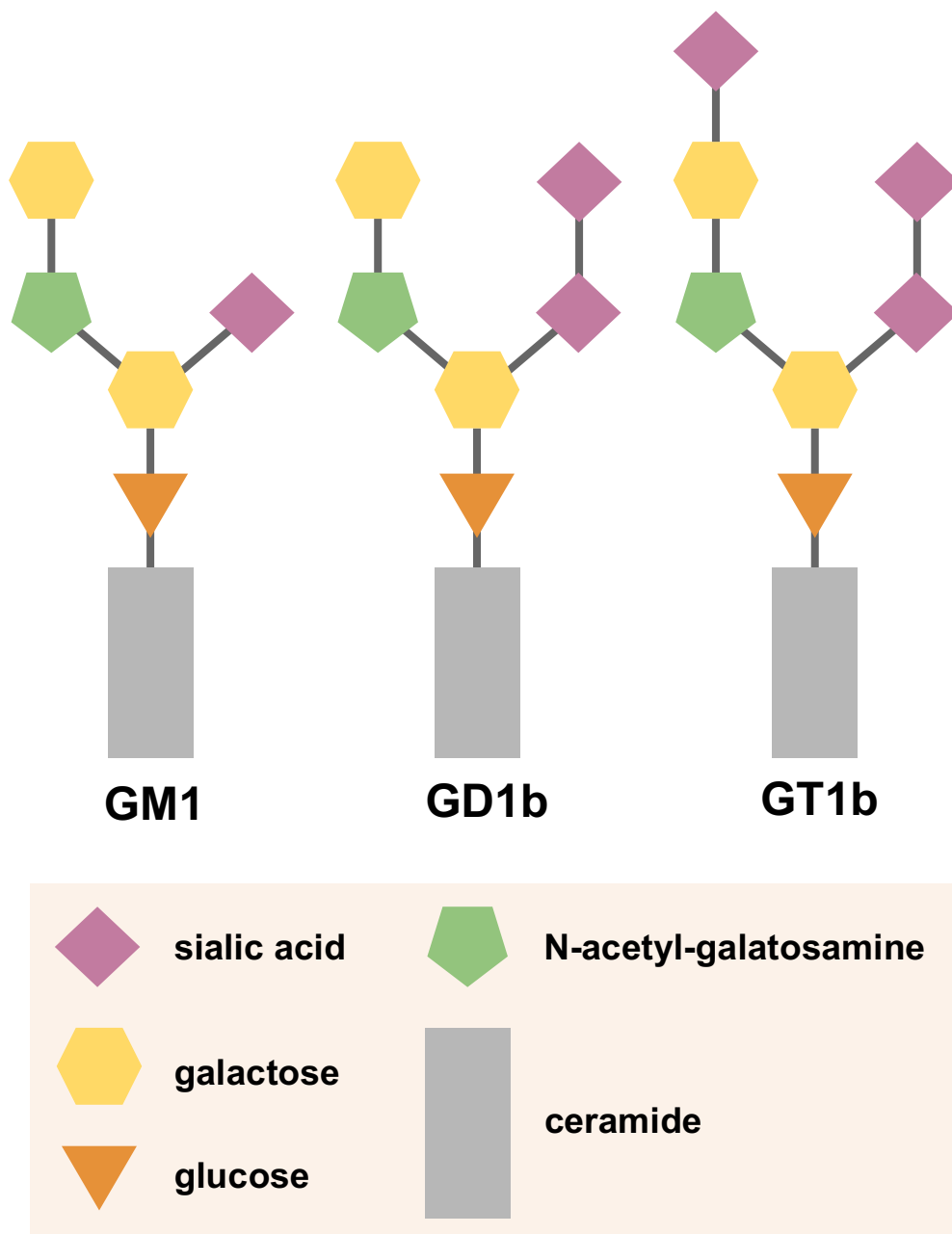


Figure 1.6: Schematic of Sialic Acid Receptors

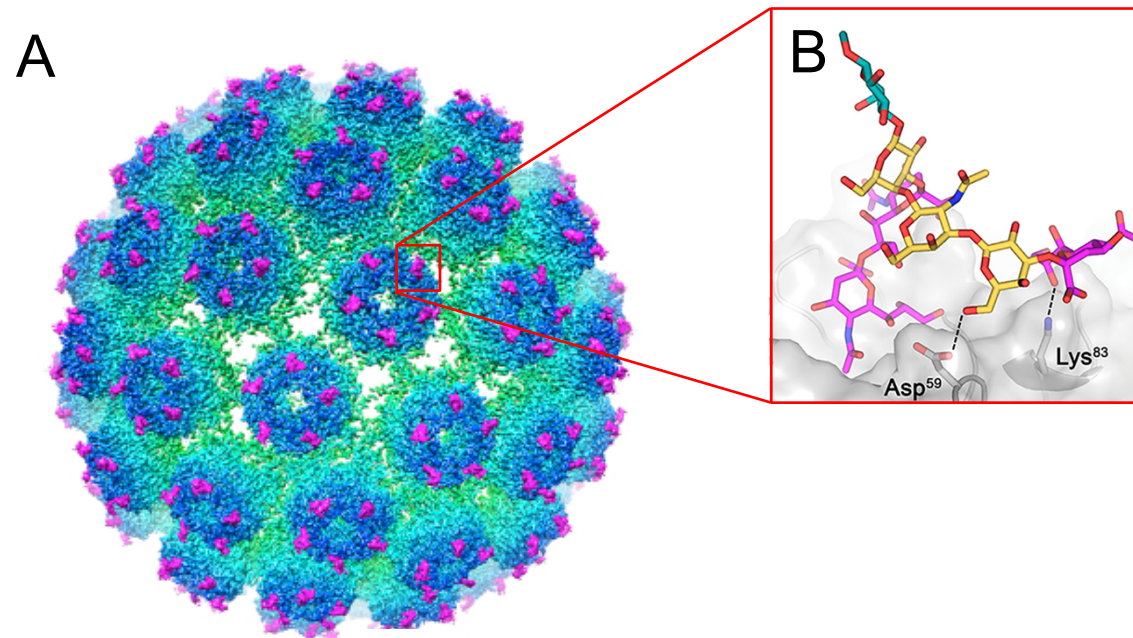


Figure 1.7: EM structure of BKPyV in complex with GT1b

(A) 3.4Å structure of native BKPyV in complex with its host cellular receptor GT1b. (B) A close up snapshot of the interaction between GT1b and the capsid surface. Molecular dynamic (MD) simulated to show the possible position of the left arm interacting with Asp59 and Lys83. Adapted from Hurdiss et al. 2018 [126].

epithelia (RPTE) cells, with the presence of GD2 and GD3 increasing the efficiency of entry [161, 171]. JCPyV can utilise GT1b and GD1b as well, but the role of this interaction during infection remains unclear. JCPyV possesses a higher affinity for pentasaccharide lactoseries tetrasaccharide c (LSTc), and serotonin receptor 5HT2A as a co-receptor, during infection of central nervous system (CNS) derived cells [172]. mPyV binds GT1b as well and has been suggested to use integrin $\beta 5$ as possible co-receptors [173, 174]. SV40 binds GM1, and MHC class I as a possible co-receptor [175]. In contrast, HPyV -6 and -7 are thought to utilise non-ganglioside receptors [176], indicated by their VP1 structure and lack of interaction found between their VP1 and sialated glycans. The differences in receptors is reflected in the binding pockets formed by VP1, where there is variation between polyomaviruses. Previously, it was shown to be possible to engineer the binding-pocket of VP1 from BKPyV to switch its receptor specificity from GD3 to GM1 [177].

1.10.1.2 Internalisation and Trafficking

Polyomaviruses has been shown to internalise into host cells through multiple endocytic pathways. The entry mechanism of HPyV remains controversial, and it is possible that these viruses have multiple mechanisms for internalisation dependent on the viral genotype [178] or cell type [163]. BKPyV has been observed to internalise independent of clathrin-coated-pit assembly, but by using caveolae-mediated endocytosis in Vero cells [179]. A dominant-negative cell line approach was used to differentiate between caveolin and clathrin-dependent endocytosis, and further experiments confirmed the colocalization of infectious virions and caveolin 1.

Similar findings were also observed in RPTE cells, suggesting that BKPyV also utilises caveolae-mediated endocytosis to enter a more physiologically relevant cell line [180, 181]. All other HPyV, except JCPyV which is internalised via clathrin-dependant endocytosis, are suggested to have similar entry mechanisms which are dependent on caveolin. However, studies that revisited BKPyV entry into RPTE cells, showed that viral entry requires gangliosides, but can occur

through a caveolin- and clathrin- independent mechanism [182]. Further studies have shown that BKPyV entry is actin-independent, and several endocytic pathways have been identified that could be utilised by polyomaviruses. These pathways implicate RhoA GTPases [183], a Cdc42-based actin machinery [184], ADP-ribosylation factor (ARF) 6 [185], and flotillin [186].

Proceeding internalisation polyomavirus containing vesicles pinch off into the cytoplasm. It has been identified in BKPyV that the trafficking of polyomavirus-containing vesicles is reliant on an intact microtubular network, but not the actin cytoskeleton [162, 181, 187]. It was observed that BKPyV could migrate along microtubules, and treatment with microtubule disrupting agents saw a reduction in levels of BKPyV infection. These studies also showed that infection levels were not inhibited by treatment with compounds which inhibited the dynamics and assembly of microtubules. Further, investigation also identified that this trafficking is dynein-independent in BKPyV, JCPyV and SV40.

Additionally, during endocytosis the pH of the polyomavirus containing vesicle drops. This acidification step is essential for a productive BKPyV infections and happens early during the viral lifecycle (2 hr post-infection). Studies that have disrupted this acidification have shown reduction in successful infections [162, 179], and subsequently BKPyV was observed to colocalise with caveolin 1, suggesting that it enters caveosomes (4 hr post-infection). Similar observations have been made for SV40 and mPyV, which both seem to traffic through endosomes to a caveosomal compartment. JCPyV, on the other hand, appears to migrate to early endosomes before arriving in a caveosome. From the caveosome, polyomaviruses migrate to the ER where capsid disassembly is initiated.

1.10.1.3 Uncoating

Capsid disassembly seems to rely on protein disulphide isomerases (PDI). PDI family members are oxidoreductases, which reduce and oxidise sulphide bonds

in newly synthesised proteins. mPyV was found to utilise the PDI family member, ERp29. ERp29 induces changes in the capsid of mPyV which exposes trypsin cleavage sites in VP1 [188, 189]. The conformational change is thought to lead to the cleavage of the C-terminal arm of VP1, which has been shown to link pentamers to adjacent pentamers. Cleavage at this site is also thought to destabilise the capsid in such that VP2/3 are exposed, facilitating their function in ER escape. Inhibition of ERp29 has been shown to reduce infection levels of SV40, BKPyV, and JCPyV, suggesting that initiation of disassembly of polyomavirus occurs through modification via ERp29 [190]. It has also been suggested, for SV40, that the viral capsid is further destabilised by treatment with EGTA. EGTA is thought to remove the calcium ions that help anchor the C-terminal arm. This is most likely occurring in a host cell by the changes in Ca^{2+} , which fall from mM outside the cell to nM in the cytosol.

It remains unclear how the viral genome is released into the nucleus, but it is thought that polyomaviruses leave the ER after initial destabilisation. It has been shown that Derlin 1 and 2 are required for mPyV's and SV40's ER escape, respectively. Derlin 1 and 2 are involved in the ERAD retrotranslocation pathway, and it is thought that the destabilisation of polyomavirus capsids results in the host cell recognising them as misfolded proteins [162]. Once recognised by the ERAD machinery the virions are thought to be transported to the cytosol, where the minor capsid nuclear localisation signals are recognised. It is not clear how polyomaviruses are trafficked through the cytosol, but it is thought that they enter the nucleus through the nuclear pore and once in the nucleus the capsid finally releases the genome [129, 165, 191]

1.10.2 Persistence

Polyomaviruses are able to chronically persist for the duration of the host's lifespan. Very little is known about how polyomaviruses establish persistence in their host, but notably these viruses are somehow capable of avoiding the host immune response to prevent clearance of their genomes. Polyomaviruses are very efficient at evading the immune system to establish lifelong persistence

infection of their host, however, HPyV replication is effectively controlled by a healthy immune system. It is evident from the pathology of PVAN and PML which results in inflammatory [26] and CD8⁺ T cell infiltration [192, 193], respectively; and existence of an antibody response in individuals who are persistently infected [194-196].

BKPyV and JCPyV DNA can be detected in the urinary and genital tracts (kidney [197], ureter, bladder [198], prostate [50], cervix [68], and sperm [198]), the central nervous system (brain tissue) [199], and the hematopoietic system (peripheral blood cells [200] and lymphoid organs). Additionally, JCPyV DNA has been found in epithelial cells of the gastrointestinal tract, whilst MCPyV, TSPyV, HPyV6, and HPyV7 were all detected in skin [19, 201]; and WUPyV and KIPyV were detected in lymphoid organs (tonsillar and adenoid tissues) [202].

It has been shown in mPyV that the viral DNA is maintained episomally, and that levels of viral promoter activity have prominent effects on persistence. The addition of enhancers to the NCCR of mPyV resulted in the loss of persistence [203]. Changes in NCCRs are also reported to affect the replicative ability of JCPyV and BKPyV, though studying these changes has proven difficult without a physiologically relevant cell model. Recently, advances have been made to develop cell culture models in physiologically relevant cell types [204], which could be used to look at the nature of episomal polyomavirus genomes.

1.10.3 Viral Replication and Transcription

Polyomaviruses use host machinery to carry out their transcription and genome replication, and therefore must replicate in dividing cells. After the viral genome is delivered to the host nucleus, the early promoter initiates expression of LT, sT, and alternative-spliced LT. The tumour antigens share an open reading frame (ORF), which is alternatively spliced to remove introns to produce transcripts for LT, sT, and alternative-spliced LT. Expression of the tumour antigens leads to the accumulation of LT and a negative feedback loop, which initiates the late promoter and viral genome replication [115]. The late genes are transcribed as a

single pre-RNA that becomes spliced into two mature RNAs, referred to as 16S and 19S. 16S encodes for VP1 and agnoprotein, whilst 19S encodes for VP2/3 [203].

Genome replication occurs during S phase. Polyomaviruses promote S phase through activation of ERK1/2 signalling pathway, leading to pRb phosphorylation which in turns initiates the G1/S phase transition [205, 206]. Polyomaviruses also cause G2/M arrest through inducing the DNA damage response [207], and this is thought to maintain a pseudo-S phase state allowing further viral replication. This is a common approach for multiple viruses which require S phase for their genome replication. There are multiple mechanisms which viruses exploit to achieve G2/M arrest. Studies have shown that the agnoprotein of JCPyV binds pRb and stimulates expression of the p21 promotor. This leads to increased levels of p21, resulting in a G2/M arrest [148].

1.10.3.1 miRNA

Polyomaviruses encode for miRNAs that are required for the regulation of early gene expression and immune evasion. BKPyV and JCPyV encodes for 2 miRNAs (miR-5P and miR-3P), which regulate viral replication through silencing LT transcripts. Studies have also shown that miR-3P is involved in the downregulation of the stress induced ligand ULBP3, making infected cells less susceptible to NK cell killing [100]. SV40 also encodes miRNAs, which are involved in the silencing of LT transcripts. However, it is believed that these miRNAs are not essential for early gene transcription, and instead required to reduce the susceptibility of infected cells to T-cell killing [208].

1.10.4 Viral Assembly

Assembly of polyomaviruses takes place in the nucleus. It has been shown for JCPyV that promyelocytic leukaemia nuclear bodies (PML-NBs) are the site of polyomavirus viral assembly [166]. However, it remains unclear how the structural proteins recognise and form capsids around the viral genomes. VP1

contains a DNA binding domain in its N-terminus, which is thought to function during viral packaging, though the interaction is not sequence specific [209]. *In vitro* studies with recombinant VP1 from mPyV, JCPyV, and BKPyV showed that VP1 has the ability to self-assemble into virus-like particles (VLP) [75, 94, 210]. Pseudo virus systems, which have been established with VLP, have shown that polyomavirus capsids are capable of packaging reporter plasmids. It is thought that interactions between VP1 and Hsp70 prevent premature capsid formation *in vivo*, by inhibiting calcium-mediated assembly [211].

1.10.5 Viral Egress and Release

Non-enveloped viruses are usually released from cells via cell lysis, however in some cases they escape through manipulating host secretory pathways. It was first observed for SV40 that polyomaviruses appear to release from host cells through the apical surface without cell lysis [212]. A similar release phenotype has also been noted for BKPyV, though the pathology of BKPyV also indicates there might be also be lytic release under certain circumstances. It has been demonstrated for BKPyV that viral egress can be aberrated by treatment with anion channel inhibitor (DIDs) [167] or by deletion of the agnogene [22]. In these circumstances, progeny virions accumulate in the nucleus, and it remains unclear how these factors are involved in viral egress. It has been suggested for JCPyV that the viroporin activity of the agnoprotein plays an important role in viral egress [141, 142], though exactly how remains unclear.

Progeny virions emerge at the plasma membrane from vesicle structures, and large proportions of the virions remain associated with the cell surface [22, 167]. Further research into alternative trafficking pathways is needed to determine how polyomaviruses migrate from the nucleus to the plasma membrane.

1.11 Viroporins

Viroporins are a family of small (≤ 100 aa) virally-encoded pore-forming proteins, which are expressed by many viruses (table 1.3). These proteins play essential functions in the manipulation of membrane permeability in order to create suitable environments for virus entry and egress [213-215].

Classification	Family	Virus	Name	Function	Ref	
ssRNA (+)	Picornaviridae	Poliovirus (PV)	2B	Particle production, Release	[216]	
			VP4	Entry	[217]	
		Coxsackievirus B (CoxV B)	2B	Particle production, Release	[216, 218]	
			Enterovirus 71 (EV71)	2B	Virus spread	[219]
	Flaviviridae	Human rhinovirus	VP4	Entry	[220]	
			Hepatitis C virus (HCV)	p7	Particle production	[221-224]
			Bovine viral diarrhea virus (BVDV)	p7	Particle production	[225]
			Classical swine fever virus (CSFV)	p7	Particle production	[225]
			Dengue virus	M	Particle production	[226]
	Togaviridae	Semliki Forest virus	6K	Particle production	[227]	
	Coronaviridae	Severe acute respiratory distress syndrome-associated coronavirus (SARS-CoV)	E	Particle production	[228]	
			3a	Virus spread	[229]	
8a			-			

		Murine hepatitis virus (MHV)	E	Particle production	[230]
ssRNA (-)	Paramyxoviridae	Human respiratory syncytial virus (hRSV)	SH	TNF antagonist, pathogenesis	[231]
	Orthomyxoviridae	Influenza A virus (IAV)	M2	Entry, Particle production	[232-235]
		Influenza B virus (IBV)	BM2	Entry	[236]
		Influenza C virus (ICV)	NB	-	[237]
ssRNA-RT	Retroviridae	Human immunodeficiency virus type-1 (HIV-1)	Vpu	Particle production	[238, 239]
		Human T-lymphotropic virus type-1 (HTLV-1)	P13ii	Mitochondrial permeability	[240]
dsRNA	Reoviridae	Rotavirus (RV)	NSP4	Particle production, Endotoxin	[241]
		Avian reovirus (ARV)	p10		[242]
dsDNA	Polyomaviridae	Simian virus 40 (SV40)	VP4	Particle production	[134]
		JC Polyomavirus (JCPyV)	Agno	Egress, Release	[141, 142]
	Papillomaviridae	Human papillomavirus 16 (HPV16)	E5	Oncogene, Signalling/trafficking	[243, 244]

Table 1.3: Table of viroporins and their functions

Viroporins from different viruses have poor sequence homology, although each contain regions of high hydrophobicity, which usually correspond to one or more transmembrane (TM) domains. Structurally viroporins are divided into 2 classes: class 1 viroporins contain a single TM domain, and class 2 viroporins contain 2

TM domains. These classes are further divided into subclasses depending on topology of their N- and C-termini (Figure 1.8) [213].

1.11.1 Influenza M2

Influenza virus (IV) is a negative sense (-) single-stranded (ss) segmented RNA virus from the *Orthomyxoviridae* family. There are four antigenic types of IV; A, B, C, and D. IV types A, B, and C are all most commonly responsible for respiratory infections in humans. Types A and B are most common, causing the seasonal epidemics and many previous pandemics. Type C is less common and usually only results in local outbreaks. Type D has only been observed to infect pigs and cattle.

The IV types A, B, C, and D all express matrix 2 (M2) proteins [234, 236, 237, 245], which are prototypic class 1a viroporins, and form proton selective ion channels in the viral membrane. M2 proteins are small integral phosphoproteins of ~97 aa in length, with a TM domain consisting of 19-20 residues, an N-termini ectodomain of ~23 residues, and a C-terminal tail of ~54 residues. Structural studies of truncated and full length M2 protein tetramerises with its TM domains forming a left-handed helical bundle creating a channel [213, 246]. IV type A M2 (AM2) [233] and type B M2 (BM2) [236] form channels that are predominantly proton channels, but have been observed to convey some permeability to small monovalent cations. Whereas, type C M2 (CM2) and type D M2 (DM2), are more selective to chloride ions with only some permeability to protons [245, 247]. The best studied of these M2 proteins is AM2. AM2 plays essential roles during the lifecycle of IV, were its functions as a pH-dependent proton channel [246] to facilitate endosomal escape, regulates viral glycoprotein transport, and protects against premature maturation of progeny virions [213].

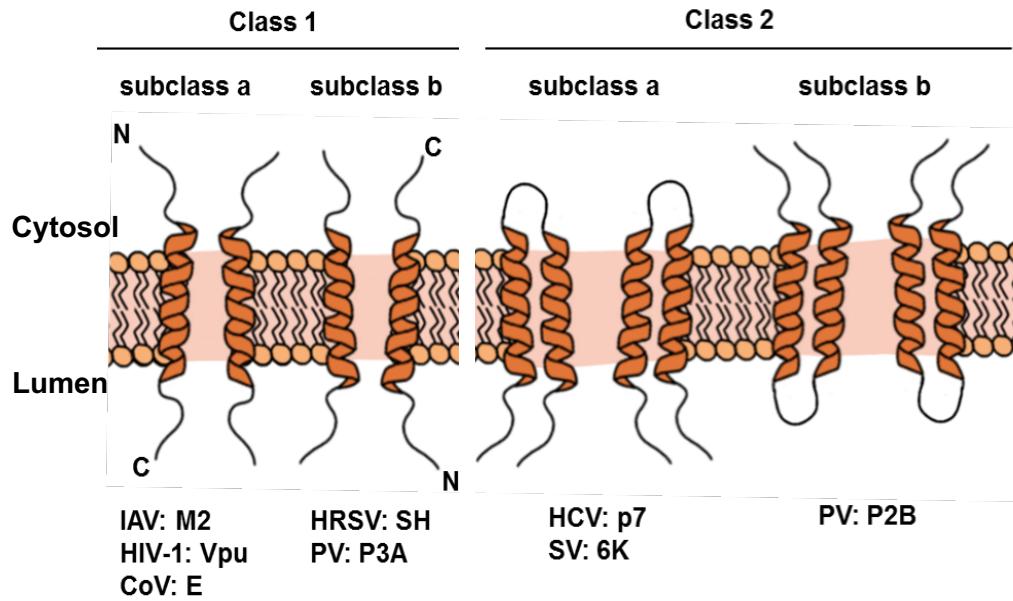


Figure 1.8: Schematic diagram of the classification of viroporin.

Viroporins for each class are shown. Influenza A (IAV); human immunodeficiency virus 1 (HIV-1); coronavirus (CoV); human respiratory syncytial virus (HRSV); polio virus (PV); hepatitis C virus (HCV); Sindbis virus (SV); matrix protein 2 (M2); viral protein U (Vpu), small hydrophobic protein (SH).

Influenza virions enter the cytoplasm of host cells via the endosomal system, where a decreasing pH triggers the activation of M2. At high pH (between 7-8) M2 exists in its closed conformation, where the four helices pack tightly together, forming a lumen of alternating stacked side chains [248]. The C-terminal end of the pore contains a gating mechanism comprising of Trp41 indole ring, which when closed, results in the dehydration of the His37 tetrad raising the protonation barrier. The His37 tetrad can exist in four protonated states, one of each His protonated. 2 of the His residues can be protonated at high pH, but the transition between open and closed requires a third protonation event. This third protonation event only occurs at low pH, where the increase in the protonation state of His37 causes the Trp41 gate to open. In M2's open conformation, the His37 deprotonation barrier is decreased and protons diffuse rapidly to His37 via an ordered water cluster. Further decreases in pH, result in expansion of the channel, and increase the proton conductance [235, 248, 249]. Activation of the M2 proton channel leads to acidification of entrapped virions and subsequent fusion of viral-endosomal membranes, via IV's glycoprotein: haemagglutinin (HA), releasing viral genome into the cytosol. Fusion of viral-endosomal membranes takes place due to a pH-dependent conversion of HA from its sialic acid receptor-binding conformation to a fusogenic conformation. This conformational change results in the exposure of a fusogenic domain that is able to anchor HA into host membranes, and bring them into contact with the viral envelope [250].

The other roles of the M2 ion channel occur late in the IV lifecycle where it assists in events during egress of progeny virions by regulating pH within the trans-Golgi network (TGN) and cytoplasm. Regulation of the local proton concentration is important at this stage of the lifecycle to prevent the premature conversion of HA. Premature conversion of HA results in the release of progeny virions lacking sialic acid binding properties. Equilibration of pH in the Golgi lumen and cytoplasm also results in the decrease in the rate of HA transport [251].

1.11.1.1 Therapeutics

Adamantane compounds were some of the first antiviral compounds licenced against IVA in the 1960s. The mechanism of these compounds was determined in the mid-1980s, revealing that they target the M2 ion channel [252, 253]. Structural studies have determined two different binding sites on M2 for adamantane compounds. The first was solved by NMR and showed that there were four rimantadine sites the subunit interfaces. This site contains residues involved in the gating of M2, and it is theorised that the binding of rimantadine stabilises the closed conformation of M2. The second binding site was solved by crystallographic studies, which observed electron density correlating to the adamantyl cage in the lumen of the M2 channel. This study suggested that adamantane compounds can also directly block the channel, by coordinating with Ser31 [254-256].

Since their discovery, IVA rapidly developed resistance to both amantadine and rimantadine [257, 258]. A S31N mutation (M2 N31) accounts for a large amount of the observed resistance [259], and supports the luminal binding site described in the crystallographic structure. Other mutations have been observed in resistance (L26F, V27A, A30T, G34E, and L38F) which are distributed across three turns of the TM domain [260, 261]. These mutations suggest that acquired resistance to amantane compounds is much more complicated than mutations localised to the binding sites. In efforts to overcome M2 N31 resistance, modified adamantane-based compounds have been developed and showed promise in inhibiting M2 N31 [262]. However, it has recently been shown that treatment with these such compounds rapidly convey resistance in culture. Further studies utilising *in silico* design and *in vitro* screening techniques have been used to develop synergistic antiviral strategies to combat drug resistance in M2. These studies have shown that a combination of drug types is much more effective at M2 N31 inhibition, and shows real promise as therapeutic approach towards IV [263].

1.11.2 Hepatitis C virus (HCV) p7

Hepatitis C virus (HCV) is a positive sense (+) ssRNA virus of the *Flaviviridae* family, which infects over 170 million worldwide. HCV infections are usually chronic infections of the liver and result in cirrhosis, end-stage liver disease, and hepatic carcinomas. The genome of HCV encodes for a polyprotein, which is subsequently cleaved into ten viral proteins, including the viroporin, p7.

HCV p7 is a 63 amino acid protein, consisting of two transmembrane domains, which are linked through a cytosolic loop containing a di-basic motif. p7 monomers form hexameric channels which are partially selective to cations, and sensitive to viroporin inhibitors. Analogous to IVA M2, p7 contains a HXXX(Y/W) motif which is integral to its gating mechanism. Mutational studies of this motif identify that His17 is critical for ion conductance across the p7 channel. It was initially identified as a potential viroporin through comparisons to 6K protein from alphaviruses, and *in silico* predictions of membrane topology [213, 224, 264-267]. *In vitro* studies in artificial membranes identified cation-selective channel forming activity, and sensitivity to amantadine [265], long-alkyl-chain derivatives (NNDGJ and NNDNJ) [268], BIT225 [269], and 5-(N,N-Hexamethylene) amiloride (HMA) [270]. Experiments in planar bilayers identified that the p7 channel conveys permeability to potassium and sodium, with some additional permeability to calcium [270].

Upon the establishment of a cell culture system using HCV isolate JFH-1 it was identified that p7 plays an essential role in virion assembly and release [222, 223]. It was shown in cell culture that expression of IVA M2 could compensate for a non-functional p7, but not the absent of p7. This suggests that viroporin functionality is essential for the HCV lifecycle, but p7 also plays other roles [266]. Additionally, mutational studies showed that the di-basic motif in the cytosolic loop of p7 were critical for channel function. L20F mutation and F25A polymorphism have also been identified in HCV p7 and are found to confer resistance to adamantanes and iminosugars [264]. Additionally, it has been shown that JFH-1 and J4 genotypes are amantadine resistant in cell culture, and

there has also been inconsistencies in data obtained from treatment of different genotypes with various inhibitors. This suggests that while p7 has been implicated as a potential drug target, and it was shown in clinical trials that BIT225 could effectively clear HCV from infected individuals, vast variation in HCV genotypes may make it unsuitable in a clinical setting.

1.11.3 Human Immunodeficiency Virus (HIV) Vpu

Human Immunodeficiency Virus (HIV) is an enveloped lentivirus from the *Retroviridae* family and is the causative agent of acquired immune deficiency syndrome (AIDS) which affects ~35 million people worldwide. HIV virions contain a (+) ssRNA copy of the viral genome, which is retrotranscribed in host cells and integrated into the host genome by a viral integrase. The genome of HIV contains 9 genes, which encode for 10 proteins; one of which is a multifunctional accessory protein named Vpu. Vpu is a 77-86 amino acid transmembrane protein, which localises to the ER, trans-Golgi network, endosomes and plasma membrane.

Vpu has important roles in adapting the host cellular environment for the lifecycle of HIV. It is well characterised for its roles in promoting degradation of CD4 and antagonising the restriction factor tetherin. Its viroporin activity is less well characterised, but it plays a critical role during viral assembly and studies have shown that the depolarisation of the plasma membrane enhances virion release. It is thought that Vpu induced permeabilisation of membranes to monovalent cations, allowing movement of these ions across intracellular membranes to induce reorganisation of raft structures which promote viral budding from infected cells [213, 238].

Further studies have also identified that viroporin activity of Vpu could be antagonised by hexamethylene amiloride (HMA) [271] and N-[5-(1-methyl-1H-pyrazol-4-yl)-naphthalene-2-carbonyl]-guanidine (BIT225) [272]. BIT225 has

been shown to disrupt HIV assembly in monocytes, by blocking viroporin activity. BIT225 is now under development as a treatment for both HIV and HCV [273].

1.11.4 Enterovirus 2B

Enteroviruses (e.g. coxsackievirus, echovirus, enterovirus, rhinovirus, and poliovirus) are +ssRNA, nonenveloped animal viruses that belong to the *Picornaviridae*. They are associated with several diseases in mammals, including humans. The genome of enteroviruses is approximately 7.5 kb and is translated into a single polyprotein of 220 kDa. This polyprotein is proteolytically processed into 11 proteins, including 2B protein (2B). 2B is a small (~100 aa) protein with two regions of hydrophobicity. The first of these hydrophobic regions forms a cationic amphipathic α -helix, which assembles to create a partially calcium-selective channel [216, 274].

Its function is thought to be the manipulation of calcium homeostasis for the purpose of viral egress. It is found located to ER, Golgi, and secretory vesicles in infected cells. It has been suggested for poliovirus (PV) 2B protein is inserted into the ER membrane by the SEC translocon as a helical hairpin with its N- and C-terminus in the cytosol, however it has also been shown to simultaneously insert into membranes *in vitro*. 2B catalyses the release intracellular calcium stores from the Golgi and ER; and increases plasma membrane permeability to calcium and small molecules. The exact mechanism of calcium release is unclear, but it has been theorised that if calcium is not directly released through the 2B channel, 2B might be indirectly activating host calcium ion channels [218, 275-277].

Extensive mutational studies have identified that alongside its role in viral egress, 2B also functions during viral replication, and it is thought that it is responsible for setting up the membranous web on which viral replication takes place. Manipulation of calcium levels has also been shown to suppress apoptosis in host cells and regulate autophagy, which again is thought to be required in membrane organisation for viral replication [213, 278, 279]. There have also been studies showing that the manipulation of calcium levels could be involved in

immune evasion by picornaviruses. It was shown that 2B proteins can antagonise the host immune response, by disrupting protein trafficking through the Golgi [278].

There are limited studies investigating 2B as a target for antivirals, but recently it has been suggested that it could serve as a potential target. There is one study that indicated that DIDs (an anion channel inhibitor) could inhibit enterovirus 71 2B protein, and have a detrimental effect on viral levels [219]. There have also been studies demonstrating that foot-and-mouth-disease virus (FMDV) is sensitive to amantadine [280]. The exact mechanism of these drugs however requires more studies to identify whether or not 2B is their target.

1.11.5 Human Papillomavirus (HPV) E5

Human Papillomavirus (HPV) is a non-enveloped double-stranded (ds) DNA virus from the *Papillomaviridae* family. There are over 200 HPV serotypes which have been classified into five genera, by the sequence identity across late protein 1 (L1) open-reading frame: Alpha-, Beta-, Gamma-, Mupa- and Nupapillomavirus. Papillomaviruses can further be characterised into high- and low-risk, depending on their pathological presentation. Low-risk HPVs cause both cutaneous and mucosal warts; whilst high-risk are a major etiological factor of cervical cancer; and a rising cause of oropharyngeal and ano-genital cancers.

The genome of HPVs encodes 8 proteins, including a minor oncoprotein called E5. E5 mRNA is highly abundant in HPV positive lesions. E5, alongside E6 and E7, is thought to be responsible for inducing the hypoplasia observed in persistently infected keratinocytes. Compared to E6 and E7, E5 is less well characterised due to the difficulties involved with the generation of reagents to carry out further investigations [243, 244].

High-risk E5s have been shown to initiate anchorage-independent growth in both murine fibroblasts and human keratinocytes, in addition to promoting tumorigenesis in mice models. One mechanism, by which E5 is thought to induce

hyperproliferation, is through activation of epidermal growth factor receptor (EGFR) leading to mitogen activated protein kinase (MAPK) signalling. Recently, EGFR is modulation by E5 was described during a productive HPV lifecycle, and the attenuation of EGFR signalling by use of dominant negative constructs led to the loss of hyperproliferation in the high-risk HPV model. How high-risk E5 increases EGFR signalling is unclear. It is thought that E5-dependant alkalisation of endosome results in aberrant recycling of EGFR [281].

It is unknown how E5-dependant alkalisation of endosomes takes place. Wetherill *et al.* [244, 282] showed that HPV16 E5 forms a rimantadine and NNDNJ sensitive viroporin, potentially consisting of 6 monomers. High-risk E5s are a small highly hydrophobic protein, with three predicted transmembrane domains. In addition, it has been demonstrated that the C-termini of HPV16 E5 is exposed to the cytosol and the N-termini is protected from digitonin permeabilisation. Considering, these data it is not possible to categorise HPV16 E5 into the current viroporin classes, as it should be categorised as a class IIIa viroporin. Little is known about how the channel forming ability of E5 functions during HPV infection, but it was shown recently that both rimantadine and NNDNJ abolished aberrant MAPK signalling. Though further investigation is required, this study suggests that the clinically available adamantane compounds and alky-imino sugars could provide a complementary antiviral option, alongside traditional chemotherapy, in cases of HPV positive cancers.

1.12 Aims and Objectives

To develop compounds targeting BKPyV, a comprehensive understanding of the roles of virus-encoded proteins during the infectious life cycle is required. Bioinformatic and biochemical studies indicate that the agnoprotein shares properties consistent with the viroporin class of virus-encoded ion channels. Viroporins are potential targets for a number of clinically available drugs. The project aims to further our functional understanding of the agnoprotein, using *in vitro* biophysical studies, to test the hypothesis that agnoprotein is a novel viroporin and to establish if this channel is a viable drug target.

Objective 1: Establish a system to generate recombinant BK agnoprotein

- An optimized expression and purification protocol will be designed to produce high yields of recombinant BK agnoprotein for functional characterization.

Objective 2: Explore biophysical characteristics of agnoprotein in vitro and within cells

- A series of biochemical and cell-based assays will be designed and optimized to analysis the characteristics of BK agnoprotein at an in vitro and physiologically relevant level. The project will also utilize a primary cell system for studying the agnoprotein in the context of an infection.

Objective 3: Screening a library of drugs and drug-like molecules against BK agnoprotein

- A library of drugs and drug-like molecules exists at Leeds which contains reported viroporin inhibitors. These will be screened against BK agnoprotein using the biochemical and cell-based assays developed in Objective 2.

Chapter 2 : Materials and Methods

2.1 Materials

2.1.1 Mammalian Cell Lines and Primary Cells

Human renal proximal tubule epithelial (RPTE) cells were purchase from ATCC, with considerations made to ensure that each subsequent batch originated from donors that had similar traits to the previous donors. African green monkey kidney (Vero) cells were kindly gifted by Dr Holly Shelton from the Pirbright Institute, UK. Human embryonic kidney 293 containing heat-sensitive SV40 large T antigen (HEK293T) cells were kindly gifted by Dr Martin Stacy from University of Leeds, UK. RPTE cells immortalised with human telomerase reverse transcriptase (RPTEC-HTERT) were kindly gifted by Professor Mike Imperiale from University of Michigan, USA.

2.1.2 Bacterial Strains

BL21(DE3) Rosetta cells, BL21(DE3) Rosetta 2 cells, BL21(DE3) Gold cells, BL21(DE3) Star, and DH5 α cells were purchased from NEB. Bacterial cells were made chemically competent following the manufacturers protocols.

2.1.3 Plasmids

pGEM7 BKPyV Dunlop was kindly gifted by Prof Mike Imperiale from University of Michigan, USA. peGFP-C1 was purchased from BD Biosciences Clontech (kanamycin resistance), and cloning of GFP agnoprotein and mutations constructs were performed by Dr Emma Prescott (Macdonald group, University of Leeds). pcDNA3.1 HA-BKPyV agnoprotein-FLAG was cloned by Dr Ethan Morgan (Macdonald group, University of Leeds). GFP-Coxsackie B3 2B wildtype and mutant constructs were a kind gift from Dr Steve Griffin from University of

Leeds. pET19bTEV (Novagene: ampicillin resistance) was kindly gifted by Dr Thomas Edwards.

2.1.4 Antibodies

Antibodies used were all diluted to working concentration in 5% skimmed milk powder in TBST. Polyclonal rabbit anti-agnoprotein (A81038P) (kindly gifted by μ Moens, University of Tromsø) was used at 1 in 10000 for western blot (WB) and 1 in 600 for immunofluorescence (IF). Monoclonal mouse anti-VP1 antibody was prepared in house from hybridoma (pAB597) (kindly gifted by Chris Buck, NIH, USA), and used at 1 in 250 for IF. Monoclonal mouse anti-6x His tag (Proteintech) was used at 1 in 5000 for WB. Polyclonal sheep anti-GST tag was produced in house and was at 1 in 5000 for WB. Monoclonal mouse anti-GAPDH (Insight Biotech) was used at 1 in 5000 for WB. Monoclonal mouse anti-GFP (Santa Cruz) was used at 1 in 5000 for WB. Monoclonal rabbit anti-epithelial growth factor receptor (EGFR) antibody (Cell Signalling Technologies) was used at 1 in 5000 for WB. Monoclonal mouse anti-HA tag antibody (Sigma) was used at 1 in 5000 for WB.

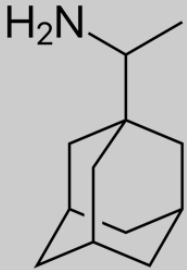
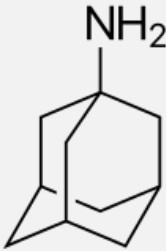
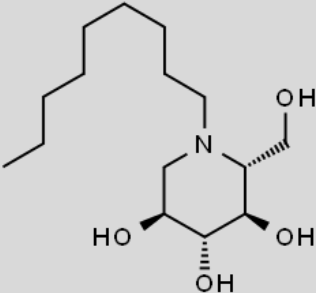
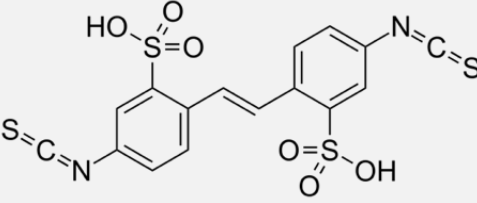
2.1.5 Lipids

L- α -Phosphatidic acid (egg monosodium salt) (PA), L- α -Phosphatidylcholine (egg) (PC) and L- α -Phosphatidylethanolamine with lissamine rhodamine B labelled head groups (PE) purchased from Avanti Polar Lipids in chloroform, as 10 mgml⁻¹ stocks. Stock solutions were aliquoted in glass vials and stored at -80 °C.

2.1.6 Inhibitors and Control Compounds

All Inhibitors and compounds (table 2.1) were stored long-term as lyophilised stocks as per the manufacturer's guidelines. Lyophilised stocks were dissolved in DMSO at the appropriate short-term stock concentrations, aliquoted and stored

at -20 °C. Inhibitors were used at experimental concentration by dilution in either liposomal buffer or cell culture media.

Compound	Structure	Source.
Rimantadine		Cambridge Biosciences (Manufacturer: LKT Laboratories Inc.)
Amantadine		Sigma
NNDNJ		Insight Biotechnology
DIDs		Sigma

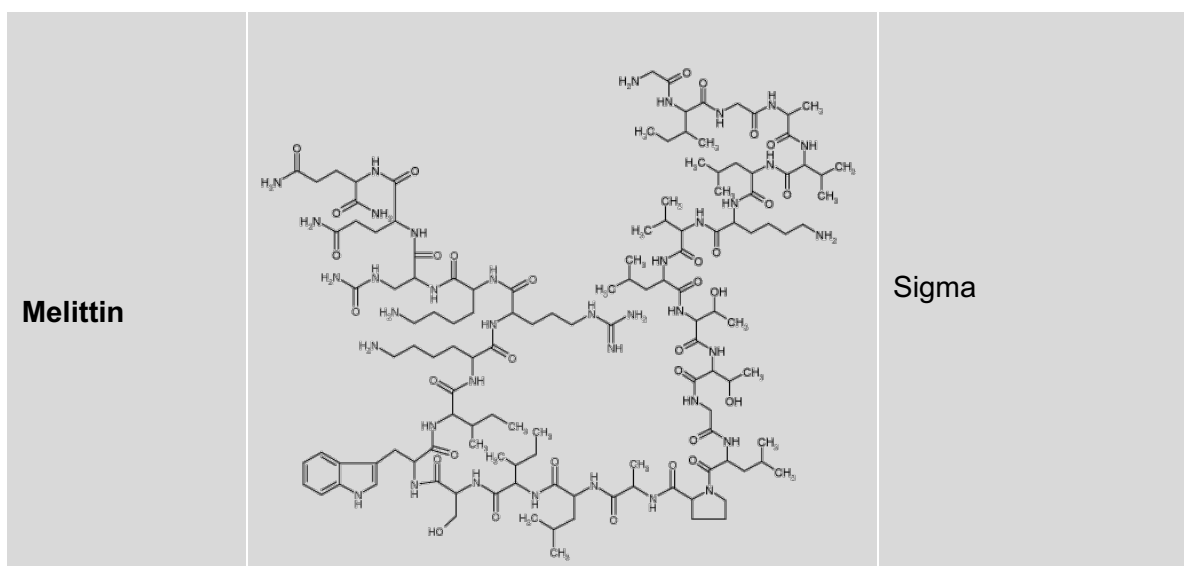


Table 2.1: Table of Inhibitors and Compounds, with their structures and source

2.2 Manipulation of Recombinant DNA

2.2.1 Oligonucleotides

DNA oligonucleotides (primers) were designed manually and purchased from Integrated DNA Technologies. Lyophilised primers were dissolved in deionised water to a stock concentration of 100 μM and were stored at $-20\text{ }^{\circ}\text{C}$. Appendix states all oligonucleotide sequences used during this project.

2.2.2 Polymerase Chain Reaction (PCR)

KOD polymerase kit (Novagen) was used to amplify DNA fragments, for the purpose of cloning, by polymerase chain reaction (PCR) using the following reaction;

Components	Vol. (μl)	Final Conc.
dd. Water	30.1	-
10x KOD Buffer	5	1x
2 mM dNTPs	5	0.2 μM

2 mM MgCl₂	2	0.08 μM
DMSO	5	10%
KOD Polymerase	0.4	1 U
Forward Primer	1	0.2 μM
Reverse Primer	1	0.2 μM
Template DNA	0.5	0.1 μM

Table 2.2: Composition of PCR mix used for amplification of agnogene

A thermocycler was programmed to perform the following PCR protocol:

Step	Temperature (°C)	Duration (sec)	N° of Cycles
Initial Melting	95	15	1
Melting	95	15	25
Annealing	52-56	5	
Elongation	72	5	
Final Elongation	72	120	1

Table 2.3: Step-by-step PCR protocol used for amplification of agnogene

After amplification, PCR products were separated for analysis on a 1% agarose gel.

2.2.3 Restriction Endonuclease Digestion

Restriction endonucleases were used for cloning and preparation of viral genomes. Restriction digestion for cloning was performed using 20 U of Kpn1-HF and BamH1-HF in 1x CutSmart buffer (NEB) with 5 μg of vector DNA or cloned PCR fragment. These digestions were incubated at 37 °C for 1hr, before

purification. Similarly, restriction digestions for the preparation of BKPyV Dunlop genomes were performed using 20U of BamH1-HF and 10 µg of pGem7 BKPyV Dunlop. These digestions were incubated at 37 °C for 2hr: an additional 20U of BamH1-HF was added at 1hr. Digested BKPyV genomes were subsequently used in downstream ligation reactions.

2.2.4 DNA Clean Up

Purification of PCR fragments and restriction digests were carried out using Monarch® PCR & DNA Cleanup Kit following the manufacturers protocol. After purification, resulting products were quantified using (nanodrop) at nm, and either carried forward to downstream applications or stored at -20 °C.

2.2.5 Agarose Gel Electrophoresis

1% agarose (Sigma) solutions were prepared in 1x TAE (appendix) supplemented with 0.1 µl/ml SYBR safe (Sigma), and used to create 1% agarose gels (appendix) for gel electrophoresis of purified PCR fragments and plasmids. Purified DNA was combined with 6x loading dye at a ratio of 1:6 (loading dye:DNA). Electrophoresis was carried out at 100 V for 70 minutes besides 6 µl of 2-log DNA ladder (NEB). Visualisation of agarose gels was performed under a UV light source.

2.2.6 DNA ligation

DNA ligations were carried out using T4 DNA ligase in 1 x T4 DNA ligase buffer (NEB). For cloning, reactions contained a vector to backbone ratio of 1:3 and were incubated overnight at 16 °C. Non-ligation controls were performed in parallel in the absence of T4 DNA ligase. Following overnight incubation, ligation products were transformed into DH5α and plated on LB agar plates with the appropriate antibiotic.

For preparation of viral genomes, 45 μ l of pGEM7-BKPyV Dunlop digestion reaction was diluted out to a total of 1 ml with 1x T4 DNA ligase buffer to reduce risk of religation of the original plasmid. T4 DNA ligase was added to catalyse ligation and reactions were incubated overnight at 16 °C.

2.2.7 Colony PCR Screening

Transformed colonies were picked and grown for several hours in 1 ml of LB broth (appendix). Colony PCR Screening of selected colonies was carried using GoTaq® G2 DNA Polymerase (Promega). The reactions were set up as follows;

Components	Vol. (μ l)	Final Conc.
5x Green GoTaq Reaction Buffer	10	1x
PCR Nucleotide Mix. 10 mM each	1	0.2 mM each dNTP
Forward primer	1	0.2 μ M
Reverse primer	1	0.2 μ M
GoTaq G2 DNA Polymerase	0.25	1.25 U
Bacterial Culture	1	Var.
dd. Water	35.75	-

Table 2.4: Composition of PCR mix used for amplification of agnogene

A thermocycler was programmed to perform the following PCR protocol:

Step	Temperature (°C)	Duration (sec)	N° of Cycles
Initial Melting	95	120	1
Melting	95	20	30
Annealing	52-56	10	
Elongation	72	20	
Final Elongation	72	120	1

Table 2.5: Step-by-step PCR protocol used for colony PCR

PCR products were then separated for analysis on a 1% agarose gel.

2.3 Preparation of Plasmid DNA

2.3.1 Transformation and Plating of Chemically Competent Bacterial Cells

1 µg plasmid DNA was incubated on ice with 50 µl of DH5α or BL21 expression strain *E. coli* (NEB) for 15 minutes. After initial incubation, bacterial/DNA suspension was heat shocked at 42 °C for 30 sec. 750 µl of LB broth (appendix) was then added and suspension was incubated at 37 °C for an hour to allow bacteria to recover. After recovery, bacteria were plated out on 0.03% LB agar plates (appendix) with the appropriate antibiotic resistance. LB agar plates (appendix) were incubated overnight at 37 °C and stored at 4 °C after colonies grew.

2.3.2 Preparation of Small-Scale Bacterial Cultures, Extraction and Purification of Plasmid DNA (Miniprep)

10 ml of LB broth (appendix) was inoculated with transformed DH5α and incubated at 37 °C overnight to produce an overnight culture. The following morning cultures were harvested via centrifugation to form pellets. Pellets were used to prep plasmid DNA using Monach DNA miniprep kit (NEB) as per the manufacturers protocol. Final elution of plasmid DNA was performed in 30 µl of deionised water.

2.3.3 Preparation of Large-Scale Bacterial Cultures, Extraction and Purification of Plasmid DNA (Maxiprep)

100 ml of LB broth was inoculated with 1 ml from an overnight culture of transformed DH5α and incubated overnight at 37 °C. The following morning

cultures were harvested via centrifugation to form pellets. Pellets were used to prep plasmid DNA using Qiagen DNA Maxi Prep kit as per the manufacturers protocol. Final elution of plasmid DNA was performed in 500 μ l of deionised water and adjusted so DNA concentration was around 1 μ g/ μ l.

2.3.4 Storage of Plasmid DNA as a Glycerol Stock

Glycerol stocks of plasmid DNA were prepared from 500 μ l of an overnight culture of transformed bacteria and 500 μ l of 50% glycerol in an eppendorf tube. Tubes were inverted several times to thoroughly mix bacterial culture with glycerol before being frozen for long-term storage at -80 °C.

2.3.5 Quantification of Plasmid DNA

Plasmid DNA was quantified using a Nanodrop spectrophotometer (Thermo Fisher Scientific) at 260 nm. Nanodrop spectrophotometer was blanked using deionised water, and 1 μ l of DNA was used to calculate concentration. Absorbances at 280 nm were also taken to assess purity of the plasmid DNA with an absorbance of 1.8 being considered as pure DNA without RNA or organic compound contaminations.

2.4 Expression and Purification of His-BK agnoprotein

2.4.1 IPTG Induced Protein Expression

Overnight cultures were grown in LB broth of BL21 Gold cells (NEB) transformed with pET19b BKPyV Agnoprotein. 5 ml of overnight culture was used to inoculate 1 L of LB broth. 1 L cultures were grown at 37 °C and monitored at 600 nm until the optical density reached 0.6. 1 mM IPTG (Sigma) was then added to the cultures to induce His-BKPyV agnoprotein expression. After induction culture were incubated overnight at 37 °C, before harvesting via centrifugation at 4000 rpm for 15 mins.

2.4.2 Bacterial Cell Lysis

Bacterial pellets were lysed in Triton X100 lysis buffer (10 mM Tris pH 8 (Sigma), 1% Triton X100 (Sigma), 500 mM NaCl (Fisher Scientific), 50 µg/ml Lysozyme (Alfa Aesar), 1x protease inhibitor cocktail (Roche), 125 U benzonase (MerckMillipore) and incubated for 1 hour at 25 °C. Bacterial lysates were clarified by centrifugation at 4000 rpm for 30 mins.

2.4.3 Nickel Affinity Purification of His-BK agnoprotein

2 ml of NiNTA resin was packed into a gravity flow column and equilibrated with Triton X100 lysis buffer. 25 mM Imidazole was added to clarified bacterial lysate, before applying the lysate to the NiNTA resin. Once the bacterial lysate had flowed through the column, the NiNTA resin was washed with three bed volumes (bv) with wash buffer (10 mM Tris pH 8, 500 mM NaCl, 50 mM imidazole). Elution took place after the NiNTA resin had been washed. Elution buffers used were the same composition as the initial wash buffer, but with increasing amounts of imidazole ranging from 100 mM to 1 mM. 2 bv of each elution buffer was passed through the column and 2 ml fractions were collected for analysis. After purification the fractions collected were resolved on a 15% SDS PAGE gel and stained with instant blue or immunoblotted an anti-agnoprotein antibody.

2.4.4 Ion Exchange Chromatography of His-BK agnoprotein

Fractions from nickel affinity chromatography were diluted 10-fold in IEX buffer A (10 mM HEPES pH 7.5, 50 mM NaCl) to reduce the high salt concentration. The diluted sample was loaded onto a 1 ml HiTrap SP column, at the rate of 1 ml min⁻¹, using a peristaltic pump. Bound proteins were eluted on a gradient from 50 mM to 1 M NaCl in IEX buffer, with 1 ml fractions collected and 220 nm absorbance being monitored for peaks which signalled protein elution. Fractions from ion exchange chromatography were resolved on a 15% SDS PAGE gel and silver stained or immunoblotted an anti-agnoprotein antibody.

2.4.5 Reverse Phase High Pressure Liquid Chromatography (rpHPLC) of 10x His BK agnoprotein

rpHPLC was performed using a Dionex HPLC system with a PDA-100 photodiode array detection unit; controlled using Chromeleon software. 500 µl of material eluted from the nickel affinity chromatography was loaded onto an Aeris wide-pore 3.6 microns C4 HPLC column (Phenomenex). Elution of bound protein species was achieved using a gradient from 100% solvent A (5% v/v acetonitrile, 0.1% v/v trifluoroacetic acid (TFA)) to 100% solvent B (95% v/v acetonitrile, 0.1% v/v TFA). Absorbance was monitored at 220 nm for eluted material, and fractions collected inside observed peaks using an automated fraction collector. Collected fractions were lyophilised using a GenVax system and re-solubilised in 1x Laemmli protein loading dye. Re-solubilised samples were resolved by 15% SDS PAGE gel and immunoblotted an anti-agnoprotein antibody or Ponceaus S stained.

2.4.6 Concentration of Recombinant 10x His BKPyV agnoprotein

Fractions from ion exchange chromatography were concentrated using C4 solid phase extraction columns. C4 solid phase extraction columns were activated using 2 bv. of 95% acetonitrile. After activation, the matrix was equilibrated with 3 bv. Of 5% acetonitrile, before samples were bound to the columns. The columns were then airdried as specified by the manufacturers protocol, before elution took place using 95% acetonitrile. Eluted material was collected and dried down to concentrate the eluted protein. Eluted protein was resuspended in DMSO to give a concentration of approximately 1 mg/ml. Samples were incubated with Laemmli loading dye for 15 minutes at room temperature, but not boiled, before SDS PAGE analysis. Boiling of recombinant agnoprotein samples was seen to cause aggregation in SDS PAGE wells.

2.4.7 Quantification of Recombinant 10x His BKPyV agnoprotein

Recombinant protein was quantified using a Nanodrop spectrophotometer (Thermo Fisher Scientific) at 280 nm. Nanodrop spectrophotometer was blanked using DMSO, and 1 μ l of recombinant protein was used to calculate concentration.

2.5 *In Vitro* Liposome Assays

2.5.1 Preparation of Unilamellar Liposomes

Lipids were measured out at a ratio of 1:1:0.1 (PA:PC:PE). Lipids were then dried using a stream of argon, and placed under vacuum for 2 hr at room temperature. Dried lipids were then reconstituted overnight in either; a self-quenching concentration of carboxyfluorescein (CF) buffer. Reconstituted lipids were extruded at 37 °C through a 0.4 μ m Nuclepore Track-Etched membrane filter, using an Avanti mini-extruder to produce unilamellar liposomes. Liposomes were purified away from excess CF buffer by washing three times in liposome buffer (recipe) and centrifugation at 100,000 xg for 15 minutes in a Sorvall S55S ultracentrifuge rotor using an RC M120 GX MicroUltra. After purification, lipids were resuspended in 500 μ l of assay buffer.

To determine liposomal concentration rhodamine fluorescence was measured at 570 nm for a pre- (diluted 10-fold) and post- extrusion sample. Absorbance values were then used in the calculation below;

$$\begin{aligned} & \text{Liposome conc. (mM)} \\ &= \frac{2.75\text{mM (average lipid molarity)}}{\text{OD}^{570} \text{ pre extrusion sample} \times \text{dilution (1: 10)}} \times \text{OD}^{570} \text{ liposomes} \end{aligned}$$

2.5.2 Real Time *In Vitro* Liposome Assay

Liposomes encapsulating self-quenching concentration of CF were used to monitor real time permeabilisation of membranes. These assays were carried out in flat-bottomed, black 96 well plates (micro-titre plate) (Greiner Bio One) where each well comprised of 50 μ M of liposomes and varying amounts of recombinant His BKPyV agnoprotein in a total volume of 100 μ l. CF release was monitored every 30 seconds over a total of 30 minutes using FLUOstar Optima plate-reader (BMG Labtech) (λ_{ex} 485/ λ_{em} 520 nm) at 37 °C.

Melittin, extracted from bee venom (Sigma), at a final concentration of 1 μ M was used as a positive control for CF release. A background fluorescence benchmark and the gain were set using liposomes that were incubated with 0.5% v/v Triton X100. Baseline readings were monitored by use of liposome only and liposomes plus 10% DMSO controls (depending on buffer in which recombinant agnoprotein was solubilised).

2.5.3 Inhibitor Assays

Dye release assays with the addition of inhibitors was carried out following the same protocol as above, but 1 μ M recombinant agnoprotein was incubated with the appropriate amount of inhibitor for 10 mins prior to the beginning of the experiment.

2.5.4 Flootation Assays

Discontinuous Ficoll gradients were prepared using liposome buffer (pH 7.4) in 2.2 ml ultracentrifuge tubes by combining 100 μ l of 40% w/v Ficoll with 100 μ l of 50 μ M liposomes in liposome buffer (final Ficoll concentration of 20% w/v). 8 μ g of recombinant agnoprotein was added to this liposome mixture. Liposomal mixture (+ 5 μ M recombinant agnoprotein) was layered under 1.7 ml of 10% Ficoll w/v, and 300 μ l 0% Ficoll was layered on top. The gradients were centrifuged at 100,000 xg for 30 minutes in a S55S ultracentrifuge rotor (Sorvall) using an RC

M120 GX MicroUltra. After centrifugation, gradients were carefully fractionated into 8 x 250 µl fractions. 40 µl of each fraction were assessed for liposome migration by rhodamine fluorescence (λ_{ex} 520 nm and λ_{em} 570 nm) using a FLUOstar Optima plate-reader (BMG Labtech). 10 µl of 1x Laemmli protein loading dye was then added to each 40 µl sample and analysed by immunoblotting with anti-agnoprotein antibody.

2.6 Mammalian Cell Culture

2.6.1 Maintenance and Passage of Cells

Vero cells and HEK 293T cells were maintained in Dulbecco's modified eagle medium (DMEM) supplemented with 1% (v/v) penicillin/streptomycin and 10% (v/v) foetal bovine serum (FBS) at 37 °C in 5% CO₂. Vero cells were passaged tri-weekly by removal of growth media, followed by a 1x PBS wash and disassociation with 1x EDTA-trypsin. Trypsinised cells were passaged at 1:10 dilution in fresh DMEM.

RPTE and RPTE-HTERT cells were maintained in Renal Epithelial Cell Growth Medium 2 (Promocell), supplemented with 0.05 ml/ml FBS, 10 ng/ml EGF, 5 µg/ml recombinant human insulin, 0.5 µg/ml epinephrine, 36 ng/ml hydrocortisone, 5 µg/ml transferrin, and 4 pg/ml triiodo-L-thyronine (purchased as a kit – Promocell). RPTE cells were maintained in a T175 flasks at 37 °C in 5% CO₂ with media replaced every 3 days to replace FBS. Flasks were passaged weekly by removal of growth media, followed by a 1x PBS wash and dissociation with 1x EDTA-trypsin. Trypsinised cells were passaged at 1:10 dilution in fresh media. RPTE cells were maintained until passage 7.

2.6.2 Seeding of Cells

Disassociated cell suspensions were mixed 1:1 with trypan blue solution (Sigma Aldrich), and counted using a haemocytometer. The average cell count from each haemocytometer quadrant was taken and multiplied by 2×10^4 to determine the

number of cells per ml. The appropriate cell density was then seeded into fresh media in tissue culture treated plasticware.

2.6.3 Storage and recovery of frozen cell stocks

Frozen cell stocks were prepared following cell disassociation. Disassociated cells were collected via centrifugation at 1000 xg, before being resuspended in fresh DMEM supplemented with 10% DMSO at a density of 1×10^6 cells/ml. Cell solution was aliquoted into cryovials and placed in an isopropanol insulated freezer container at -80 °C overnight. The following day, cell vials were transferred to liquid nitrogen for long-term storage.

Frozen cell stocks were recovered by thawing at 37 °C and transferred to a T75 flask containing 10 ml of warm DMEM. Cells were allowed to attach overnight, before media was replaced with fresh DMEM the following morning to remove 1% DMSO from the culture. Flasks are then maintained as described above.

2.7 Preparation of BK Polyomavirus Stocks

2.7.1 Transfection of RPTE cells with BKPyV genome

1×10^6 RPTE cells were seeded in T175 cm tissue culture flask the day before transfection. On day of transfection, 4 µg of BKPyV genome was incubated for 10 mins with TransIT LT (Mirus), at a ratio of 1:3 (DNA: transfection reagent). 15 ml of fresh media was placed on RPTE cells and then transfection mix was introduced to the media. The transfected RPTE cells were incubated for 3 weeks, or until cytopathic effects reduced cellular viability (figure 2.1A). Harvesting of transfected RPTE cells was then performed by scrapping the cells into the media. The cell suspension was then sonicated for 5 minutes to rupture cells, and centrifuged to remove large pieces of cell debris.

2.7.2 Infection of RPTE cells with BKPyV

1x10⁶ RPTE cells were seeded in T175 cm tissue culture flask the day before infection. Virus harvested from transfected RPTE cells was placed onto the naïve RPTE cells and incubated for a further 2 weeks (figure 2.1B). After incubation, virus was harvested by scrapping the cells into the media and sonicating to rupture the cells. Resulting crude viral lysate was then quantified and used for downstream assays.

2.7.3 Quantification of BKPyV – Fluorescence Focus Assay

1x10⁴ RPTE cells were seeded into 7 wells of a 96 well plate. Crude viral lysate was diluted 1 in 10 into the first well, and sequentially diluted 1 in 2 across the next 5 wells to produce a dilution series. The seventh well was left as an uninfected control. Crude viral lysate was removed from cells after 2 hrs and cells were incubated for 48 hrs, before fixation with 4% PFA. After fixation cells were permeabilised with 0.1% Triton x100 in 1x PBS for 10 min at 25 °C. Permeabilised cells were then blocked in 1% BSA in 1x PBS for 30 mins at 25 °C, before incubation with anti-VP1 antibody in 1% BSA in 1x PBS overnight at 4 °C. The next day cells were washed 3 times with 1x PBS, and then incubated for 1hr at 25 °C with chicken anti-mouse Alexa Fluor 488 in 1% BSA in 1x PBS. Subsequently, cells were washed a further 3 times with 1x PBS and imaged using IncuCyte (figure 2.1C).

Number of VP1 positive cells was counted using IncuCyte ZOOM software. Quantification of viral titre was then carried out by calculating infectious units (IU) per ml for each dilution as follows;

$$N^{\circ} \text{ of VP1 positive cells} \times \text{dilution} \times \text{volume of media (in ml)} = \text{IU/ml}$$

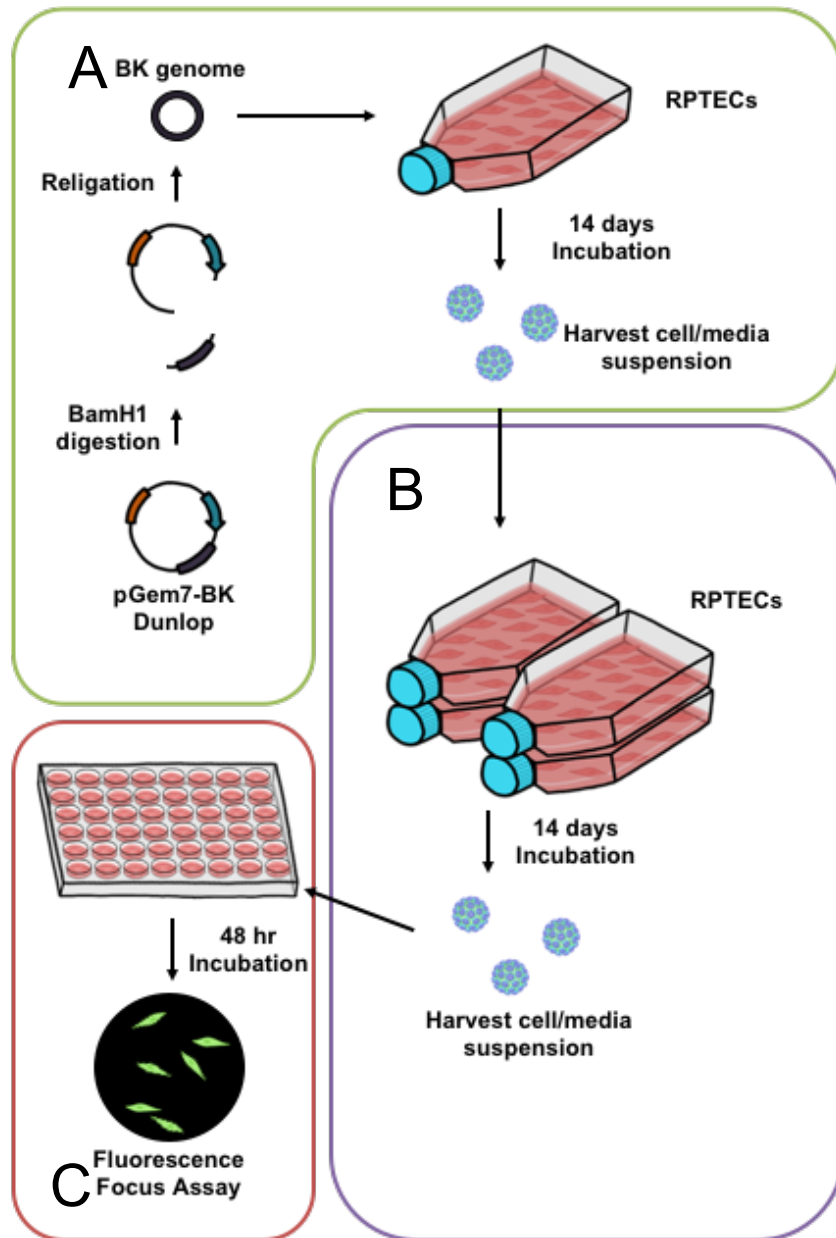


Figure 2.1: Schematic of BKPyV production

(A) Digestion of pGem7 BK Dunlop by BamH1, followed by religation and transfection into naïve RPTE cells using TransIT LT. (B) Infection of naïve RPTE cells using crude virus lysate from transfected cells. (C) Fluorescence focus assay used to titre final viral lysate, imaged and quantified using IncuCyte ZOOM software.

Calculated IU/ml were then averaged together to give an average IU/ml for the crude viral lysate. The average IU/ml was used, as follows, to calculate the amount of crude viral lysate required to give a specific multiplicity of infection (MOI).

$$\frac{\text{Required MOI} \times \text{N}^{\circ} \text{ of cells}}{\text{IU/ml}} = \text{vol of crude viral lysate (in ml)}$$

2.8 Protein Biochemistry

2.8.1 Preparation of Cell Lysates for SDS Polyacrylamide Gel Electrophoresis (PAGE)

Quantification of cell lysates was carried out using a bicinchoninic acid (BCA) protein assay. 5 µl of cell lysate was incubated with 200 µl of BCA reagent for 15 min, as per the manufacturers protocol, alongside a set of protein standards ranging from 2000 – 25 µg/ml. After incubation, absorbance at 562 nm were taken and concentration of cell lysates was calculated against the protein standards.

Calculated concentrations were used to load equal amounts of cell lysates onto SDS PAGE. Samples were made up to equal volumes using appropriate lysis buffer and 1x Laemmli protein loading dye (appendix).

2.8.2 Preparation of Immunoprecipitations/GST Pull Down for SDS PAGE

Samples from immunoprecipitations and GST pull downs were eluted from beads directly into 50 µl Laemmli protein loading dye in preparation for analysis via SDS PAGE. Equal amounts of each elution were loading onto SDS PAGE gels.

2.8.3 Preparing and Running SDS PAGE Gels

SDS PAGE gels were prepared following the recipe below, using BioRad's electrophoresis format. Resolving gel (table 2.6) was prepared first and placed between glass plates under a layer of 70% ethanol to prevent formation of bubbles. Stacking gel (table 2.6) was layered on top of polymerized resolving gel, with a plastic comb inserted to form wells. Prepared protein samples were loaded into the wells formed in the stacking gel, and were resolved at 140 V for 190 min.

Resolving Gel	12.5%	15%	10%	Stacking Gel	2 gels
1M Tris pH 8.8	2.5 ml	2.5 ml	2.5 ml	1M Tris pH 6.8	0.5 ml
dd. Water	3.1 ml	2.4 ml	4 ml	dd. Water	2.85 ml
30% Bis-Acrylamide	4.2 ml	4.9 ml	3.3 ml	30% Bis-Acrylamide	0.6 ml
10% SDS	100 μ l	100 μ l	100 μ l	10% SDS	40 μ l
10% APS	100 μ l	100 μ l	100 μ l	10% APS	40 μ l
TEMED	16 μ l	16 μ l	16 μ l	TEMED	10 μ l

Table 2.6: Recipe for resolving and stacking acrylamide gels

2.8.4 Semi-Dry Transfer of Proteins to Nitrocellulose

SDS PAGE gels were transferred to nitrocellulose membrane using BioRad's semi-dry transfer rig, according to the manufacturers protocol. The conditions used during transfer were 25 V for 30 mins with a current set to not exceed 1 amp.

2.8.5 Western Blotting

Nitrocellulose membranes were blocked for 30 min at room temperature in 5% skimmed milk powder in Tris Buffer Saline with 0.1% Tween (TBST). Blocked membranes were either incubated overnight at 4 °C or for 1 hr at room

temperature with the appropriate primary antibody. Primary antibody was then removed, and membranes washed thrice in 1x TBST, before being incubated for 1 hr at room temperature with the appropriate horse radish peroxidase conjugated secondary antibody. Secondary antibody was then removed, and membrane washed thrice in 1x TBST.

Detection of antibodies was then performed by incubating nitrocellulose membrane with electrochemiluminescence (ECL) western blotting detection reagent (GE healthcare life science). Membranes were then exposed to CL-XPosure photographic film (ThermoFisher) and developed using an xograph in a dark room.

2.8.6 Coomassie-based Staining of Polyacrylamide Gels

SDS PAGE gels were stained using PAGEBlue protein staining solution (ThermoFisher). After electrophoresis, gels were washed 3x with deionised water and then incubated overnight with PAGEBlue protein stain. Gels were destained the following morning by washing with water until the background was light enough to see protein bands.

2.8.7 GST Pull Down

pGex6P1-FLAG BkPyV agnoprotein was transformed into Rosetta 2 BL21 E. coli. Transformed cells were grown in LB broth overnight at 37 °C and used to inoculate 50 ml cultures. 50 ml cultures were grown at 37 °C until OD₆₀₀ was equal to 0.6. GST-FLAG-BkPyV agnoprotein expression was then induced by addition of 1 mM IPTG. After induction, bacterial cultures were incubated overnight at 37C, prior to harvesting via centrifugation at 4000 rpm for 20 minutes. Bacterial pellets were lysed on ice for 30 min in Triton X100 lysis buffer, followed by sonication for 5 min in a sonicating water bath. Bacterial cell lysate was clarified by centrifugation at 4000 rpm, and supernatant incubated with glutathione agarose beads for 2 hr at 4 °C. After incubation, the glutathione agarose beads were collected via centrifugation and washed 3 times in RIPA lysis buffer. HEK293T cells were transfected using PEI with GFP and GFP-agno

constructs. These cells were incubated for 48 hr and harvested by scrapping cells into RIPA lysis buffer. The cell suspension was incubated on ice for 20 mins and then sonicated for 3 cycles of 30 sec on and 30 sec off. 100 μ l of cell lysate was diluted in 400 μ l of RIPA lysis buffer and incubated with 20 μ l of GST/GST-agnoprotein primed glutathione agarose beads. GST pull downs were incubated at 4 °C overnight, and then washed 3 times with RIPA lysis buffer and twice with TBS. Proteins were eluted from glutathione agarose beads by resuspending the beads in SDS PAGE loading dye.

2.9 Cell-based Assays

2.9.1 Transfection

2.9.1.1 TransIT LT

RPTE and HTERT RPTE cells were transfected with TransIT LT (Mirus) at a ratio of 1:3 (DNA:reagent). The required amount of DNA was diluted into 250 μ l of OptiMEM. TransIT LT was added to the diluted DNA and incubated for 20 mins. After 20 mins of incubation the mixture was evenly distributed onto cells in full media.

2.9.1.2 PEI

HEK293T or HEK293 cells were transfected with PEI at a ratio of 1:4 (DNA:PEI). The required amount of DNA was diluted into 250 μ l of OptiMEM. PEI was added to the diluted DNA and incubated for 10 mins. The media from the cells was replaced with OptiMEM, and after 10 mins of incubations the transfection mixture was evenly distributed onto cells. The following morning the transfection mixture and OptiMEM was replaced by full DMEM.

2.9.2 Preparation of Cells for Immunofluorescence

Cells for immunofluorescence or fluorescence analysis were fixed in paraformaldehyde for 10 min at room temperature. After fixation, cells were permeabilised with 0.1% Triton X100 in PBS for 10 mins at room temperature, before being blocked in 5% BSA in PBS for 30 mins. For Topology studies the same method was used, but the permeabilisation step was missed out.

2.9.3 Lysis of Mammalian Cells

Mammalian cell lysates were prepared by scrapping cells into RIPA buffer, unless stated otherwise. Cell suspension was then sonicated for 3 cycles of 30 sec on and 30 sec off in a sonicating water bath. After sonication cells were left on ice for 30 minutes, before being used in downstream analyse.

2.9.4 Merocyanine 540 Assay

4×10^5 HEK293T were seeded into 6 well plates and allowed to settle for 48 hr. Cells were then transfected with the appropriate GFP constructs and incubated for a further 48 hr. After incubation, cells were gently washed with 1x PBS and disassociated with enzyme free disassociation buffer (Gibco). Disassociated cells were harvested via centrifugation at 1000 xg and resuspended in 1ug/ml of Merocyanine 540 (MC540). Once resuspended cells were incubated for 10 mins at 37 °C. Cells were then wash in 1x PBS and analysed by flow cytometry. Analysis was performed with a BD Fortessa used at 488 nm excitation and 575 nm emission wavelengths. Gates were applied to the live population of cells, and within that population a secondary gate was applied to GFP positive cells. These gates were selected using non-stained and GFP only cells, and compensation was performed between GFP and MC540 to account for any bleed through.

2.9.5 Hygromycin Assay

2x10⁵ HEK293T cells were seeded into 12 well plates and allowed to settle for 48 hr. Cells were then transfected with the appropriate GFP constructs. After 48 hr cells were treated with Click-iT® Plus OPP Alexa Fluor® 594 Protein Synthesis Assay Kit (Thermo Fisher) following the manufacturer's protocol but detaching cells prior to staining with azide dye. Hygromycin was used as the treatment in this assay and was used at a concentration of 500µg/ml. Cells were analysed using a Becton Dickinson BD-LSRFortessa at 488 nm and 610 nm. Gates were applied to the live population of cells, and within that population a secondary gate was applied to GFP positive cells. These gates were selected using non-stained and GFP only cells, and compensation was performed between GFP and Alexa Fluor® 594 to account for any bleed through.

2.9.6 Subcellular Fractionations

Membrane/Cytoplasmic fractionations were carried out in HEK293T cells transfected with pcDNA 3.1 FLAG-BKPyV agnoprotein-HA. Cells were disassociated into enzyme free disassociation buffer and centrifuged to retrieve a cell pellet. Cell pellets were resuspended in M1 (10 mM PIPES pH 7.4, 0.5mM MgCl₂, and protease inhibitors). Cell suspension was sonicated for 3 cycles of 30 sec on, 30 sec off; and salt concentration was readjusted using M2 (10 mM PIPES pH 7.4, 600 mM KCl, 150 mM NaCl, and 22.5 mM MgCl₂) using a ration of 4:1. Readjusted lysate was centrifuged at 3000 xg for 10 minutes to remove the nuclear fraction. Supernatant was then centrifuged at 100,000 xg for 30 minutes to separate out cytoplasmic and membranous fractions. The cytoplasmic fraction was acetone precipitated at -20 °C for 20 mins. Precipitated material was collected by centrifugation at 4000 rpm for 30 minutes and resuspended in 100 µl of SDS loading buffer. The membrane fraction was washed 3 times with M1/M2 buffer (at ratio of 4:1), before being resuspended in 100 µl of SDS loading buffer. 40 µl samples of each fraction were analysed by SDS PAGE.

2.9.7 Cytotoxicity Assay

1×10^3 RPTE cells were seeded into 96 well plate. The following day compounds to be tested for cytotoxicity or DMSO was placed on the cells at varying concentrations. The cells were incubated in the presences of the compounds for 24 hr. After 24 hr, media on cells was replaced with MTT reagent and incubated in the dark for 1 hr. MTT reagent was then replaced with DMSO to permeabilise cells and resolubilise precipitate that had formed. Quantification of precipitate formation was carried out at 560 nm and absorbance used to determine cell viability compared to the DMSO control.

2.9.8 Treatment of BK polyomavirus Infection

RPTE cells infected with Dunlop BK polyomavirus where treated 24 hr post-infection with drugs of interest. Infected RPTE cells were incubated for 24 hr (48 hr post-infection) and then media was collected. Collected media was stored at -80C until analysis of released virus.

Release virus was quantified by placing 200 μ l of collected media on naïve RPTE cells. After 2 hr media was replaced with fresh media, before cells were incubated for 48 hr. RPTE cells were then stained for IncuCyte analysis as described in 2.8.2.

2.10 Statistical Analysis

Statistical analysis of data throughout this project was performed using standard error and significance was calculated using the students' T test.

Chapter 3 : Expression and Purification of Recombinant BKPyV Agnoprotein

3.1 Introduction

Agnoproteins drastically vary in size from 30 to 154 amino acids [135], but share common key features, such as, regions of hydrophobicity and a high content of basic residues (figure 3.1). These features have hindered production of recombinant agnoprotein for extensive biochemical and structural analysis. The agnoproteins of BKPyV, JCPyV, and SV40 are highly conserved in their N-termini, with some variation at their C-termini after residue 50 (figure 3.2A). Comparatively across the full peptide sequence there is an 80% similarity between BKPyV and JCPyV, and a 60% similarity between BKPyV and SV40.

Further similarities between these agnoproteins are also evident from other characteristics, such as hydrophobicity (figure 3.2B) and the helical tendency (figure 3.2C). The agnoprotein of BKPyV, JCPyV, and SV40 contain a 21 amino acids region (between residues 21-42) which corresponds to high hydrophobicity and helical tendency. NMR studies utilising synthetically synthesised JCPyV agnoprotein [157, 159] have confirmed the existence of a stable helical structure between residues 24 and 39, which corresponds to the characteristic described above in JCPyV, BKPyV, and SV40 agnoproteins. The predicted helical domain (figure 3.2D) is amphipathic with two hydrophobic sides, an aromatic side, and a hydrophilic side, which suggests this helical domain may function both as a transmembrane (TM) domain and dimerization surface within the protein.

```

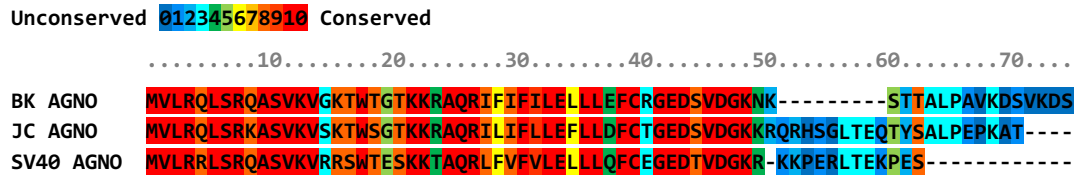
BKPyV  MVLRLQ--SRQASVKVG-KTWTGTTKRAQRIFIFI-LE-LLLEF--CRGEDSDGKKNK-----STTALPAVKDSVKD-----S-----
JCPyV  MVLRLQ--SRKASVKVS-KTWSGTTKRAQRILIFL-LE-FLLDF--CTGEDSDGKKRQRHSGLTE----Q--TYSALPEPKAT-----
SV40   MVLRRLL--SRQASVKVR-RSWTESKKTARLFVVFV-LE-LLLQF--CEGEDTVDGK-RKKPERLT-----EKPES-----
ChPyV  MVLRLQ--SRQASVKVG-KTWTGTTKRAQRIFIFI-LE-ILLEF--CRGEDSDGKQKRESTLT-----DKTGY-----
BPyV   MALQVWVLCRLKSLRNN-KL----MMCR--ILIEL-LK-ILLDV--LDSGDYADGPSDNPVTGIA-----KEEIVKCIDFLK-MLEA-----GDDIDKY--GFPEL----LA-----AHFANCLAV-CLKAARESDAMFCCS-LEANSDFN----
MaPyV  M-IQVLWQTLKCLLRVF-SI----SHASAAVLGDI-MC-ILEEFYKLAKEHKTVLNKVECGWELAR----FKQKINYYMDKVKATLKHCGKVQVMYFSKQGTDSVDRNLACVPELKGKGLALSLGHSEQEREETACDCLACQDMRQQLNLAEHLRSLTEELQKLLM
SqPyV  M-ARKL-MARKTPPLVGLDT---VQLRVETIWLTSQMDLFLVLT---KGEPRITASRASASRVATF-----GMTSVWL---KNSCF-----
CSLPyV  ---MKKILRLA-LCPDGVRLPACPGFAYW-----AVAPPSA-GPFGPQLLLL-----TRGAQPK-----
MyPyV  --MRGR-----SSW--YRRWKDLLKIFVNL-----NKRSGAPPR-----

```

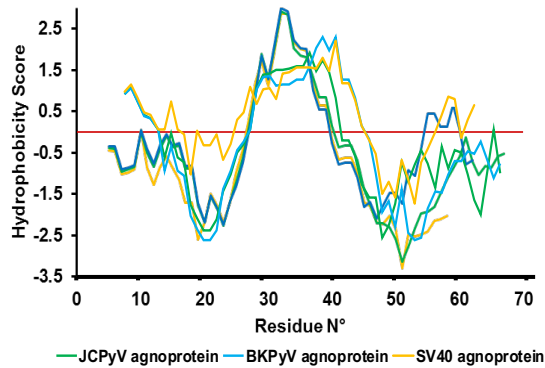
Figure 3.1: Amino acid conservation and hydrophobicity of polyomavirus agnoproteins

Alignment of agnoproteins encoded by BK polyomavirus (BKPyV), JC polyomavirus (JCPyV), Simian Vacuolating 40 (SV40) polyomavirus, Chimpanzee polyomavirus (ChPyV), Bovine polyomavirus (BPyV), Mastomys polyomavirus (MaPyV), squirrel monkey polyomavirus (SqPyV), California sea lion polyomavirus (CSLPyV), and Myotis polyomavirus (MyPyV). Alignment was performed by PRALINE (<http://www.ibi.vu.nl/programs/pralinewww/>) using BLOSUM62 matrix. Residues highlighted in red are basic residues and those highlighted in green are hydrophobic residues.

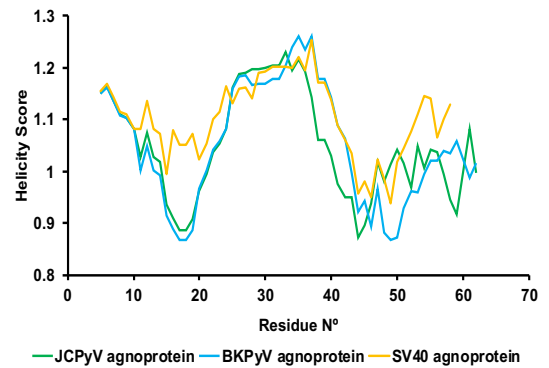
A



B



C



D

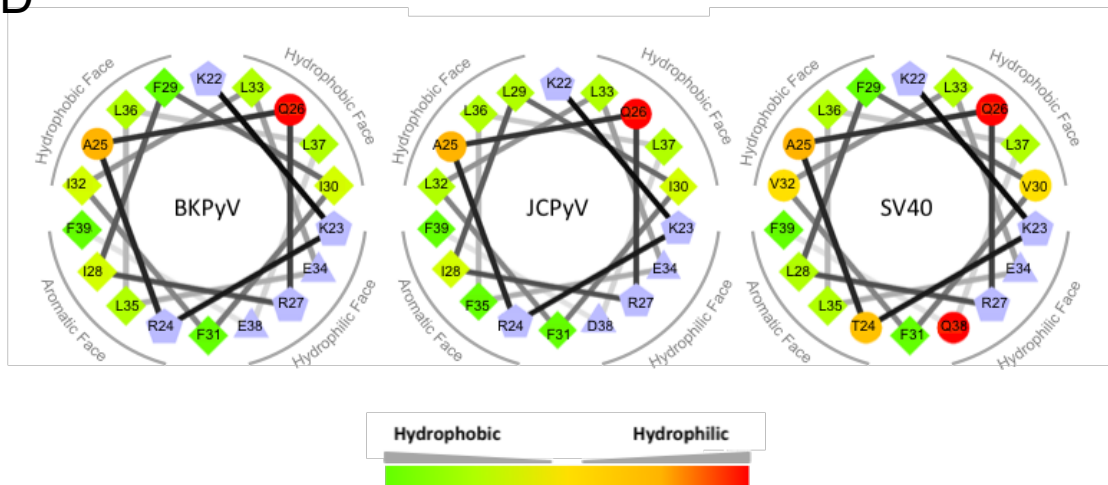


Figure 3.2: Computational Characterisation of agnoproteins from BKPyV, JCPyV and SV40

(A) Sequence Alignment: BKPyV, JCPyV, and SV40 Agnoprotein performed by PRALINE server. (B) Hydrophobicity score (Kyte Dolittle matrix [283]) across BKPyV and JCPyV agnoprotein amino acid sequence. (C) Helicity score (Deleage & Roux matrix [284]) across BKPyV, JCPyV, and SV40 agnoprotein amino acid sequence. (D) Helical wheel diagram representation of central helical structure for BKPyV, JCPyV, and SV40 agnoprotein, with each amino acid coloured either on the displayed hydrophobic to hydrophilic scale (green to red) or blue for polar residues.

Given the high degree of similarity, it is likely that the agnoproteins of JCPyV, BKPyV and SV40 have an analogous function within their respective virus lifecycles. Knockout studies in JCPyV [139, 140, 285], SV40 [140, 286], and BKPyV [22] have revealed that the absence of an agnoprotein results in a reduction in viral titre. In BKPyV polyomavirus, it was shown that this reduced virus titre is linked to a defect in viral egress. Infections with agnoprotein knockout virus generate progeny that are trapped in the nucleus, indicating a function for agnoprotein in nuclear and/or cytoplasmic egress [22]. The exact role that agnoprotein plays in viral egress is unknown as mechanistic studies are limited, however, there are multiple binding partners listed in the literature (table 1.2), and JC polyomavirus agnoprotein has previously been reported to exhibit viroporin function, linked to its ability to form oligomers [141, 142].

Viroporins are a family of small hydrophobic viral proteins, which form higher order oligomers for the purpose of permeabilising membranes to facilitate viral entry and egress [213-215]. When lysates from JCPyV infected cells are analysed by SDS PAGE, their agnoproteins have been observed to form dimers and higher order oligomers [142, 144, 157]. It is unclear how these oligomeric species function in the polyomavirus lifecycle, however alongside the predicted TM domain, these oligomeric species provide further support of a viroporin function. To establish if BKPyV agnoprotein functions as a viroporin, a comprehensive biochemical analysis was required. For this, a robust method for producing pure recombinant BKPyV agnoprotein needed to be developed. This expression and purification system needed to be compatible with downstream biochemical analysis and with future structural studies.

Purification of membrane associated proteins is challenging, technically difficult, and often requires significant optimisation. Previous studies on JCPyV agnoprotein [159] and HCV p7 [267] have used peptide synthesis to generate large quantities of functional viroporin. However, this method is very expensive and sometimes, as in the case of HCV p7, generates peptide which requires purification via rpHPLC [267]. An alternative technique is to overexpress proteins

in prokaryotic [287] or eukaryotic systems [288] and subsequently purify the recombinant proteins using chromatography. This technique theoretically provides a cheaper and more rapid pipeline for the expression of protein, however, purification via chromatography requires optimisation and yields are often sub-optimal.

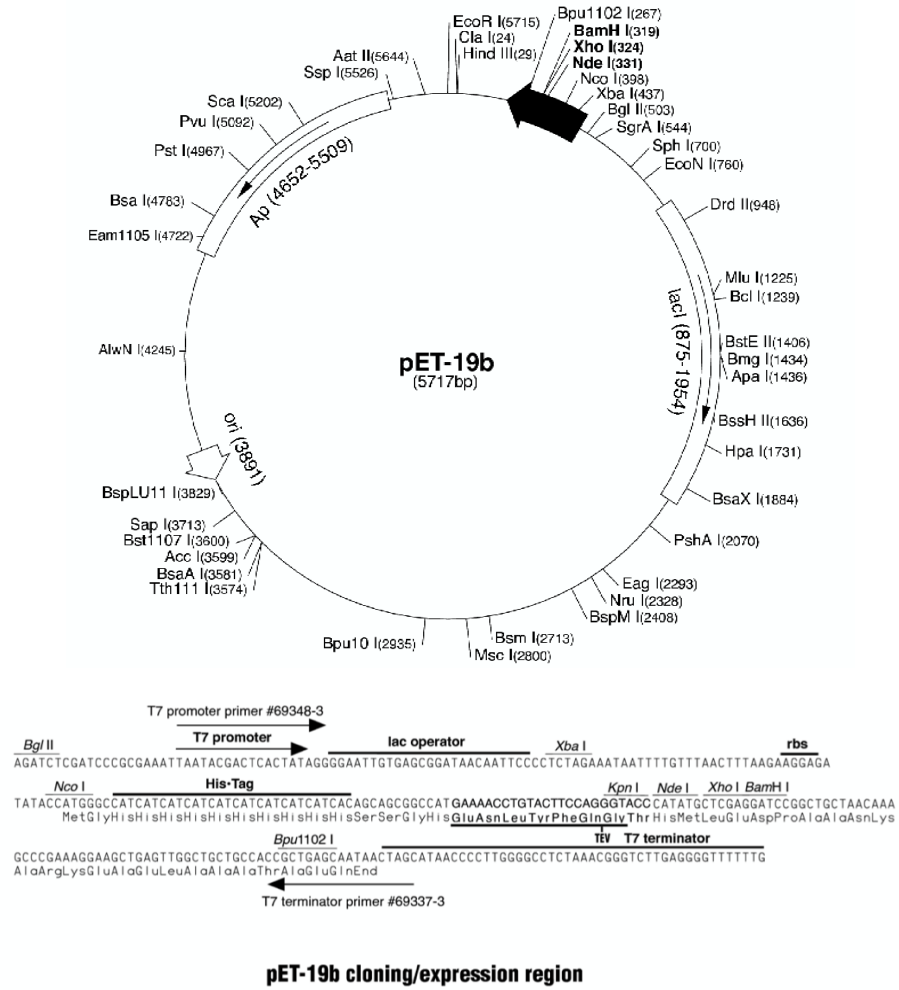
Previously, HCV p7 [264], hRSV SH [289], and HPV E5 [244] have been expressed in prokaryotic systems, as glutathione-S-transferase (GST) fusion proteins, which encourages hydrophobic proteins to aggregate and enter inclusion bodies. Insoluble inclusion bodies, containing GST-viroporin fusion proteins, were isolated, and following cleavage of the GST tag, reverse-phase high pressure liquid chromatography (rpHPLC) was used to purify the viroporin of interest. The major limitations of this purification method were poor reproducibility, and a dramatic reduction in yield during both inclusion body purification and rpHPLC.

This chapter describes a method of expression and purification for BKPyV agnoprotein, which moves away from the historical method of purifying viroporins. Importantly this method results in the final product being a 'detergent free' recombinant protein for biochemical analysis in liposomal membranes.

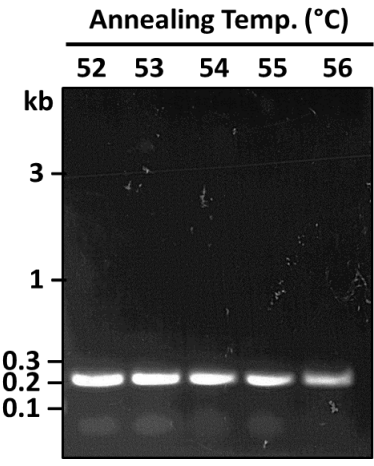
3.2 Cloning of 10x His BKPyV agnoprotein

The agnogene from BK polyomavirus DIK strain (AB211369.1) was codon optimised for expression in *E. coli* and synthesised as a DNA fragment (GeneWiz), which was amplified by PCR using pET19b BKPyV agnoprotein primer set (appendix). The resulting amplified fragment was cloned into pET19b TEV (figure 3.3A/B) between Kpn1 and BamH1 restriction sites, and successful insertion was determined via colony PCR (figure 3.3C). Two colonies produced bands at the correct size (~200bp) of the optimised agnogene insert. Plasmid DNA was prepped from these colonies and sent for sequencing, which confirmed the expected agnogene sequence.

A



B



C

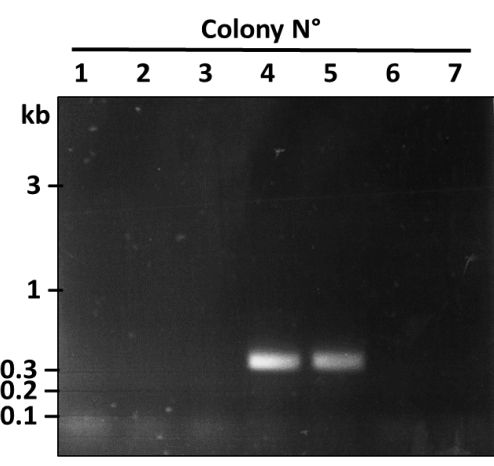


Figure 3.3: Cloning of pET19b BKP_yV agnoprotein

(A) Schematic of pET19b plasmid map. (B) 1% agarose gel showing annealing temperature gradient for the amplification of the codon optimised agnogene. (C) 1% agarose gel showing colony PCR for agnogene after ligation of pET19b vector and agnogene insert. 2-Log DNA Ladder (NEB) was used to confirm size of fragments.

3.3 Expression of Recombinant 10x His BKPyV agnoprotein

3.3.1 Provisional Optimisation of Expression

BKPyV agnoprotein was expressed as a fusion with a 10x His tag (figure 3.4A) to enable purification via nickel chromatography, and to negate the required cleavage of a larger affinity tag during purification. Previous unpublished work demonstrated that while BKPyV agnoprotein could be purified as a GST fusion protein, solubility and co-elution became an issue post-cleavage of the GST tag. Cleavage of the 10x His tag was not required for downstream applications as, unlike the GST tag, it was not expected to inhibit drug compounds from reaching the agnoprotein due to its smaller size.

Expression of 10x His BK agnoprotein was provisionally assessed in Rosetta, Rosetta 2, BL21 Gold, and BL21* strains of *E. coli*, at temperatures ranging from 27-37 °C, for optimal overnight expression by 1 mM IPTG induction. Resulting bacterial pellets were lysed; analysed by western blot, and agnoprotein expression levels were compared to an uninduced control.

The results of these expression trials showed that 10x His BK agnoprotein universally expressed under all conditions (figure 3.4B). An agnoprotein dimer, but not high order oligomers, of recombinant protein was also detected under all conditions during these expression trials, which supports previous observations that agnoproteins oligomerise under SDS PAGE conditions. In addition, the Rosetta stain was observed to have unfavourable “leaky” expression with a 10 kDa band visible in the non-induced control; and a non-specific band, which migrated just below the ~ 20 kDa recombinant dimer, was seen in both BL21 Gold and BL21*. The highest level of expression was seen the BL21 Gold stain at 37 °C, so these conditions were carried forward to a larger bacterial culture.

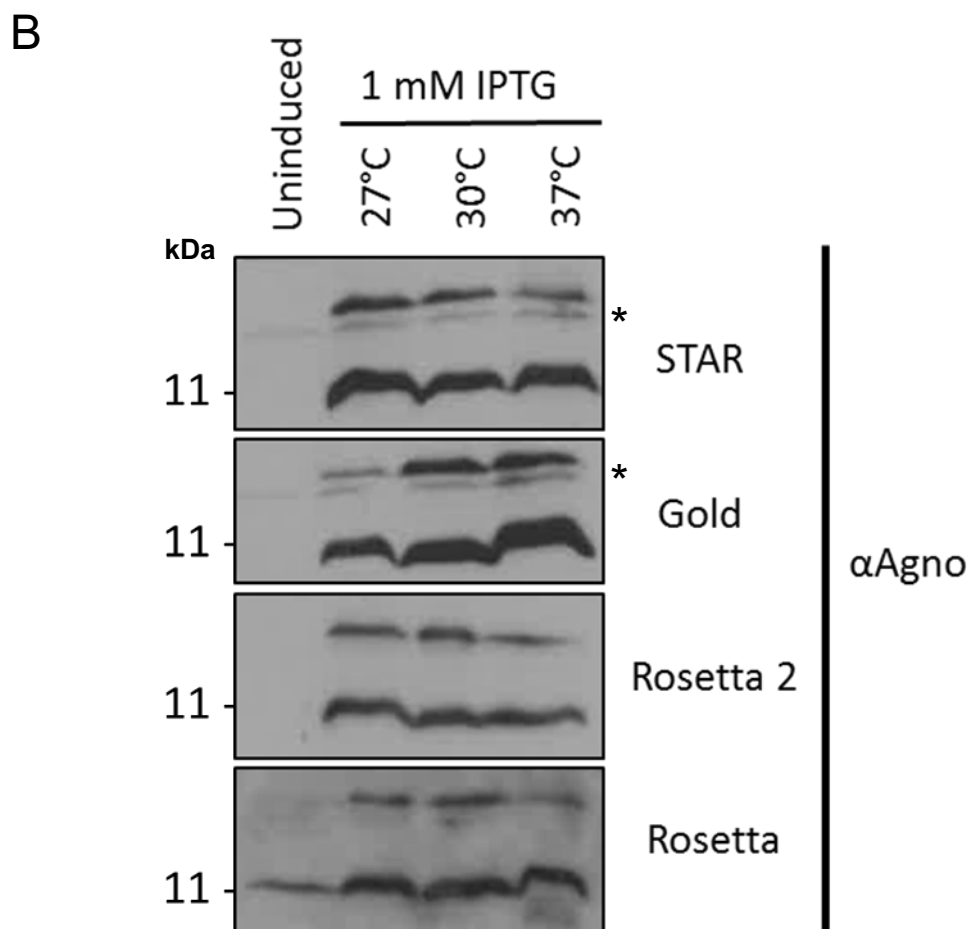
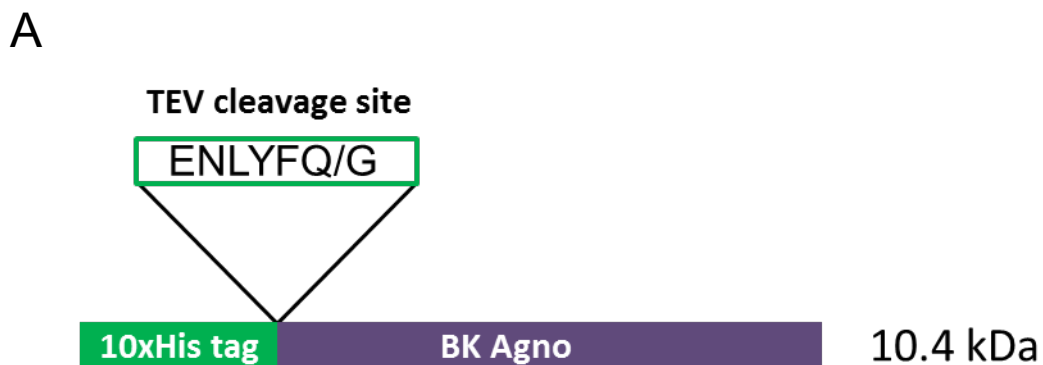


Figure 3.4: Test Expression of pET17b BKPyV agnoprotein

(A) Schematic of recombinant HIS BK agnoprotein expressed from pET19b BK agnoprotein. (B) Western blot using anti-agnoprotein antibody (pAB81058) [290] showing the test expression of 10x His BKPyV agnoprotein in multiple *E. coli* strains under varying temperatures. * denotes non-specific bands visible just below the dimer of recombinant agnoprotein.

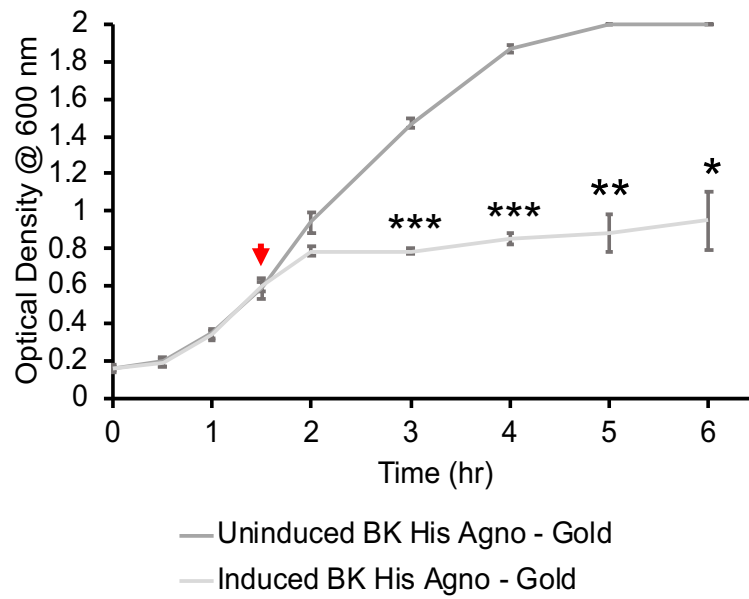
3.3.1 Toxicity of Recombinant BKPyV agnoprotein

Overexpression of recombinant proteins can result in unforeseen toxicity issues, often reducing yields of the target protein. In relation to our work, overexpression of HPV E5 [244], leads to deleterious effects on the growth and survival of bacterial cultures.

The toxicity of recombinant 10x His BKPyV agnoprotein was investigated in BL21 Gold cells by monitoring the optical density at 600nm (OD₆₀₀) of bacterial cultures during IPTG induction. OD₆₀₀ was measured over a period of six hours, and compared to an uninduced control, to obtain bacterial growth curves (figure 3.5A). The uninduced culture produced a typical bacterial growth curve containing a lag, exponential, and stationary phase. Whereas, the IPTG-induced culture produced a growth curve that indicated that 10x His BKPyV agnoprotein had a dramatic effect on bacterial growth. The overexpression of 10x His BKPyV agnoprotein was able to significantly hinder the bacterial exponential phase and result in a plateau of the growth curve approximately 30 mins after IPTG induction. By the third hour (1.5 hr post-induction), there was an average decrease in bacterial growth of 46.4% (P=0.00008), which increased to a 52.5% (P=0.01) decrease by the end of the observed time.

Samples of bacteria were also collected at each time point post-induction and analysed by western blot to confirm that agnoprotein expression had taken place (figure 3.5B). Analysis of induced bacterial lysates showed rapid expression of 10x His BKPyV agnoprotein to a level, which in general remained stable. Analysis of uninduced lysates, on the other hand, showed there was a small amount of “leaky” protein expression, which was then absent 4 ½ hr post-induction. This “leaky” expression suggests there was a threshold of 10x His BKPyV agnoprotein which the bacterial culture could tolerate. Taking these observations of bacterial growth into consideration it was decided to increase the volume of future large-scale protein expression to account for the reduction in final biomass obtained.

A



B

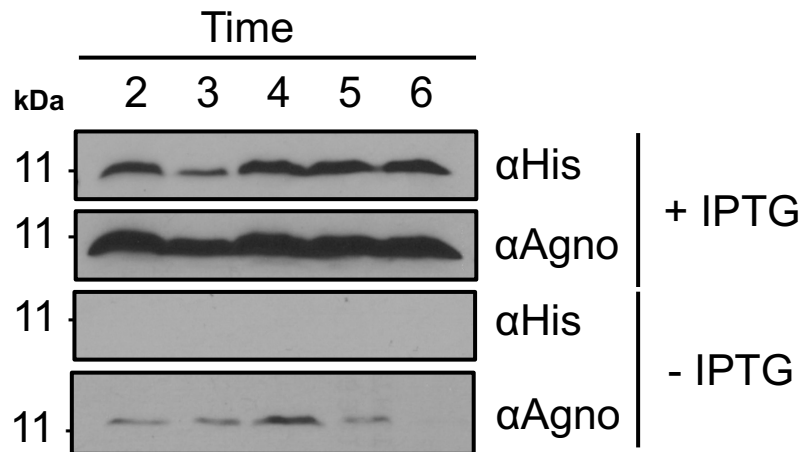


Figure 3.5: Effect of His BK agnoprotein on *E. coli* proliferation

(A) OD₆₀₀ measurements taken over a 6hr period. Arrow indicates the time of IPTG induction. (B) Representative western blot of bacterial lysate samples taken every hour after induction. Significance calculated using students' t-test: * ≤ 0.05 , ** ≤ 0.005 , *** ≤ 0.0005 , **** ≤ 0.00005 .

3.4 Isolation of 10x His BKPyV agnoprotein

Purification of recombinant proteins utilising an affinity tag [291] is a common method for initial extraction of proteins overexpressed in both eukaryotic and prokaryotic expression systems. However, in the case of membrane proteins, detergents [292] are often involved to solubilise recombinant protein in order to produce a eukaryotic/prokaryotic lysate containing the overexpressed recombinant protein. The choice of detergent used is often determined by downstream assays and can make purification more expensive as synthesis of some detergents involves high costs. Previous evidence in the literature [143], and within the Macdonald group, has shown that GST BKPyV agnoprotein can be solubilised in Triton x100.

To determine if 10x His BKPyV agnoprotein could also be solubilised, bacterial pellets were lysed in the presence of Triton x100 prior to analysis by 15% SDS PAGE (figure 3.6A) and staining with a Coomassie-based protein dye. Comparing non-induced bacterial lysates and lysates from bacteria induced with IPTG, there was no band visible at the expected size of 10x His BKPyV agnoprotein (~10 kDa). This was not entirely unexpected, as it has been observed that viroporins do not generally express to high levels, and in comparison with other proteins, they do not bind well to Coomassie stains.

In light of these observations, the lysate from an IPTG-induced culture was placed on a nickel chromatography column, and the bound protein was eluted on an imidazole gradient. Eluted fractions were then analysed by 15% SDS PAGE and Coomassie-based staining for the presence of 10x His BKPyV agnoprotein (figure 3.6B). In contrast to the analysis of whole cell lysates, a ~10 kDa band could be seen in the elution fractions, indicating that recombinant BKPyV agnoprotein could be solubilised by Triton x100. This ~10 kDa band could be seen eluting from the column in several fractions with a concentration of imidazole between 100 mM and 200 mM, along with contamination by higher molecular weight proteins.

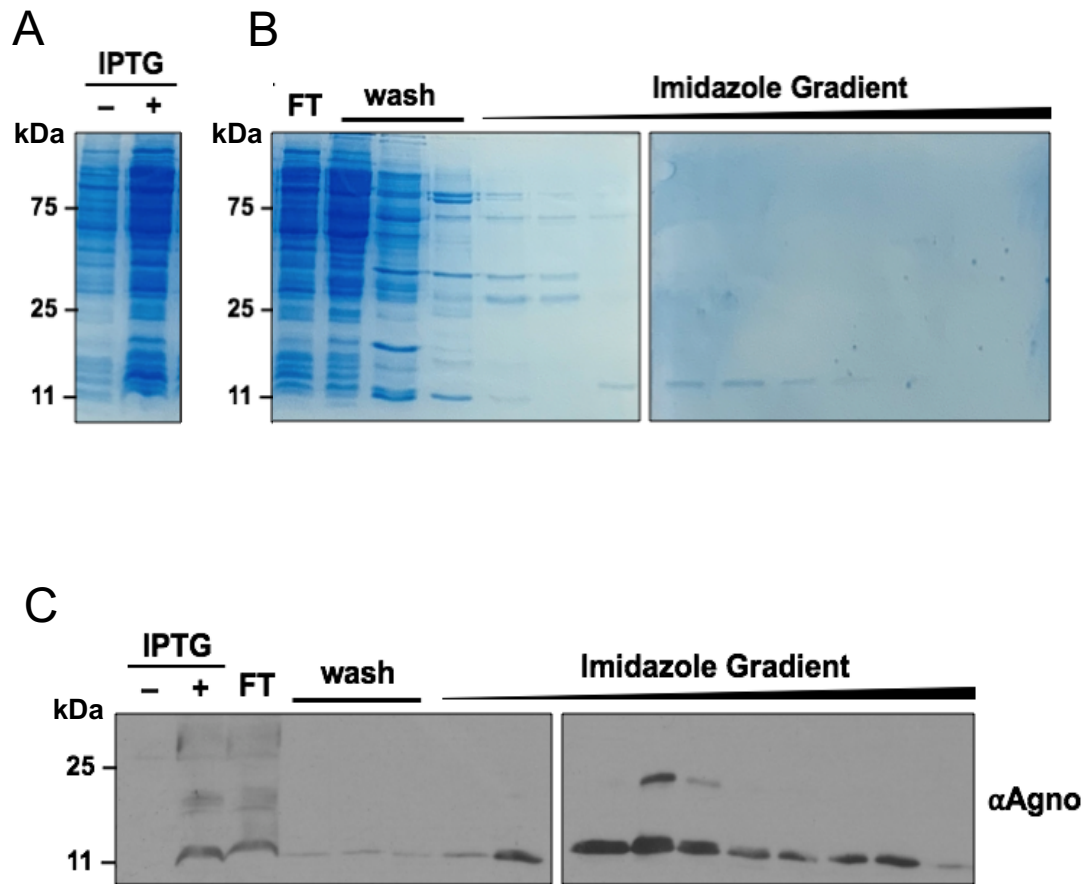


Figure 3.6: Nickel affinity chromatography purification of 10x His BkPyV agnoprotein

(A) 15% SDS PAGE of IPTG induced vs uninduced BL21 Gold cells transformed with pET19b TEV BkPyV Agnoprotein, stained with Coomassie protein stain. (B) 15% SDS PAGE of fractions collected during Ni affinity, stained with Coomassie protein stain. (C) Western blot of fractions collected during Ni affinity chromatography, blotted with anti-agnoprotein antibody.

Fractions were also analysed by western blot with an anti-agnoprotein antibody [290] to confirm the identity of the eluted protein (figure 3.6C). Western blot confirmed the ~10 kDa band as recombinant 10x His BKPyV agnoprotein and revealed that a small proportion of recombinant agnoprotein eluted in the 25 mM wash fractions, as well as, in all fractions across the imidazole gradient. With this in mind, only the fractions that were shown to be positive during Coomassie staining were taken forward, as these provided the highest concentration and purity of recombinant agnoprotein.

3.5 Purification of isolated 10x His BKPyV agnoprotein

Recombinant protein purification often involves a second round of purification in order to increase the purity of the target protein. There are many chromatography techniques, and selecting the appropriate technique depends on the biophysical characteristics of the protein. In the case of agnoprotein, the techniques investigated included rpHPLC, size exclusion chromatography (SEC), and ion exchange chromatography (IEX).

3.5.1 Reverse Phase High Pressure Liquid Chromatography (rpHPLC)

Purification of recombinant BKPyV agnoprotein was first achieved in the Macdonald group using C4 reverse-phase high pressure liquid chromatography (rpHPLC) (unpublished data). rpHPLC using low-hydrocarbon number matrices is useful for the purification of viroporins [244, 264, 289] as they bind to hydrocarbon-based matrices through hydrophobic interactions and can be eluted using volatile organic solvents, which can then be removed by lyophilisation. Previous attempts at purifying recombinant BKPyV agnoprotein used a GST-FLAG-BKPyV agnoprotein fusion construct, similar to those used for HCV p7 [264], hRSV SH [289] and HPV E5 [244, 282], and followed methodology outlined in those cases. The technique has previously worked well for HCV p7 [264] and hRSV SH [289], however, it was often unreliable when used for HPV E5 [244] and BKPyV agnoprotein.

The three caveats with this system were:

- Recombinant GST-FLAG-BKPyV agnoprotein was lost during inclusion body purification as only a proportion of overexpressed protein entered inclusion bodies and the construct suffered undesirable auto-cleavage of the GST tag.
- The final purified inclusion body supernatant contained many proteins, corresponding to a range of insoluble material from the *E coli* expression system. This was thought to cause high back-pressure and blockage of the C4 HPLC column.
- The FLAG-BKPyV agnoprotein construct behaved inconsistently on the C4 column; it often co-eluted with the cleaved GST tag due to a broad retention time, and sometimes either did not elute at all or eluted at a concentration below that of the sensitivity of the anti-agnoprotein antibody.

rpHPLC was investigated for the further purification of recombinant 10x His BKPyV agnoprotein after nickel affinity chromatography as the technique has worked well in the past for viroporins. Samples from nickel affinity were injected onto a new C4 column and eluted using a 5 to 95% acetonitrile gradient. Two sets of peaks were detected at 280 nm during this rpHPLC: the first set at 2-3 min and the second set at 17-20 min (figure 3.7A). Fractions collected at these retention times were dried down, resuspended in DMSO, and resolved by 15% SDS PAGE. A ~10 kDa band was visible in the 17-20 min fractions using both Ponceau S staining (figure 3.7B) and western blotting with anti-agnoprotein antibody (figure 3.7C). These results were repeated several times, before the HPLC column began experiencing high back-pressure and ultimately became blocked. Attempts to unblock the C4 column were unsuccessful, indicating that to continue using this technique the column would need regenerating weekly.

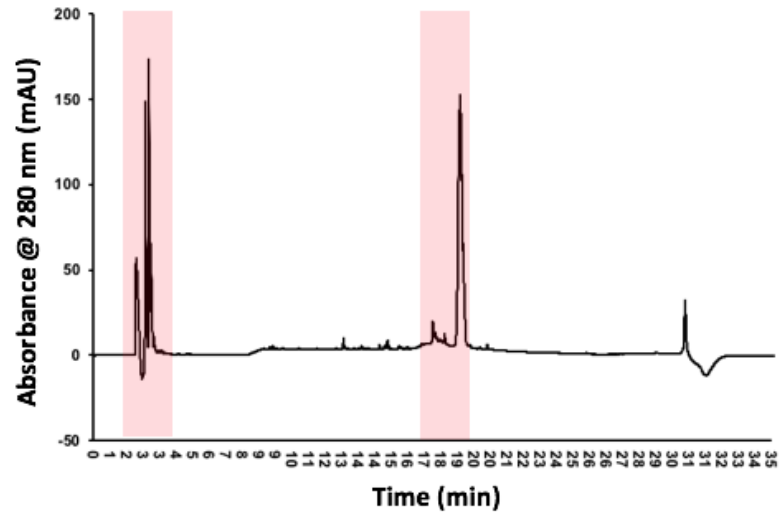
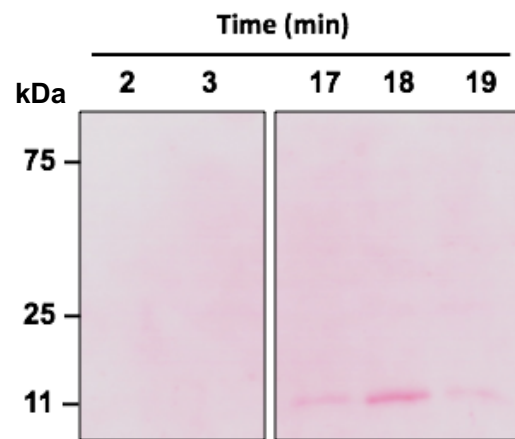
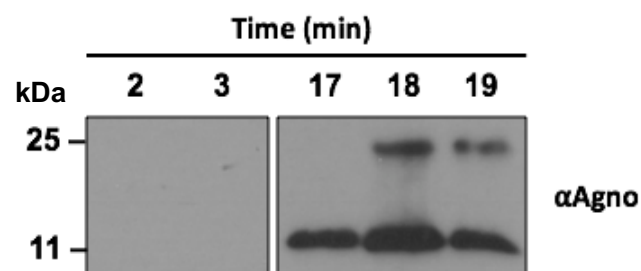
A**B****C**

Figure 3.7: rpHPLC of 10x His BKPvV agnoprotein

(A) 280 nm chromatogram of protein eluted from the C4 HPLC column during acetonitrile gradient from 5% to 95%. Red shading indicates were fractions were collected for the visible peaks. (B) 15% SDS PAGE of collected fractions, transferred to nitrocellulose and stained with Ponceau S protein stain. (C) Western blot of 15% SDS PAGE incubated with anti-agnoprotein antibody.

3.5.2 Size Exclusion Chromatography (SEC)

SEC was investigated as a potential technique for the purification of recombinant BKPyV agnoprotein, because native *E coli* proteins are typically >10 kDa [293], meaning 10x His BKPyV agnoprotein would likely have a different retention time compared to contaminating *E coli* proteins. Previously, SEC was used to purify a recombinant maltose-binding protein (MBP) JCPyV agnoprotein fusion protein [294]. MBP-JCPyV agnoprotein was eluted from a Sephacryl HR 2000 gel filtration column as a single peak, while analysis via 4-20% SDS PAGE showed dimeric and higher order oligomeric species [294]. This indicates that the agnoprotein fusions migrated through the gel filtration matrix as a single species, which was promising as there was a potential concern that agnoprotein oligomers may migrate across many fractions, diluting the recovered protein yield.

Recombinant 10x His BKPyV agnoprotein isolated via nickel affinity chromatography was injected onto a Superdex 200 increase 3.2/300 gel filtration column. Eluted material was monitored at 280 nm and 220 nm over the 2.4 ml bed volume, and collected as 50 µl fractions. Chromatograms obtained (not shown) contained no observable peaks, and when fractions were analysed by western blot (not shown) no detectable band was seen with the anti-agnoprotein antibody.

3.5.3 Cation Ion Exchange Chromatography (cIEX)

Cation ion exchange chromatography (cIEX) was also investigated in the purification of recombinant 10x His BKPyV agnoprotein. BKPyV agnoprotein has an unusually high isoelectric point of pH 10.1. This is a useful characteristic as native *E coli* proteins have isoelectric points which typically range from pH 5 to pH 9 [293]. 10x His BKPyV agnoprotein would therefore elute from a cation exchange column away from contaminating *E coli* proteins. Eluted fractions from nickel affinity chromatography were diluted 10-fold to lower the concentration of NaCl from 500 mM to 50 mM. This was necessary to ensure 10x His BKPyV agnoprotein bound to the cation exchange column. Resulting diluted sample was loaded onto a HiTrap SP ion exchange column at a rate of 1 ml/minute. Bound

protein was eluted using a NaCl gradient from 50 mM to 1 M. A single peak was detected at 220 nm towards the middle of the NaCl gradient (figure 3.8A); fractions were collected across this peak for analysis. 15% SDS PAGE analysis of collected fractions identified a ~10 kDa band via silver stain (figure 3.8B). This band was extracted and sent for mass spec analysis, which confirmed the ~10 kDa protein was recombinant 10x His BKPyV agnoprotein.

With this result in mind, cIEX was chosen as the method used to further purify 10x His BKPyV agnoprotein. cIEX chromatography successfully purified recombinant 10x His BKPyV agnoprotein, although it often diluted the protein below a concentration that was useful for downstream applications. Therefore, a method for concentration needed to be developed.

3.6 Concentration of purified 10x His BKPyV agnoprotein

Traditional concentration and dialysis techniques could not be used for BKPyV agnoprotein. These techniques both use synthetic membranes which BKPyV agnoprotein binds tightly to, meaning during concentration or dialysis there is a near complete loss of recombinant BKPyV agnoprotein.

To avoid this, recombinant 10x His BKPyV agnoprotein was concentrated using C4 solid phase extraction columns. Fractions from cIEX were applied to these columns and washed with 5% acetonitrile to remove salt. Bound protein was then eluted in 95% acetonitrile; dried down under a vacuum; and re-dissolved in DMSO. Samples of the same volume for pre- and post- concentration were resolved on 15% SDS PAGE and analysed by western blot (figure 3.8C).

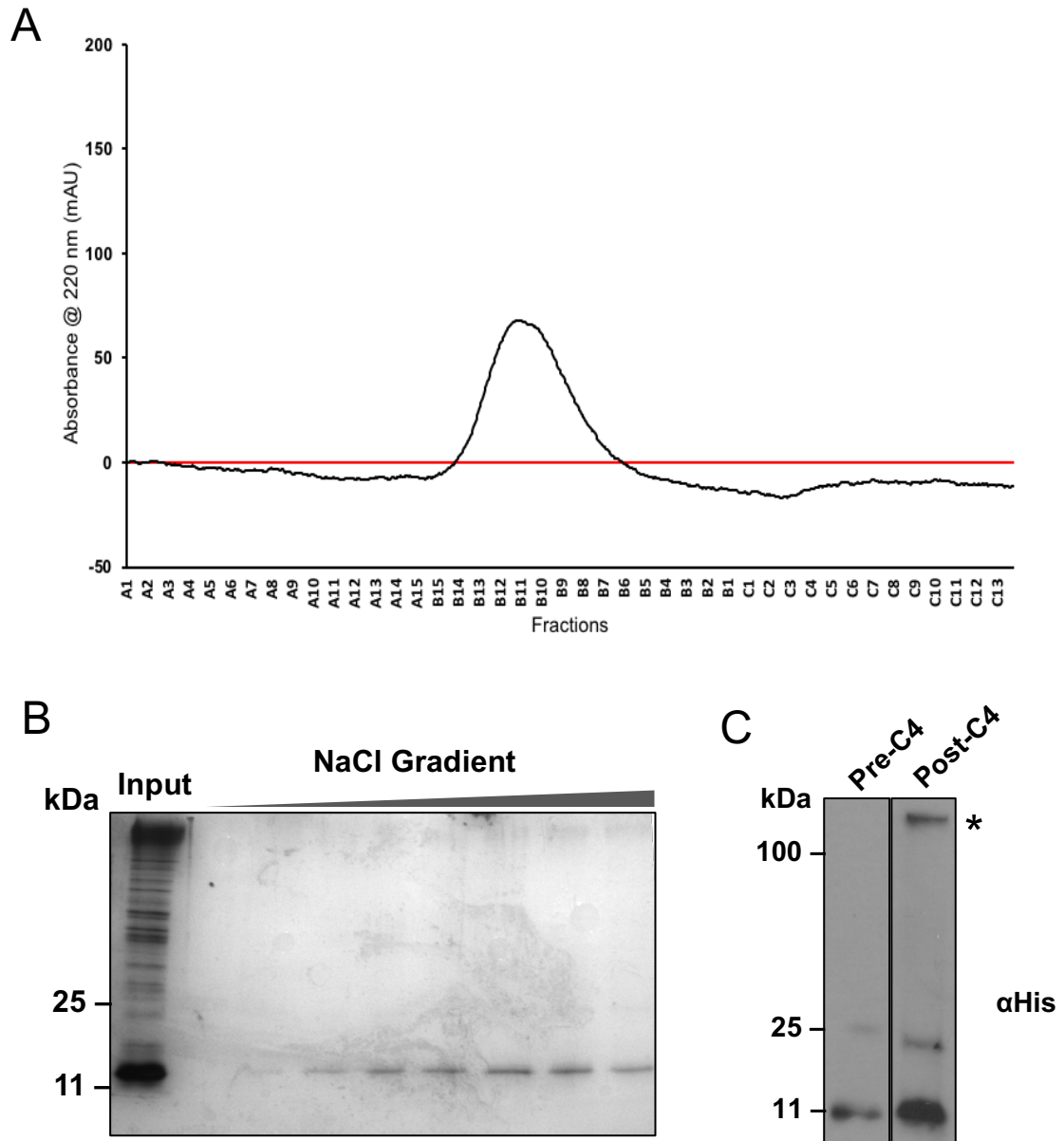


Figure 3.8: cIEX purification of recombinant 10x His BKPyV agnoprotein

(A) Chromatogram of 220 nm absorbance of material eluted from cation exchange column. (B) 15% SDS PAGE of fractions collected from observed peak, stained with silver stain (C) Western blot analysis of pre-C4 and post-C4 concentration. * notates potential aggregation species of 10x His BKPyV agnoprotein.

Both samples were positive for 10x His BKPyV agnoprotein, but the ~10 kDa band was more intense in the post-concentration sample and the less abundant dimeric species could be seen. Concentration of 10x His BKPyV agnoprotein also produced a much larger band, which is too large to be considered an oligomer and is probably the result of BKPyV agnoproteins aggregation-prone nature (figure 3.9). This larger band has also been seen in other examples of agnoprotein purification [294], with the MBP JCPyV agnoprotein construct. In this instance, this larger band is termed a higher order oligomer, but perhaps it is simply an aggregated species.

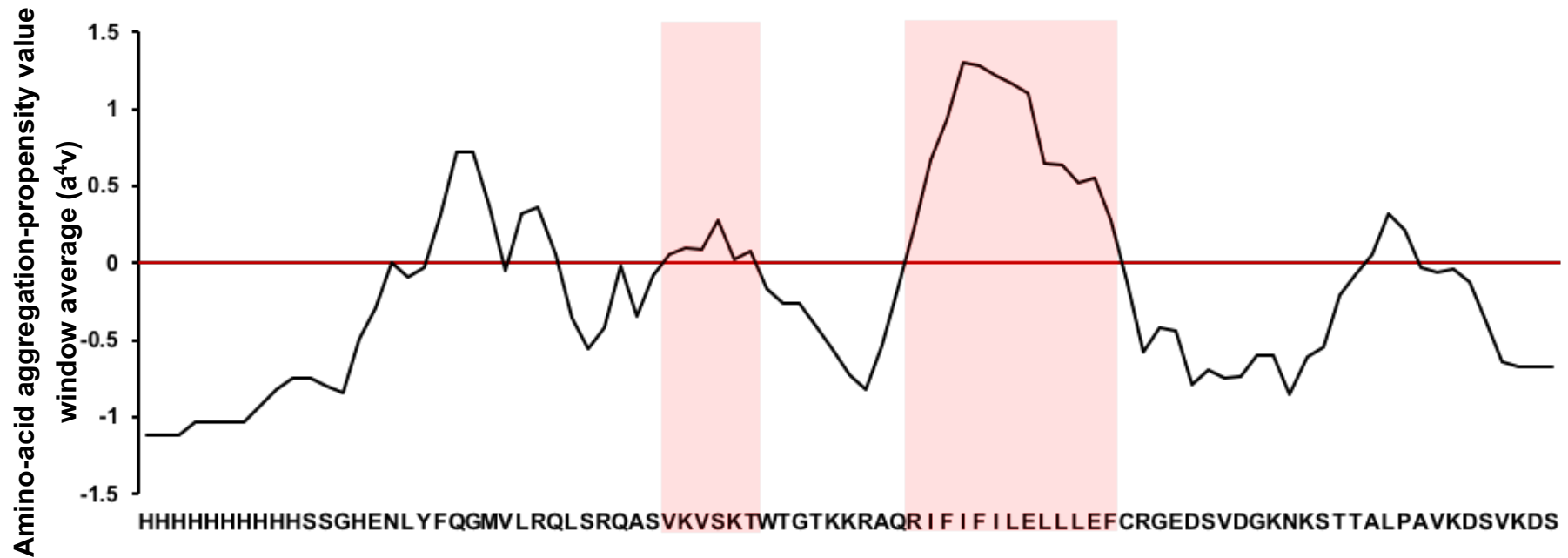


Figure 3.9: Aggrescan prediction of aggregation-prone “hot spots” in 10x His BkPyV agnoprotein

Analysis of aggregation-propensity of 10x His BkPyV agnoprotein using Aggrescan. Aggrescan looks at individual amino-acid aggregation-propensity in the context of the surrounding amino acids to produce a value termed a^4v . a^4v is derived, from a^3v values that are stated in N. Sánchez de Groot et al., by taking an average a^3v of individual amino acids and adjacent amino acids. Aggregation-prone hot spots are determined by 5 or more consecutive having a^4v values below the hot spot threshold which is currently -0.02. Regions highlighted in red show the predicted aggregation hot-spots for 10x His BkPyV agnoprotein [295].

3.7 Discussion

There is limited understanding of the role of agnoprotein in BKPyV infection and an absence in mechanistic detail. The difficulties associated with purification of recombinant BKPyV agnoprotein has led to a lack of biochemical characterisation and structural analysis. The hydrophobic nature of BKPyV agnoprotein and traditional methods of viroporin purification has hindered the development of a purification system for BKPyV agnoprotein, which produces a significant amount of protein.

This chapter has discussed the previous methods used to purify viroporins for biochemical characterisation, and the development of a more reliable purification system to improve upon previous limitations. The expression construct for BKPyV agnoprotein was redesigned to switch affinity tag from GST to 10x His. This avoided the difficulties faced with cleaved BKPyV agnoprotein co-eluting with cleaved GST, and avoided the inclusion body purification which produced a final sample that often blocked the HPLC column.

In redesigning the construct, the agnogene was codon optimised (appendix) for expression in *E coli* and cloned into pET19b (figure 3.3). Initial expression trials of 10x His BKPyV agnoprotein demonstrated that the construct expressed best in the BL21 Gold strain of *E coli* (figure 3.4). Although, further investigation into bacterial toxicity during IPTG induction revealed that this protein had a dramatic effect on bacterial growth. There was a 52.5% decrease in growth (figure 3.5), by the end of the observed growth period, in bacterial culture induced to express 10x His BKPyV agnoprotein.

These deleterious effects on growth were also seen with overexpression of other viroporins, when expressed in similar bacterial systems. HPV E5 [unpublished, Wetherill thesis, 2012], Rotavirus NSP4 [296], poliovirus 2B [297], IAV M2 [232], Semliki Forest virus 6K [227], and HIV1 Vpu [239] have all been observed to cause a decrease in optical density (OD) of bacterial cultures. Investigation into this phenotype, revealed that viroporins are capable of insertion into the bacterial membrane, resulting in destabilisation. This destabilisation can result in leakage

of bacterial cytoplasmic components into the periplasmic space [297], and disruption to osmotic balance across the bacterial membrane, resulting in lysis of the bacterial cell.

Although, BKPyV agnoprotein results in a decrease in growth, the effect was not dramatic enough to cause a decrease in OD. This suggests that unlike the other viroporins (mentioned above), BKPyV agnoprotein either does not induce rapid lysis of bacterial cells, or is inhibiting growth through other mechanisms. It has been shown in mammalian cells, that both JCPyV [148] and BKPyV [144] agnoprotein can inhibit cell proliferation, by dysregulating the cell cycle and inhibiting PCNA-dependent DNA synthesis, respectively. These mechanisms both rely on host protein-agnoprotein interactions, which are unlikely to take place in a bacterial host. Although, because of the aggregation-prone nature of BKPyV agnoprotein, it could be possible that overexpression caused a nucleation event for aggregation native *E. coli* proteins required for cell proliferation. Fortunately, the deleterious effects on bacterial growth did not hinder 10x His BKPyV agnoprotein overexpression and could be resolved by increasing bacterial culture volume.

Increasing the bacterial culture volume enabled an increased yield of recombinant 10x His BKPyV agnoprotein to take forward for purification. Overexpressed 10x His BKPyV agnoprotein could be visualised and identified, by 15% SDS PAGE using an anti-agnoprotein antibody (figure 3.6C), in the induced bacterial lysate. It was not possible to visualise the overexpression using a Coomassie-based protein stain when induced lysate was resolved beside a non-induced control (figure 3.6A).

Previously, it has been observed that, in our hands, Coomassie-based protein stains do not bind well to recombinant BKPyV agnoprotein. This observation made little sense, because BKPyV agnoprotein contains a high percentage of basic residues (5 arginine and 8 lysine residues), which should make it compatible with Coomassie-based stains. This is another observation that is shared by HPV E5 and BKPyV agnoprotein, though it remained unclear why Coomassie-based stains would bind so poorly to these proteins.

From initial analysis of bacterial lysates, it appeared that Coomassie-based stains also bound poorly to recombinant 10x His BKPyV agnoprotein. However, after nickel affinity chromatography a ~10 kDa band corresponding to 10x His BKPyV agnoprotein could be seen via Coomassie-based protein staining (figure 3.6B). These observations indicate that Coomassie-based stains could bind to 10x His BKPyV agnoprotein, but the sample concentration must overcome a certain threshold for visualisation to be successful.

Nickel affinity chromatography proved to be a consistent technique for the isolation of recombinant 10x His BKPyV agnoprotein from bacterial lysates. However, further purification was required to remove contaminating *E coli* proteins. Three distinct chromatography techniques were investigated for this further purification. C4 rpHPLC was revisited, as this technique has been successful in the purification of a selection of recombinant viroporins [20-22]. It was considered that the previous caveats of this technique could be avoided by using the nickel affinity chromatography isolation approach. Initially, C4 rpHPLC seemed very effective at the further purification of recombinant 10x His BKPyV agnoprotein. Two sets of peaks were detected at 280 nm (first set at 2-3 min and second set at 17-20 min) (figure 3.7A), from which samples were collected and resolved by SDS PAGE. The first of these peaks (2-3 min) were absent of protein and probably the imidazole carried forward from the nickel affinity chromatography. The second of these peaks were positive for a ~10 kDa band by Ponceau S staining (figure 3.7B); and further analysis by western blot confirmed that this band was recombinant 10x His BKPyV agnoprotein (figure 3.7C).

Subsequent C4 rpHPLC produced similar results for several attempts, before the peak corresponding to 10x His BKPyV agnoprotein began to decrease in absorbance units. This was followed shortly by high back-pressure within the system and ultimately complete blockage of the C4 rpHPLC column. Attempts were made to unblock the column, but these attempts were unsuccessful, and the column required regeneration. From these observations, it became clear that this was a major disadvantage of purifying viroporins via rpHPLC, as it seemed

residual recombinant protein accumulates on the column over time. To continue using rpHPLC the C4 column would have to be regenerated on a weekly bases to remove residual proteins. These residual recombinant proteins would also pose considerable complications should we attempt to generate and purify agnoprotein mutants, as we would not be entirely confident that our preparations would not be contaminated by wildtype agnoprotein.

Moving on from C4 rpHPLC, SEC and cIEX were investigated to separate 10x His BKPyV agnoprotein from the contaminating *E coli* proteins. These techniques would take advantage of BKPyV agnoproteins small size and high isoelectric point (IP), respectively.

There were initial concerns with SEC, as it was not clear if 10x His BKPyV agnoprotein would migrate through a gel filtration column as a monomeric or a range of oligomeric species. If 10x His BKPyV agnoprotein migrated through the column as a mixture of species, there would be the risk of diluting the protein sample and not being able to visualise its elution. SEC has previously been used in the purification of MBP-JCPyV agnoprotein [294], with a single peak being observed, suggesting that agnoproteins do migrate as a single species through a gel filtration matrix. Though, in the case of MBP-JCPyV agnoprotein, SEC seemed unable to separate out the oligomeric states as bands for dimeric and a high order oligomeric species were observed on SDS PAGE.

Attempts to repeat this result with recombinant 10x His BKPyV agnoprotein were unsuccessful. No visible 220 nm absorbance was observed, and no bands were detected via western blot. This indicates that 10x His BKPyV agnoprotein either eluted at a concentration below the detection sensitivity of the detector and anti-agnoprotein antibody; or did not elute at all. It was unknown if recombinant protein bound irreversible to the gel filtration matrix and would accumulate overtime as was seen with rpHPLC. If recombinant protein remained in the column matrix, when it comes to expressing mutant agnoproteins this technique would be unsuitable as it would be impractical to have a gel filtration column for each mutation.

For these reasons, cIEX was a very appealing technique as disposable columns could be used without too much cost. 10x His BKPyV agnoprotein has a relatively high IP of 10.01, meaning it would bind a cation exchange matrix. To achieve this the salt concentration in the fractions from nickel affinity chromatography needed to be reduced. This could not be achieved by dialysis, because BKPyV agnoprotein has a strong binding affinity to dialysis membranes. Therefore, samples were diluted 10-fold and loaded onto cIEX columns at 1 ml/min using a peristaltic pump. Eluted fractions from the cIEX columns were collected from the observed peak and resolved on 15% SDS PAGE. Coomassie-based staining of these SDS PAGE did not detect any protein, but with silver staining ~10 kDa bands could be found in the elution fractions. These bands were confirmed to be 10x His BKPyV agnoprotein by mass spec.

The resulting recombinant protein samples from cIEX were often diluted to a concentration that was unsuitable for downstream applications. This was problematic as, similar to dialysis membranes, BKPyV agnoprotein also has a high binding affinity to membranes used in protein concentrators. Therefore, to concentrate recombinant 10x His BKPyV agnoprotein, C4 solid phase extraction columns were used. rpHPLC has shown that recombinant viroporins bind to C4 matrices; so, by using C4 solid phase extraction columns, 10x His BKPyV agnoprotein could be captured, washed to remove salt, and eluted in 95% acetonitrile. These samples could then be lyophilised and re-dissolved, at the appropriate concentration, in DMSO.

The current expression and purification system (figure 3.10) described in this chapter has considerably improved the expression of recombinant agnoprotein, but still does not produce enough for the optimisation of structural techniques.

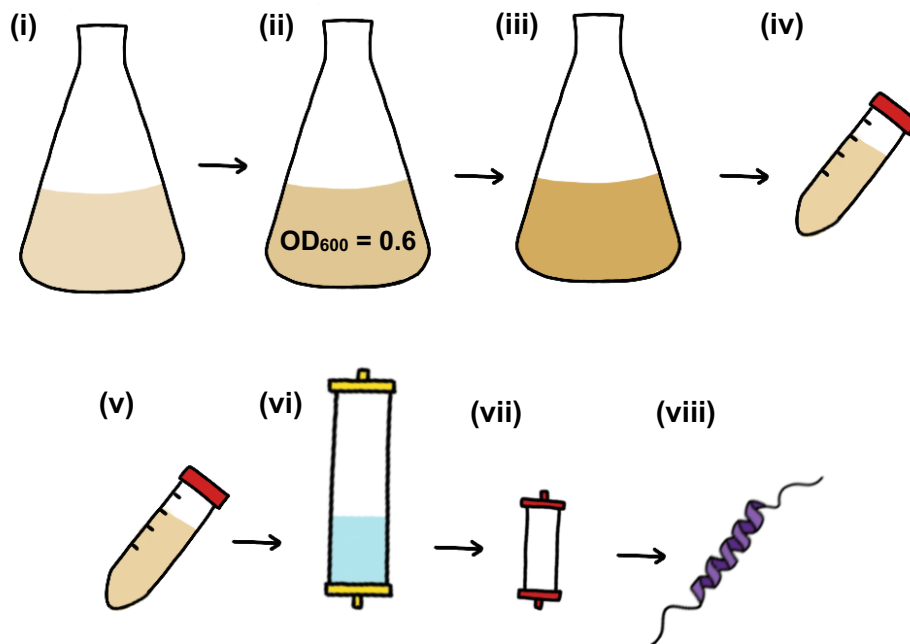


Figure 3.10: Schematic of purification method for recombinant 10x His BKPyV agnoprotein

(i) LB broth was inoculated with *E. coli* GOLD transformed with pET19b BKPyV agnoprotein. (ii) Protein expression was induced at OD_{600} 0.6 with IPTG. (iii) Bacterial culture was incubated overnight at 37°C. (iv) Bacterial biomass was harvested by centrifugation. (v) Bacterial pellet was lysed at room temperature followed by sonication and clarification via centrifugation. (vi) Clarified supernatant was supplemented with 25 mM imidazole and applied to NiNTA resin. Resin was washed in 25 mM imidazole, and bound proteins eluted. Fractions of eluted proteins were collected. (vii) Positive fractions were diluted 10-fold and applied to a cation exchange column. Bound proteins were eluted on a NaCl gradient. (viii) Collected fractions were passed through a C4 cartridge. Cartridge was washed 3x with 5% acetonitrile, and bound protein eluted in 95% acetonitrile. Eluted protein was dried down and resolubilised in DMSO.

Moving forward, with the aim of structural analysis, it would be worth considering the use of an *E coli* expression strain, such as C41(DE3) and C43(DE3), which were developed from *E coli* BL21(DE3) to have high tolerance to the expression of toxic recombinant proteins. These strains would potentially be beneficial in obtaining a higher yield of 10x His BKPyV agnoprotein, however, in doing so further optimisation would be required during purification. It became clear during the development of the strategy described above, that simply up-scaling the protocol had negative effects on final protein yields. This has also been observed in the expression of HCV p7 during the development of a high-throughput screen of potential viroporin inhibitors [221]. These limitations were probably due to local concentrations of BKPyV agnoprotein, on the chromatography column, reaching a threshold that catalysed aggregation. At the time, this issue was resolved by dividing initial bacterial cultures for multiple rounds of purification. Although, in moving towards achieving concentrations required for structural analysis, it would be attractive to develop the protocol to avoid the problems described.

Chapter 4 : BKPyV agnoprotein Oligomerises and Displays Channel-Forming Ability

4.1 Introduction

JCPyV agnoprotein has been shown to primarily localise to ER membranes, with an additional diffuse population in the cytoplasm [142]. Further studies investigating the localisation of BKPyV agnoprotein also observed a diffuse distribution in the cytoplasm, but also saw the formation of large, doughnut-like structures, which were determined to be lipid droplets [155, 156]. Lipid droplets are dynamic organelles that are thought to primarily act as lipid storage sites. They consist of hydrophobic cores (neutral lipids, triacylglycerols and sterol esters) surrounded by a monolayer of polar phospholipids [298]. Lipid droplets have been reported to act as the site of viral assembly in many viruses, such as HCV [299], dengue virus [300], and rotavirus [301]. As polyomaviruses assemble in the nucleus [166], it is more likely that lipid droplets participate in the anterograde transport of polyomavirus to the plasma membrane for release.

It was previously shown that the loss of agnoprotein, through siRNA knock-down, resulted in the inhibition of JCPyV infections [285]. Similar defects in viral replication have also been observed in SV40 and BKPyV infections when agnoprotein is absent [22, 286]. In the absence of a functioning agnoprotein, there was an observed decrease in viral titres for JCPyV, SV40, and BKPyV [22, 140, 285]. There have also been suggestions of a defect in virion packaging for agnoprotein-deficient JCPyV and SV40; and a visible defect, by electron microscopy, for agnoprotein-deficient JCPyV. These defects have never been reported for agnoprotein-deficient BKPyV. BKPyV infections that lack agnoprotein expression, result in a major defect in viral egress where progeny virions accumulate in the nucleus. The virions produced were thought to be fully mature infectious particles, and shown to be capable of consecutive infection of naive cells [22]. These data all suggest that agnoproteins play an essential role in nuclear, and possible cytoplasmic, egress of progeny virions. This is also

suggested by the observed cellular localisation of JCPyV and BKPyV agnoprotein which seem to originate at the ER and diffuse out to the plasma membrane.

Suzuki *et al.* (2010) reported that the agnoprotein of JCPyV was an integral membrane protein, which oligomerised *in vitro* and displayed a novel viroporin activity *in vivo*. The viroporin function of JCPyV agnoprotein was further characterised to be regulated by adaptor protein 3 (AP-3) in order to facilitate JCPyV agnoprotein trafficking to the plasma membrane, where agnoprotein increased membrane permeability to both hygromycin and Ca^{2+} [141, 142]. Calcium plays a critical role in the stability of polyomaviral capsids, so a mechanism by which progeny virus is protected in a calcium rich environment during its release would potentially prevent mature capsids disassembling [302, 303]. However, it remains unknown if manipulation of calcium homeostasis observed in Suzuki *et al.* was directly associated with agnoprotein or if there was an indirect mechanism through activation of host ion channels.

Currently the precise role of the viroporin activity of agnoprotein is not fully defined. If agnoprotein is hijacking host exocytic pathways to facilitate viral egress and release, then it is likely that both interactions with host proteins (table 1.2) and viroporin function may be involved. This chapter describes the characterisation of the channel forming ability of BKPyV-agnoprotein using recombinant agnoprotein in liposome-based assays and cell-based assays.

4.2 BKPyV agnoprotein Forms Oligomers

Oligomerisation is an essential step in the formation of a channel protein. To investigate the ability of BKPyV agnoprotein to form oligomers by self-associating, recombinant GST-FLAG BKPyV agnoprotein was first expressed in bacteria. This recombinant protein was then captured on glutathione agarose beads and used as the bait in a GST pull down assay. GFP BKPyV agnoprotein was expressed in HEK293T cell, and lysate prepared from these cells was incubated with the agnoprotein-primed glutathione agarose. After incubation the glutathione agarose was washed extensively, and bound proteins analysed via western blot to determine if there was an interaction between the agnoproteins. The western blot analysis (figure 4.1A) showed that GST-FLAG BKPyV agnoprotein successfully pulled down GFP BKPyV agnoprotein, indicating that BKPyV agnoprotein could at the very least self-associate, as has been previously suggested for JCPyV agnoprotein [294].

In addition, when recombinant 10x His BKPyV agnoprotein was analysed by SDS PAGE it displayed characteristic SDS-resistant dimeric and oligomeric species (figure 4.1B). This distinct oligomerisation pattern was concentration dependent, with tetramers and pentamers only clearly visible when >2ug of protein was loaded. Similar analyses were performed with lysates from BKPyV infected cells, although we were unable to observe the agnoprotein dimers seen in other studies. To increase the likelihood of dimer formation, MOI of virus up to 50 were used to infect cells but even those were unable to provide evidence of dimerization in infections; and this will be discussed later in the chapter.

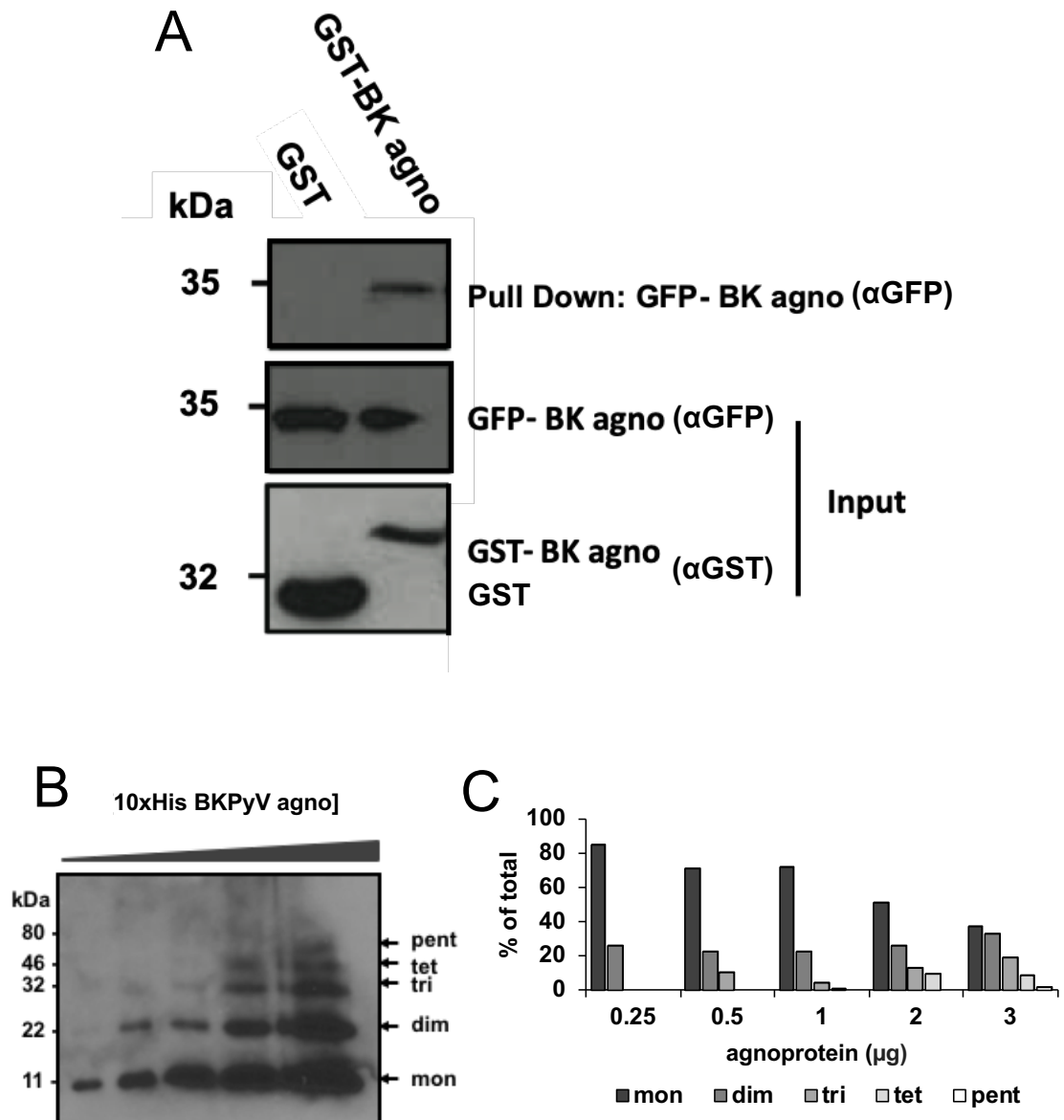


Figure 4.1: Oligomerisation of BKPyV agnoprotein

(A) Western blot analysis of GST pull down of GFP BKPyV agnoprotein using GST-FLAG BKPyV agnoprotein construct. (B) Oligomerisation analysis via western blot of recombinant 10x His BKPyV agnoprotein from SDS PAGE. Recombinant agnoprotein increases in concentration loaded across the lanes. These samples were not boiled. N=2 (C) Densitometry analysis of oligomeric species seen in (B) N=2.

4.3 BKPyV agnoprotein associates with membranes in mammalian cells.

HEK293T cells were transfected with FLAG-BKPyV agnoprotein-HA (method 2.1.3) to investigate if BKPyV agnoprotein associates with membranes in cells. Cell lysates were fractionated by ultracentrifugation to isolate the membranes fraction. Membrane fractions were washed to remove residual cytoplasmic proteins, before western blot analysis (figure 4.2). This showed successful fractionation as evidenced by the presence of the epidermal growth factor receptor (EGFR) in the membrane fraction and GAPDH in the cytosolic fraction. FLAG-BKPyV agnoprotein-HA was located in the membrane fraction, confirming it associates with membranes in cells. Similar experiments were attempted in virally infected RPTE cells, though levels of agnoprotein varied greatly and reliable repeats were unable to be obtained.

4.4 BKPyV agnoprotein has a varying orientation in membranes

The topology of agnoproteins has never been investigated, but they have been observed to localise to ER, lipid droplet, and plasma membranes in mammalian cells [142, 155, 156]. The topology of BKPyV agnoprotein was first predicted using the CCTOP server [304], which makes predictions using several different methods to come to a consensus topology. Using this server, BKPyV agnoprotein was predicted to have its N-terminus in cytosol and its C-terminus in the lumen of vesicles/ER (figure 4.3A). To validate of this prediction a dual tagged construct was designed with a FLAG tag at the N-terminus and a HA tag at the C-terminus. These dual tagged constructs have been successfully used in selective permeabilisation experiments to determine protein topology [305]. Digitonin is used in these experiments to selectively permeabilise (figure 4.3B) the plasma membrane, leaving organelle membranes intact. This allows the determination of topology based on the cytoplasmic availability of the tags.

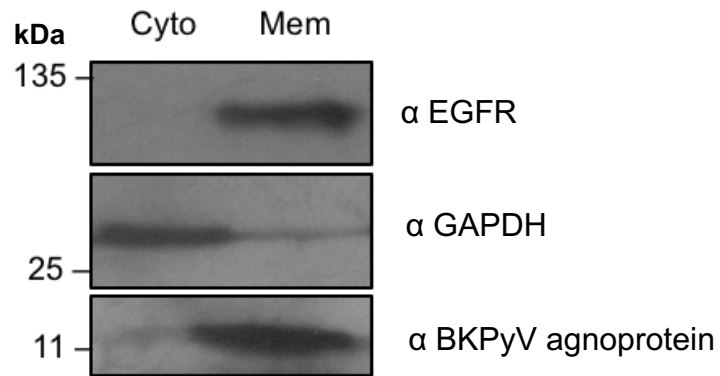


Figure 4.2: Subcellular fractionation of BKPyV agnoprotein

Western blot analysis of membrane/cytosol fractionation from HEK293T cells transfected with FLAG-BKPyV agnoprotein-HA. N=3.

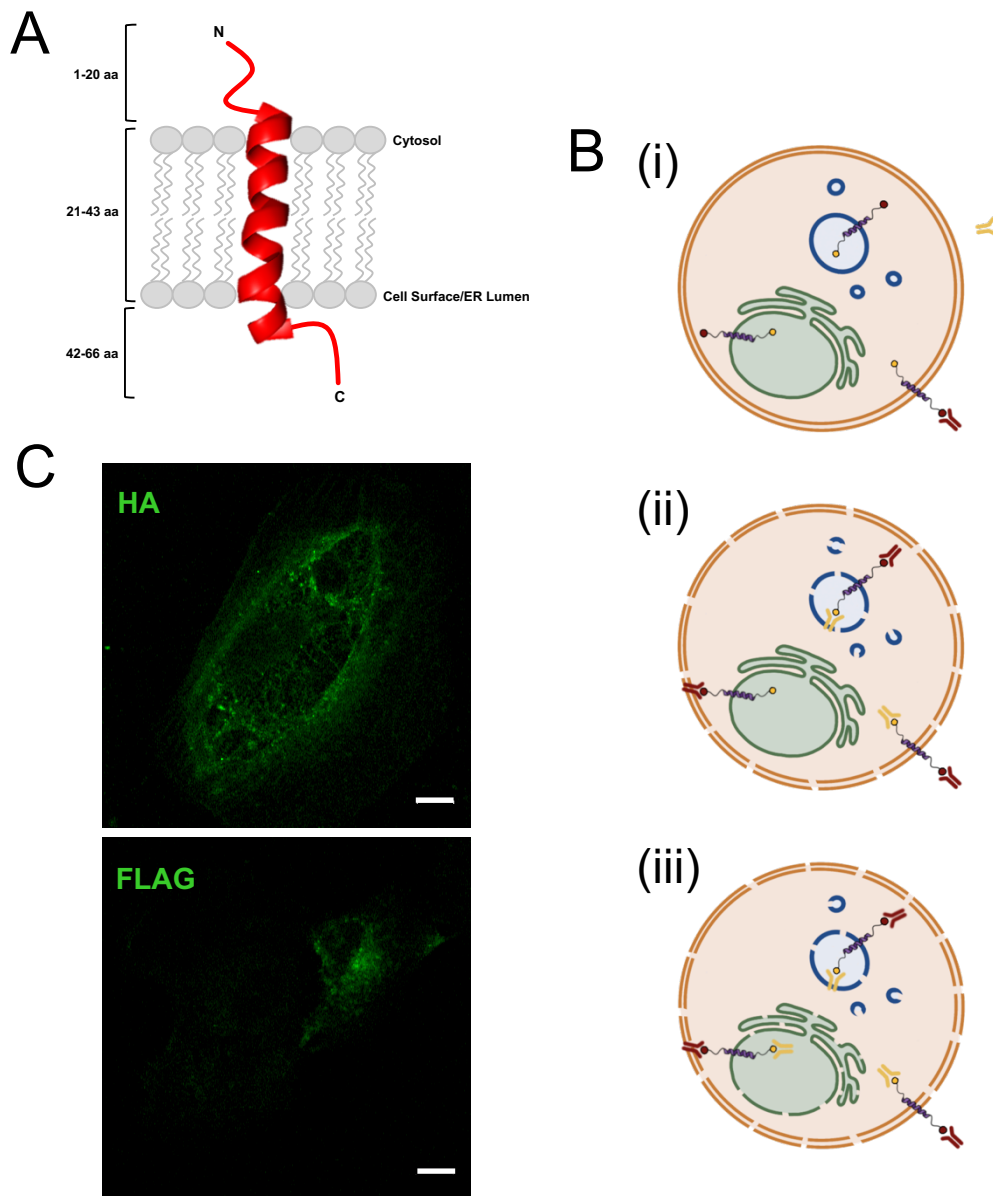


Figure 4.3: Topology of BKPyV agnoprotein

(A) A schematic of the predicted topology of BKPyV agnoprotein using the CCTOP server. (B) A schematic of selective permeabilisation experiment. (i) Non-permeabilised control; only surface exposed antigens bind antibodies. (ii) Digitonin permeabilisation; plasma membrane (orange) and lipid droplets (blue) permeabilised. Cytosolic and lipid droplet luminal antigens bind antibodies. (iii) Triton x100 permeabilisation; all membranes permeabilised. All antigens bind antibodies. (C) Immunofluorescence images of HTERT RPTEC cells transfected with pcDNA 3 FLAG-BKPyV agnoprotein-HA. Left panel was stained with mouse anti-HA antibody and right panel was stained with mouse anti-FLAG antibody. Scale bars = 10 μ m. N=1.

Upon investigation, BKPyV agnoprotein, was found to be unsuitable for this type of experiment. Firstly, the immunofluorescence analysis demonstrated that it localises to the plasma membrane and therefore both tags would likely be exposed during digitonin permeabilisation. Secondly, Digitonin can permeabilise lipid droplets due to their high cholesterol content and this is where a substantial population of BKPyV agnoprotein has been observed to localise. Thus, any agnoprotein residing in lipid droplets would also likely have both tags exposed during permeabilization.

Therefore, to determine the topology of BKPyV agnoprotein, we simply utilised a dual tagged construct to investigate which tag was exposed at the cell surface when staining non-permeabilised cells. HTERT RPTE cells were transfected with 3 FLAG-BKPyV agnoprotein-HA with TransIT LT. Following transfection, these cells were fixed and stained with either anti-HA or anti-FLAG antibodies to determine which terminus was exposed at the cell surface. Imaging of stained cells (figure 4.3C) showed that both HA and FLAG antibodies detected their respective tags. This could have indicated that BKPyV agnoprotein was positioned in membranes in both topological orientations. If time had permitted further experiments would have been performed to validate this initial observation. This is unusual for a viroporin, although molecular dynamic modelling of JCPyV agnoprotein dimers has suggested that it forms antiparallel dimers [306]. The implications of this will be discussed further, but these results suggest that BKPyV agnoprotein could be forming oligomeric species with an antiparallel structure. Dapi staining was not included in these images as TransIT LT forms complexes which interfere with staining. At the time of these experiments an alternative non-cytotoxic transfection reagent had not been found.

4.5 10x His BKPyV agnoprotein Displays Channel-forming Activity

4.5.1 BKPyV agnoprotein disrupts cellular membranes

To examine if BKPyV agnoprotein disrupted cellular membranes a functional assay was performed using the Merocyanine 540 (MC540) dye, which can measure the effect on lipid packing in cellular membranes. MC540 consists of a chromophore, comprised of heterocyclic, sulfonate, and two methylenic-tail groups, which emits at 570 nm. MC540 has been extensively used to probe cellular membrane structure, integrity and function [307-309]. The presence of its two methylenic groups enables MC540 to embed into biological membranes, where it forms an equilibrium between a fluorescent monomeric and non-fluorescent dimeric state (figure 4.4A). The MC540 equilibrium in membranes can be affected by changes in lipid packaging [141, 142, 308] and membrane potential [310]. This enabled an increase in MC540 fluorescence to be used to investigate protein-membrane association within live cells using flow cytometry (figure 4.4B).

To optimise MC540 staining, we took advantage of the available coxsackie B virus 2B protein, which has been extensively characterised and shown to display viroporin characteristics in cells. HEK293T cells were transfected with a GFP-CoxV 2B fusion and stained with MC540 for imaging by confocal microscopy. Images obtained from this staining confirmed that MC540 is capable of staining HEK293T membranes, and that the observed staining colocalised with GFP-CoxV 2B (figure 4.4C). Further optimisation was then carried out to achieve a suitable level of staining for flow cytometry, and appropriate gates were designed to quantify the change in MC540 fluorescence (figure 4.5). GFP-CoxV 2B was transfected into cells alongside GFP alone and a non-functional CoxV 2B mutant (L46N/V47N/I49N/I50N) (GFP-CoxV 2B mt) [311]. This mutation disrupted the oligomerisation and pore-forming activity of CoxV 2B, so was a useful control for determining if MC540 could be used to look at functionality of viroporins.

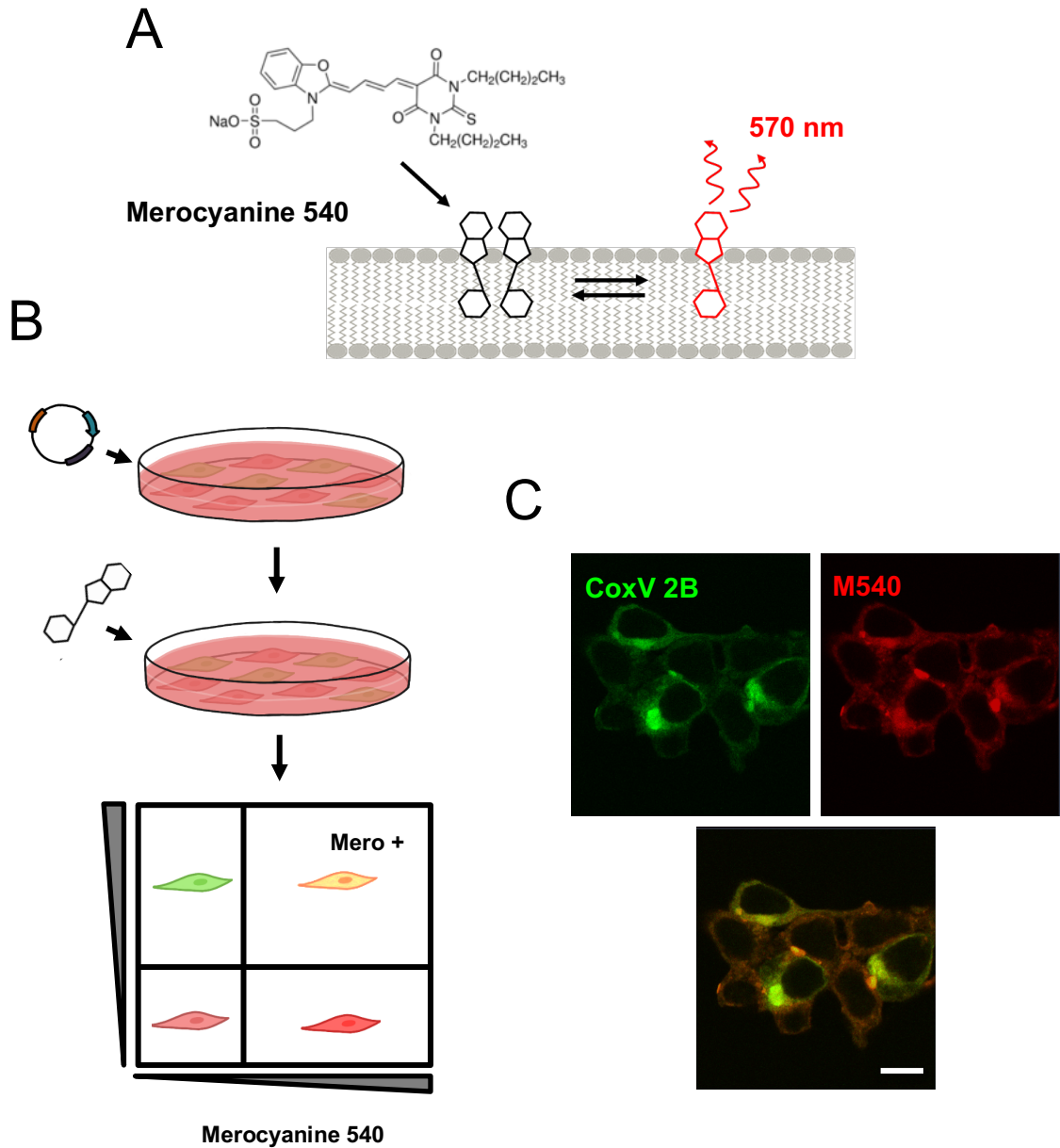


Figure 4.4: Merocyanine 540 (MC540) Assay

(A) Schematic showing the structure of MC540, and the equilibrium that it forms in cellular membranes. Dimeric MC540 was non-fluorescent and monomeric MC540 was fluorescent at 570 nm. (B) Schematic of experimental procedure. Cells were transfected with GFP constructs and stained with MC540 48hr post-transfection. Cells were then analysed by flow cytometry, by determining the percentage of green cells which are co-stained with MC540. (C) Confocal microscopy of HEK293T cells transfected with GFP-Coxsackie B virus 2B protein and stained with MC540. Scale bars = 10 μ m.

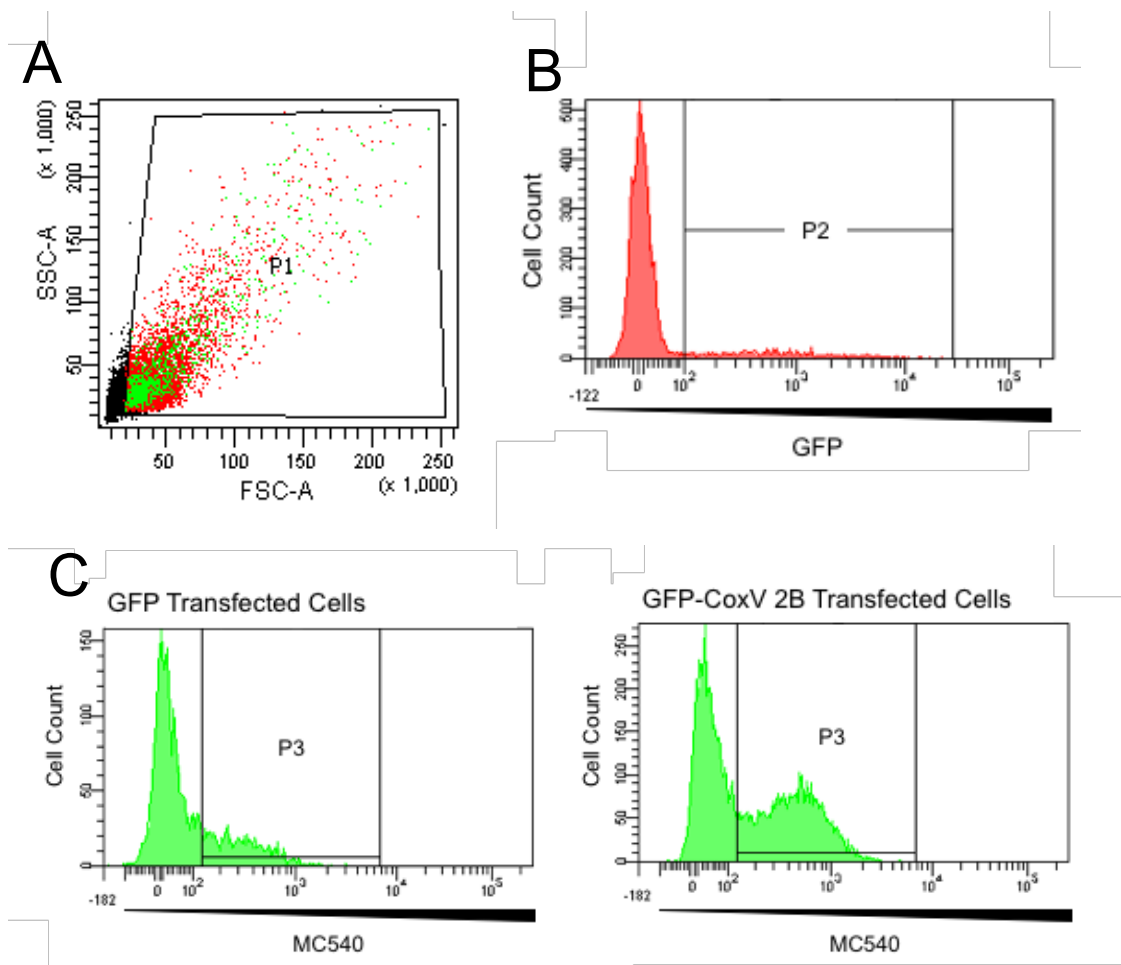


Figure 4.5: Flow cytometry gates applied during merocyanine analysis

(A) Dot plot showing area of side scatter (SSC) vs. area of forward scatter for cells analysed by flow cytometry during merocyanine assay. P1 was the gate applied to remove dead cells and cell debris, leaving the live population of cells. (B) A histogram of P1 cells against GFP signal. P2 was the gate applied to the GFP positive population of cells; determined by using a GFP negative control. (C) Histograms of P2 cells against MC540 signal. P3 was the gate applied to distinguish MC540 positive cells; determined by using a MC540 negative control.

GFP-CoxV 2B showed a significant ($P=0.001$) 2-fold increase in merocyanine fluorescence compared to the GFP control, and this increase was absent in cells transfected with GFP-CoxV 2B mt (figure 4.6). Significant increases in the merocyanine positive population were also seen for both GFP-BKPyV agnoprotein and GFP-JCPyV agnoprotein ($P= 0.002$, and 0.02 respectively). A series of truncated BKPyV agnoproteins (figure 4.7) were next tested in the MC540 assay to as part of a strategy to determine the regions of agnoprotein required for cellular membrane disruption. The truncations were designed to distinguish between the C-terminal region, the predicted helical domain, and the N-terminal region of BKPyV agnoprotein. Confocal microscopy was first used to determine the cellular localisation of the truncations (figure 4.8A). As expected, full length (FL) GFP-BKPyV agnoprotein distributed to the cytosol and formed multiple puncta in what are most likely lipid droplets. While the number of puncta was reduced by all truncations, this ability to form puncta was only lost completely from the truncations that lacked the predicted helical domain. A similar trend was seen with the MC540 assay, as the increase in MC540 positive cells observed for FT agnoprotein was significantly reduced only in GFP-BK agnoprotein 1-20 ($P=0.049$) and GFP-BK agnoprotein 42-66 ($P=0.007$) (figure 4.8B/C). These data from the truncational analysis suggest that the minimum sequence required for membrane disruption is amino acids 20-42, comprising the helical domain, though future studies are required to investigate this further.

Next, a series of point mutations (figure 4.7) were designed to identify residues in the helical domain critical for membrane disruption. Previous studies have investigated the Leu/Ile/Phe-rich region in the helical domain of JCPyV agnoprotein [158], showing that it is potentially important in the stability of the protein. Therefore, we designed L33/35/36/37A (GFP-BK agnoprotein 4L), F29/31/39A (GFP-BK agnoprotein 3F), and I28/30/32A (GFP-BK agnoprotein 3I) to characterise the role these residues might have in membrane disruption. In addition, the dibasic motif K8K9 in JCPyV agnoprotein was shown to be critical for viroporin function [142]. This dibasic motif is not conserved in BKPyV agnoprotein, though there is a dibasic motif at the N-terminus of its helical domain.

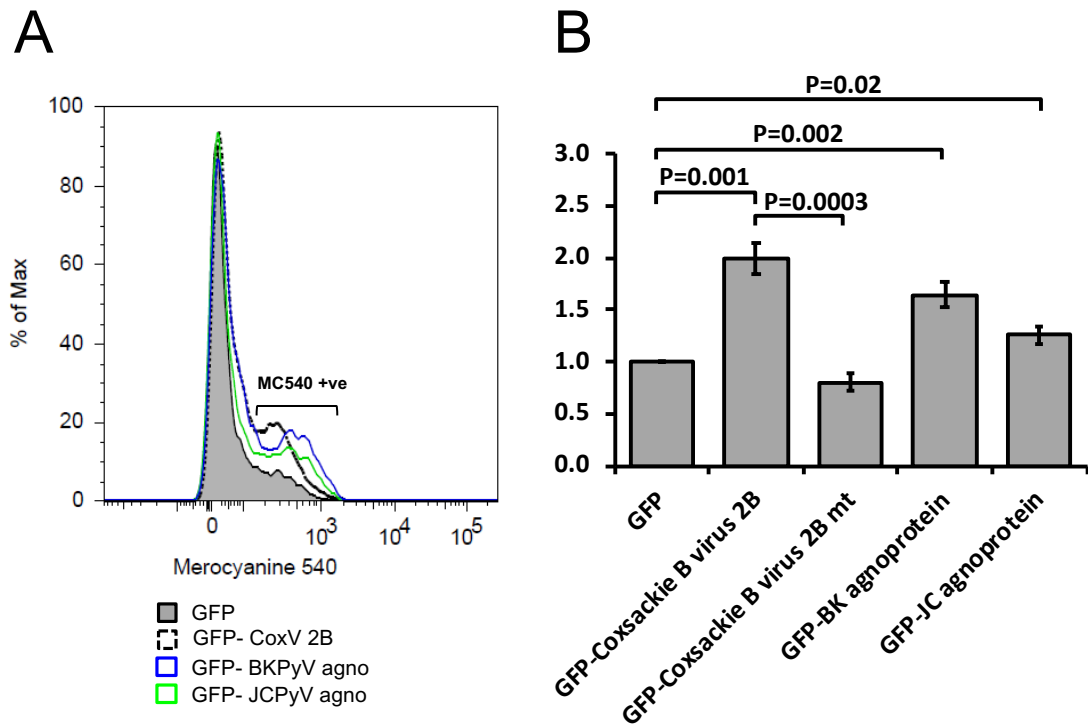


Figure 4.6: Merocyanine 540 Assay with BKPyV and JCPyV agnoprotein

(A) Histogram overlay of Merocyanine staining in HEK293T cells transfected with GFP constructs for CoxV 2B protein, BKPyV agnoprotein, and JCPyV agnoprotein. (B) Quantification of merocyanine positive population of cells relative to GFP control. N=5 in technical triplicate.

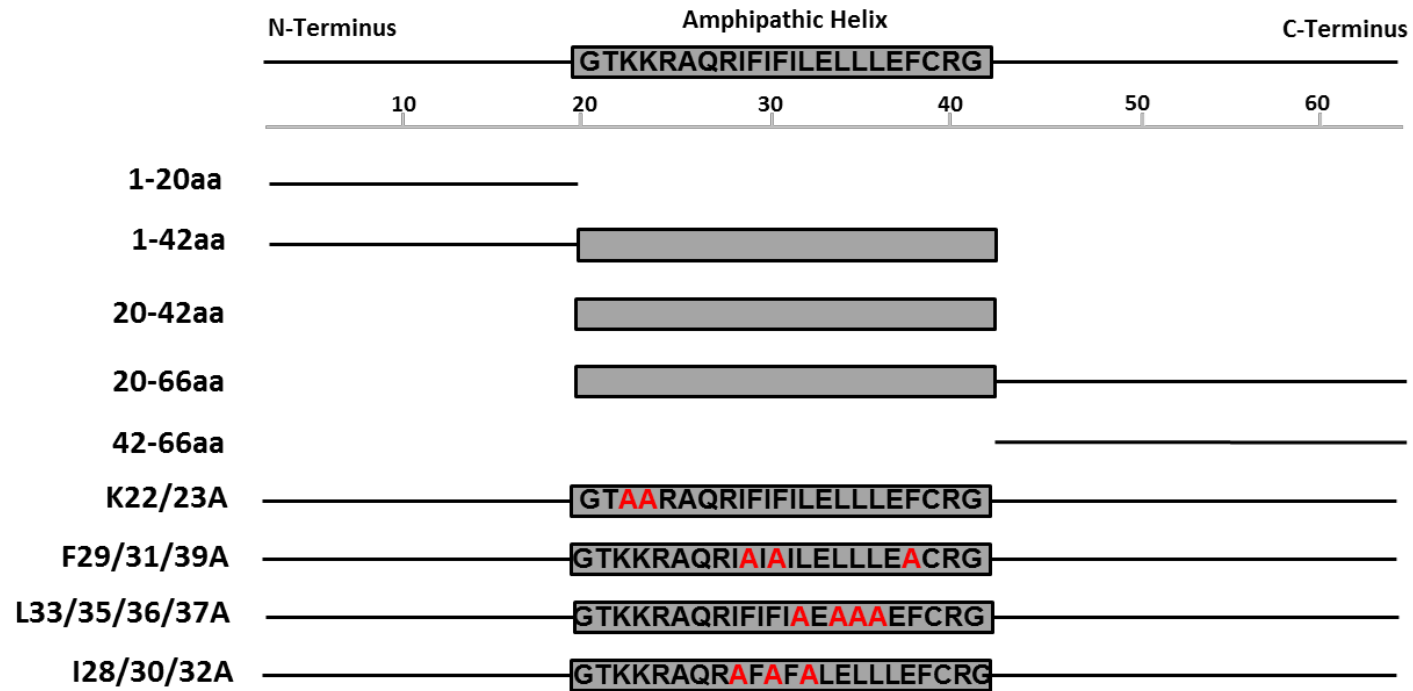


Figure 4.7: A schematic of BKPyV agnoprotein mutants cloned into peGFP-C1

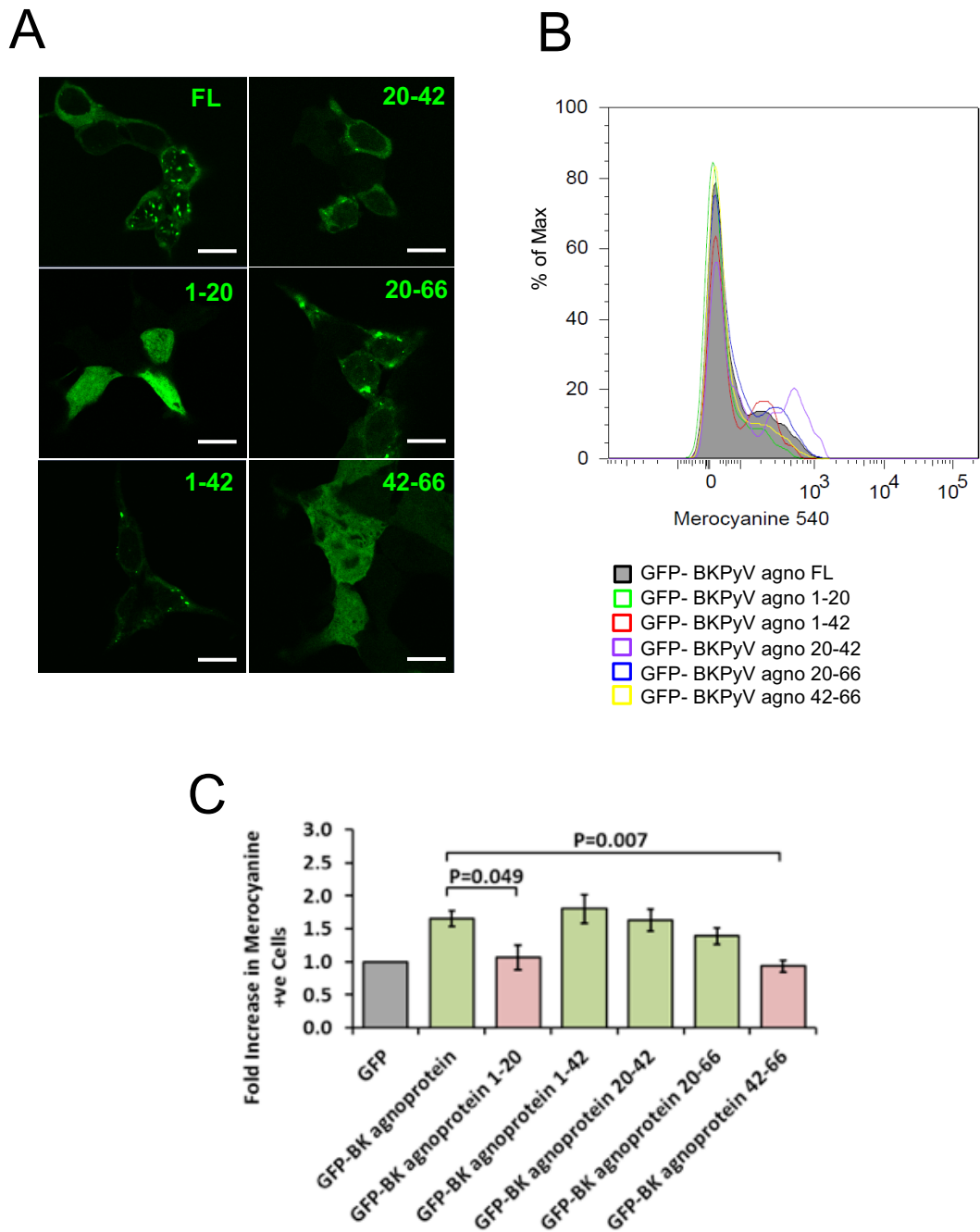


Figure 4.8: Merocyanine 540 Assay with BKPyV agnoprotein truncations

(A) Confocal images of truncated BKPyV agnoprotein constructs at 40x magnification. Scale bars = 10 μ m. (B) Histogram overlay of Merocyanine staining in HEK293T cells transfected with GFP-truncated BKPyV agnoprotein constructs against full length BKPyV agnoprotein. (C) Quantification of merocyanine positive population of cells relative to GFP control. N=5 in technical triplicate.

The point mutation K23/24A (GFP-BK agnoprotein 2K) was designed to determine if this dibasic motif had a similar role to K8K9 in JCPyV. Initially, these point mutations were analysed by confocal microscopy to investigate cellular localisation (figure 4.9A). GFP-BK agnoprotein 2K, GFP-BK agnoprotein 3F, and GFP-BK agnoprotein 3I all reduced the number of puncta observed within the cytoplasm, whilst GFP-BK agnoprotein 3F was noted to have visually larger puncta. Furthermore, results from the MC540, showed that GFP-BK agnoprotein 3F ($P=0.02$) and GFP-BK agnoprotein 4L ($P=0.006$) significantly decreased MC540 positive cells compared to wt. (figure 4.9B/C). GFP-BK agnoprotein. This indicates that phenylalanine and leucine residues could be essential residues involved in BKPyV agnoprotein's ability to disrupt cellular membranes.

4.5.2 BKPyV agnoprotein does not permeabilise the plasma membrane

JCPyV agnoprotein has been observed to permeabilise the plasma membrane [141] in assays which investigated the ability of hygromycin to enter mammalian cells. If mammalian plasma membranes are intact then - at low concentrations - hygromycin is unable to enter the cell. If the plasma membrane is compromised, then hygromycin enters and the inhibition of translation can be observed as a read-out. This assay has classically been utilised to investigate membrane integrity in both mammalian cells and has previously shown that CoxV 2B permeabilises the plasma membrane [218].

In order to investigate if BKPyV agnoprotein permeabilises the plasma membrane; GFP, GFP-CoxV 2B, GFP-CoxV2B mt, GFP-BKPyV agnoprotein and GFP-JCPyV agnoprotein were transfected into HEK293T cells. Transfected cells were treated with low concentration hygromycin, and then O-propargyl-puromycin was used to probe for protein translation. O-propargyl-puromycin is a puromycin analogue, which becomes incorporated into newly synthesized protein chains. It contains an alkyne function group that can be used to perform a copper(I)-catalyzed azide alkyne cycloaddition with an azide functionalized fluorescence probe.

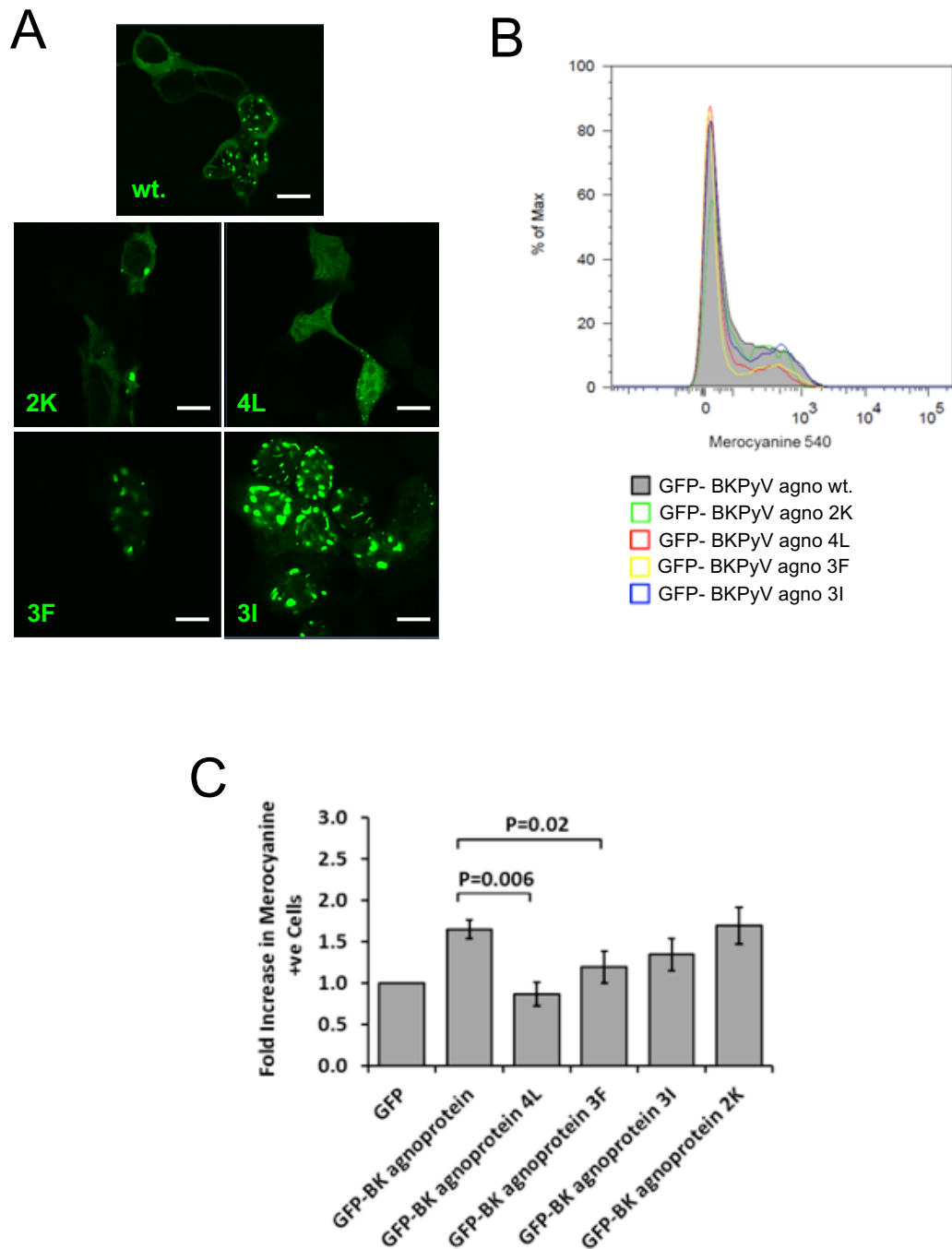


Figure 4.9: Merocyanine 540 Assay with BKPvV agnoprotein point mutants

(A) Confocal images of alanine mutant BKPvV agnoprotein constructs at 40x magnification. Scale bars = 10 μ m. (B) Histogram overlay of Merocyanine staining in HEK293T cells transfected with GFP-alanine mutant BKPvV agnoprotein constructs against wt. BKPvV agnoprotein. (C) Quantification of merocyanine positive population of cells relative to GFP control. N=5 in technical triplicate.

This enabled visualisation of active protein translation, by flow cytometry using similar gates to the MC540 assay to isolate the GFP positive population (figure 4.5A/B), in the population of cells which expressed GFP fusion proteins (figure 4.10A/B). If the plasma membrane became compromised by the protein that was expressed, then the number of cells which were both translationally active and green would decrease. This was seen with the control protein GFP CoxV 2B, which resulted in a significant 3-fold decrease ($P= 0.02$) in translationally active cells (figure 4.11).

GFP CoxV 2B mt did not result in the decrease of translationally active cells, confirming that plasma membrane permeabilisation to hygromycin was a consequence of the channel forming activity of 2B. GFP BKPyV agnoprotein and GFP JCPyV agnoprotein also did not result in the decrease of translationally active cells (figure 4.11), suggesting they do not permeabilise the plasma membrane. This is contradictory to what Suzuki *et al.* [141] observed in a similar assay, though this will be discussed further later in this chapter.

4.5.3 10x His BKPyV agnoprotein associated with and integrates into Liposomal membranes

To further explore the nature of the interaction, between BKPyV agnoprotein and membranes, we assessed the behaviour of 10x His BKPyV agnoprotein in an artificial membrane environment. Liposomal membranes, which have previously been utilised to investigate the interaction of viral protein with membranes, were employed to characterise this interaction.

Liposomes were composed of L- α -Phosphatidic acid (PA) and L- α -Phosphatidylcholine (PC) at a ratio of 50:50. This lipid profile was chosen to mimic host cell endoplasmic reticulum membranes [244, 312], which agnoprotein colocalises with and may potentially be the origin of agnoprotein lipid droplets [155].

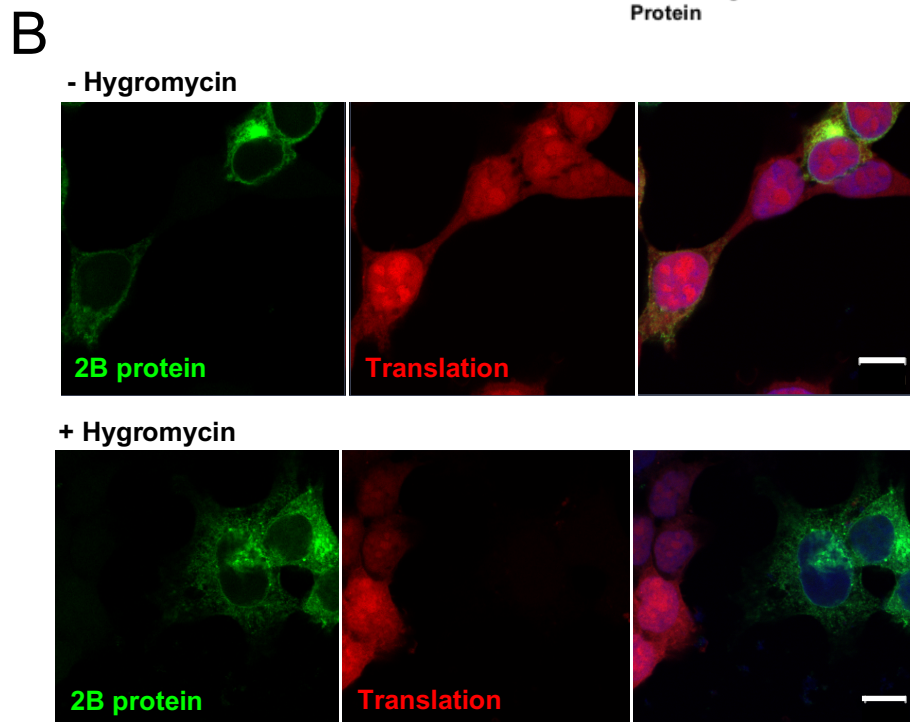
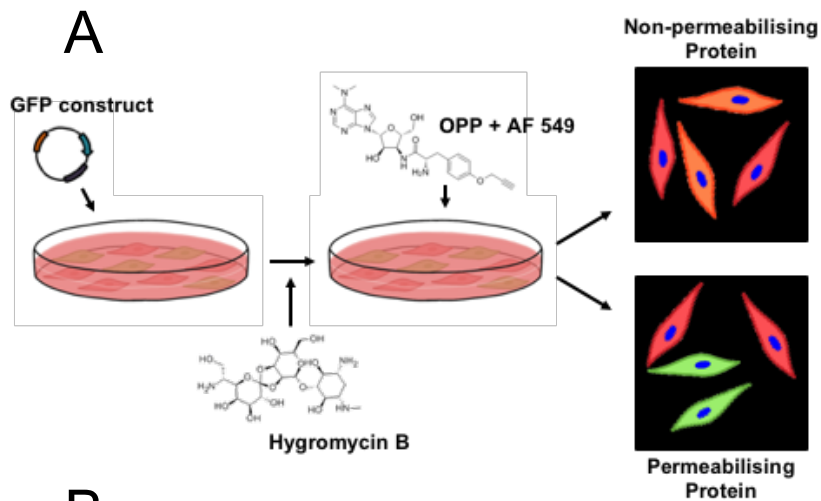


Figure 4.10: Hygromycin Assay

(A) A schematic of the workflow for analysis of plasma membrane integrity using hygromycin B and OPP. (B) Confocal images of untreated and hygromycin treated cells transfected with CoxV 2B. Scale bars = 10 μ m.

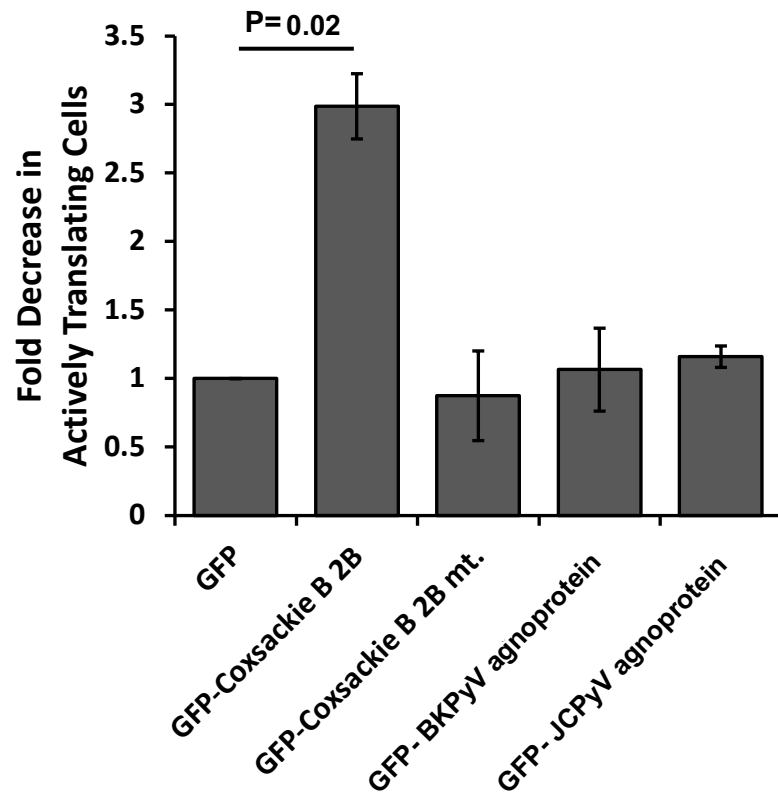


Figure 4.11: Hygromycin Assay with BKPyV and JCPyV agnoprotein

Quantification of fold decrease in translationally active cells expressing GFP-viroporin constructs after hygromycin treatment. Flow cytometry gates were applied to live population and sub-gates applied to the GFP positive cells. N=3.

5% L- α -Phosphatidylethanolamine with lissamine rhodamine B labelled head groups (PE) was added to the liposomes to enable their visualisation and quantification. Lipid mixtures were dried down under a stream argon, followed by 2 hr incubation in a vacuum. Dried lipid mix was resuspended in the presence of the self-quenching dye; carboxyfluorescein (50mM). Resuspended lipid mix was extruded through 0.4 μ m filters to form liposomes of a consistent size. Purification of liposomes was carried out to remove excess carboxyfluorescein, and concentration of liposomes calculated as described in (methods 2.5.2) using rhodamine fluorescence (λ_{ex} 570 nm).

Recombinant 10x His BKPyV agnoprotein was added to liposomes prior to floatation on a discontinuous Ficoll gradient (methods 2.5.4). Post-centrifugation, the gradient was then divided into 8 equal fractions and migration of the liposomes was determined by rhodamine fluorescence. Intact liposomal membranes migrate to the top of the Ficoll gradient between the 0-10% interface, meaning maximum fluorescence was observed in fractions 2/3. Liposomes disrupted with Triton X100 remain at the bottom in fraction 8 (figure 4.12A). Samples of each fraction were taken for western blot analysis to determine if recombinant 10x His BKPyV agnoprotein had co-migrated alongside the liposomes. The majority of recombinant agnoprotein co-migrated with the liposome to the top of the gradient (figure 4.12B). High-salt conditions and Triton X100 were used to distinguish if agnoprotein formed a peripheral or integral interaction with the liposomal membranes. Migration was completely disrupted by treatment with Triton X100, and partially disrupted by treatment with high-salt conditions. High-salt conditions appear to preferentially disrupt agnoprotein monomer co-migration, compared to dimer co-migration, this will be discussed later in this chapter.

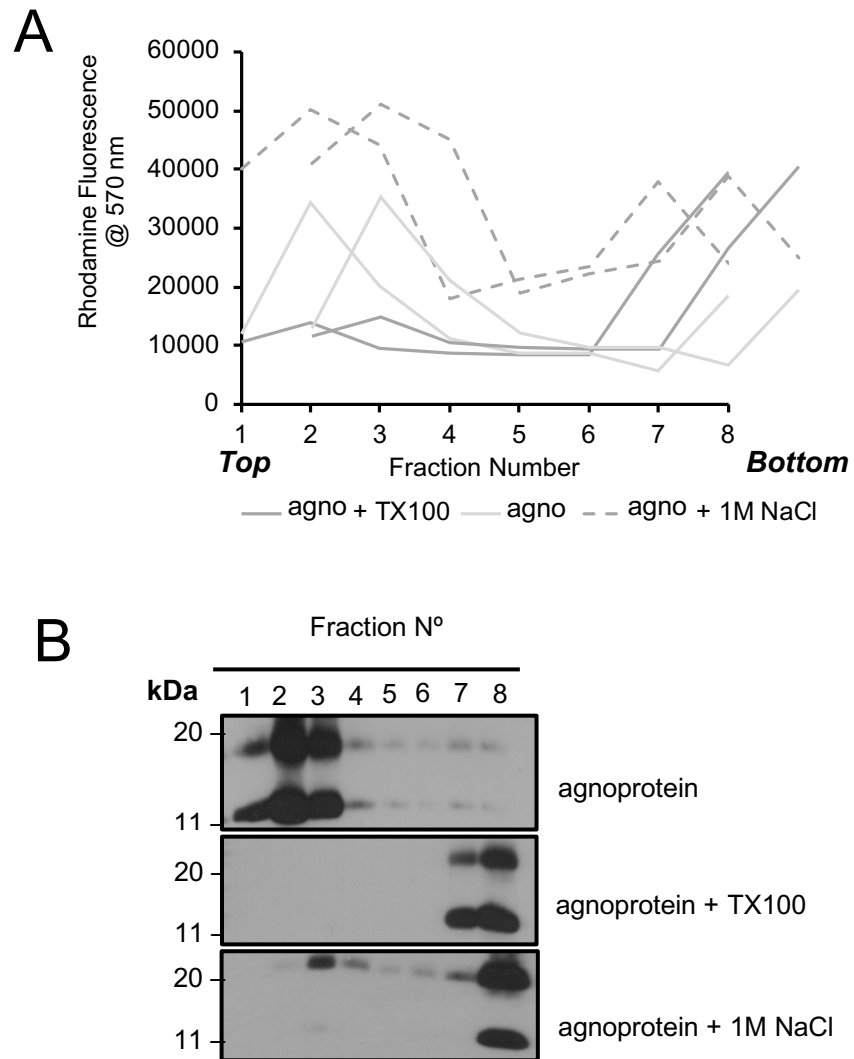


Figure 4.12: Floatation Assay with recombinant BKPyV agnoprotein

(A) Rhodamine fluorescence measured across fractions taken from Ficoll gradients to track the migration of liposomes. (B) Western blot analysis using anti-agnoprotein antibody of fractions taken from Ficoll gradients after centrifugation to monitor the migration of BKPyV agnoprotein. N=3.

4.5.4 10x His BKPyV agnoprotein facilitates dose-dependent release of carboxyfluorescein from Liposomes

To investigate if BKPyV agnoprotein oligomers form channels, dye release assays were carried out in liposomes. Liposomes were packed with a self-quenching dye; carboxyfluorescein, which fluoresces if released from liposomes (figure 4.13A). BKPyV agnoprotein was incubated with liposomes and fluorescence was monitored over 30 minutes at 30 sec intervals. Alongside BKPyV agnoprotein, Melittin peptide from honeybee venom (sigma) was incubated with liposomes as a positive control for dye release. Melittin is a well characterised pore forming peptide, which is capable of forming tetramers and simultaneously integrates into membranes. Addition of Triton x100 to rupture liposomes and buffer only conditions were used in order to assess their integrity.

Recombinant BKPyV agnoprotein was shown to initiate dye release over the observed time course (figure 4.13B), though this release was not as rapid as Melittin. The increase in fluorescence seen for Melittin plateaued after approximately 120 sec, whereas for recombinant BKPyV agnoprotein fluorescence increased steadily until towards the end of the time course. Neither Melittin or recombinant BKPyV agnoprotein resulted in complete dye release as seen with Triton X100, and the plateau in fluorescence probably suggests that in these experiments the liposomes were in excess. To further characterise recombinant BKPyV agnoproteins ability to initiate dye release, liposomes were incubated with increasing concentrations of recombinant protein. Fluorescent values were taken at the end of these time courses as a measure of dye release (figure 4.13C). These data showed that significant dye release was achieved with concentrations greater than 1.3 μM , and that amount of dye release is concentration dependant.

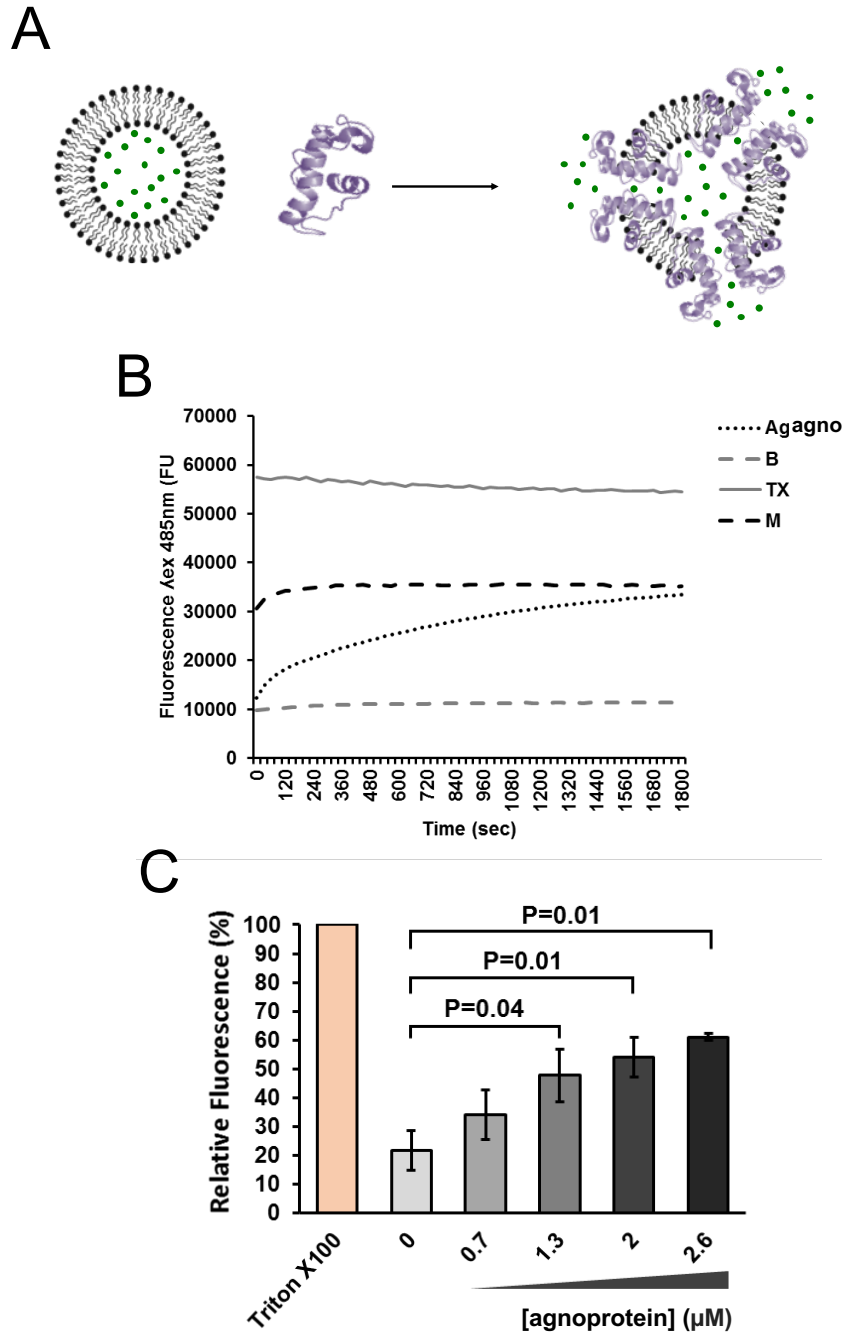


Figure 4.13: Dye Release Assay with recombinant BKPyV agnoprotein

(A) A schematic of dye-release assay. (B) Carboxyfluorescein release over the course of 30 minutes after liposomes are incubated with Triton x100 (TX), buffer (B), melittin (M), or recombinant 10x His BKPyV agnoprotein (agno). (C) Dye release, measured by relative fluorescence compared to Triton X100 control, of increasing amounts of recombinant 10x His BKPyV agnoprotein. $N=3$.

In addition, we designed a synthetic peptide spanning the helical domain (appendix) to investigate whether the truncation mutant BKPyV agnoprotein 20-42 caused membrane disruption through pore formation. 5 μ M of peptide was incubated with liposomes over the course of 30 min (figure 4.14A) and resulted in 21.8 percent increase in endpoint fluorescence (figure 4.14B). These data indicate that the peptide was able to form pores in liposomes, though not as effectively as the full-length recombinant protein. However, repeats to investigate this peptide future showed that it lost complete activity after one round of freeze thaw.

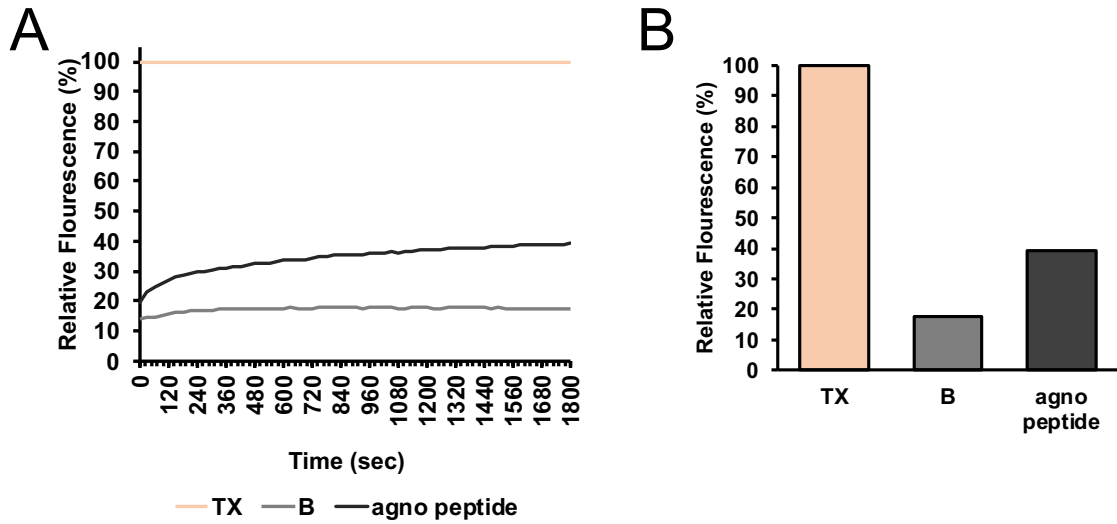


Figure 4.14: Dye Release Assay with Agnoprotein 20-42 aa. Peptide

(A) Carboxyfluorescein release over the course of 30 minutes after liposomes are incubated with Triton x100 (TX), buffer (B), or recombinant BKPyV agnoprotein peptide (agno peptide). (C) Quantification of endpoint fluorescence for agno peptide dye release assay. N=1.

4.6 Discussion

Viroporins have become ubiquitous across a wide range of viral families. Very little was known about the function of BKPyV agnoprotein, and as a whole it is less well studied than JCPyV agnoprotein. In 2010, JCPyV agnoprotein was reported to have a novel viroporin function, but mechanistic detail of how it functioned during the viral life cycle remains unknown [141, 142]. The experiments in this chapter aimed to determine if this viroporin function was conserved in BKPyV.

To begin with, it was shown that BKPyV agnoprotein could at least dimerize through GST pull downs (figure 4.1A). Had time permitted, we would have liked to investigate if BKPyV agnoprotein could also associate with JCPyV and SV40 agnoproteins. Previous work in the lab has suggested that BKPyV agnoprotein was able to interact with JCPyV agnoprotein, but further experiments are required to validate this observation. This is particularly interesting as the co-infection of multiple polyomaviruses has yet to be studied, though there is evidence that BKPyV and JCPyV are both capable of infecting renal cells [197]. Co-infections could therefore potentially lead to a hybrid agnoprotein oligomers.

Furthermore, future experiments should characterise the interaction between BKPyV agnoprotein monomers, through performing GST pull downs with the agnoprotein mutant constructs described in this chapter. These GFP-fusion constructs were found to be unstable in cell lysates, so could never be used in GST pull downs. Similar observations have been made with truncation mutants of JCPyV agnoprotein, which were shown to be unstable in mammalian cells [148]. Cloning these mutants across into a pGEX-6P1 vector could result in their stable expression in bacteria as GST-fusion constructs. If this proved possible these mutations could then be used as bait to pull down GFP BKPyV agnoprotein. Alternatively, these mutants could be clones as fusion partners into a FRET system to look at their interaction with wt. BKPyV agnoprotein in cells.

Although, if dimerization and/or oligomerisation are required for membrane disruption, then the MC540 data presented in this chapter indicates the regions

of BKPyV agnoprotein that required for monomer-monomer interactions. The MC540 assay showed that both JCPyV and BKPyV agnoproteins disrupted membranes in mammalian cells (figure 4.6), causing an increase in MC540 fluorescence. Introducing truncation mutants (figure 4.8) of BKPyV agnoprotein into this assay, showed that the loss of the helical domain resulted in significant loss in membrane disruption. These data also suggested that the minimum sequence required for disruption was BKPyV agnoprotein 20-42, which consists of the residues encompassing the predicted helical domain. Further investigation is required to determine if residues 20-42 could form channels in cell membranes. A BKPyV agnoprotein peptide, which spanned the helical domain, was shown to initiate dye release from liposomes (figure 4.14), however the peptide proved difficult to work with due to insolubility and instability issues. In the future, revisiting peptides could be a potential option for determining if truncations are able to form channels in membranes.

All of these mutants also displayed a loss in cytosolic punctate formation, which potentially suggests that their integration into lipid droplets [155] was affected. To validate this observation co-staining with a lipid droplet dye could be performed, and imaging of a larger data set of cells would enable quantitative analysis of punctate loss. Rescue assays with BKPyV Δ agno should also be revisited with these constructs to determine if they are able to rescue the loss of agnoprotein in infection. In the time frame of this project, these rescue assays were unable to be optimised, and a more complex system was found to be required to reintroduce agnoprotein to BKPyV Δ agno. If a system could be optimised for rescue assays, rescuing BKPyV Δ agno should be attempted with JCPyV agnoprotein and other viroporins. This could indicate how viroporin activity functions within the polyomavirus lifecycle.

In addition to this, alanine mutants in the helical domain showed that the loss of phenylalanine and leucine residues results in the significant loss of membrane disruption (figure 4.9). This compares with molecular dynamic modelling that has previously been performed with JCPyV agnoprotein [159]. In this modelling, it was suggested that the dimerisation interface between antiparallel monomers contains leucine and isoleucine residues. It was unclear for the data described

above, which leucine residue was essential, or if the loss of hydrophobicity had resulted in the loss of membrane integration. This could be investigated by producing individual leucine alanine mutants and testing them in the MC540 assay. Moreover, phenylalanine residues have been indicated in HPV E5 oligomerisation through pi-stacking (unpublished, Wetherill thesis). This could potentially also explain the role of phenylalanine residues in BKPyV agnoprotein, but again it remained unclear which phenylalanine residue was essential. To perform a more detailed analysis of essential residues required for membrane disruption an alanine scan should be performed across the sequence of BKPyV agnoprotein. It would also be interesting to look at phosphorylation mutants in the MC540 assay as they have been suggested to play an important role in agnoprotein regulation. Considering the detrimental effect that recombinant 10x His BKPyV agnoprotein had on bacterial growth, its regulation in mammalian cells would be required to ensure a proliferative environment for viral replication.

In following up the interaction seen between GST-Flag BKPyV agnoprotein and GFP-BKPyV agnoprotein, it was shown that recombinant 10x His BKPyV agnoprotein formed SDS-resistant oligomerisation (figure 4.1B) which has previously been reported in the literature [158, 294]. Larger oligomers, up to pentamers, were seen in this analysis; the formation of which was observed to be concentration dependent. To validate these oligomeric states, native PAGE should be performed to rule out any artefacts that might have been introduced by SDS PAGE. Native PAGE was attempted during this project, but optimisation was required and not possible within the project's timeframe. Notably these oligomers could never be observed in cell lysates from BKPyV infected cells. This was potentially a result of low expression levels during infection, which could possibly be a mechanism employed by BKPyV to prevent the cytotoxic effect of agnoprotein. In investigating the agnogene of BKPyV, it was found to have poor codon optimisation for host translation, and it would be interesting to look at the effect of codon optimising the agnogene in a viral genome.

Subsequently, the membrane association of BKPyV agnoprotein was investigated in mammalian cells and liposomal membranes. Subcellular fractionations (figure 4.2) were performed, showing that overexpressed

agnoprotein was found in membranous fractions. These fractionations were also attempted in BKPyV infected cells, but further optimisation was unable to be performed due to time frames. Low viral titres were the main problem with this assay, as it resulted in low MOI infections and membrane fractions often did not contain a concentration of agnoprotein that could be detected. Preliminary topology studies were also performed in mammalian cells and could have indicated that BKPyV agnoprotein was located to the plasma membrane in both topological orientations (figure 4.3). This was unusual for a viroporin but agreed with the molecular dynamic modelling of JCPyV agnoprotein dimers [157]. Moreover, investigation of membrane association in liposomal membranes confirmed that recombinant 10x His BKPyV agnoprotein co-migrates with liposomes along a Ficoll gradient (figure 4.13). This co-migration was completely disrupted by Triton X100, but only partially disrupted by high-salt conditions.

This indicates that BKPyV agnoprotein integrates into membranes as an integral protein, as well as a proportion of it associating peripherally. This analysis showed that the dimeric form of BKPyV agnoprotein remained associated with liposomal membranes under high-salt conditions, while the majority of the monomeric species disassociated. This might suggest that agnoprotein was dimeric when associated with lipids, whereas it remains monomeric if a lipid environment was not present. To test this native PAGE could be carried out in the presence and absence of a lipid mimetic to determine how lipids might affect oligomerisation.

The integral integration into membranes and oligomerisation described by these data, indicated that BKPyV agnoprotein may possess viroporin activity. Next it was investigated if recombinant BKPyV agnoprotein could form channels in liposomal membranes. Dye release assays revealed that liposomes incubated with recombinant 10x His BKPyV agnoprotein released carboxyfluorescein (figure 4.13). This carboxyfluorescein release was concentration dependent and was significant when more than 1.3 mM of recombinant protein was present. To further characterise this channel formation, similar dye release assays should be carried out at different varying pH and with liposome packaged with different sized dextran dyes.

Performing these assays at varying pH could determine if the channel formed by BKPyV agnoprotein has a gating mechanism similar to IVA M2, and indicate where in mammalian cells the channel was likely to form. The floatation assay described above could also be performed at varying pH to distinguish between a closing of the channel and a disruption to integration. Moreover, different sized dextran dyes could be used in a dye release assay to determine the diameter of the channel lumen, giving indication of the sort of substrates which were likely to pass through the channel, and guide *in silico* modelling of an oligomeric structure.

To further investigate pore-formation in mammalian cells, hygromycin assay were performed. This has previously been performed for JCPyV agnoprotein where it was shown that JCPyV agnoprotein permeabilised the plasma membrane [141]. Although, our observation from the hygromycin assay, suggest that BKPyV and JCPyV agnoprotein were incapable of forming pores at the plasma membrane (figure 4.11). This result may have been an artefact of the GFP fusion, which might have disrupted integration at the plasma membrane, or blocked hygromycin from accessing the pore. These experiments were initially planned to be revisited using a bicistronic system lentiviral system to introduce agnoprotein to cells. This system appeared promising with both western blot and MC50 analysis indicating that agnoprotein was expressed and active, respectively. However, overtime it was found that the cells rapidly lost expression of agnoprotein, whilst still maintaining selection markers. It is unclear why this happened, but similar loss of expression has been observed in an HEK-derived inducible agnoprotein cell line. The previous experiments with JCPyV agnoprotein was also performed in HeLa cells, which constitutively express HPV E6 and E7 proteins. Our lab has shown that these proteins alone have a profound effect on membrane stability, so this may have caused the permeabilisation seen in the JCPyV agnoprotein experiments.

Alternatively, these data might indicate that agnoprotein only formed pore in intracellular membranes. If the agnoprotein forms pores in intracellular membranes it might be forming them in the vesicles that traffic progeny virus out of infected cells, or as part of a nuclear export pathway. The pore may not,

therefore, be present at the plasma membrane as the viroporin function of agnoprotein is no longer required. This theory could be tested using the dye release assay described above, if different lipid compositions were used to mimic different cellular membranes. This approach has been successfully applied for Hepatitis A virus 2B protein [313], providing a simple approach to determining the types of locations and stages of viral lifecycles where viroporins may function.

4.6.1 *in silico* Modelling of BKPyV agnoprotein

Reflecting on the data presented in this chapter, it was identified that BKPyV agnoprotein possesses a viroporin activity. There were plans within this project to create an *in silico* modelling of the oligomeric form of BKPyV agnoprotein as a tool to predict drug compound binding sites.

An *in silico* model of BKPyV agnoprotein monomer (figure 4.15) was previously created, by Richard Foster's group, using a combination of secondary structure prediction (from the PSIPRED server (figure 14.5A)) and MEMSAT3 software. The secondary structure was built amino acid by amino acid in Maestro software (Schrödinger Inc.) and energy minimisation was performed (Merck-Molecular ForceField (MMF) in a simulated water dielectric), allowing the relaxation into a tertiary structure with the lowest energy state. This monomeric structure was then docked into an oligomeric arrangement to generate a pentameric species (figure 4.15C), with further rounds of energy minimisation.

Unlike other viroporins, which have been modelled in a similar way [244, 264], this initial model of BKPyV agnoprotein has some unusual features. Its N- and C-terminus fold back on its helical domain, which seems peculiar when considering that conventionally the terminal domains of viroporin protrude from membranes. It is possible that this monomeric structure may be an artefact of the modelling environment. Hydrophobic collapse is an energetically favoured event during the folding of globular proteins in an aqueous environment.

Considering the data, it was sensible to assume that under the correct conditions the N- and C- termini of BKPyV agnoprotein might collapse around its helical domain to protect the hydrophobic region of the helix.

Additionally, the pentameric model does not have a continuous lumen. This was not too concerning, because we could not say for certain that the channel-forming species was pentameric, and we could not say that there was not a gating mechanism that regulates movement of substrate through the agnoprotein. IVA M2 is a well-characterised example of a gated-viroporin [213], and similarly BKPyV agnoprotein also contains a tryptophan in close proximity to C- terminus of its predicted TM domain. To investigate the possibility of a gating mechanism, further liposomal dye release assays described above will need to be carried out. These experiments would indicate if the channel formed by BKPyV agnoprotein was gated.

Considering our experimental data, this initial model was considered unsuitable for *in silico* docking of drug compounds. Further *in silico* modelling was not possible using the approach described above, but other options were investigated to generate a model which was more realistic. CCbuilder 2.0 was used to assemble an initial coiled-coil structure of BKPyV agnoprotein's helical domain. The CCbuilder 2.0 server [314] applies generalised coiled-coil parameters to flexibly fit protein sequences into a coiled-coil conformation. The server allows for parameters such as; helix orientation, helical pitch, radius, and interface angles, to be adjusted and generates a BUDE energy to indicate how energetically favourable each conformation is. An iterative approach was first applied to investigate the most appropriate oligomeric state for the model. Viroporins have previously been described as tetramers (e.g. IV M2), pentamers (e.g. CoV E protein), hexamers (e.g. HCV p7 and HPVE5), and heptamers (e.g. SH hRVS). Each of these oligomeric states were modelled (figure 4.16). Tetrameric and pentameric arrangements did not feature a lumen so were ruled out for now, as there is currently no evidence supporting that BKPyV agnoprotein is a gated channel. Hexameric and heptameric arrangements did both feature

lumens and were suggested to be more energetically favourable. Hexameric was chosen for further modelling because the suggested antiparallel nature of BKPyV would indicate the formation of an oligomer of an even number of subunits.

Considering the experimental data described in this chapter and evidence from the literature, it was decided that any further model generated using CCbuilder 2.0 should contain antiparallel alpha helices. In addition to this, data from the MC540 assay was used to indicate that leucine and phenylalanine residues might be positioned at the monomer-monomer interfaces. The model generated using CCbuilder 2.0 (figure 4.17A) will require further optimisation, although agrees with the experimental data better than the initial *in silico* model.

The CCbuilder model shows two potential interfaces between monomers; the first of which (indicated by burgundy shading in figure 4.17B) contains F39, L36, and F29. Mutating these residues individually in MC540 assay could validate this feature of the model. The second interface (indicated by orange shading in figure 4.15B) was formed from K23, R27, I30, and E34; and will need further experimental investigation to validate. Moving forward, future work should revisit the modelling of BKPyV agnoprotein, by attempted *in silico* modelling in a lipid environment to produce an oligomeric structure which takes in to account cellular membranes.

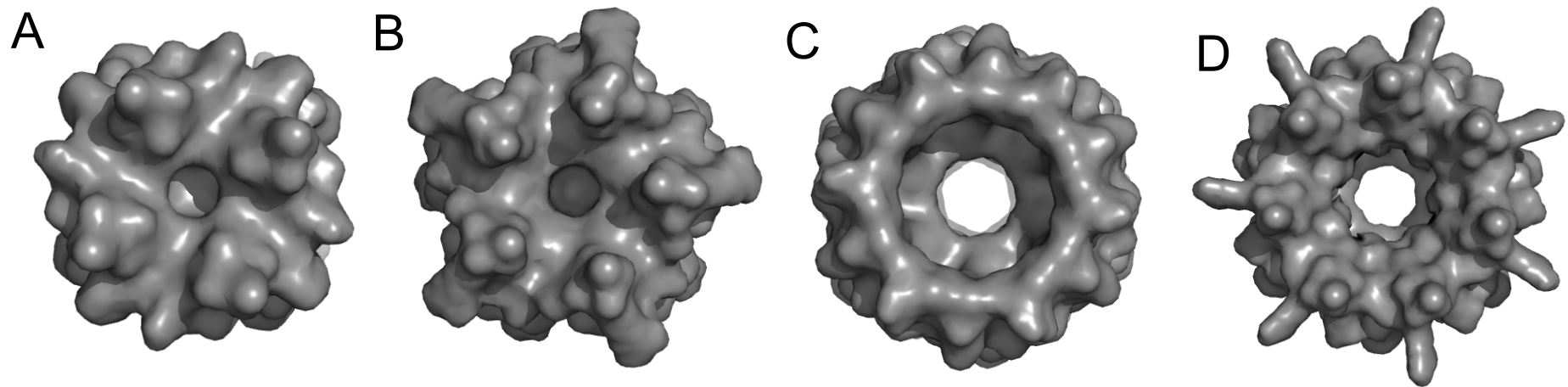


Figure 4.16: Iterative Oligomeric Modelling of BKPyV agnoprotein using CCbuilder

Surface render top-down view of a (A) tetrameric, (B) pentameric, (C) hexameric, and (D) heptameric arrangement of agnoprotein monomers. Generated using an iterative approach on CC builder 2.0 (<http://coiledcoils.chm.bris.ac.uk/ccbuilder2/builder>).

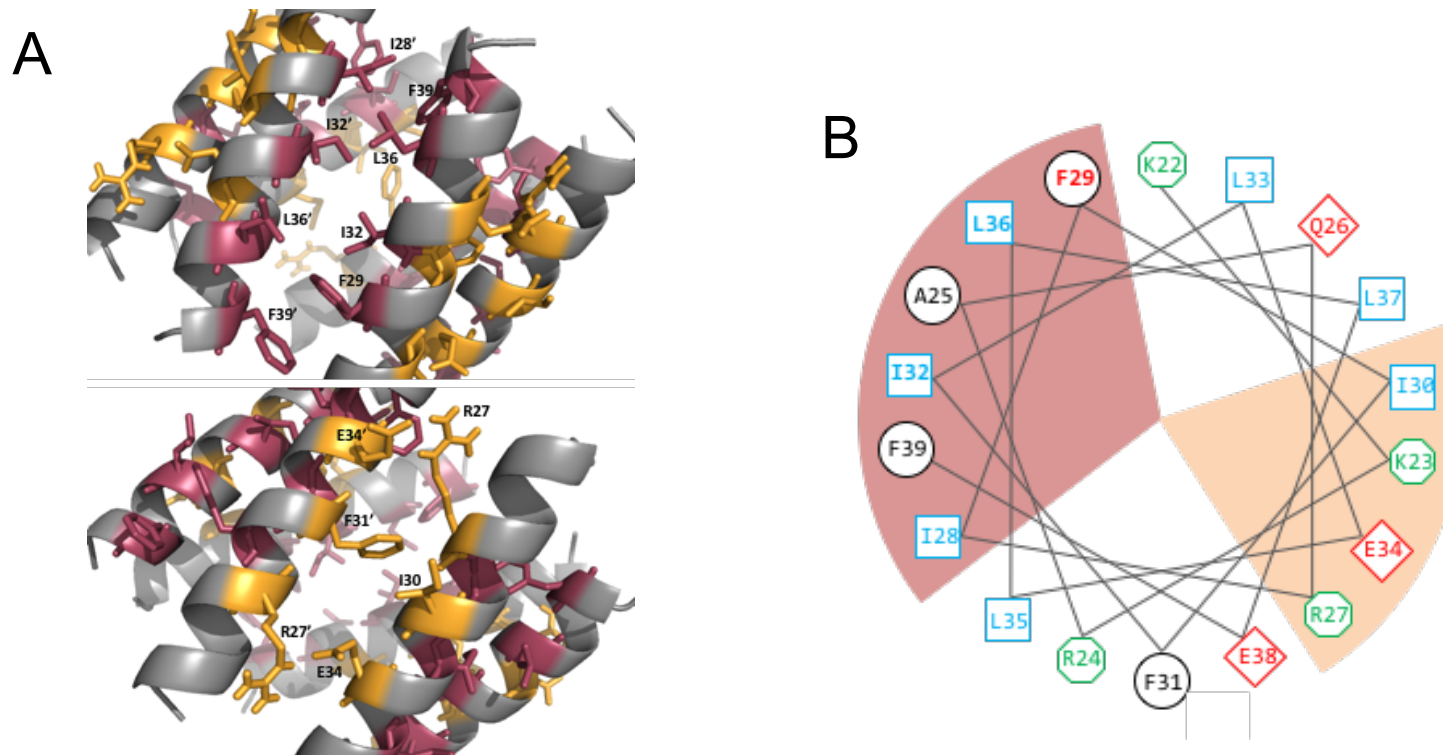


Figure 4.17: CCbuilder 2.0 Model of BKPyV agnoprotein

(A) A hexameric structure generated using CCbuilder 2.0, using data described in this chapter. Radius: 12, Interface: 24, Pitch: 200, BUDE energy: -367.2 Burgundy residues highlight the first oligomerisation interface and yellow residues highlight the second oligomerisation interface.

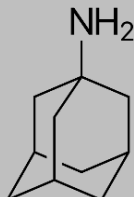
(B) A helical wheel diagram highlighting the residues involved in the interfaces suggested by the mode

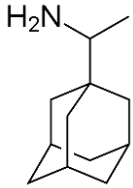
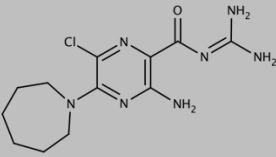
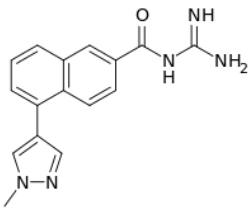
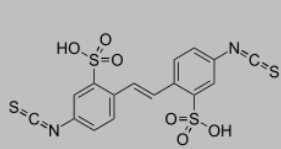
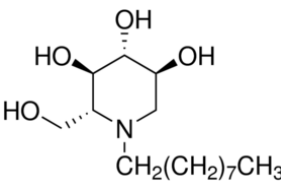
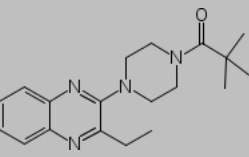
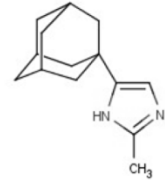
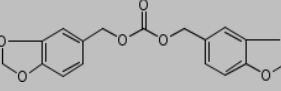
Chapter 5 : Inhibition of BKPyV agnoprotein Channel Activity

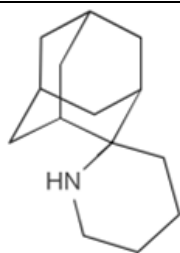
5.1 Introduction

Many studies have directed the development of new antivirals towards the inhibition of viroporins. With viroporins playing critical roles within viral lifecycles they are ideal candidates for antivirals, as inhibiting/knocking out their function is often seen to dysregulate the viral lifecycle [213, 214]. The best developed antivirals, whose mechanisms are through the inhibition of a viroporin, are adamantanes. In 1964, it was observed that amantadine selectively inhibited Influenza A virus (IAV) in tissue culture, chick embryos, and mice [315]. Following these findings, the U.S. Food and Drug Administration (FDA) approved amantadine as a prophylactic agent against Asian flu in 1966, but it was not until 1985 that its mechanism of action was described, and it was shown that amantadine blocks the channel formed by the Influenza M2 protein [252, 253].

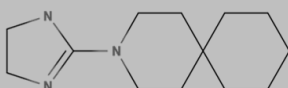
Since, then the amantadine derivative, rimantadine [253], has also been shown to be an antiviral; though both compounds are no longer clinically used due to the development of resistance in Influenza A [257-259]. Other viroporin inhibitors have now been published; most of which seem to have the ability to block multiple viroporin proteins (Table 5.1)

Inhibitor	Structure	Viroporin Targets	System
Adamantane		<ul style="list-style-type: none">- IVA M2 [315, 316]- HCV p7 [265, 266]- Dengue M protein [226]	<ul style="list-style-type: none">Cell culture, artificial membranesArtificial membranes, cell culture, clinical studiesArtificial membranes

Rimantadine		- IVA M2 [253] - HPV16 E5 [244]	Cell culture, artificial membranes Artificial membranes
Hexamethylene amiloride (HMA)		- HCV p7 [317] - <i>Coronaviridae</i> E protein [228] - Dengue M Protein [226]	Artificial membranes, cell culture Cell culture, Artificial membranes Artificial membranes
BIT225		- HIV Vpu [272, 273] - HCV p7 [269] - BVDV p7 [269]	Cell culture Artificial membranes, early stage Phase Ib/IIa trials Cell culture
4,4'-Diisothiocyano-2,2'-stilbenedisulfonic acid (DIDs)		- EV71 2B protein [219]	<i>Xenopus laevis</i> oocytes, cell culture
NNDNJ		- HCV p7 [268] - HPV E5 [282]	Cell culture, clinical studies
MV006		- HPV16 E5 [244]	Artificial membranes
“H”:5-(1-adamantyl)-2-methyl-1H-imidazole		- HCV p7 [215]	Artificial membranes, cell culture
MV266		- HPV16 E5 [244]	Artificial membranes
Spiro[piperidine-2,29-adamantane] 3		- IVA M2 [215]	Artificial membranes



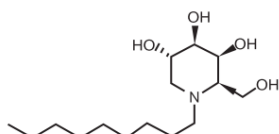
BL-1743:(2-[3-azaspiro(5,5)undecan-2-ylidene]imidazole)



- IVA M2 [215]

Artificial membranes

MNDGJ



- HCV p7 [268]

Cell culture

Table 5.1: List of characterised viroporin inhibitors, their structures, target and system in which they were characterised

Viroporin inhibitors have never been tested against agnoproteins. This chapter describes the sensitivity of the channel formed by BKPyV agnoprotein to classical viroporin inhibitors.

5.2 Channel formed by BKPyV agnoprotein is sensitive to classical viroporin inhibitors

Adamantanes; rimantadine and amantadine, and the alkyl-imino sugar; MNDNJ have been previously characterised to inhibit multiple viroporins. The following data shows the results of using these compounds to inhibit the channel formed by BKPyV agnoprotein. Controls were carried out with all compounds to confirm that they did not affect the integrity of the liposomes on their own or effect the fluorescence of carboxyfluorescein by looking at dye release initiating by melittin (appendix).

5.2.1 Adamantanes

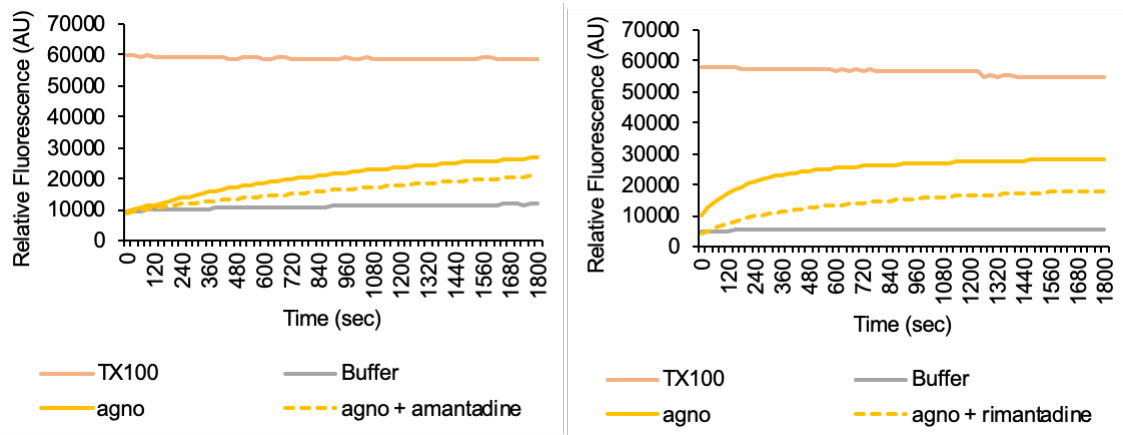
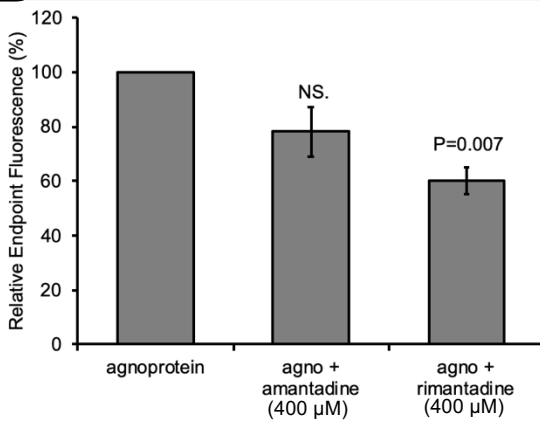
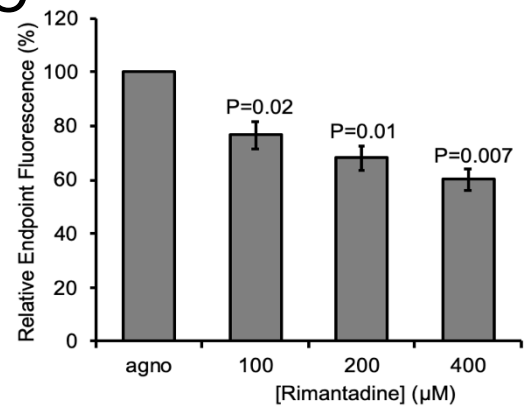
To investigate if the channel formed by BKPyV was sensitive to rimantadine and amantadine, 400 μM of each compound was incubated with recombinant BKPyV agnoprotein. After 10 minutes, the pre-treated recombinant BKPyV agnoprotein was incubated with liposomes and carboxyfluorescein fluorescence was observed over time (figure 5.1A). Amantadine and rimantadine treatment resulted a 22% (non-significant) and 38% ($P=0.007$) reduction in dye release observed at the end of the time course, respectively (figure 5.1B). Additionally, a titration of rimantadine concentration was tested at 100 μM , 200 μM , and 400 μM (figure 5.1C). This showed that rimantadine caused a significant reduction in dye release at all concentrations compared to the untreated control.

5.2.2 NNDNJ

Similarly to the adamantanes, 400 μM of NNDNJ was incubated with recombinant BKPyV agnoprotein to investigate any potential inhibitor effect. BKPyV agnoprotein pre-treated with NNDNJ resulted in a 23.4% ($P=0.008$) reduction in dye release compared to the untreated control (figure 5.2).

5.3 Channel formed by BKPyV agnoprotein is sensitive to the anion channel inhibitor DIDs

4,4'-Diisothiocyano-2,2'-stilbenedisulfonic acid (DIDs) has previously been shown to have an inhibitory effect on the release of BKPyV polyomavirus [167]. The mechanism by which DIDs inhibits BKPyV polyomavirus infection remains unknown. However, it has previously been shown that DIDs can inhibit the 2B protein from enterovirus 71. To examine if DIDs was inhibiting BKPyV agnoprotein, DIDs was pre-incubated with recombinant BKPyV agnoprotein at 25 μM , 50 μM , and 100 μM . This pre-treated BKPyV agnoprotein was then incubated with liposomes and ~80% reduction in dye release was seen with all concentrations (figure 5.3).

A**B****C****Figure 5.1: Inhibition of Dye Release with Adamantanes**

(A) Relative fluorescence overtime monitoring dye release with recombinant agnoprotein pre-treated with 400 μ M of rimantadine and amantadine. TX100 and buffer only controls were performed to monitor liposome integrity. (B) Quantification of endpoint fluorescence relative to an untreated control. (C) Quantification of endpoint fluorescence relative to an untreated control for a titration of rimantadine concentrations. $N=3$ in technical duplicate.

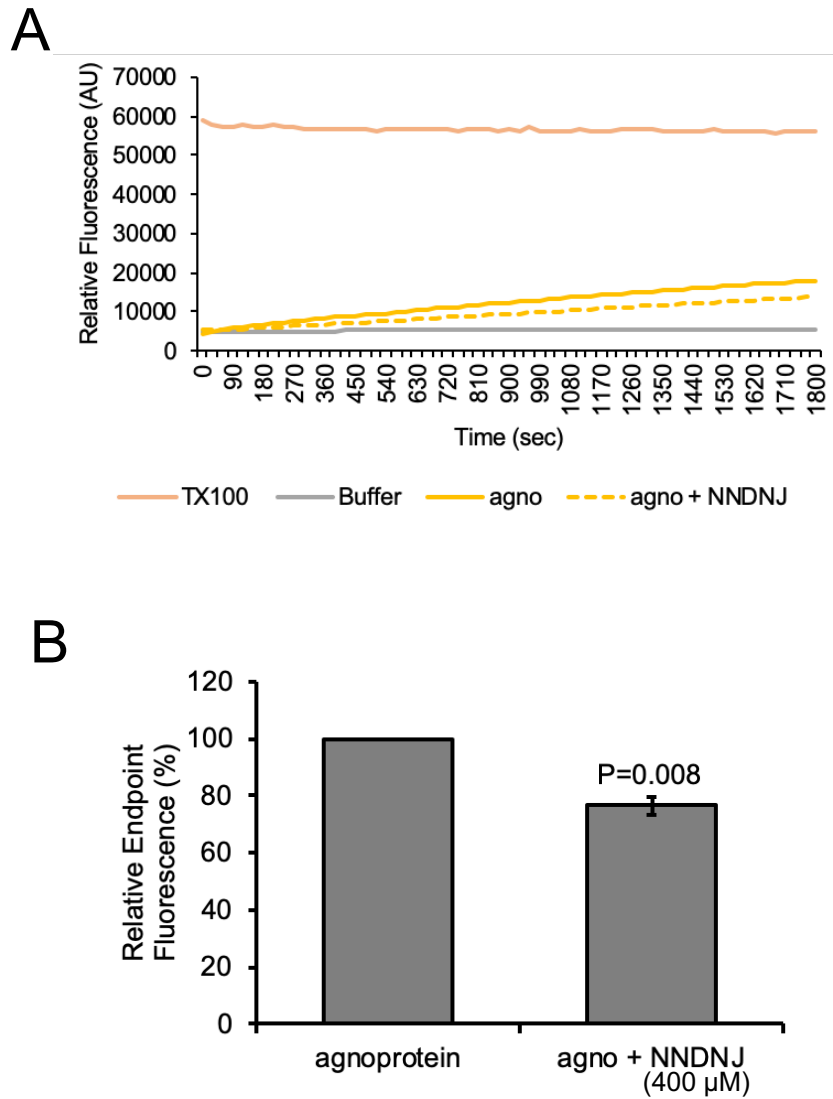


Figure 5.2: Inhibition of Dye Release with NNDNJ

(A) Relative fluorescence overtime monitoring dye release with recombinant agnoprotein pre-treated with 400 μM of NNDNJ. TX100 and buffer only controls were performed to monitor liposome integrity. (B) Quantification of endpoint fluorescence relative to an untreated control. N=3 in technical duplicate.

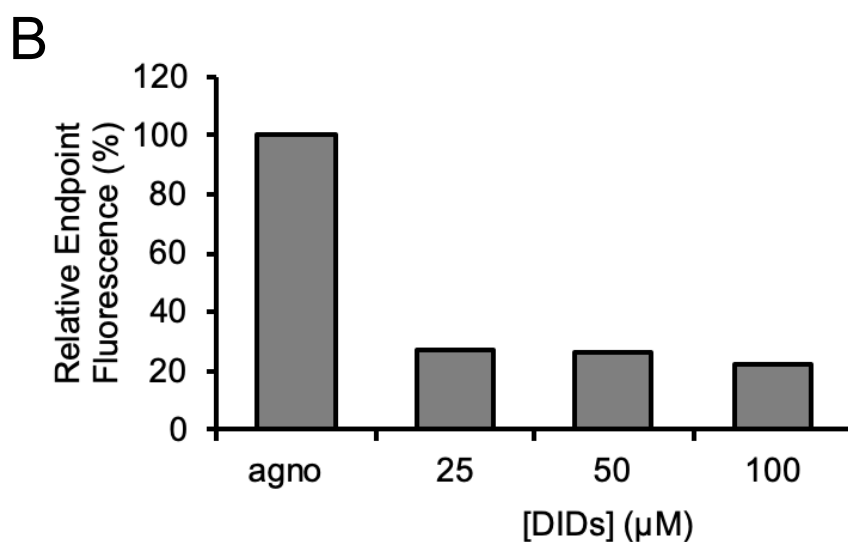
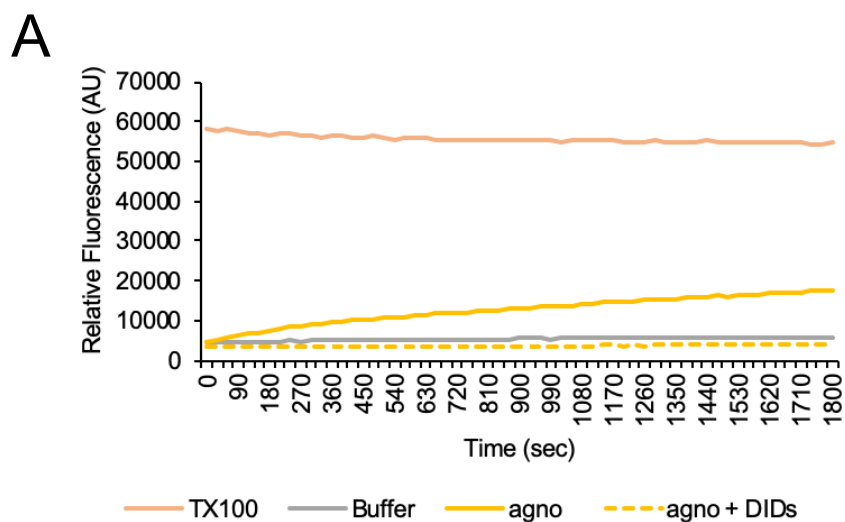


Figure 5.3: Inhibition of Dye Release with DIDs

(A) Relative fluorescence overtime monitoring dye release with recombinant agnoprotein pre-treated with 100 μM of DIDs. $N=1$. TX100 and buffer only controls were performed to monitor liposome integrity. (B) Quantification of endpoint fluorescence relative to an untreated control for a titration of DIDs concentrations. $N=1$.

Alongside this assay controls with melittin were performed to confirm that DIDs did not adversely affect fluorescence (appendix). This control confirmed that carboxyfluorescein fluorescence was not affected by DIDs, though DIDs pre-treatment resulted in a delay to the dye release caused by melittin. This will be discussed later in this chapter.

5.3.1 Rimantadine, NNDNJ, and DIDs inhibit BKPyV viral release from RPTE cells.

To further investigate rimantadine, NNDNJ, and DIDs on BKPyV agnoprotein infected cells were treated to see the effect on viral release. RPTE cells were infected with 0.5 MOI of BKPyV Dunlop, and compounds of interest added in fresh media at 24 hr post-infection. Media from treated cells was harvested at 48 hr post-infection and applied to naïve cells to quantify released virus.

Prior to treating RPTE cells, cell viability assays were carried out over a 24 hr timeframe at a range of drug concentrations (figure 5.4) for amantadine, rimantadine, and NNDNJ. No concentration of the drugs tested showed significant toxicity in RPTE cells, though all compounds showed a possible reduction cell viability at higher concentrations. 100 μ M of each compound was used in subsequent experiments. DIDs has previously been studied in RPTE cells and shown to have no significant toxicity [167], so 25 μ M was used in the following experiments.

A significant reduction in released virus was observed for rimantadine, NNDNJ, and DIDs treated cells. Rimantadine a 69%, NNDNJ a 70%, and DIDs a 60% reduction in viral release (figure 5.5). Amantadine treated cells had no significant reduction in virus release, which was similar to the dye release assays where it was not as effective as rimantadine.

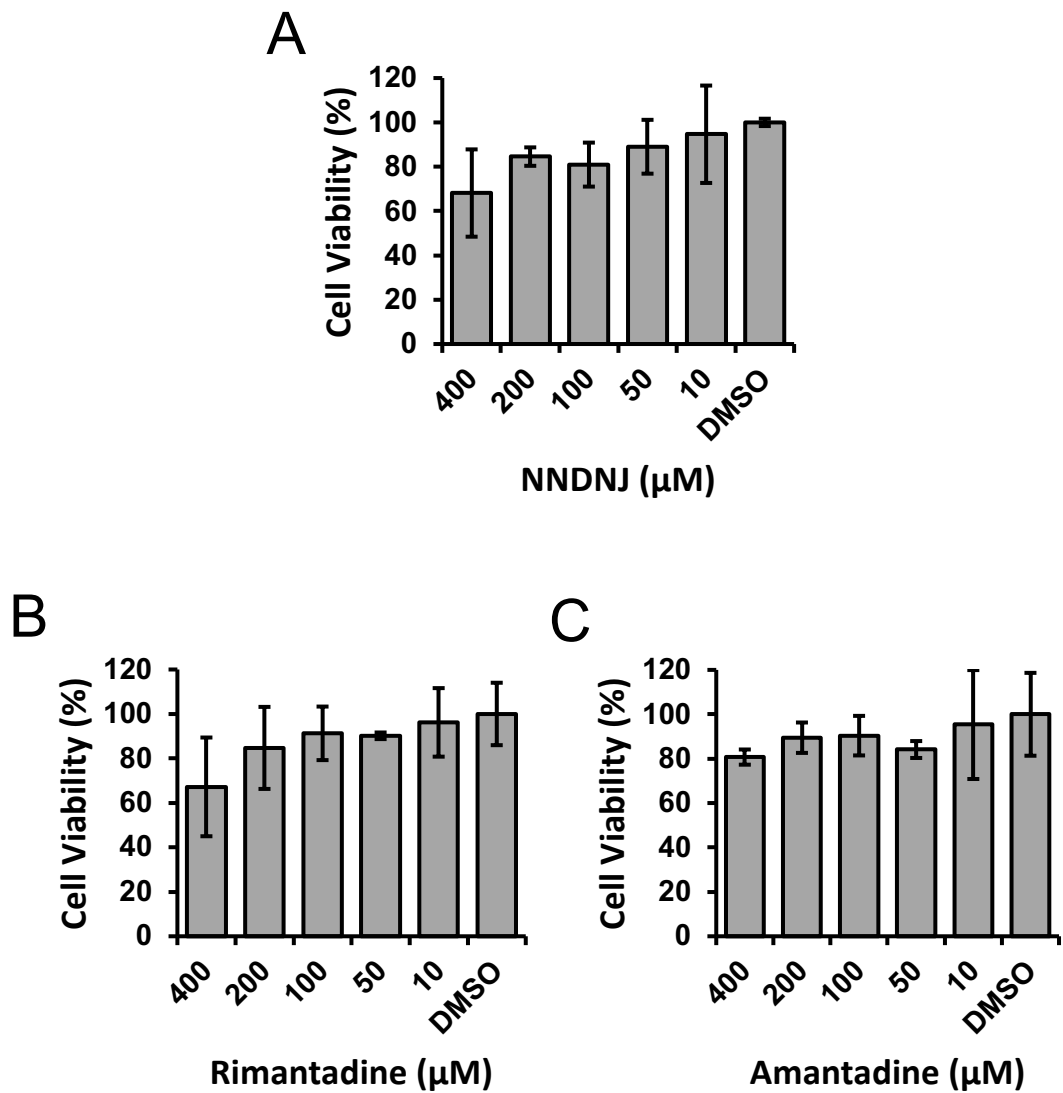
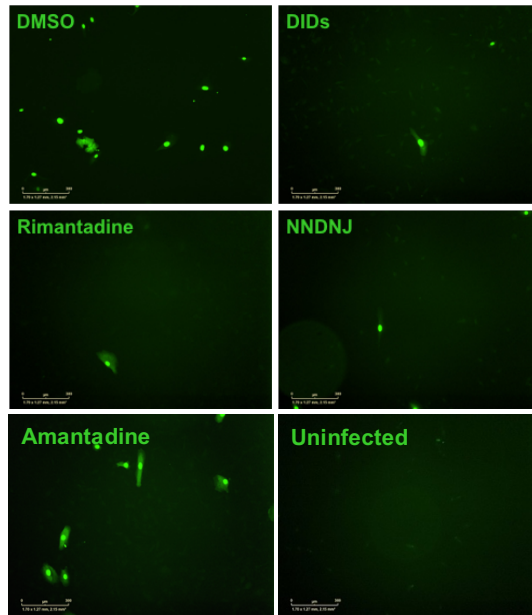


Figure 5.4: MTT Assays in RPTE cells

(A) Cell viability assay for NNDNJ 24 hr treatment of RPTE cells at varying concentrations. (B) Cell viability assay for rimantadine 24 hr treatment of RPTE cells at varying concentrations. (C) Cell viability assay for amantadine 24 hr treatment of RPTE cells at varying concentrations. $N=3$.

A



B

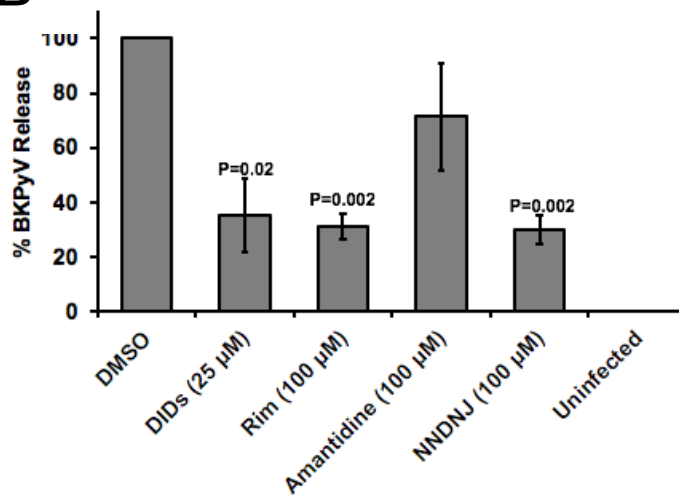


Figure 5.5: Treatment of BKPvV Infections in RPTE cells

(A) Fluorescence images from IncuCyte analysis of quantification of virus released from RPTE cells treated with inhibitor compounds. Scale bar = 300 μm. (B) Quantification of VP1 positive cells, (stained with VP1 antibody) in a 60% confluent 12 well, relative to the DMSO control from images obtained via the IncuCyte. Analysis carried out using IncuCyte ZOOM software.

5.4 Discussion

There is a desperate need for direct acting antivirals against BKPyV infections. In 2016 there were 70,000 kidney transplants worldwide, with 3% of the NHS's budget used in kidney failure services (NHS annual report, 2018). This chapter demonstrated that the agnoprotein of BKPyV could be a potential drug target for the development of new antivirals.

The dye release assays, described above, with recombinant protein showed that dye release could be significantly inhibited with rimantadine (figure 5.1), MNDNJ (figure 5.2), and DIDs (figure 5.3). Moving forward these liposomal-based assays need further investigation and repeats, particularly the DIDs inhibition. DIDs has previously been shown to have an inhibitory effect in BKPyV infections [167], although it had been contributed to the inhibition of a host ion channel required by BKPyV. The results described in this chapter suggest that the mechanism of DIDs inhibition could be through the inhibition of agnoprotein. Future work should investigate rimantadine, MNDNJ, and DIDs in floatation assays to determine if their inhibitory effect is pre- or post- insertion into membranes. The melittin control performed for DIDs indicated that perhaps DIDs was able to hinder the insertion of melittin into the liposomal membranes, causing a delay in dye release. If DIDs does prevent the insertion of agnoprotein into membranes, then it would disrupt the co-migration of agnoprotein and liposomes along a Ficoll gradient.

Interestingly, rimantadine, MNDNJ, and DIDs all also performed as potent inhibitors in BKPyV Dunlop infected cells (figure 5.5), reducing the virus released after 48 hr. To further investigate this observation, each compound will need testing on BKPyV Δ agno to determine if they have an additive affect when agnoprotein is absent. This would allow us to distinguish any off target affects and indicate if the compound act on agnoprotein. This was attempted during this project but needs further optimisation to allow for the release of enough BKPyV Δ agno to give reliable results in a fluorescence focus assay. In addition to this, titrations of rimantadine and MNDNJ should be performed to conclude the lowest

concentration required to significantly inhibit viral release. In addition to these characterisation, nuclear/cytoplasmic fractionations could be performed in BKPyV Dunlop infected cells to see if a similar phenotype is observed in treated cells compared to BKPyV Δ agno. In a recently published study [22] it was shown that the loss of agnoprotein resulted in virions becoming trapped in the nucleus, therefore if nuclear egress requires the viroporin function of agnoprotein then treatment with these compounds should result in increased nuclear associated virions.

Furthermore, *in silico* docking of these compounds onto a model of BKPyV agnoprotein should also be considered if a suitable model can be produced. This would give indication of how these compounds interact with BKPyV agnoprotein and allow for guided design of resistant mutants, which could be tested in the liposome and cell-based assays described in this project.

5.4.1 Could Resistant Strains of BKPyV form?

Resistance is an unprecedented problem in the design and discovery of new antimicrobial therapies. The sheer diversity in viral serotypes and the tendency to rely on error-prone replication machine means mutations in viral genomes can rapidly occur. RNA viruses, in particular, have rapid mutation rates as their viral encoded polymerases are often highly error prone. The RNA-polymerase of IAV lacks a proofreading function, therefore incorrect nucleotides are inserted into replicated genomes at a rate of 10^{-4} to 10^{-3} [318]. This is advantageous from the pathogens prospective as produces a wide variation in the progeny virus, enabling small proportions of overcome either the human immune system, or antiviral intervention. In comparison, DNA viruses rely on host replicative machine, and therefore have a lower mutation rate in the order of 10^{-8} to 10^{-6} [319]. Recent studies to develop novel antivirals have turned their attention to regions of viral proteins which are essential for function, or to essential host proteins required by the virus.

To investigate the rate of mutation with BKPyV agnoprotein, 252 genomes from clinical isolates were analysed and their agnoprotein sequences aligned (appendix). This analysis revealed that there was a series of common mutations that occur across the sequence of BKPyV agnoprotein. Considering the helical domain alone (aa 21-42), the following mutations were observed; K23R, R24I, Q26H, F29L, E38K, and F39L (table 5.2). It is important to note that of these mutations all, except Q26H, occur in agnoprotein from other polyomaviruses. This indicates that if the function of agnoprotein is conserved across polyomaviruses, then these mutations would be tolerated without affecting function. This would indicate that the compounds tested in this chapter may not provide a pan-inhibitory affect across all polyomaviruses.

Mutation	Frequency (tot. 252)	Source of Isolation	Example Strain(s)
K23R	26	Urine	FUJ-13 (AB269826.1) JPN-15 (AB269834.1) KOM-2 (AB211387.1)
R24I	1	Integrated into host genome	CH-2 (KY487998.1)
Q26H	1	Unpublished, source not recorded	TOM-11 (LC309239.1)
F29L	11	Blood, Urine	5682/KW (KY114803.1) A-37H (AB369089.1) A-66H (AB369093.1) GRC-4 (AB269830.1) ITA-4 (AB269833.1)
E38K	2	Urine of patient with Lupus	Mtclone18 (AB485698.1) Mtclone44 (AB485701.1)
F39L	1	Urine	OKN-42 (AB365153.1)

Table 5.2: Mutations found in the helical domain of agnoprotein from clinically isolated BKPyV stains

Other mutations are seen in the N- and C- terminal domains, and these regions seem to acquire a greater amount of mutations compared to the helical domain, including deletion/insertion mutations. Notable of these mutations was AS (M23122.1) stain; isolated from the urine of a pregnant woman, which contains an insertion of FCRPKNLV to the N-terminus of its agnoprotein. This mutation results in the extension of the small alpha helix predicted within the N-terminal domain. It is unlikely that this extended helix contributes to a further TM domain, as it is 13 aa in length, however it does not seem to hinder viral replication. In addition, it is worth mentioning HI-u6 (AY628237.1) strain, which contains a deletion of the phosphorylation at S11. S11 has been shown to be key to the regulation of agnoprotein during BKPyV infection.

We have shown that the viroporin function of BKPyV agnoprotein can be inhibited by Rimantadine and *MNDNJ*, and that these drugs result in a decrease in released virus. Providing a suitable model was created, *in silico* docking would be a sensible step in determining where these drugs might bind to agnoprotein. This would allow for rational design of resistant mutants in order to assess whether a resistant strain could arise. Alongside *in silico* docking, it would also be worth considering other viroporins, which have acquired resistance to adamantanes and imino-sugars, with the purpose of looking for trends. Rimantadine resistance has been observed in IAV M2 [261] and HCV p7 [264]; notably mutations of L26F and L20F, respectively, have been observed. If L>F mutations are common in generating rimantadine resistance, it made be rational to produce similar mutations in BKPyV agnoprotein with the hope of generating resistant mutants. Interestingly, L35 in BKPyV agnoprotein is replaced by F35 in JCPyV agnoprotein. Had more time been available this would have been easy to investigate this substitution, by carrying out viral release assays with JCPyV infection treated with rimantadine.

MNDNJ resistance, on the other hand, is most well characterised in HCV p7. Clinical isolates of HCV have been observed carrying the mutation F25A [264].

Previous work in the lab has demonstrated that BKPyV agnoprotein F39A (F39A), reduces viral titre though the mutant maintains similar cellular localisation to wt. This mutant could be easily treated with NNDNJ to determine if resistance has been conveyed, though in the timeframe of this project there was not enough time to produce BKPyV F39A virus.

Chapter 6 : Conclusions

Viroporins have been shown to play essential roles in viral lifecycles across many viral families. These roles are usually associated with viral entry and egress, where with many viruses it is important that the local concentration of ions is carefully rebalanced to prevent aberrant viral disassembly [213-215]. There have been many studies investigating viroporins as potential antiviral targets, and adamantane compounds have been clinically available against IAV M2 viroporin [252, 258]. The agnoprotein of JCPyV has previously been described to have viroporin activity [141, 142], however its function during the polyomavirus lifecycle remains unclear. It was previously shown that the loss of agnoprotein in BKPyV infections results in an egress defect where virions become trapped in the nucleus [22]. Agnoproteins are found in many members of the *Polyomaviridae* and are highly conserved. It is unknown if viroporin function was conserved across the members, and the role of this function is unknown in context of the viral lifecycle [135].

This study has described a robust detergent-free purification system to produce recombinant 10x His BKPyV agnoprotein in order to characterise its function. Previously the purification of a sufficient recombinant protein yield has limited the *in vitro* characterisation of BKPyV agnoprotein and other viroporins [244, 264]. The purification system described in this study significantly improved recombinant protein yields and improved upon the limitations in the previous method described above. The purification platform described (figure 3.10) in this study will allow for purification of mutant agnoproteins, without contamination from previously purified proteins, which had always been a concern when using rpHPLC.

Obtaining an improved protein yield enabled *in vitro* characterisation of channel forming activity by dye release assay in a liposomal based assay. These assays

have previously been used to characterise several viroporins, such as HCV p7 [264, 265] and HPV E5 [244, 282]. The data from these assays showed that BKPyV agnoprotein forms pores that release carboxyfluorescein from liposomes (figure 4.12). Furthermore, these data demonstrated that BKPyV agnoprotein catalysed release of carboxyfluorescein from liposomes in a concentration-dependent manner. Recombinant protein was also shown to form SDS resistant oligomers via western blot analysis (figure 4.1). This has previously been seen with JCPyV agnoprotein [158, 294], though often contributed as an artefact of SDS PAGE. Without validation of these oligomeric states, it remains unknown how many protomers form the channel, although the further work described above should address this.

To investigate the viroporin function of BKPyV agnoprotein in a more physiological context, a flow cytometry-based assay was used in mammalian cells. MC540 was a lipophilic dye, which fluoresces when cellular membranes become disrupted [308, 309] (figure 4.4). It was shown that MC540 fluorescence could distinguish between functional and non-functional CoxV 2B protein [311], suggesting this assay could be used to look at viroporin functionality (figure 4.5). The MC540 data showed that GFP- BKPyV agnoprotein was able to disrupt cellular membranes, and a series of BKPyV agnoprotein mutants revealed that the helical domain was essential to this ability (figure 4.7). Moreover, these experiments also suggested that phenylalanine and leucine were critical to membrane disruption (figure 4.8), and potentially indicating that these residues are positioned on the dimerisation interface. Following on from these studies, a BKPyV agnoprotein peptide was designed to span the helical domain, and showed channel forming activity in dye release assays (figure 4.13). Future work could design more peptides with the point mutations described to look at effects on channel formation.

Alongside MC540 assays, cell fractionations were performed and showed that BKPyV agnoprotein localises to the membranous fraction (figure 4.2). Furthermore, topology investigations showed that BKPyV agnoprotein was

positioned in both topological orientations in cells (figure 4.3), which has previously been suggested from dynamic modelling with JCPyV agnoprotein. However, hygromycin assays showed that the pore formed by BKPyV agnoprotein does not permeabilise the plasma membrane (figure 4.9). This indicates the viroporin function of BKPyV agnoprotein potentially plays a role in the viral lifecycle before the protein reaches the plasma membrane. Further investigation in cells is required to determine where the viroporin function of agnoprotein is functional in the polyomavirus lifecycle.

Having characterised the viroporin function of BKPyV agnoprotein, inhibitor molecules were tested for their effectiveness at impairing agnoprotein viroporin activity. BKPyV agnoprotein mediated dye release was shown to be significantly reduced by rimantadine (figure 5.1), *MNDNJ* (figure 5.2), and *DIDs* (figure 5.3), but not by amantadine. In this study, *DIDs* proved the most effective inhibitor, though further repeats are required. *DIDs* has previously been shown to inhibit BKPyV release in infected cells [167]. This study also observed *DIDs* to have a similar inhibitory effect in BKPyV infected cells, and furthermore it was shown that rimantadine and *MNDNJ* also inhibited release of virus from infected cells (figure 5.5).

In summary, this study has developed an improved platform for the purification of recombinant BKPyV agnoprotein. Using liposomal based assays, it was shown that BKPyV agnoprotein has a novel viroporin function. The channel formed by BKPyV agnoprotein was sensitive to rimantadine, *MNDNJ*, and *DIDs*; and these compounds are also affective at significantly reducing the viral release from BKPyV infected primary cells.

Chapter 7 : Reference

1. Eddy, B.E. and S.E. Stewart, *Characteristics of the SE Polyoma Virus*. American Journal of Public Health and the Nations Health, 1959. 49(11): p. 1486-1492.
2. Buck, C.B., et al., *The Ancient Evolutionary History of Polyomaviruses*. PLoS pathogens, 2016. 12(4): p. e1005574.
3. Fauquet, C.M. and M.A. Mayo, *The 7th ICTV Report*. Archives of Virology, 2001. 146(1): p. 189-194.
4. Calvignac-Spencer, S., et al., *A taxonomy update for the family Polyomaviridae*. Archives of virology, 2016. 161(6): p. 1739-1750.
5. Moens, U., et al., *ICTV Virus Taxonomy Profile: Polyomaviridae*. Journal of General Virology, 2017. 98(6): p. 1159-1160.
6. Van Doorslaer, K., et al., *Fish polyomaviruses belong to two distinct evolutionary lineages*. The Journal of general virology, 2018. 99(4): p. 567-573.
7. Zu Rhein, G.M. and S.-M. Chou, *Particles Resembling Papova Viruses in Human Cerebral Demyelinating Disease*. Science, 1965. 148(3676): p. 1477-1479.
8. Padgett, B.L., et al., *Cultivation of papova-like virus from human brain with progressive multifocal leucoencephalopathy*. Lancet, 1971. 1(7712): p. 1257-60.
9. Gardner, S.D., et al., *New human papovavirus (B.K.) isolated from urine after renal transplantation*. Lancet, 1971. 1(7712): p. 1253-7.
10. Babakir-Mina, M., et al., *Identification of the novel KI Polyomavirus in paranasal and lung tissues*. J Med Virol, 2009. 81(3): p. 558-61.
11. Gaynor, A.M., et al., *Identification of a novel polyomavirus from patients with acute respiratory tract infections*. PLoS Pathog, 2007. 3(5): p. e64.
12. Feng, H., et al., *Clonal integration of a polyomavirus in human Merkel cell carcinoma*. Science, 2008. 319(5866): p. 1096-100.
13. van der Meijden, E., et al., *Discovery of a new human polyomavirus associated with trichodysplasia spinulosa in an immunocompromized patient*. PLoS Pathog, 2010. 6(7): p. e1001024.

14. Siebrasse, E.A., et al., *Identification of MW polyomavirus, a novel polyomavirus in human stool*. J Virol, 2012. 86(19): p. 10321-6.
15. Lim, E.S., et al., *Discovery of STL polyomavirus, a polyomavirus of ancestral recombinant origin that encodes a unique T antigen by alternative splicing*. Virology, 2013. 436(2): p. 295-303.
16. Mishra, N., et al., *Identification of a novel polyomavirus in a pancreatic transplant recipient with retinal blindness and vasculitic myopathy*. J Infect Dis, 2014. 210(10): p. 1595-9.
17. Yu, G., et al., *Discovery of a novel polyomavirus in acute diarrheal samples from children*. PloS one, 2012. 7(11): p. e49449-e49449.
18. Gheit, T., et al., *Isolation and characterization of a novel putative human polyomavirus*. Virology, 2017. 506: p. 45-54.
19. Schowalter, R.M., et al., *Merkel cell polyomavirus and two previously unknown polyomaviruses are chronically shed from human skin*. Cell Host Microbe, 2010. 7(6): p. 509-15.
20. Scuda, N., et al., *A novel human polyomavirus closely related to the african green monkey-derived lymphotropic polyomavirus*. J Virol, 2011. 85(9): p. 4586-90.
21. Korup, S., et al., *Identification of a novel human polyomavirus in organs of the gastrointestinal tract*. PloS one, 2013. 8(3): p. e58021.
22. Panou, M.-M., et al., *Agnoprotein Is an Essential Egress Factor during BK Polyomavirus Infection*. International Journal of Molecular Sciences, 2018. 19(3): p. 902.
23. DeCaprio, J.A. and R.L. Garcea, *A cornucopia of human polyomaviruses*. Nat Rev Microbiol, 2013. 11(4): p. 264-76.
24. Kamminga, S., et al., *Seroprevalence of fourteen human polyomaviruses determined in blood donors*. PLOS ONE, 2018. 13(10): p. e0206273.
25. De Gascun, C.F. and M.J. Carr, *Human polyomavirus reactivation: disease pathogenesis and treatment approaches*. Clinical & Developmental Immunology, 2013. 2013: p. 373579.
26. Drachenberg, C.B. and J.C. Papadimitriou, *Polyomavirus-associated nephropathy: update in diagnosis*. Transpl Infect Dis, 2006. 8(2): p. 68-75.
27. Coleman, D.V., et al., *Human polyomavirus (BK) infection and ureteric stenosis in renal allograft recipients*. J Clin Pathol, 1978. 31(4): p. 338-47.

28. Höller, K., et al., *Dynamics of BKPyV reactivation and risk of hemorrhagic cystitis after allogeneic hematopoietic stem cell transplantation*. European Journal of Haematology, 2017. 99(2): p. 133-140.
29. Nguyen, K.D., et al., *Human polyomavirus 6 and 7 are associated with pruritic and dyskeratotic dermatoses*. J Am Acad Dermatol, 2017. 76(5): p. 932-940 e3.
30. Wu, J.H., et al., *Dysregulation of the MEK/ERK/MNK1 signaling cascade by middle T antigen of the trichoydsplasia spinulosa polyomavirus*. J Eur Acad Dermatol Venereol, 2017: p. n/a-n/a.
31. Nicol, J.T., et al., *Seroprevalence of human Malawi polyomavirus*. J Clin Microbiol, 2014. 52(1): p. 321-3.
32. Yu, G., et al., *Discovery of a Novel Polyomavirus in Acute Diarrheal Samples from Children*. PLOS ONE, 2012. 7(11): p. e49449.
33. Lim, E.S., et al., *Common exposure to STL polyomavirus during childhood*. Emerg Infect Dis, 2014. 20(9): p. 1559-61.
34. Saundh, B.K., *The Association Between Human Polyomaviruses and Renal Transplant Rejection*, in *Faculty of Biological Sciences*. 2011, University of Leeds.
35. Limate, A.P., et al., *Polyomavirus nephropathy in native kidneys of non-renal transplant recipients*. Am J Transplant, 2005. 5(3): p. 614-20.
36. Cubukcu-Dimopulo, O., et al., *BK virus infection in AIDS*. Am J Surg Pathol, 2000. 24(1): p. 145-9.
37. Khalili, K., et al., *Reactivation of JC virus and development of PML in patients with multiple sclerosis*. Neurology, 2007. 68(13): p. 985-90.
38. Del Valle, L. and S. Piña-Oviedo, *Human Polyomavirus JCPyV and Its Role in Progressive Multifocal Leukoencephalopathy and Oncogenesis*. Frontiers in Oncology, 2019. 9(711).
39. Velásquez, C., et al., *Characterization of a Merkel Cell Polyomavirus-Positive Merkel Cell Carcinoma Cell Line CVG-1*. Frontiers in Microbiology, 2018. 9(713).
40. Moens, U. and M. Johannessen, *Human polyomaviruses and cancer: expanding repertoire*. JDDG: Journal der Deutschen Dermatologischen Gesellschaft, 2008. 6(9): p. 704-708.

41. González-Vela, M.d.C., et al., *Shared Oncogenic Pathways Implicated in Both Virus-Positive and UV-Induced Merkel Cell Carcinomas*. *Journal of Investigative Dermatology*, 2017. 137(1): p. 197-206.
42. Kenan, D.J., et al., *The oncogenic potential of BK-polyomavirus is linked to viral integration into the human genome*. *The Journal of Pathology*, 2015. 237(3): p. 379-389.
43. Kenan, D.J., et al., *BK Polyomavirus Genomic Integration and Large T Antigen Expression: Evolving Paradigms in Human Oncogenesis*. *American Journal of Transplantation*, 2016.
44. Dalianis, T. and H.H. Hirsch, *Human polyomaviruses in disease and cancer*. *Virology*, 2013. 437(2): p. 63-72.
45. Bofill-Mas, S., S. Pina, and R. Girones, *Documenting the Epidemiologic Patterns of Polyomaviruses in Human Populations by Studying Their Presence in Urban Sewage*. *Applied and Environmental Microbiology*, 2000. 66(1): p. 238-245.
46. Varughese, E.A., et al., *Estimating virus occurrence using Bayesian modeling in multiple drinking water systems of the United States*. *The Science of the total environment*, 2018. 619-620: p. 1330-1339.
47. Bofill-Mas, S., et al., *Potential transmission of human polyomaviruses through the gastrointestinal tract after exposure to virions or viral DNA*. *Journal of virology*, 2001. 75(21): p. 10290-10299.
48. Jeffers, L.K., V. Madden, and J. Webster-Cyriaque, *BK virus has tropism for human salivary gland cells in vitro: Implications for transmission*. *Virology*, 2009. 394(2): p. 183-193.
49. Das, D., R.B. Shah, and M.J. Imperiale, *Detection and expression of human BK virus sequences in neoplastic prostate tissues*. *Oncogene*, 2004. 23(42): p. 7031-7046.
50. Keller, E.X., et al., *Polyomavirus BK and prostate cancer: a complex interaction of potential clinical relevance*. *Reviews in Medical Virology*, 2015. 25(6): p. 366-378.
51. Cheungpasitporn, W., et al., *Reactivation of BK polyomavirus during pregnancy, vertical transmission, and clinical significance: A meta-analysis*. *Journal of Clinical Virology*, 2018. 102: p. 56-62.

52. Arthur, R.R., et al., *Association of BK viruria with hemorrhagic cystitis in recipients of bone marrow transplants*. N Engl J Med, 1986. 315(4): p. 230-4.
53. Hirsch, H., et al., *BK Polyomavirus Replication in Renal Tubular Epithelial Cells Is Inhibited by Sirolimus, but Activated by Tacrolimus Through a Pathway Involving FKBP-12*. American Journal of Transplantation, 2015.
54. Bennett, S.M., N.M. Broekema, and M.J. Imperiale, *BK polyomavirus: emerging pathogen*. Microbes Infect, 2012. 14(9): p. 672-83.
55. Ginevri, F. and H.H. Hirsch, *Polyomavirus-Associated Nephropathy*. Evidence-Based Nephrology, 2008: p. 277-284.
56. Stracke, S., et al., *Polyoma virus-associated interstitial nephritis in a patient with acute myeloic leukaemia and peripheral blood stem cell transplantation*. Nephrol Dial Transplant, 2003. 18(11): p. 2431-3.
57. Milstone, A., et al., *Polyomavirus simian virus 40 infection associated with nephropathy in a lung-transplant recipient*. Transplantation, 2004. 77(7): p. 1019-24.
58. Schwarz, A., et al., *Polyoma virus nephropathy in native kidneys after lung transplantation*. Am J Transplant, 2005. 5(10): p. 2582-5.
59. Bratt, G., et al., *BK virus as the cause of meningoencephalitis, retinitis and nephritis in a patient with AIDS*. AIDS, 1999. 13(9): p. 1071-1075.
60. Hedquist, B.G., et al., *Identification of BK virus in a patient with acquired immune deficiency syndrome and bilateral atypical retinitis*. Ophthalmology, 1999. 106(1): p. 129-132.
61. Cabrejo, L., et al., *Leucoencéphalopathie multifocale progressive à BK virus chez un patient immunodéprimé par une corticothérapie*. Revue Neurologique, 2005. 161(3): p. 326-330.
62. White, M.K., et al., *Human polyomaviruses and brain tumors*. Brain Research Reviews, 2005. 50(1): p. 69-85.
63. Corallini, A., et al., *Association of BK virus with human brain tumors and tumors of pancreatic islets*. International journal of cancer, 1987. 39(1): p. 60-67.
64. Flægstad, T., et al., *A possible contributory role of BK virus infection in neuroblastoma development*. Cancer Research, 1999. 59(5): p. 1160-1163.

65. Yin, W.-Y., et al., *BK virus as a potential oncovirus for bladder cancer in a renal transplant patient*. Journal of the Formosan Medical Association, 2015. 114(4): p. 373-374.
66. Starrett, G.J. and C.B. Buck, *The case for BK polyomavirus as a cause of bladder cancer*. Current Opinion in Virology, 2019. 39: p. 8-15.
67. Abend, J.R., M. Jiang, and M.J. Imperiale, *BK virus and human cancer: Innocent until proven guilty*. Seminars in Cancer Biology, 2009. 19(4): p. 252-260.
68. Comar, M., et al., *High prevalence of BK polyomavirus sequences in human papillomavirus-16-positive precancerous cervical lesions*. Journal of medical virology, 2011. 83(10): p. 1770-1776.
69. Levican, J., et al., *Role of BK human polyomavirus in cancer*. Infectious agents and cancer, 2018. 13: p. 12-12.
70. Lamarche, C., et al., *BK Polyomavirus and the Transplanted Kidney: Immunopathology and Therapeutic Approaches*. Transplantation, 2016. 100(11): p. 2276-2287.
71. Kadambi, P.V., et al., *Treatment of refractory BK virus-associated nephropathy with cidofovir*. Am J Transplant, 2003. 3(2): p. 186-91.
72. Cekmen, M.B., et al., *BK virus nephropathy developing after renal transplantation and its treatment with ciprofloxacin: a case report*. Transplant Proc, 2012. 44(10): p. 3044-7.
73. Leung, A.Y., et al., *Ciprofloxacin decreased polyoma BK virus load in patients who underwent allogeneic hematopoietic stem cell transplantation*. Clin Infect Dis, 2005. 40(4): p. 528-37.
74. Williams, J.W., et al., *Leflunomide for polyomavirus type BK nephropathy*. N Engl J Med, 2005. 352(11): p. 1157-8.
75. Pastrana, D.V., et al., *Neutralization Serotyping of BK Polyomavirus Infection in Kidney Transplant Recipients*. PLOS Pathogens, 2012. 8(4): p. e1002650.
76. Astrom, K., E. Mancall, and E. Richardson, *Progressive multifocal leukoencephalopathy*. Brain, 1958. 81(1): p. 93-111.
77. Howatson, A.F., M. Nagai, and G.M. Zurhein, *POLYOMA-LIKE VIRIONS IN HUMAN DEMYELINATING BRAIN DISEASE*. Canadian Medical Association journal, 1965. 93(9): p. 379-386.

78. Avsenik, J., A. Horvat Ledinek, and K. Šurlan Popovič, *Progressive multifocal leukoencephalopathy - immune reconstitution inflammatory syndrome (PML-IRIS) in liver transplant recipient*. Multiple Sclerosis and Related Disorders, 2017. 17: p. 135-137.
79. Mateen, F.J., et al., *Progressive multifocal leukoencephalopathy in transplant recipients*. Annals of neurology, 2011. 70(2): p. 305-322.
80. Aksamit, A.J., et al., *AIDS-associated progressive multifocal leukoencephalopathy (PML)*. Comparison to non-AIDS PML with in situ hybridization and immunohistochemistry, 1990. 40(7): p. 1073-1073.
81. Hernández, B., F. Dronda, and S. Moreno, *Treatment options for AIDS patients with progressive multifocal leukoencephalopathy*. Expert Opinion on Pharmacotherapy, 2009. 10(3): p. 403-416.
82. Randhawa, P., et al., *JC VIRUS INFECTION IN ALLOGRAFT KIDNEYS: Analysis by Polymerase Chain Reaction and Immunohistochemistry*. Transplantation, 2001. 71(9): p. 1300-1303.
83. Kazory, A., et al., *THE FIRST CASE OF JC VIRUS ALLOGRAFT NEPHROPATHY*. Transplantation, 2003. 76(11): p. 1653-1655.
84. Wen, M.-C., et al., *Association of JC virus with tubulointerstitial nephritis in a renal allograft recipient*. Journal of Medical Virology, 2004. 72(4): p. 675-678.
85. Rencic, A., et al., *Detection of JC virus DNA sequence and expression of the viral oncoprotein, tumor antigen, in brain of immunocompetent patient with oligoastrocytoma*. Proceedings of the National Academy of Sciences, 1996. 93(14): p. 7352-7357.
86. Enam, S., et al., *Association of Human Polyomavirus JCV with Colon Cancer*. Evidence for Interaction of Viral T-Antigen and β -Catenin, 2002. 62(23): p. 7093-7101.
87. Clifford, D.B., et al., *HAART improves prognosis in HIV-associated progressive multifocal leukoencephalopathy*. Neurology, 1999. 52(3): p. 623-623.
88. Salmaggi, A., et al., *Reversal of CSF positivity for JC virus genome by cidofovir in a patient with systemic lupus erythematosus and progressive multifocal leukoencephalopathy*. Neurological Sciences, 2001. 22(1): p. 17-20.

89. Gasnault, J., et al., *Cidofovir in AIDS-associated progressive multifocal leukoencephalopathy: A monocenter observational study with clinical and JC virus load monitoring*. *Journal of NeuroVirology*, 2001. 7(4): p. 375-381.
90. O'Riordan, T., et al., *Progressive multifocal leukoencephalopathy-remission with cytarabine*. *Journal of Infection*, 1990. 20(1): p. 51-54.
91. Gofton, T.E., et al., *Mefloquine in the treatment of progressive multifocal leukoencephalopathy*. *Journal of Neurology, Neurosurgery & Psychiatry*, 2011. 82(4): p. 452-455.
92. Przepiorka, D., et al., *Successful treatment of progressive multifocal leukoencephalopathy with low-dose interleukin-2*. *Bone Marrow Transplantation*, 1997. 20(11): p. 983-987.
93. Cettomai, D. and J.C. McArthur, *Mirtazapine Use in Human Immunodeficiency Virus–Infected Patients With Progressive Multifocal Leukoencephalopathy*. *Archives of Neurology*, 2009. 66(2): p. 255-258.
94. Ray, U., et al., *JC polyomavirus mutants escape antibody-mediated neutralization*. *Science Translational Medicine*, 2015. 7(306): p. 306ra151-306ra151.
95. Seif, I., G. Khoury, and R. Dhar, *The genome of human papovavirus BKV*. *Cell*, 1979. 18(4): p. 963-77.
96. Ferenczy, M.W., et al., *Molecular Biology, Epidemiology, and Pathogenesis of Progressive Multifocal Leukoencephalopathy, the JC Virus-Induced Demyelinating Disease of the Human Brain*. *Clinical Microbiology Reviews*, 2012. 25(3): p. 471-506.
97. Brodsky, J.L. and J.M. Pipas, *Polyomavirus T antigens: molecular chaperones for multiprotein complexes*. *J Virol*, 1998. 72(7): p. 5329-34.
98. An, P., M.T. Saenz Robles, and J.M. Pipas, *Large T antigens of polyomaviruses: amazing molecular machines*. *Annu Rev Microbiol*, 2012. 66(1): p. 213-36.
99. Bauman, Y., et al., *An identical miRNA of the human JC and BK polyoma viruses targets the stress-induced ligand ULBP3 to escape immune elimination*. *Cell Host Microbe*, 2011. 9(2): p. 93-102.
100. Broekema, N.M. and M.J. Imperiale, *miRNA regulation of BK polyomavirus replication during early infection*. *Proceedings of the National Academy of Sciences of the United States of America*, 2013. 110(20): p. 8200-8205.

101. Henriksen, S., et al., *The Presumed Polyomavirus Viroporin VP4 of Simian Virus 40 or Human BK Polyomavirus Is Not Required for Viral Progeny Release*. J Virol, 2016. 90(22): p. 10398-10413.
102. Jay, G., et al., *Identification of the SV40 agnogene product: a DNA binding protein*. Nature, 1981. 291(5813): p. 346-349.
103. Rinaldo, C.H., T. Traavik, and A. Hey, *The agnogene of the human polyomavirus BK is expressed*. Journal of virology, 1998. 72(7): p. 6233-6236.
104. Bethge, T., et al., *Sp1 sites in the noncoding control region of BK polyomavirus are key regulators of bidirectional viral early and late gene expression*. J Virol, 2015. 89(6): p. 3396-411.
105. Gosert, R., et al., *Rearranged JC Virus Noncoding Control Regions Found in Progressive Multifocal Leukoencephalopathy Patient Samples Increase Virus Early Gene Expression and Replication Rate*. Journal of Virology, 2010. 84(20): p. 10448-10456.
106. Gosert, R., et al., *Polyomavirus BK with rearranged noncoding control region emerge in vivo in renal transplant patients and increase viral replication and cytopathology*. The Journal of experimental medicine, 2008. 205(4): p. 841-852.
107. Carr, M.J., et al., *Unique BK virus non-coding control region (NCCR) variants in hematopoietic stem cell transplant recipients with and without hemorrhagic cystitis*. Journal of Medical Virology, 2006. 78(4): p. 485-493.
108. Burger-Calderon, R., et al., *Distinct BK polyomavirus non-coding control region (NCCR) variants in oral fluids of HIV- associated Salivary Gland Disease patients*. Virology, 2016. 493: p. 255-266.
109. Marshall, L.J., et al., *JC virus promoter/enhancers contain TATA box-associated Spi-B-binding sites that support early viral gene expression in primary astrocytes*. Journal of General Virology, 2012. 93(3): p. 651-661.
110. Sharma, P.M., et al., *Polyomavirus BK non-coding control region rearrangements in health and disease*. Journal of Medical Virology, 2007. 79(8): p. 1199-1207.
111. Wortman, M.J., et al., *Opportunistic DNA Recombination With Epstein-Barr Virus at Sites of Control Region Rearrangements Mediating JC Virus*

- Neurovirulence*. The Journal of Infectious Diseases, 2015. 213(9): p. 1436-1443.
112. Johnson, E.M., et al., *Polyomavirus JC in the Context of Immunosuppression: A Series of Adaptive, DNA Replication-Driven Recombination Events in the Development of Progressive Multifocal Leukoencephalopathy*. Clinical and Developmental Immunology, 2013. 2013: p. 10.
 113. Cheng, J., et al., *Cellular transformation by Simian Virus 40 and Murine Polyoma Virus T antigens*. Semin Cancer Biol, 2009. 19(4): p. 218-28.
 114. Cheng, J., et al., *Merkel cell polyomavirus large T antigen has growth-promoting and inhibitory activities*. Journal of virology, 2013. 87(11): p. 6118-6126.
 115. Farmerie, W.G. and W.R. Folk, *Regulation of polyomavirus transcription by large tumor antigen*. Proceedings of the National Academy of Sciences, 1984. 81(22): p. 6919-6923.
 116. Prezioso, C., et al., *Efficient propagation of archetype JC polyomavirus in COS-7 cells: evaluation of rearrangements within the NCCR structural organization after transfection*. Archives of Virology, 2017. 162(12): p. 3745-3752.
 117. Broekema, N.M. and M.J. Imperiale, *Efficient propagation of archetype BK and JC polyomaviruses*. Virology, 2012. 422(2): p. 235-241.
 118. Ahuja, D., M.T. Saenz-Robles, and J.M. Pipas, *SV40 large T antigen targets multiple cellular pathways to elicit cellular transformation*. Oncogene, 0000. 24(52): p. 7729-7745.
 119. Watanabe, G., et al., *Induction of cyclin D1 by simian virus 40 small tumor antigen*. Proc Natl Acad Sci U S A, 1996. 93(23): p. 12861-6.
 120. Griffiths, D.A., et al., *Merkel cell polyomavirus small T antigen targets the NEMO adaptor protein to disrupt inflammatory signaling*. J Virol, 2013. 87(24): p. 13853-67.
 121. Riley, M.I., et al., *Tiny T antigen: an autonomous polyomavirus T antigen amino-terminal domain*. J Virol, 1997. 71(8): p. 6068-74.
 122. Abend, J.R., et al., *A truncated T antigen expressed from an alternatively spliced BK virus early mRNA*. J Gen Virol, 2009. 90(Pt 5): p. 1238-45.

123. Bollag, B., et al., *Purified JC virus T and T' proteins differentially interact with the retinoblastoma family of tumor suppressor proteins*. *Virology*, 2000. 274(1): p. 165-78.
124. Zerrahn, J., et al., *Independent expression of the transforming amino-terminal domain of SV40 large T antigen from an alternatively spliced third SV40 early mRNA*. *EMBO J*, 1993. 12(12): p. 4739-46.
125. Hurdiss, D.L., et al., *New Structural Insights into the Genome and Minor Capsid Proteins of BK Polyomavirus using Cryo-Electron Microscopy*. *Structure*, 2016. 24(4): p. 528-36.
126. Hurdiss, D.L., et al., *The Structure of an Infectious Human Polyomavirus and Its Interactions with Cellular Receptors*. *Structure*, 2018. 26(6): p. 839-847.e3.
127. Stehle, T., et al., *The structure of simian virus 40 refined at 3.1 Å resolution*. *Structure*, 1996. 4(2): p. 165-182.
128. Daniels, R., et al., *SV40 VP2 and VP3 insertion into ER membranes is controlled by the capsid protein VP1: implications for DNA translocation out of the ER*. *Mol Cell*, 2006. 24(6): p. 955-66.
129. Inoue, T. and B. Tsai, *A large and intact viral particle penetrates the endoplasmic reticulum membrane to reach the cytosol*. *PLoS Pathog*, 2011. 7(5): p. e1002037.
130. Bennett, S.M., et al., *Role of a nuclear localization signal on the minor capsid Proteins VP2 and VP3 in BKPyV nuclear entry*. *Virology*, 2015. 474: p. 110-116.
131. Soldatova, I., et al., *Interaction of the Mouse Polyomavirus Capsid Proteins with Importins Is Required for Efficient Import of Viral DNA into the Cell Nucleus*. *Viruses*, 2018. 10(4): p. 165.
132. Gasparovic, M.L., G.V. Gee, and W.J. Atwood, *JC virus minor capsid proteins Vp2 and Vp3 are essential for virus propagation*. *J Virol*, 2006. 80(21): p. 10858-61.
133. Huerfano, S., et al., *Minor capsid proteins of mouse polyomavirus are inducers of apoptosis when produced individually but are only moderate contributors to cell death during the late phase of viral infection*. *FEBS journal*, 2010. 277(5): p. 1270-1283.

134. Raghava, S., et al., *The SV40 Late Protein VP4 Is a Viroporin that Forms Pores to Disrupt Membranes for Viral Release*. PLoS pathogens, 2011. 7(6): p. e1002116.
135. Gerits, N. and U. Moens, *Agnoprotein of mammalian polyomaviruses*. Virology, 2012. 432(2): p. 316-26.
136. Khalili, K., et al., *The agnoprotein of polyomaviruses: a multifunctional auxiliary protein*. J Cell Physiol, 2005. 204(1): p. 1-7.
137. Del Valle, L., et al., *Expression of human neurotropic polyomavirus JCV late gene product agnoprotein in human medulloblastoma*. J Natl Cancer Inst, 2002. 94(4): p. 267-73.
138. Leuenberger, D., et al., *Human polyomavirus type 1 (BK virus) agnoprotein is abundantly expressed but immunologically ignored*. Clinical and Vaccine Immunology, 2007. 14(8): p. 959-968.
139. Suzuki, T., et al., *Role of JC virus agnoprotein in virion formation*. Microbiol Immunol, 2012. 56(9): p. 639-46.
140. Sariyer, I.K., et al., *Infection by agnoprotein-negative mutants of polyomavirus JC and SV40 results in the release of virions that are mostly deficient in DNA content*. Virology journal, 2011. 8(1): p. 1.
141. Suzuki, T., et al., *Viroporin activity of the JC polyomavirus is regulated by interactions with the adaptor protein complex 3*. Proc Natl Acad Sci U S A, 2013. 110(46): p. 18668-73.
142. Suzuki, T., et al., *The human polyoma JC virus agnoprotein acts as a viroporin*. PLoS Pathog, 2010. 6(3): p. e1000801.
143. Johannessen, M., et al., *BKV agnoprotein interacts with alpha-soluble N-ethylmaleimide-sensitive fusion attachment protein, and negatively influences transport of VSVG-EGFP*. PloS one, 2011. 6(9): p. e24489.
144. Gerits, N., et al., *Agnoprotein of polyomavirus BK interacts with proliferating cell nuclear antigen and inhibits DNA replication*. Virol J, 2015. 12(1): p. 7.
145. Suzuki, T., et al., *Identification of FEZ1 as a protein that interacts with JC virus agnoprotein and microtubules: role of agnoprotein-induced dissociation of FEZ1 from microtubules in viral propagation*. J Biol Chem, 2005. 280(26): p. 24948-56.

146. Okada, Y., et al., *Dissociation of heterochromatin protein 1 from lamin B receptor induced by human polyomavirus agnoprotein: role in nuclear egress of viral particles*. EMBO Rep, 2005. 6(5): p. 452-7.
147. Darbinyan, A., et al., *Role of JC virus agnoprotein in DNA repair*. J Virol, 2004. 78(16): p. 8593-600.
148. Darbinyan, A., et al., *Evidence for dysregulation of cell cycle by human polyomavirus, JCV, late auxiliary protein*. Oncogene, 2002. 21(36): p. 5574-81.
149. Endo, S., et al., *JC virus agnoprotein colocalizes with tubulin*. J Neurovirol, 2003. 9 Suppl 1(sup1): p. 10-4.
150. Kaniowska, D., et al., *Cross-interaction between JC virus agnoprotein and human immunodeficiency virus type 1 (HIV-1) tat modulates transcription of the HIV-1 long terminal repeat in glial cells*. Journal of virology, 2006. 80(18): p. 9288-9299.
151. Safak, M., et al., *Functional interaction between JC virus late regulatory agnoprotein and cellular Y-box binding transcription factor, YB-1*. Journal of virology, 2002. 76(8): p. 3828-3838.
152. Safak, M., et al., *Interaction of JC virus agno protein with T antigen modulates transcription and replication of the viral genome in glial cells*. J Virol, 2001. 75(3): p. 1476-86.
153. Sariyer, I.K., K. Khalili, and M. Safak, *Dephosphorylation of JC virus agnoprotein by protein phosphatase 2A: inhibition by small t antigen*. Virology, 2008. 375(2): p. 464-79.
154. Okada, Y., et al., *Distribution and function of JCV agnoprotein*. J Neurovirol, 2001. 7(4): p. 302-6.
155. Unterstab, G., et al., *The polyomavirus BK agnoprotein co-localizes with lipid droplets*. Virology, 2010. 399(2): p. 322-31.
156. Unterstab, G., J. Manzetti, and H.H. Hirsch, *Corrigendum to "The polyomavirus BK agnoprotein co-localizes with lipid droplets"*[Virology 399 (2)(2010) 322–331]. Virology, 2013. 441(2): p. 197-199.
157. Coric, P., et al., *Nuclear magnetic resonance structure revealed that the human polyomavirus JC virus agnoprotein contains an α -helix encompassing the Leu/Ile/Phe-rich domain*. Journal of virology, 2014. 88(12): p. 6556-6575.

158. Sami Saribas, A., et al., *Essential roles of Leu/Ile/Phe-rich domain of JC virus agnoprotein in dimer/oligomer formation, protein stability and splicing of viral transcripts*. *Virology*, 2013. 443(1): p. 161-76.
159. Coric, P., et al., *Nuclear Magnetic Resonance Structure of the Human Polyoma JC Virus Agnoprotein*. *J Cell Biochem*, 2017: p. n/a-n/a.
160. Zhao, L., et al., *Caveolin- and clathrin-independent entry of BKPyV into primary human proximal tubule epithelial cells*. *Virology*, 2016. 492: p. 66-72.
161. Low, J.A., et al., *Identification of Gangliosides GD1b and GT1b as Receptors for BK Virus*. *Journal of Virology*, 2006. 80(3): p. 1361-1366.
162. Jiang, M., et al., *Early Events during BK Virus Entry and Disassembly*. *Journal of Virology*, 2009. 83(3): p. 1350-1358.
163. Bennett, S.M., M. Jiang, and M.J. Imperiale, *Role of Cell-Type-Specific Endoplasmic Reticulum-Associated Degradation in Polyomavirus Trafficking*. *Journal of Virology*, 2013. 87(16): p. 8843-8852.
164. Geiger, R., et al., *BAP31 and BiP are essential for dislocation of SV40 from the endoplasmic reticulum to the cytosol*. *Nature Cell Biology*, 2011. 13(11): p. 1305-1314.
165. Dupzyk, A. and B. Tsai, *How Polyomaviruses Exploit the ERAD Machinery to Cause Infection*. *Viruses*, 2016. 8(9): p. 242.
166. Erickson, K.D., et al., *Virion assembly factories in the nucleus of polyomavirus-infected cells*. *PLoS Pathog*, 2012. 8(4): p. e1002630.
167. Evans, G.L., et al., *Anion homeostasis is important for non-lytic release of BK polyomavirus from infected cells*. *Open Biology*, 2015. 5(8): p. 150041.
168. Stehle, T. and S.C. Harrison, *High-resolution structure of a polyomavirus VP1-oligosaccharide complex: implications for assembly and receptor binding*. *EMBO J*, 1997. 16(16): p. 5139-48.
169. Rauvala, H., *Gangliosides of human kidney*. *Journal of Biological Chemistry*, 1976. 251(23): p. 7517-7520.
170. Yu, R.K., et al., *Structures, biosynthesis, and functions of gangliosides--an overview*. *Journal of oleo science*, 2011. 60(10): p. 537-544.
171. O'Hara, S.D., T. Stehle, and R. Garcea, *Glycan receptors of the Polyomaviridae: structure, function, and pathogenesis*. *Current Opinion in Virology*, 2014. 7: p. 73-78.

172. Assetta, B., et al., *5-HT2 receptors facilitate JC polyomavirus entry*. Journal of virology, 2013. 87(24): p. 13490-13498.
173. Erickson, K.D., R.L. Garcea, and B. Tsai, *Ganglioside GT1b Is a Putative Host Cell Receptor for the Merkel Cell Polyomavirus*. Journal of Virology, 2009. 83(19): p. 10275.
174. Akgül, B., et al., *Lack of integrin $\beta 5$ in Merkel cell carcinomas and derived cell lines is frequently associated with Merkel cell polyomavirus positivity*. Journal of Dermatological Science, 2012. 67(1): p. 66-68.
175. Tsai, B., et al., *Gangliosides are receptors for murine polyoma virus and SV40*. The EMBO Journal, 2003. 22(17): p. 4346-4355.
176. Ströh, L.J., et al., *Structure Analysis of the Major Capsid Proteins of Human Polyomaviruses 6 and 7 Reveals an Obstructed Sialic Acid Binding Site*. Journal of Virology, 2014. 88(18): p. 10831.
177. Neu, U., et al., *A structure-guided mutation in the major capsid protein retargets BK polyomavirus*. PLoS Pathog, 2013. 9(10): p. e1003688.
178. Pastrana, D.V., et al., *BK Polyomavirus Genotypes Represent Distinct Serotypes with Distinct Entry Tropism*. Journal of Virology, 2013. 87(18): p. 10105-10113.
179. Eash, S., W. Querbes, and W.J. Atwood, *Infection of Vero Cells by BK Virus Is Dependent on Caveolae*. Journal of Virology, 2004. 78(21): p. 11583-11590.
180. Moriyama, T., et al., *Caveolar endocytosis is critical for BK virus infection of human renal proximal tubular epithelial cells*. J Virol, 2007. 81(16): p. 8552-62.
181. Moriyama, T. and A. Sorokin, *Intracellular trafficking pathway of BK Virus in human renal proximal tubular epithelial cells*. Virology, 2008. 371(2): p. 336-49.
182. Zhao, L.B., et al., *Caveolin- and clathrin-independent entry of BKPyV into primary human proximal tubule epithelial cells*. Virology, 2016. 492: p. 66-72.
183. Lamaze, C., et al., *Interleukin 2 Receptors and Detergent-Resistant Membrane Domains Define a Clathrin-Independent Endocytic Pathway*. Molecular Cell, 2001. 7(3): p. 661-671.

184. Chadda, R., et al., *Cholesterol-Sensitive Cdc42 Activation Regulates Actin Polymerization for Endocytosis via the GEEC Pathway*. *Traffic*, 2007. 8(6): p. 702-717.
185. Radhakrishna, H. and J.G. Donaldson, *ADP-ribosylation factor 6 regulates a novel plasma membrane recycling pathway*. *The Journal of cell biology*, 1997. 139(1): p. 49-61.
186. Glebov, O.O., N.A. Bright, and B.J. Nichols, *Flotillin-1 defines a clathrin-independent endocytic pathway in mammalian cells*. *Nature Cell Biology*, 2006. 8(1): p. 46-54.
187. Eash, S. and W.J. Atwood, *Involvement of cytoskeletal components in BK virus infectious entry*. *J Virol*, 2005. 79(18): p. 11734-41.
188. Rainey-Barger, E.K., B. Magnuson, and B. Tsai, *A chaperone-activated nonenveloped virus perforates the physiologically relevant endoplasmic reticulum membrane*. *J Virol*, 2007. 81(23): p. 12996-3004.
189. Rainey-Barger, E.K., S. Mkrтчian, and B. Tsai, *The C-terminal domain of ERp29 mediates polyomavirus binding, unfolding, and infection*. *Journal of virology*, 2009. 83(3): p. 1483-1491.
190. Magnuson, B., et al., *ERp29 triggers a conformational change in polyomavirus to stimulate membrane binding*. *Mol Cell*, 2005. 20(2): p. 289-300.
191. Inoue, T., et al., *ERdj5 Reductase Cooperates with Protein Disulfide Isomerase To Promote Simian Virus 40 Endoplasmic Reticulum Membrane Translocation*. *Journal of virology*, 2015. 89(17): p. 8897-8908.
192. Mockus, T.E., et al., *CD4 T cells control development and maintenance of brain-resident CD8 T cells during polyomavirus infection*. *PLoS pathogens*, 2018. 14(10): p. e1007365-e1007365.
193. Gheuens, S., et al., *Role of CD4+ and CD8+ T-cell responses against JC virus in the outcome of patients with progressive multifocal leukoencephalopathy (PML) and PML with immune reconstitution inflammatory syndrome*. *Journal of virology*, 2011. 85(14): p. 7256-7263.
194. Randhawa, P.S., et al., *Polyomavirus BK neutralizing activity in human immunoglobulin preparations*. *Transplantation*, 2010. 89(12): p. 1462-1465.

195. Stuyver, L.J., et al., *An antibody response to human polyomavirus 15-mer peptides is highly abundant in healthy human subjects*. *Virology journal*, 2013. 10: p. 192-192.
196. Pietrobon, S., et al., *Specific IgG Antibodies React to Mimotopes of BK Polyomavirus, a Small DNA Tumor Virus, in Healthy Adult Sera*. *Frontiers in immunology*, 2017. 8: p. 236-236.
197. Randhawa, P., R. Shapiro, and A. Vats, *Quantitation of DNA of Polyomaviruses BK and JC in Human Kidneys*. *The Journal of Infectious Diseases*, 2005. 192(3): p. 504-509.
198. Replogue, M.D., G.A. Storch, and D.B. Clifford, *BK Virus: A Clinical Review*. *Clinical Infectious Diseases*, 2001. 33(2): p. 191-202.
199. Elsner, C. and K. Dörries, *Evidence of human polyomavirus BK and JC infection in normal brain tissue*. *Virology*, 1992. 191(1): p. 72-80.
200. Dörries, K., et al., *Infection of Human Polyomaviruses JC and BK in Peripheral Blood Leukocytes from Immunocompetent Individuals*. *Virology*, 1994. 198(1): p. 59-70.
201. van der Meijden, E., et al., *Different Serologic Behavior of MCPyV, TSPyV, HPyV6, HPyV7 and HPyV9 Polyomaviruses Found on the Skin*. *PLOS ONE*, 2013. 8(11): p. e81078.
202. Comar, M., et al., *Secondary lymphoid tissue as an important site for WU polyomavirus infection in immunocompetent children*. *Journal of Medical Virology*, 2011. 83(8): p. 1446-1450.
203. Imperiale, M.J. and M. Jiang, *Polyomavirus Persistence*. *Annual Review of Virology*, 2016. 3(1): p. 517-532.
204. Zhao, L. and M.J. Imperiale, *Establishing RPTE-derived cell lines expressing hTERT for studying BK polyomavirus*. *bioRxiv*, 2019: p. 766675.
205. DuShane, J.K., et al., *ERK Is a Critical Regulator of JC Polyomavirus Infection*. *Journal of Virology*, 2018. 92(7): p. e01529-17.
206. Seamone, M.E., et al., *MAP kinase activation increases BK polyomavirus replication and facilitates viral propagation in vitro*. *Journal of Virological Methods*, 2010. 170(1): p. 21-29.

207. Dahl, J., J. You, and T.L. Benjamin, *Induction and Utilization of an ATM Signaling Pathway by Polyomavirus*. Journal of Virology, 2005. 79(20): p. 13007.
208. Sullivan, C.S., et al., *SV40-encoded microRNAs regulate viral gene expression and reduce susceptibility to cytotoxic T cells*. Nature, 2005. 435(7042): p. 682-6.
209. Chang, D., X. Cai, and R.A. Consigli, *Characterization of the DNA binding properties of polyomavirus capsid protein*. Journal of Virology, 1993. 67(10): p. 6327.
210. TEGERSTEDT, K., et al., *Murine Polyomavirus Virus-like Particles (VLPs) as Vectors for Gene and Immune Therapy and Vaccines against Viral Infections and Cancer*. Anticancer Research, 2005. 25(4): p. 2601-2608.
211. Cripe, T.P., et al., *In vivo and in vitro association of hsc70 with polyomavirus capsid proteins*. Journal of Virology, 1995. 69(12): p. 7807.
212. Clayson, E.T., L.V.J. Brando, and R.W. Compans, *Release of Simian Virus-40 Virions from Epithelial-Cells Is Polarized and Occurs without Cell-Lysis*. Journal of virology, 1989. 63(5): p. 2278-2288.
213. Nieva, J.L., V. Madan, and L. Carrasco, *Viroporins: structure and biological functions*. Nat Rev Microbiol, 2012. 10(8): p. 563-74.
214. Royle, J., et al., *Emerging Roles of Viroporins Encoded by DNA Viruses: Novel Targets for Antivirals?* Viruses, 2015. 7(10): p. 5375-87.
215. Scott, C. and S. Griffin, *Viroporins: structure, function and potential as antiviral targets*. Journal of General Virology, 2015. 96(8): p. 2000-2027.
216. Agirre, A., et al., *Viroporin-mediated membrane permeabilization. Pore formation by nonstructural poliovirus 2B protein*. J Biol Chem, 2002. 277(43): p. 40434-41.
217. Danthi, P., et al., *Genome delivery and ion channel properties are altered in VP4 mutants of poliovirus*. Journal of virology, 2003. 77(9): p. 5266-5274.
218. van Kuppeveld, F.J., et al., *Coxsackievirus protein 2B modifies endoplasmic reticulum membrane and plasma membrane permeability and facilitates virus release*. EMBO J, 1997. 16(12): p. 3519-32.
219. Xie, S., et al., *DIDS blocks a chloride-dependent current that is mediated by the 2B protein of enterovirus 71*. Cell research, 2011. 21(8): p. 1271.

220. Davis, M.P., et al., *Recombinant VP4 of human rhinovirus induces permeability in model membranes*. Journal of virology, 2008. 82(8): p. 4169-4174.
221. Gervais, C., et al., *Development and validation of a high-throughput screening assay for the hepatitis C virus p7 viroporin*. J Biomol Screen, 2011. 16(3): p. 363-9.
222. Madan, V. and R. Bartenschlager, *Structural and Functional Properties of the Hepatitis C Virus p7 Viroporin*. Viruses, 2015. 7(8): p. 4461-81.
223. Steinmann, E., et al., *Hepatitis C virus p7 protein is crucial for assembly and release of infectious virions*. PLoS pathogens, 2007. 3(7): p. 962-971.
224. StGelais, C., et al., *Inhibition of hepatitis C virus p7 membrane channels in a liposome-based assay system*. Antiviral Res, 2007. 76(1): p. 48-58.
225. Largo, E., et al., *Pore-forming activity of pestivirus p7 in a minimal model system supports genus-specific viroporin function*. Antiviral Research, 2014. 101(Supplement C): p. 30-36.
226. Premkumar, A., C.R. Horan, and P.W. Gage, *Dengue virus M protein C-terminal peptide (DVM-C) forms ion channels*. J Membr Biol, 2005. 204(1): p. 33-8.
227. Sanz, M.A., L. Pérez, and L. Carrasco, *Semliki Forest virus 6K protein modifies membrane permeability after inducible expression in Escherichia coli cells*. Journal of Biological Chemistry, 1994. 269(16): p. 12106-12110.
228. Wilson, L., P. Gage, and G. Ewart, *Hexamethylene amiloride blocks E protein ion channels and inhibits coronavirus replication*. Virology, 2006. 353(2): p. 294-306.
229. Lu, W., et al., *Severe acute respiratory syndrome-associated coronavirus 3a protein forms an ion channel and modulates virus release*. Proceedings of the National Academy of Sciences, 2006. 103(33): p. 12540-12545.
230. Madan, V., et al., *Viroporin activity of murine hepatitis virus E protein*. FEBS letters, 2005. 579(17): p. 3607-3612.
231. Perez, M., et al., *Membrane Permeability Changes Induced in Escherichia coli by the SH Protein of Human Respiratory Syncytial Virus*. Virology, 1997. 235(2): p. 342-351.

232. Guinea, R. and L. Carrasco, *Influenza virus M2 protein modifies membrane permeability in E. coli cells*. FEBS Letters, 1994. 343(3): p. 242-246.
233. Ma, C., et al., *Identification of the functional core of the influenza A virus A/M2 proton-selective ion channel*. Proc Natl Acad Sci U S A, 2009. 106(30): p. 12283-8.
234. Pinto, L.H., L.J. Holsinger, and R.A. Lamb, *Influenza-Virus M2 Protein Encodes Ion Channel Activity*. Faseb Journal, 1992. 6(1): p. A11-A11.
235. Stouffer, A.L., et al., *Structural basis for the function and inhibition of an influenza virus proton channel*. Nature, 2008. 451(7178): p. 596-9.
236. Mould, J.A., et al., *Influenza B virus BM2 protein has ion channel activity that conducts protons across membranes*. Developmental cell, 2003. 5(1): p. 175-184.
237. Hongo, S., et al., *Detection of ion channel activity in Xenopus laevis oocytes expressing Influenza C virus CM2 protein*. Archives of virology, 2003. 149(1): p. 35-50.
238. González, M.E., *Vpu protein: The viroporin encoded by HIV-1*. Viruses, 2015. 7(8): p. 4352-4368.
239. González, M.E. and L. Carrasco, *The Human Immunodeficiency Virus Type 1 Vpu Protein Enhances Membrane Permeability*. Biochemistry, 1998. 37(39): p. 13710-13719.
240. Silic-Benussi, M., et al., *Effects of human T-cell leukemia virus type 1 (HTLV-1) p13 on mitochondrial K⁺ permeability: A new member of the viroporin family?* FEBS letters, 2010. 584(10): p. 2070-2075.
241. Hyser, J.M., et al., *Rotavirus disrupts calcium homeostasis by NSP4 viroporin activity*. MBio, 2010. 1(5): p. e00265-10.
242. Bodelón, G., et al., *Modification of Late Membrane Permeability in Avian Reovirus-infected Cells VIROPORIN ACTIVITY OF THE S1-ENCODED NONSTRUCTURAL p10 PROTEIN*. Journal of Biological Chemistry, 2002. 277(20): p. 17789-17796.
243. Conrad, M., V.J. Bubb, and R. Schlegel, *The Human Papillomavirus Type-6 and 16-E5 Proteins Are Membrane-Associated Proteins Which Associate with the 16-Kilodalton Pore-Forming Protein*. Journal of virology, 1993. 67(10): p. 6170-6178.

244. Wetherill, L.F., et al., *High-risk human papillomavirus E5 oncoprotein displays channel-forming activity sensitive to small-molecule inhibitors*. J Virol, 2012. 86(9): p. 5341-51.
245. Kesinger, E., et al., *Influenza D virus M2 protein exhibits ion channel activity in Xenopus laevis oocytes*. PLOS ONE, 2018. 13(6): p. e0199227.
246. Wang, J., et al., *Structure of the transmembrane region of the M2 protein H⁺ channel*. Protein Science, 2001. 10(11): p. 2241-2250.
247. Betakova, T. and E. Kollerova, *pH modulating activity of ion channels of influenza A, B, and C viruses*. Acta virologica, 2006. 50(3): p. 187.
248. Wang, J., et al., *Structural and dynamic mechanisms for the function and inhibition of the M2 proton channel from influenza A virus*. Current Opinion in Structural Biology, 2011. 21(1): p. 68-80.
249. Sugrue, R.J. and A.J. Hay, *Structural Characteristics of the M2 Protein of Influenza-a Viruses - Evidence That It Forms a Tetrameric Channel*. Virology, 1991. 180(2): p. 617-624.
250. Pielak, R.M. and J.J. Chou, *Influenza M2 proton channels*. Biochimica et Biophysica Acta (BBA) - Biomembranes, 2011. 1808(2): p. 522-529.
251. Sakaguchi, T., G.P. Leser, and R.A. Lamb, *The ion channel activity of the influenza virus M2 protein affects transport through the Golgi apparatus*. The Journal of Cell Biology, 1996. 133(4): p. 733.
252. Hay, A.J., et al., *The molecular basis of the specific anti-influenza action of amantadine*. EMBO J, 1985. 4(11): p. 3021-4.
253. Intharathep, P., et al., *How amantadine and rimantadine inhibit proton transport in the M2 protein channel*. J Mol Graph Model, 2008. 27(3): p. 342-8.
254. Rosenberg, M.R. and M.G. Casarotto, *Coexistence of two adamantane binding sites in the influenza A M2 ion channel*. Proceedings of the National Academy of Sciences, 2010. 107(31): p. 13866.
255. Huang, R.-B., et al., *An in-depth analysis of the biological functional studies based on the NMR M2 channel structure of influenza A virus*. Biochemical and Biophysical Research Communications, 2008. 377(4): p. 1243-1247.

256. Hong, M. and W.F. DeGrado, *Structural basis for proton conduction and inhibition by the influenza M2 protein*. Protein Science, 2012. 21(11): p. 1620-1633.
257. Mast, E.E., et al., *Emergence and possible transmission of amantadine-resistant viruses during nursing home outbreaks of influenza A (H3N2)*. Am J Epidemiol, 1991. 134(9): p. 988-97.
258. Sweet, C., et al., *Virulence of rimantadine-resistant human influenza A (H3N2) viruses in ferrets*. J Infect Dis, 1991. 164(5): p. 969-72.
259. Wang, J., et al., *Structure and inhibition of the drug-resistant S31N mutant of the M2 ion channel of influenza A virus*. Proceedings of the National Academy of Sciences, 2013. 110(4): p. 1315.
260. Pielak, R.M. and J.J. Chou, *Solution NMR structure of the V27A drug resistant mutant of influenza A M2 channel*. Biochemical and Biophysical Research Communications, 2010. 401(1): p. 58-63.
261. Pielak, R.M., J.R. Schnell, and J.J. Chou, *Mechanism of drug inhibition and drug resistance of influenza A M2 channel*. Proc Natl Acad Sci U S A, 2009. 106(18): p. 7379-84.
262. Wang, J., F. Li, and C. Ma, *Recent progress in designing inhibitors that target the drug-resistant M2 proton channels from the influenza A viruses*. Peptide Science, 2015. 104(4): p. 291-309.
263. Scott, C., et al., *Site-directed M2 proton channel inhibitors enable synergistic combination therapy for rimantadine-resistant pandemic influenza*. bioRxiv, 2019: p. 713636.
264. Foster, T.L., et al., *Resistance mutations define specific antiviral effects for inhibitors of the hepatitis C virus p7 ion channel*. Hepatology, 2011. 54(1): p. 79-90.
265. Griffin, S.D.C., et al., *The p7 protein of hepatitis C virus forms an ion channel that is blocked by the antiviral drug, Amantadine*. FEBS letters, 2003. 535(1-3): p. 34-38.
266. Griffin, S.D.C., et al., *A conserved basic loop in hepatitis C virus p7 protein is required for amantadine-sensitive ion channel activity in mammalian cells but is dispensable for localization to mitochondria*. Journal of General Virology, 2004. 85(2): p. 451-461.

267. Luik, P., et al., *The 3-dimensional structure of a hepatitis C virus p7 ion channel by electron microscopy*. Proc Natl Acad Sci U S A, 2009. 106(31): p. 12712-6.
268. Pavlović, D., et al., *The hepatitis C virus p7 protein forms an ion channel that is inhibited by long-alkyl-chain iminosugar derivatives*. Proceedings of the National Academy of Sciences, 2003. 100(10): p. 6104.
269. Luscombe, C.A., et al., *A novel Hepatitis C virus p7 ion channel inhibitor, BIT225, inhibits bovine viral diarrhea virus in vitro and shows synergism with recombinant interferon-alpha-2b and nucleoside analogues*. Antiviral Res, 2010. 86(2): p. 144-53.
270. Premkumar, A., et al., *Cation-selective ion channels formed by p7 of hepatitis C virus are blocked by hexamethylene amiloride*. FEBS Letters, 2004. 557(1-3): p. 99-103.
271. Ewart, G.D., Mills, K., Cox, G.B. et al., *Amiloride derivatives block ion channel activity and enhancement of virus-like particle budding caused by HIV-1 protein Vpu*. Eur Biophys J, 2001. 31(1): p. 26-35.
272. Khoury, G., et al., *Antiviral Efficacy of the Novel Compound BIT225 against HIV-1 Release from Human Macrophages*. Antimicrobial Agents and Chemotherapy, 2010. 54(2): p. 835.
273. Wilkinson, J., et al., *A Phase 1b/2a study of the safety, pharmacokinetics and antiviral activity of BIT225 in patients with HIV-1 infection*. Journal of Antimicrobial Chemotherapy, 2015. 71(3): p. 731-738.
274. de Jong, A.S., et al., *The coxsackievirus 2B protein increases efflux of ions from the endoplasmic reticulum and Golgi, thereby inhibiting protein trafficking through the Golgi*. J Biol Chem, 2006. 281(20): p. 14144-50.
275. de Jong, A.S., et al., *Determinants for membrane association and permeabilization of the coxsackievirus 2B protein and the identification of the Golgi complex as the target organelle*. J Biol Chem, 2003. 278(2): p. 1012-21.
276. Van kuppeveld, F.J., et al., *Structure-function analysis of coxsackie B3 virus protein 2B*. Virology, 1997. 227(1): p. 111-8.
277. van Kuppeveld, F.J., et al., *Homomultimerization of the coxsackievirus 2B protein in living cells visualized by fluorescence resonance energy transfer microscopy*. J Virol, 2002. 76(18): p. 9446-56.

278. de Jong, A.S., et al., *Functional Analysis of Picornavirus 2B Proteins: Effects on Calcium Homeostasis and Intracellular Protein Trafficking*. Journal of Virology, 2008. 82(7): p. 3782.
279. Nieva, J.L., et al., *Mechanisms of membrane permeabilization by picornavirus 2B viroporin*. FEBS Letters, 2003. 552(1): p. 68-73.
280. Ao, D., et al., *Viroporin Activity of the Foot-and-Mouth Disease Virus Non-Structural 2B Protein*. PLOS ONE, 2015. 10(5): p. e0125828.
281. Wasson, C.W., et al., *Human papillomavirus type 18 E5 oncogene supports cell cycle progression and impairs epithelial differentiation by modulating growth factor receptor signalling during the virus life cycle*. Oncotarget, 2017. 8(61): p. 103581-103600.
282. Wetherill, L.F., et al., *Alkyl-imino sugars inhibit the pro-oncogenic ion channel function of human papillomavirus (HPV) E5*. Antiviral Research, 2018. 158: p. 113-121.
283. Kyte, J. and R.F. Doolittle, *A simple method for displaying the hydropathic character of a protein*. Journal of Molecular Biology, 1982. 157(1): p. 105-132.
284. Deléage, G. and B. Roux, *An algorithm for protein secondary structure prediction based on class prediction*. Protein Engineering, Design and Selection, 1987. 1(4): p. 289-294.
285. Ellis, L.C., et al., *Agnogene deletion in a novel pathogenic JC virus isolate impairs VP1 expression and virion production*. PloS one, 2013. 8(11): p. e80840.
286. Ng, S.C., et al., *Simian virus 40 maturation in cells harboring mutants deleted in the agnogene*. J Biol Chem, 1985. 260(2): p. 1127-32.
287. Rosano, G.L. and E.A. Ceccarelli, *Recombinant protein expression in Escherichia coli: advances and challenges*. Frontiers in microbiology, 2014. 5: p. 172-172.
288. Geisse, S., et al., *Eukaryotic Expression Systems: A Comparison*. Protein Expression and Purification, 1996. 8(3): p. 271-282.
289. Carter, S.D., et al., *Direct visualization of the small hydrophobic protein of human respiratory syncytial virus reveals the structural basis for membrane permeability*. FEBS Letters, 2010. 584(13): p. 2786-2790.

290. Hey, A.W., et al., *A two fusion partner system for raising antibodies against small immunogens expressed in bacteria*. J Immunol Methods, 1994. 173(2): p. 149-56.
291. Arnau, J., et al., *Reprint of: Current strategies for the use of affinity tags and tag removal for the purification of recombinant proteins*. Protein Expr Purif, 2011.
292. Seddon, A.M., P. Curnow, and P.J. Booth, *Membrane proteins, lipids and detergents: not just a soap opera*. Biochimica et Biophysica Acta (BBA) - Biomembranes, 2004. 1666(1): p. 105-117.
293. Schwartz, R., C.S. Ting, and J. King, *Whole Proteome pI Values Correlate with Subcellular Localizations of Proteins for Organisms within the Three Domains of Life*. Genome Research, 2001. 11(5): p. 703-709.
294. Saribas, A.S., et al., *Human polyomavirus JC small regulatory agnoprotein forms highly stable dimers and oligomers: Implications for their roles in agnoprotein function*. Virology, 2011. 420(1): p. 51-65.
295. Conchillo-Solé, O., et al., *AGGRESKAN: a server for the prediction and evaluation of "hot spots" of aggregation in polypeptides*. BMC Bioinformatics, 2007. 8(1): p. 65.
296. Browne, E.P., A.R. Bellamy, and J.A. Taylor, *Membrane-destabilizing activity of rotavirus NSP4 is mediated by a membrane-proximal amphipathic domain*. Journal of General Virology, 2000. 81(8): p. 1955-1959.
297. Lama, J. and L. Carrasco, *Expression of poliovirus nonstructural proteins in Escherichia coli cells. Modification of membrane permeability induced by 2B and 3A*. Journal of Biological Chemistry, 1992. 267(22): p. 15932-15937.
298. Walther, T.C. and R.V. Farese, *Lipid Droplets and Cellular Lipid Metabolism*. Annual Review of Biochemistry, 2012. 81(1): p. 687-714.
299. Miyanari, Y., et al., *The lipid droplet is an important organelle for hepatitis C virus production*. Nature Cell Biology, 2007. 9(9): p. 1089-1097.
300. Heaton, N.S. and G. Randall, *Dengue Virus-Induced Autophagy Regulates Lipid Metabolism*. Cell Host & Microbe, 2010. 8(5): p. 422-432.
301. Cheung, W., et al., *Rotaviruses Associate with Cellular Lipid Droplet Components To Replicate in Viroplasms, and Compounds Disrupting or*

- Blocking Lipid Droplets Inhibit Viroplasm Formation and Viral Replication.* Journal of Virology, 2010. 84(13): p. 6782.
302. Ishizu, K.-I., et al., *Roles of Disulfide Linkage and Calcium Ion-Mediated Interactions in Assembly and Disassembly of Virus-Like Particles Composed of Simian Virus 40 VP1 Capsid Protein.* Journal of Virology, 2001. 75(1): p. 61.
303. Chen, P.-L., et al., *Disulfide bonds stabilize JC virus capsid-like structure by protecting calcium ions from chelation.* FEBS Letters, 2001. 500(3): p. 109-113.
304. Dobson, L., I. Reményi, and G.E. Tusnády, *CCTOP: a Consensus Constrained TOPology prediction web server.* Nucleic Acids Research, 2015. 43(W1): p. W408-W412.
305. Maeda, J., et al., *Membrane Topology of Coronavirus E Protein.* Virology, 2001. 281(2): p. 163-169.
306. Saribas, A.S., et al., *Emerging From the Unknown: Structural and Functional Features of Agnoprotein of Polyomaviruses.* J Cell Physiol, 2016. 231(10): p. 2115-27.
307. Mandal, D., et al., *Photophysical processes of merocyanine 540 in solutions and in organized media.* Journal of Physical Chemistry A, 1999. 103(41): p. 8156-8159.
308. Verkman, A.S., *Mechanism and kinetics of merocyanine 540 binding to phospholipid membranes.* Biochemistry, 1987. 26(13): p. 4050-6.
309. Williamson, P., K. Mattocks, and R.A. Schlegel, *Merocyanine 540, a fluorescent probe sensitive to lipid packing.* Biochimica Et Biophysica Acta, 1983. 732(2): p. 387-93.
310. Dragsten, P.R. and W.W. Webb, *Mechanism of the membrane potential sensitivity of the fluorescent membrane probe merocyanine 540.* Biochemistry, 1978. 17(24): p. 5228-5240.
311. de Jong, A.S., et al., *Mutational analysis of different regions in the coxsackievirus 2B protein: requirements for homo-multimerization, membrane permeabilization, subcellular localization, and virus replication.* J Biol Chem, 2004. 279(19): p. 19924-35.

312. Van Meer, G., D.R. Voelker, and G.W. Feigenson, *Membrane lipids: where they are and how they behave*. Nature reviews Molecular cell biology, 2008. 9(2): p. 112-124.
313. Shukla, A., et al., *The C-terminal region of the non-structural protein 2B from Hepatitis A Virus demonstrates lipid-specific viroporin-like activity*. Scientific Reports, 2015. 5(1): p. 15884.
314. Wood, C.W. and D.N. Woolfson, *CCBuilder 2.0: Powerful and accessible coiled-coil modeling*. Protein Science, 2018. 27(1): p. 103-111.
315. Davies, W.L., et al., *Antiviral Activity of 1-Adamantanamine (Amantadine)*. Science, 1964. 144(3620): p. 862-3.
316. Wang, C., et al., *Ion channel activity of influenza A virus M2 protein: characterization of the amantadine block*. J Virol, 1993. 67(9): p. 5585-94.
317. Clarke, D., et al., *Evidence for the formation of a heptameric ion channel complex by the hepatitis C virus p7 protein in vitro*. J Biol Chem, 2006. 281(48): p. 37057-68.
318. Luke, C.J., S.S. Lakdawala, and K. Subbarao, *32 - Influenza Vaccine—Live*, in *Plotkin's Vaccines (Seventh Edition)*, S.A. Plotkin, et al., Editors. 2018, Elsevier. p. 489-510.e7.
319. Sanjuán, R., et al., *Viral Mutation Rates*. Journal of Virology, 2010. 84(19): p. 9733.

Appendix

Oligonucleotides

Name	Sequence
pET19b BKPyV agnoprotein forward	5' - AAA AAA GGT ACC ATG GTT CTG CGC CAG CTG AG - 3'
pET19b BKPyV agnoprotein reverse	5' - AAA AAA GGA TCC TTA GCT ATC CTT CAC GCT ATC TTT CAC G - 3'
T7 forward sequencing	5' - TAA TAC GAC TCA CTA TAG GG - 3'

Table A.1: List of Oligonucleotides

Recipes

10x TEA buffer (1 L)

- 48.4 g of Tris base
- 11.4 mL of glacial acetic acid
- 3.7 g of EDTA
- Deionised water

1% agarose gel (50 ml)

- 0.5 g of agarose
- 5 µl of SYBR safe
- Deionised water

LB broth (1 L) - autoclaved

- 10 g of tryptone
- 5 g of yeast extract
- 10 g of NaCl
- Deionised water

- 500 ml was supplemented with 7 g agar to make LB agar.

Laemmli SDS PAGE Protein Dye (250 ml)

- 1M Tris pH6.8 31.25 ml
- Glycerol 22.5 ml
- SDS 10% 50 ml
- Bromophenol blue 1% 5 ml
- Deionised water 131.25 ml

- β -mercaptoethanol was added at 1:100 to a working stock, which disposed of after 2 months.

Agnogene Codon Optimisation

```
0    ATGGTTCTGC GCCAGCTGAG CCGTCAGGCC AGCGTTAAAG TGAGCAAGAC
51   CTGGACCGGT ACCAAAAAAC GCGCCCAGCG CATCTTCATC TTCATCCTGG
101  AGCTGCTGCT GGAATTTTGC CGCGGCGAGG ATAGCGTGGA TGGCAAAAAC
151  AAGAGCACCA CCGCCCTGCC GGCCGTGAAA GATAGCGTGA AGGATAGCTA A
```

Agnoprotein Peptide Sequence

```
aa. 20.....30.....40...
     GTKKRAQRIFIFILELLEFCRGEDKKKKKK
```

Dye Release Controls

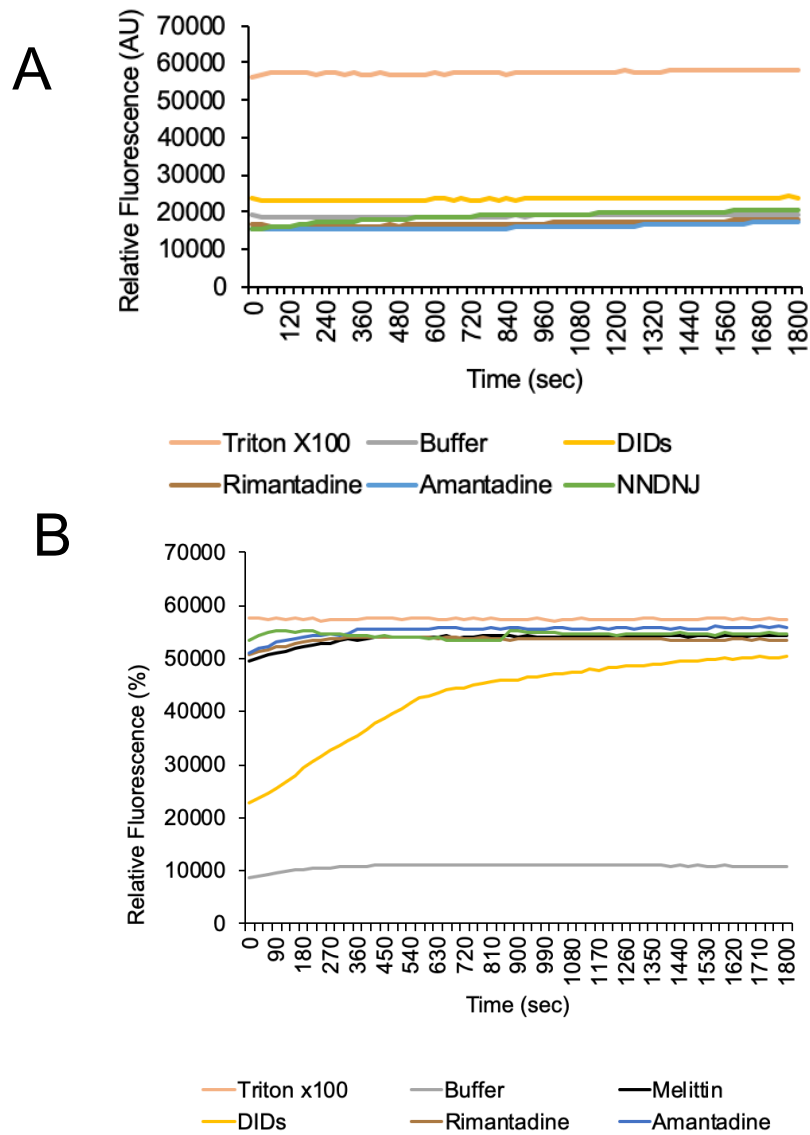


Figure A.1: Dye Release Controls

(A) Dye release over time from liposomes incubated with drug compounds in the absence of a pore forming protein. (B) Dye release over time from liposomes incubated with melittin pre-treated with drug compounds.

Multiple BKPyV Agnoprotein Alignment

	cov	pid	1 [:] 74
1 MMR29	100.0%	100.0%	-----	MVLRQLSRQASVRSVSKTWTG	TKKRAQRIFILELLELLEFCRGL---HGKNKSTTALPAVKDSVKDS
2 FUJ13	95.2%	84.8%	-----	MVLRQLSRQASVKVSKTWTG	TKKRAQRIFILELLELLEFCRGE
3 JPN15	95.2%	84.8%	-----	MVLRQLSRQASVKVSKTWTG	TKKRAQRIFILELLELLEFCRGE
4 KOM2	95.2%	84.8%	-----	MVLRQLSRQASVKVSKTWTG	TKKRAQRIFILELLELLEFCRGE
5 KOM7	95.2%	84.8%	-----	MVLRQLSRQASVKVSKTWTG	TKKRAQRIFILELLELLEFCRGE
6 MMR1	95.2%	84.8%	-----	MVLRQLSRQASVKVSKTWTG	TKKRAQRIFILELLELLEFCRGE
7 NEB10	95.2%	84.8%	-----	MVLRQLSRQASVKVSKTWTG	TKKRAQRIFILELLELLEFCRGE
8 OKN19	95.2%	84.8%	-----	MVLRQLSRQASVKVSKTWTG	TKKRAQRIFILELLELLEFCRGE
9 OKN22	95.2%	84.8%	-----	MVLRQLSRQASVKVSKTWTG	TKKRAQRIFILELLELLEFCRGE
10 RYU3	95.2%	84.8%	-----	MVLRQLSRQASVKVSKTWTG	TKKRAQRIFILELLELLEFCRGE
11 KOM1	95.2%	81.8%	-----	MVLRQLSRQASVKVSKTWTG	TKKRAQRIFILELLELLEFCRGE
12 GBR12	95.2%	80.3%	-----	MVLRQLSRQASVKIKGKTWTG	TKKRAQRIFILELLELLEFCRGE
13 J/1025/05	95.2%	80.3%	-----	MVLRQLSRQASVKIKGKTWTG	TKKRAQRIFILELLELLEFCRGE
14 J2B11	95.2%	80.3%	-----	MVLRQLSRQASVKIKGKTWTG	TKKRAQRIFILELLELLEFCRGE
15 BDX_2015_BKV1	95.2%	78.8%	-----	MVLRQLSRQASVKIKGKTWTG	TKKRAQRIFILELLELLEFCRGE
16 ITA5	95.2%	80.3%	-----	MVLRQLSRQASVKIKGKTWTG	TKKRAQRIFILELLELLEFCRGE
17 APJ	98.4%	87.9%	-----	MVLRQLSRQASVKVSKTWTG	TKKRAQRIFILELLELLEFCRGE
18 HIu6	93.7%	80.3%	-----	MVLRQ-----LSRKVSKTWTG	TKKRAQRIFILELLELLEFCRGE
19 TUR5	100.0%	86.4%	-----	MVLRQLSRQASVKIKGKTWTG	TKKRAQRIFILELLELLEFCRGE
20 MMR6	100.0%	89.4%	-----	MVLRQLSRQASVVRVGKTWTG	TKKRAQRIFILELLELLEFCRGE
21 PHL7	100.0%	89.4%	-----	MVLRQLSRQASVVRVGKTWTG	TKKRAQRIFILELLELLEFCRGE
22 SJHLG168	100.0%	89.4%	-----	MVLRQLSRQASVVRVGKTWTG	TKKRAQRIFILELLELLEFCRGE
23 FIN10	100.0%	86.4%	-----	MVLRQLSRQASVKIKGKTWTG	TKKRAQRIFILELLELLEFCRGE
24 CH1	100.0%	87.9%	-----	MVLRQLSRQASVKVVGKTWTG	TKKRAQRIFILELLELLEFCRGE
25 BK2	100.0%	86.4%	-----	MVLRQLSRQASVKVVGKTWTG	TKKRAQRIFILELLELLEFCRGE
26 CH2	100.0%	86.4%	-----	MVLRQLSRQASVKVVGKTWTG	TKKRAQRIFILELLELLEFCRGE
27 AS	100.0%	77.0%	MFCEPKNLV	MVLRQLSRQASVKVVGKTWTG	TKKRAQRIFILELLELLEFCRGE
28 A23H	100.0%	84.8%	-----	MVLRQLSRQASVKIKGKTWTG	TKKRAQRIFILELLELLEFCRGE
29 RU12	100.0%	84.8%	-----	MVLRQLSRQASVKIKGKTWTG	TKKRAQRIFILELLELLEFCRGE
30 RU18	100.0%	84.8%	-----	MVLRQLSRQASVKIKGKTWTG	TKKRAQRIFILELLELLEFCRGE
31 RU19	100.0%	84.8%	-----	MVLRQLSRQASVKIKGKTWTG	TKKRAQRIFILELLELLEFCRGE
32 RU3	100.0%	84.8%	-----	MVLRQLSRQASVKIKGKTWTG	TKKRAQRIFILELLELLEFCRGE
33 RU4	100.0%	84.8%	-----	MVLRQLSRQASVKIKGKTWTG	TKKRAQRIFILELLELLEFCRGE
34 RU5	100.0%	84.8%	-----	MVLRQLSRQASVKIKGKTWTG	TKKRAQRIFILELLELLEFCRGE
35 RU6	100.0%	84.8%	-----	MVLRQLSRQASVKIKGKTWTG	TKKRAQRIFILELLELLEFCRGE

36	RU8	100.0%	84.8%	-----MVLRLSRQASVKLGKTTWTGTTKKRAQRIFILELLELLEFCRGE	DSVDGKNKSTTALPAVKDSVKDS
37	Dunlop	100.0%	87.9%	-----MVLRLSRQASVKVGGKTTWTGTTKKRAQRIFILELLELLEFCRGE	DSVDGKNKSTTALPAVKDSVKDS
38	1474/KW	100.0%	87.9%	-----MVLRLSRQASVKVGGKTTWTGTTKKRAQRIFILELLELLEFCRGE	DSVDGKNKSTTALPAVKDSVKDS
39	342	100.0%	87.9%	-----MVLRLSRQASVKVGGKTTWTGTTKKRAQRIFILELLELLEFCRGE	DSVDGKNKSTTALPAVKDSVKDS
40	A62H	100.0%	87.9%	-----MVLRLSRQASVKVGGKTTWTGTTKKRAQRIFILELLELLEFCRGE	DSVDGKNKSTTALPAVKDSVKDS
41	BKVD	100.0%	87.9%	-----MVLRLSRQASVKVGGKTTWTGTTKKRAQRIFILELLELLEFCRGE	DSVDGKNKSTTALPAVKDSVKDS
42	CAF15	100.0%	87.9%	-----MVLRLSRQASVKVGGKTTWTGTTKKRAQRIFILELLELLEFCRGE	DSVDGKNKSTTALPAVKDSVKDS
43	CAF5	100.0%	87.9%	-----MVLRLSRQASVKVGGKTTWTGTTKKRAQRIFILELLELLEFCRGE	DSVDGKNKSTTALPAVKDSVKDS
44	CAF9	100.0%	87.9%	-----MVLRLSRQASVKVGGKTTWTGTTKKRAQRIFILELLELLEFCRGE	DSVDGKNKSTTALPAVKDSVKDS
45	FUJ34	100.0%	87.9%	-----MVLRLSRQASVKVGGKTTWTGTTKKRAQRIFILELLELLEFCRGE	DSVDGKNKSTTALPAVKDSVKDS
46	KEN1	100.0%	87.9%	-----MVLRLSRQASVKVGGKTTWTGTTKKRAQRIFILELLELLEFCRGE	DSVDGKNKSTTALPAVKDSVKDS
47	KEN4	100.0%	87.9%	-----MVLRLSRQASVKVGGKTTWTGTTKKRAQRIFILELLELLEFCRGE	DSVDGKNKSTTALPAVKDSVKDS
48	KT514USA	100.0%	87.9%	-----MVLRLSRQASVKVGGKTTWTGTTKKRAQRIFILELLELLEFCRGE	DSVDGKNKSTTALPAVKDSVKDS
49	KT815.4USA	100.0%	87.9%	-----MVLRLSRQASVKVGGKTTWTGTTKKRAQRIFILELLELLEFCRGE	DSVDGKNKSTTALPAVKDSVKDS
50	KT867USA	100.0%	87.9%	-----MVLRLSRQASVKVGGKTTWTGTTKKRAQRIFILELLELLEFCRGE	DSVDGKNKSTTALPAVKDSVKDS
51	PittNP4	100.0%	87.9%	-----MVLRLSRQASVKVGGKTTWTGTTKKRAQRIFILELLELLEFCRGE	DSVDGKNKSTTALPAVKDSVKDS
52	PittNP5	100.0%	87.9%	-----MVLRLSRQASVKVGGKTTWTGTTKKRAQRIFILELLELLEFCRGE	DSVDGKNKSTTALPAVKDSVKDS
53	PittVR4	100.0%	87.9%	-----MVLRLSRQASVKVGGKTTWTGTTKKRAQRIFILELLELLEFCRGE	DSVDGKNKSTTALPAVKDSVKDS
54	PittVR9	100.0%	87.9%	-----MVLRLSRQASVKVGGKTTWTGTTKKRAQRIFILELLELLEFCRGE	DSVDGKNKSTTALPAVKDSVKDS
55	SAU3	100.0%	87.9%	-----MVLRLSRQASVKVGGKTTWTGTTKKRAQRIFILELLELLEFCRGE	DSVDGKNKSTTALPAVKDSVKDS
56	SHA62	100.0%	87.9%	-----MVLRLSRQASVKVGGKTTWTGTTKKRAQRIFILELLELLEFCRGE	DSVDGKNKSTTALPAVKDSVKDS
57	SHA9	100.0%	87.9%	-----MVLRLSRQASVKVGGKTTWTGTTKKRAQRIFILELLELLEFCRGE	DSVDGKNKSTTALPAVKDSVKDS
58	SJHLG310	100.0%	87.9%	-----MVLRLSRQASVKVGGKTTWTGTTKKRAQRIFILELLELLEFCRGE	DSVDGKNKSTTALPAVKDSVKDS
59	UT	100.0%	87.9%	-----MVLRLSRQASVKVGGKTTWTGTTKKRAQRIFILELLELLEFCRGE	DSVDGKNKSTTALPAVKDSVKDS
60	ZAF1	100.0%	87.9%	-----MVLRLSRQASVKVGGKTTWTGTTKKRAQRIFILELLELLEFCRGE	DSVDGKNKSTTALPAVKDSVKDS
61	A36H	100.0%	86.4%	-----MVLRLSRQASVKLGKTTWTGTTKKRAQRIFILELLELLEFCRGE	DSVDGKNKSTTALPAVKDSVKDS
62	A47H	100.0%	86.4%	-----MVLRLSRQASVKLGKTTWTGTTKKRAQRIFILELLELLEFCRGE	DSVDGKNKSTTALPAVKDSVKDS
63	ESP2	100.0%	86.4%	-----MVLRLSRQASVKLGKTTWTGTTKKRAQRIFILELLELLEFCRGE	DSVDGKNKSTTALPAVKDSVKDS
64	ETH4	100.0%	86.4%	-----MVLRLSRQASVKLGKTTWTGTTKKRAQRIFILELLELLEFCRGE	DSVDGKNKSTTALPAVKDSVKDS
65	FIN11	100.0%	86.4%	-----MVLRLSRQASVKLGKTTWTGTTKKRAQRIFILELLELLEFCRGE	DSVDGKNKSTTALPAVKDSVKDS
66	FIN13	100.0%	86.4%	-----MVLRLSRQASVKLGKTTWTGTTKKRAQRIFILELLELLEFCRGE	DSVDGKNKSTTALPAVKDSVKDS
67	FIN14	100.0%	86.4%	-----MVLRLSRQASVKLGKTTWTGTTKKRAQRIFILELLELLEFCRGE	DSVDGKNKSTTALPAVKDSVKDS
68	FIN23	100.0%	86.4%	-----MVLRLSRQASVKLGKTTWTGTTKKRAQRIFILELLELLEFCRGE	DSVDGKNKSTTALPAVKDSVKDS
69	FNL12	100.0%	86.4%	-----MVLRLSRQASVKLGKTTWTGTTKKRAQRIFILELLELLEFCRGE	DSVDGKNKSTTALPAVKDSVKDS
70	FNL22	100.0%	86.4%	-----MVLRLSRQASVKLGKTTWTGTTKKRAQRIFILELLELLEFCRGE	DSVDGKNKSTTALPAVKDSVKDS
71	GBR4	100.0%	86.4%	-----MVLRLSRQASVKLGKTTWTGTTKKRAQRIFILELLELLEFCRGE	DSVDGKNKSTTALPAVKDSVKDS
72	GBR8	100.0%	86.4%	-----MVLRLSRQASVKLGKTTWTGTTKKRAQRIFILELLELLEFCRGE	DSVDGKNKSTTALPAVKDSVKDS
73	GBR9	100.0%	86.4%	-----MVLRLSRQASVKLGKTTWTGTTKKRAQRIFILELLELLEFCRGE	DSVDGKNKSTTALPAVKDSVKDS
74	HCu2	100.0%	86.4%	-----MVLRLSRQASVKLGKTTWTGTTKKRAQRIFILELLELLEFCRGE	DSVDGKNKSTTALPAVKDSVKDS
75	HCu5	100.0%	86.4%	-----MVLRLSRQASVKLGKTTWTGTTKKRAQRIFILELLELLEFCRGE	DSVDGKNKSTTALPAVKDSVKDS
76	HCu9	100.0%	86.4%	-----MVLRLSRQASVKLGKTTWTGTTKKRAQRIFILELLELLEFCRGE	DSVDGKNKSTTALPAVKDSVKDS

77	JL	100.0%	86.4%	-----MVLRLSRQASVKLGKTTWTGTTKKRAQRIFILELLELLEFCRGE
78	LAB11	100.0%	86.4%	-----MVLRLSRQASVKLGKTTWTGTTKKRAQRIFILELLELLEFCRGE
79	LAB20	100.0%	86.4%	-----MVLRLSRQASVKLGKTTWTGTTKKRAQRIFILELLELLEFCRGE
80	LAB29	100.0%	86.4%	-----MVLRLSRQASVKLGKTTWTGTTKKRAQRIFILELLELLEFCRGE
81	LAB7	100.0%	86.4%	-----MVLRLSRQASVKLGKTTWTGTTKKRAQRIFILELLELLEFCRGE
82	PittNP2	100.0%	86.4%	-----MVLRLSRQASVKLGKTTWTGTTKKRAQRIFILELLELLEFCRGE
83	PittNP3	100.0%	86.4%	-----MVLRLSRQASVKLGKTTWTGTTKKRAQRIFILELLELLEFCRGE
84	PittVM1	100.0%	86.4%	-----MVLRLSRQASVKLGKTTWTGTTKKRAQRIFILELLELLEFCRGE
85	PittVM3	100.0%	86.4%	-----MVLRLSRQASVKLGKTTWTGTTKKRAQRIFILELLELLEFCRGE
86	PittVM4	100.0%	86.4%	-----MVLRLSRQASVKLGKTTWTGTTKKRAQRIFILELLELLEFCRGE
87	PittVM5	100.0%	86.4%	-----MVLRLSRQASVKLGKTTWTGTTKKRAQRIFILELLELLEFCRGE
88	PittVR1	100.0%	86.4%	-----MVLRLSRQASVKLGKTTWTGTTKKRAQRIFILELLELLEFCRGE
89	PittVR10	100.0%	86.4%	-----MVLRLSRQASVKLGKTTWTGTTKKRAQRIFILELLELLEFCRGE
90	PittVR2	100.0%	86.4%	-----MVLRLSRQASVKLGKTTWTGTTKKRAQRIFILELLELLEFCRGE
91	PittVR3	100.0%	86.4%	-----MVLRLSRQASVKLGKTTWTGTTKKRAQRIFILELLELLEFCRGE
92	PittVR5	100.0%	86.4%	-----MVLRLSRQASVKLGKTTWTGTTKKRAQRIFILELLELLEFCRGE
93	PittVR6	100.0%	86.4%	-----MVLRLSRQASVKLGKTTWTGTTKKRAQRIFILELLELLEFCRGE
94	PittVR7	100.0%	86.4%	-----MVLRLSRQASVKLGKTTWTGTTKKRAQRIFILELLELLEFCRGE
95	RU16	100.0%	86.4%	-----MVLRLSRQASVKLGKTTWTGTTKKRAQRIFILELLELLEFCRGE
96	RU2	100.0%	86.4%	-----MVLRLSRQASVKLGKTTWTGTTKKRAQRIFILELLELLEFCRGE
97	RU7	100.0%	86.4%	-----MVLRLSRQASVKLGKTTWTGTTKKRAQRIFILELLELLEFCRGE
98	RU9	100.0%	86.4%	-----MVLRLSRQASVKLGKTTWTGTTKKRAQRIFILELLELLEFCRGE
99	SJHLG253	100.0%	86.4%	-----MVLRLSRQASVKLGKTTWTGTTKKRAQRIFILELLELLEFCRGE
100	SJHLG305	100.0%	86.4%	-----MVLRLSRQASVKLGKTTWTGTTKKRAQRIFILELLELLEFCRGE
101	SJHLG308	100.0%	86.4%	-----MVLRLSRQASVKLGKTTWTGTTKKRAQRIFILELLELLEFCRGE
102	SWE2	100.0%	86.4%	-----MVLRLSRQASVKLGKTTWTGTTKKRAQRIFILELLELLEFCRGE
103	ETH3	100.0%	86.4%	-----MVLRLSRQASVKLGKTTWTGTTKKRAQRIFILELLELLEFCRGE
104	DIK	100.0%	89.4%	-----MVLRLSRQASVKVSKTTWTGTTKKRAQRIFILELLELLEFCRGE
105	A43H	100.0%	89.4%	-----MVLRLSRQASVKVSKTTWTGTTKKRAQRIFILELLELLEFCRGE
106	A68H	100.0%	89.4%	-----MVLRLSRQASVKVSKTTWTGTTKKRAQRIFILELLELLEFCRGE
107	Any13	100.0%	89.4%	-----MVLRLSRQASVKVSKTTWTGTTKKRAQRIFILELLELLEFCRGE
108	Any2	100.0%	89.4%	-----MVLRLSRQASVKVSKTTWTGTTKKRAQRIFILELLELLEFCRGE
109	Any29	100.0%	89.4%	-----MVLRLSRQASVKVSKTTWTGTTKKRAQRIFILELLELLEFCRGE
110	ANY3	100.0%	89.4%	-----MVLRLSRQASVKVSKTTWTGTTKKRAQRIFILELLELLEFCRGE
111	Any32	100.0%	89.4%	-----MVLRLSRQASVKVSKTTWTGTTKKRAQRIFILELLELLEFCRGE
112	Any33	100.0%	89.4%	-----MVLRLSRQASVKVSKTTWTGTTKKRAQRIFILELLELLEFCRGE
113	Any38	100.0%	89.4%	-----MVLRLSRQASVKVSKTTWTGTTKKRAQRIFILELLELLEFCRGE
114	Any56	100.0%	89.4%	-----MVLRLSRQASVKVSKTTWTGTTKKRAQRIFILELLELLEFCRGE
115	Any57	100.0%	89.4%	-----MVLRLSRQASVKVSKTTWTGTTKKRAQRIFILELLELLEFCRGE
116	Any63	100.0%	89.4%	-----MVLRLSRQASVKVSKTTWTGTTKKRAQRIFILELLELLEFCRGE
117	Any7	100.0%	89.4%	-----MVLRLSRQASVKVSKTTWTGTTKKRAQRIFILELLELLEFCRGE

118	AR11	100.0%	89.4%	-----MVLRLSRQASVKVSKTWTGTTKRAQRIFILELLELLEFCRGE
119	BDX_2015_BKV3	100.0%	89.4%	-----MVLRLSRQASVKVSKTWTGTTKRAQRIFILELLELLEFCRGE
120	CAPH2	100.0%	89.4%	-----MVLRLSRQASVKVSKTWTGTTKRAQRIFILELLELLEFCRGE
121	CAPH22	100.0%	89.4%	-----MVLRLSRQASVKVSKTWTGTTKRAQRIFILELLELLEFCRGE
122	CAPH8	100.0%	89.4%	-----MVLRLSRQASVKVSKTWTGTTKRAQRIFILELLELLEFCRGE
123	CAPm13	100.0%	89.4%	-----MVLRLSRQASVKVSKTWTGTTKRAQRIFILELLELLEFCRGE
124	CAPm2	100.0%	89.4%	-----MVLRLSRQASVKVSKTWTGTTKRAQRIFILELLELLEFCRGE
125	CAPm5	100.0%	89.4%	-----MVLRLSRQASVKVSKTWTGTTKRAQRIFILELLELLEFCRGE
126	CAPm9	100.0%	89.4%	-----MVLRLSRQASVKVSKTWTGTTKRAQRIFILELLELLEFCRGE
127	FUJ15	100.0%	89.4%	-----MVLRLSRQASVKVSKTWTGTTKRAQRIFILELLELLEFCRGE
128	FUJ27	100.0%	89.4%	-----MVLRLSRQASVKVSKTWTGTTKRAQRIFILELLELLEFCRGE
129	FUJ31	100.0%	89.4%	-----MVLRLSRQASVKVSKTWTGTTKRAQRIFILELLELLEFCRGE
130	FUJ36	100.0%	89.4%	-----MVLRLSRQASVKVSKTWTGTTKRAQRIFILELLELLEFCRGE
131	FUJ4	100.0%	89.4%	-----MVLRLSRQASVKVSKTWTGTTKRAQRIFILELLELLEFCRGE
132	FUJ6	100.0%	89.4%	-----MVLRLSRQASVKVSKTWTGTTKRAQRIFILELLELLEFCRGE
133	HIu5	100.0%	89.4%	-----MVLRLSRQASVKVSKTWTGTTKRAQRIFILELLELLEFCRGE
134	HIu8	100.0%	89.4%	-----MVLRLSRQASVKVSKTWTGTTKRAQRIFILELLELLEFCRGE
135	J2B1	100.0%	89.4%	-----MVLRLSRQASVKVSKTWTGTTKRAQRIFILELLELLEFCRGE
136	J2B2	100.0%	89.4%	-----MVLRLSRQASVKVSKTWTGTTKRAQRIFILELLELLEFCRGE
137	KEN3	100.0%	89.4%	-----MVLRLSRQASVKVSKTWTGTTKRAQRIFILELLELLEFCRGE
138	KOM3	100.0%	89.4%	-----MVLRLSRQASVKVSKTWTGTTKRAQRIFILELLELLEFCRGE
139	KOM5	100.0%	89.4%	-----MVLRLSRQASVKVSKTWTGTTKRAQRIFILELLELLEFCRGE
140	KOM6	100.0%	89.4%	-----MVLRLSRQASVKVSKTWTGTTKRAQRIFILELLELLEFCRGE
141	LAB18	100.0%	89.4%	-----MVLRLSRQASVKVSKTWTGTTKRAQRIFILELLELLEFCRGE
142	LAB27	100.0%	89.4%	-----MVLRLSRQASVKVSKTWTGTTKRAQRIFILELLELLEFCRGE
143	MT	100.0%	89.4%	-----MVLRLSRQASVKVSKTWTGTTKRAQRIFILELLELLEFCRGE
144	Mtclone29	100.0%	89.4%	-----MVLRLSRQASVKVSKTWTGTTKRAQRIFILELLELLEFCRGE
145	Mtclone47	100.0%	89.4%	-----MVLRLSRQASVKVSKTWTGTTKRAQRIFILELLELLEFCRGE
146	Mtclone87	100.0%	89.4%	-----MVLRLSRQASVKVSKTWTGTTKRAQRIFILELLELLEFCRGE
147	Mtclone97	100.0%	89.4%	-----MVLRLSRQASVKVSKTWTGTTKRAQRIFILELLELLEFCRGE
148	Mtclone104	100.0%	89.4%	-----MVLRLSRQASVKVSKTWTGTTKRAQRIFILELLELLEFCRGE
149	Mtclone111	100.0%	89.4%	-----MVLRLSRQASVKVSKTWTGTTKRAQRIFILELLELLEFCRGE
150	NAR9	100.0%	89.4%	-----MVLRLSRQASVKVSKTWTGTTKRAQRIFILELLELLEFCRGE
151	NAR15	100.0%	89.4%	-----MVLRLSRQASVKVSKTWTGTTKRAQRIFILELLELLEFCRGE
152	NAR16	100.0%	89.4%	-----MVLRLSRQASVKVSKTWTGTTKRAQRIFILELLELLEFCRGE
153	NAR17	100.0%	89.4%	-----MVLRLSRQASVKVSKTWTGTTKRAQRIFILELLELLEFCRGE
154	NAR21	100.0%	89.4%	-----MVLRLSRQASVKVSKTWTGTTKRAQRIFILELLELLEFCRGE
155	NAR41	100.0%	89.4%	-----MVLRLSRQASVKVSKTWTGTTKRAQRIFILELLELLEFCRGE
156	NEA27	100.0%	89.4%	-----MVLRLSRQASVKVSKTWTGTTKRAQRIFILELLELLEFCRGE
157	NEC15	100.0%	89.4%	-----MVLRLSRQASVKVSKTWTGTTKRAQRIFILELLELLEFCRGE
158	NEC7	100.0%	89.4%	-----MVLRLSRQASVKVSKTWTGTTKRAQRIFILELLELLEFCRGE

159	NEC8	100.0%	89.4%	-----MVLRLSRQASVKVSKTWTGTTKRAQRIFILELLELLEFCRGE
160	NER1	100.0%	89.4%	-----MVLRLSRQASVKVSKTWTGTTKRAQRIFILELLELLEFCRGE
161	OKN16	100.0%	89.4%	-----MVLRLSRQASVKVSKTWTGTTKRAQRIFILELLELLEFCRGE
162	OKN28	100.0%	89.4%	-----MVLRLSRQASVKVSKTWTGTTKRAQRIFILELLELLEFCRGE
163	OKN36	100.0%	89.4%	-----MVLRLSRQASVKVSKTWTGTTKRAQRIFILELLELLEFCRGE
164	OKN48	100.0%	89.4%	-----MVLRLSRQASVKVSKTWTGTTKRAQRIFILELLELLEFCRGE
165	OKN50	100.0%	89.4%	-----MVLRLSRQASVKVSKTWTGTTKRAQRIFILELLELLEFCRGE
166	OKN58	100.0%	89.4%	-----MVLRLSRQASVKVSKTWTGTTKRAQRIFILELLELLEFCRGE
167	PHL6	100.0%	89.4%	-----MVLRLSRQASVKVSKTWTGTTKRAQRIFILELLELLEFCRGE
168	PittNP1	100.0%	89.4%	-----MVLRLSRQASVKVSKTWTGTTKRAQRIFILELLELLEFCRGE
169	PittVM2	100.0%	89.4%	-----MVLRLSRQASVKVSKTWTGTTKRAQRIFILELLELLEFCRGE
170	PittVR8	100.0%	89.4%	-----MVLRLSRQASVKVSKTWTGTTKRAQRIFILELLELLEFCRGE
171	RYU1	100.0%	89.4%	-----MVLRLSRQASVKVSKTWTGTTKRAQRIFILELLELLEFCRGE
172	SHA10	100.0%	89.4%	-----MVLRLSRQASVKVSKTWTGTTKRAQRIFILELLELLEFCRGE
173	SHA13	100.0%	89.4%	-----MVLRLSRQASVKVSKTWTGTTKRAQRIFILELLELLEFCRGE
174	SHA19	100.0%	89.4%	-----MVLRLSRQASVKVSKTWTGTTKRAQRIFILELLELLEFCRGE
175	SHA22	100.0%	89.4%	-----MVLRLSRQASVKVSKTWTGTTKRAQRIFILELLELLEFCRGE
176	SHA23	100.0%	89.4%	-----MVLRLSRQASVKVSKTWTGTTKRAQRIFILELLELLEFCRGE
177	SHA25	100.0%	89.4%	-----MVLRLSRQASVKVSKTWTGTTKRAQRIFILELLELLEFCRGE
178	SHA4	100.0%	89.4%	-----MVLRLSRQASVKVSKTWTGTTKRAQRIFILELLELLEFCRGE
179	SHA40	100.0%	89.4%	-----MVLRLSRQASVKVSKTWTGTTKRAQRIFILELLELLEFCRGE
180	SHA41	100.0%	89.4%	-----MVLRLSRQASVKVSKTWTGTTKRAQRIFILELLELLEFCRGE
181	SHA56	100.0%	89.4%	-----MVLRLSRQASVKVSKTWTGTTKRAQRIFILELLELLEFCRGE
182	SHA7	100.0%	89.4%	-----MVLRLSRQASVKVSKTWTGTTKRAQRIFILELLELLEFCRGE
183	SHA70	100.0%	89.4%	-----MVLRLSRQASVKVSKTWTGTTKRAQRIFILELLELLEFCRGE
184	SHA72	100.0%	89.4%	-----MVLRLSRQASVKVSKTWTGTTKRAQRIFILELLELLEFCRGE
185	SJHLG152	100.0%	89.4%	-----MVLRLSRQASVKVSKTWTGTTKRAQRIFILELLELLEFCRGE
186	SJHLG166	100.0%	89.4%	-----MVLRLSRQASVKVSKTWTGTTKRAQRIFILELLELLEFCRGE
187	SJHLG304	100.0%	89.4%	-----MVLRLSRQASVKVSKTWTGTTKRAQRIFILELLELLEFCRGE
188	SJHLG313	100.0%	89.4%	-----MVLRLSRQASVKVSKTWTGTTKRAQRIFILELLELLEFCRGE
189	THK11	100.0%	89.4%	-----MVLRLSRQASVKVSKTWTGTTKRAQRIFILELLELLEFCRGE
190	THK6	100.0%	89.4%	-----MVLRLSRQASVKVSKTWTGTTKRAQRIFILELLELLEFCRGE
191	THK9	100.0%	89.4%	-----MVLRLSRQASVKVSKTWTGTTKRAQRIFILELLELLEFCRGE
192	THK9a	100.0%	89.4%	-----MVLRLSRQASVKVSKTWTGTTKRAQRIFILELLELLEFCRGE
193	TOM16	100.0%	89.4%	-----MVLRLSRQASVKVSKTWTGTTKRAQRIFILELLELLEFCRGE
194	TW1	100.0%	89.4%	-----MVLRLSRQASVKVSKTWTGTTKRAQRIFILELLELLEFCRGE
195	TW1a	100.0%	89.4%	-----MVLRLSRQASVKVSKTWTGTTKRAQRIFILELLELLEFCRGE
196	TW1b	100.0%	89.4%	-----MVLRLSRQASVKVSKTWTGTTKRAQRIFILELLELLEFCRGE
197	TW2	100.0%	89.4%	-----MVLRLSRQASVKVSKTWTGTTKRAQRIFILELLELLEFCRGE
198	TW4	100.0%	89.4%	-----MVLRLSRQASVKVSKTWTGTTKRAQRIFILELLELLEFCRGE
199	TW5	100.0%	89.4%	-----MVLRLSRQASVKVSKTWTGTTKRAQRIFILELLELLEFCRGE

200	TW7	100.0%	89.4%	-----MVLRLSRQASVKVSKTWTGTTKRAQRIFILELLELLEFCRGE
201	TW8	100.0%	89.4%	-----MVLRLSRQASVKVSKTWTGTTKRAQRIFILELLELLEFCRGE
202	TW8a	100.0%	89.4%	-----MVLRLSRQASVKVSKTWTGTTKRAQRIFILELLELLEFCRGE
203	VNM9	100.0%	89.4%	-----MVLRLSRQASVKVSKTWTGTTKRAQRIFILELLELLEFCRGE
204	WW	100.0%	89.4%	-----MVLRLSRQASVKVSKTWTGTTKRAQRIFILELLELLEFCRGE
205	TOM11	100.0%	87.9%	-----MVLRLSRQASVKVSKTWTGTTKRAHRIFILELLELLEFCRGE
206	TW3	100.0%	89.4%	-----MVLRLSLQASVKVSKTWTGTTKRAQRIFILELLELLEFCRGE
207	MMR24	100.0%	89.4%	-----MVLRLSRQASVKVSKTWTGTTKRAQRIFILELLELLEFCRGE
208	FUJ18	100.0%	92.4%	-----MVLRLSRQASVRVSKTWTGTTKRAQRIFILELLELLEFCRGE
209	MON1	100.0%	92.4%	-----MVLRLSRQASVRVSKTWTGTTKRAQRIFILELLELLEFCRGE
210	NWC14	100.0%	92.4%	-----MVLRLSRQASVRVSKTWTGTTKRAQRIFILELLELLEFCRGE
211	SHA28	100.0%	92.4%	-----MVLRLSRQASVRVSKTWTGTTKRAQRIFILELLELLEFCRGE
212	SHA30	100.0%	92.4%	-----MVLRLSRQASVRVSKTWTGTTKRAQRIFILELLELLEFCRGE
213	SHA47	100.0%	92.4%	-----MVLRLSRQASVRVSKTWTGTTKRAQRIFILELLELLEFCRGE
214	SHA55	100.0%	92.4%	-----MVLRLSRQASVRVSKTWTGTTKRAQRIFILELLELLEFCRGE
215	SHA78	100.0%	92.4%	-----MVLRLSRQASVRVSKTWTGTTKRAQRIFILELLELLEFCRGE
216	SWC1	100.0%	92.4%	-----MVLRLSRQASVRVSKTWTGTTKRAQRIFILELLELLEFCRGE
217	NEA28	100.0%	90.9%	-----MVLRLSRQASVKVSKTWTGTTKRAQRIFILELLELLEFCRGE
218	NEB26	100.0%	90.9%	-----MVLRLSRQASVKVSKTWTGTTKRAQRIFILELLELLEFCRGE
219	NEB27	100.0%	90.9%	-----MVLRLSRQASVKVSKTWTGTTKRAQRIFILELLELLEFCRGE
220	NGY19	100.0%	90.9%	-----MVLRLSRQASVKVSKTWTGTTKRAQRIFILELLELLEFCRGE
221	PHL8	100.0%	90.9%	-----MVLRLSRQASVKVSKTWTGTTKRAQRIFILELLELLEFCRGE
222	SHA43	100.0%	90.9%	-----MVLRLSRQASVKVSKTWTGTTKRAQRIFILELLELLEFCRGE
223	THK8	100.0%	90.9%	-----MVLRLSRQASVKVSKTWTGTTKRAQRIFILELLELLEFCRGE
224	TW3a	100.0%	90.9%	-----MVLRLSRQASVKVSKTWTGTTKRAQRIFILELLELLEFCRGE
225	VNM7	100.0%	90.9%	-----MVLRLSRQASVKVSKTWTGTTKRAQRIFILELLELLEFCRGE
226	5682/KW	100.0%	87.9%	-----MVLRLSRQASVKVSKTWTGTTKRAQRIFILELLELLEFCRGE
227	A37H	100.0%	87.9%	-----MVLRLSRQASVKVSKTWTGTTKRAQRIFILELLELLEFCRGE
228	A66H	100.0%	87.9%	-----MVLRLSRQASVKVSKTWTGTTKRAQRIFILELLELLEFCRGE
229	FIN2	100.0%	87.9%	-----MVLRLSRQASVKVSKTWTGTTKRAQRIFILELLELLEFCRGE
230	FIN4	100.0%	87.9%	-----MVLRLSRQASVKVSKTWTGTTKRAQRIFILELLELLEFCRGE
231	GRC4	100.0%	87.9%	-----MVLRLSRQASVKVSKTWTGTTKRAQRIFILELLELLEFCRGE
232	ITA4	100.0%	87.9%	-----MVLRLSRQASVKVSKTWTGTTKRAQRIFILELLELLEFCRGE
233	RU10	100.0%	87.9%	-----MVLRLSRQASVKVSKTWTGTTKRAQRIFILELLELLEFCRGE
234	RU11	100.0%	87.9%	-----MVLRLSRQASVKVSKTWTGTTKRAQRIFILELLELLEFCRGE
235	RU13	100.0%	87.9%	-----MVLRLSRQASVKVSKTWTGTTKRAQRIFILELLELLEFCRGE
236	RU15	100.0%	87.9%	-----MVLRLSRQASVKVSKTWTGTTKRAQRIFILELLELLEFCRGE
237	CAMB1055	100.0%	89.4%	-----MVLRLSRQASVKVSKTWTGTTKRAQRIFILELLELLEFCRGE
238	Mtclone32	100.0%	89.4%	-----MVLRLSRQASVKVSKTWTGTTKRAQRIFILELLELLEFCRGE
239	Mtclone51	100.0%	89.4%	-----MVLRLSRQASVKVSKTWTGTTKRAQRIFILELLELLEFCRGE
240	Mtclone54	100.0%	89.4%	-----MVLRLSRQASVKVSKTWTGTTKRAQRIFILELLELLEFCRGE

241	Mtclone59	100.0%	89.4%	-----MVLRLSRQASVKVSKTWTGTTKKRAQRIFILELLELLEFCRGGKDSVDGKNKSTTALPAVKDSVKDS
242	Mtclone93	100.0%	89.4%	-----MVLRLSRQASVKVSKTWTGTTKKRAQRIFILELLELLEFCRGGKDSVDGKNKSTTALPAVKDSVKDS
243	Mtclone108	100.0%	89.4%	-----MVLRLSRQASVKVSKTWTGTTKKRAQRIFILELLELLEFCRGGKDSVDGKNKSTTALPAVKDSVKDS
244	SJHLG309	100.0%	89.4%	-----MVLRLSRQASVKVSKTWTGTTKKRAQRIFILELLELLEFCRGGKDSVDGKNKSTTALPAVKDSVKDS
245	CAPH5	100.0%	87.9%	-----MVLRLSRQASVKVSKTWTGTTKKRAQRIFILELLELLEFCRGGKDSVDGKNKSTTALPAVKDSVKDS
246	CAPm18	100.0%	87.9%	-----MVLRLSRQASVKVSKTWTGTTKKRAQRIFILELLELLEFCRGGKDSVDGKNKSTTALPAVKDSVKDS
247	GBR6	100.0%	89.4%	-----MVLRLSRQASVKVSKTWTGTTKKRAQRIFILELLELLEFCRGGKDSVDGKNKSTTALPAVKDSVKDS
248	Mtclone18	100.0%	87.9%	-----MVLRLSRQASVKVSKTWTGTTKKRAQRIFILELLELLEFCRGGKDSVDGKNKSTTALPAVKDSVKDS
249	Mtclone44	100.0%	87.9%	-----MVLRLSRQASVKVSKTWTGTTKKRAQRIFILELLELLEFCRGGKDSVDGKNKSTTALPAVKDSVKDS
250	Mtclone50	100.0%	87.9%	-----MVLRLSRQASVKVSKTWTGTTKKRAQRIFILELLELLEFCRGGKDSVDGKNKSTTALPAVKDSVKDS
251	RYU2	100.0%	87.9%	-----MVLRLSRQASVKVSKTWTGTTKKRAQRIFILELLELLEFCRGGKDSVDGKNKSTTALPAVKDSVKDS
252	NEC12	100.0%	87.9%	-----MVLRLSRQASVKVSKTWTGTTKKRAQRIFILELLELLEFCRGGKDSVDGKNKSTTALPAVKDSVKDS
253	OKN42	100.0%	87.9%	-----MVLRLSRQASVKVSKTWTGTTKKRAQRIFILELLELLEFCRGGKDSVDGKNKSTTALPAVKDSVKDS

Figure A.2: Alignment of BKPyV agnoproteins from multiple stains

Multiple sequence alignment was performed using Clustal Omega server. Coverage (cov.) and percentage identity (pid.) were calculated compared to a determined consensus sequence determined by the server. Amino acids are colour coded as green=hydrophobic, red=basic, purple=neutral charge, dark blue=acidic yellow=thiol, and light blue=polar

